Mesoscale Structure and Techno-functional Properties of Enzymatically Cross-linked α-Lactalbumin Nanoparticles

Surender Kumar Dhayal

Thesis committee

Promotor

Prof. Dr H. Gruppen
Professor of Food Chemistry
Wageningen University

Co-promotors

Dr P. A. Wierenga
Assistant professor, Laboratory of Food Chemistry
Wageningen University

Dr R. J. de Vries
Associate professor, Laboratory of Physical Chemistry and Colloid Science
Wageningen University

Other members

Prof. Dr W. J. H. van Berkel, Wageningen University
Dr P. Venema, Wageningen University
Dr M. B. J. Meinders, Wageningen UR Food & Biobased Research
Dr A. Alting, FrieslandCampina, The Netherlands

This research was conducted under the auspices of the Graduate School VLAG (Advanced studies in Food Technology, Agrobiotechnology, Nutrition and Health Sciences).

Mesoscale Structure and Techno-functional Properties of Enzymatically Cross-linked α-Lactalbumin Nanoparticles

Surender Kumar Dhayal

Thesis
submitted in fulfilment of the requirements for the degree of doctor
at Wageningen University
by the authority of the Rector Magnificus
Prof. Dr M.J. Kropff,
in the presence of the
Thesis Committee appointed by the Academic Board
to be defended in public
on Monday 11 May 2015
at 4 p.m. in the Aula.

Surender Kumar Dhayal
Mesoscale Structure and Techno-functional Properties of
Enzymatically Cross-linked α-Lactalbumin Nanoparticles
162 pages.

PhD thesis, Wageningen University, Wageningen, NL (2015)
With references, with summaries in English and Dutch.

ISBN: 978-94-6257-281-2

Abstract

The aim of this thesis is to understand the connection between molecular, meso and macroscales of enzymatically cross-linked proteins. It was hypothesised that the techno-functional properties at macroscale, such as bulk rheology and foam stability, are affected by the structure of nanoparticles at mesoscale. The approach was to make α-lactalbumin (α-LA) nanoparticles by using two different enzymes, horseradish peroxidase (HRP) or microbial transglutaminase (mTG), to produce an open and compact mesoscale structure, respectively. In addition to the control over the mesoscale structure, the size of the nanoparticles can be independently controlled by varying the dosage of hydrogen peroxide in the case of HRP and by thermal inactivation in the case of mTG. The other important parameters determining the size are protein concentration and ionic strength. The size (radius of gyration) range that could be achieved by varying the above mentioned control parameters is $20 - 200$ nm. The polydispersed nanoparticles were separated by asymmetrical flow field flow fractionation (AF4) and characterised inline with multi angle light scattering (MALS). Polymerization of apo α-LA with HRP and mTG proceeds in a step growth way i.e. first monomers react to form oligomers and the oligomers are cross-linked to form polymers (nanoparticles). Extensive cross-linking of α-LA with HRP gives rise to not only di-tyrosine cross-links, but also tri$-$octa tyrosine cross-links, which was hitherto unknown. The two different mesoscale structures result in gels of different storage moduli. The storage modulus of gels made by concentrating the α-LA/mTG nanoparticles was around ten times higher than that made with open nanoparticles. The half-life time ($t_{0.5}$) of the foam made with α-LA nanoparticles was two to six times higher than that of the monomeric α-LA. The higher foam-stability of the α-LA nanoparticles as compared to the monomeric α-LA is due to their higher thickness of the interfacial layer and thin films. In conclusion, it is shown that the techno-functional properties of α-LA are directly correlated to the size and meso-scale structures of the nanoparticles and enzymatic cross-linking is an effective way to control them.

Contents

Chapter 1

General Introduction

Proteins are important functional ingredients in foods [1]. In addition to nutritional and bio-functionality, proteins also have important techno-functional properties, such as gelation, emulsification and foam stabilisation [2–5]. There are many physico-chemical parameters that determine the techno-functional properties of proteins, molar mass (M_w) and size (hydrodynamic radius, R_h or radius of gyration, R_g) being two of them. The size and mass of small native proteins can be increased, for example, by heating the native proteins to induce aggregation and form protein particles [6]. Heat-induced protein particles are known to increase the foam stability in many systems [7–9]. The size and mass can also be increased by chemical or enzymatic cross-linking [5, 10–12]. In past decades, there have been many articles on functionality of enzymatically cross-linked proteins, mostly *in situ* i.e. in bulk [10, 13–15]. From *in situ* studies it is not easy to understand the relation between the molecular scale details and macroscale functionality. In contrast to those studies, this thesis focusses on the use of enzymatic cross-linking to modify the proteins. In this way nanoparticles (polymers) can be prepared *ex situ* that can later be used to impart a specific functionality (figure 1.1). This approach may allow us to better understand the link between molecular scale details and macroscale functionality and this is the main goal of this thesis. It should be noted that the use of adjective nano in the case of enzymatic cross-linking is to highlight that that the typical size of enzymatically cross-linked protein particles aimed in this thesis is in the range $5 - 500$ nm [16] (figure 1.1). Main questions in this topic were what range of properties can be obtained by enzymatic cross-linking and how these properties are affected by enzyme, substrate and solution conditions. In addition, routine methods are needed for the characterisation of the structure of the protein nanoparticles. Once these questions are answered, the aim of this thesis is to link various length scales, such as molecular, meso, and macroscale in enzymatic cross-linking of proteins. The aim is to see if the macroscale functionality is related to the physico-chemical properties of the protein nanoparticles at mesoscale. Information available on the structure-function relation in the case of enzymatic cross-linking of globular proteins is rather limited as

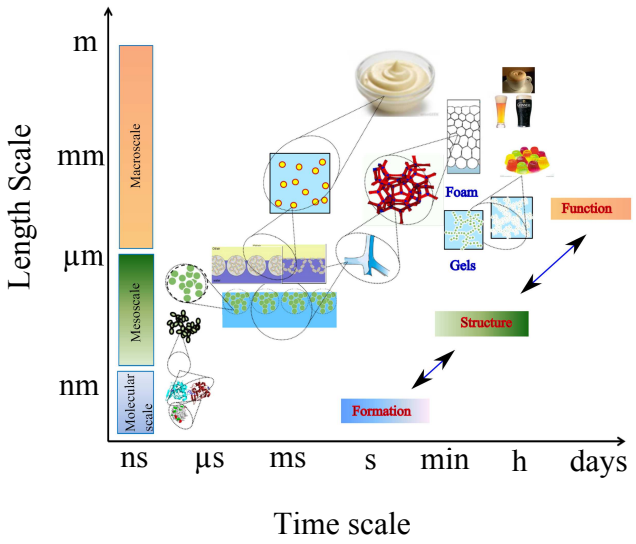

Figure 1.1: *Various length and time scales used to describe the formation, structure and functionality of enzymatically cross-linked protein nanoparticles.*

compared to heat-induced protein particles. To illustrate the point, lets consider the example of globular milk proteins. From an abundance perspective, the major globular protein in bovine milk is β-lactoglobulin (β-LG), followed by α-LA-lactalbumin (α-LA) and minor amount of bovine serum albumin (BSA). These proteins have been extensively studied in the case of heat-induced protein particles e.g. [5, 6, 17]. Various types of β-LG particles have been made by heating at different pH and ionic strengths [17]. There have been many studies on the relation between the types of protein particles obtained by heating and their functional properties e.g. [5, 18]. In comparison to heating studies, studies on enzymatic cross-linking of globular milk proteins to obtain nanoparticles are scant. A few examples of cross-linking of globular milk proteins in the past two decades are provided in table 1.1. The examples were selected from studies where there was also a characterization of particle mass or structure or functionality done.

Current state of enzymatic cross-linking of proteins

Different types of enzymes have been reported to cross-link food proteins. Examples are oxidative enzymes, such as peroxidase, tyrosinase, laccase and transferases, such as transglutaminase [10, 11]. Due to formation of inter-molecular covalent bonds between monomeric proteins, protein polymers or (nano-)particles are formed e.g. see [19–29] in table 1.1. Most of the work on enzymatic cross-linking of proteins has so far focused on the molecular details, such as; 1) The effect of the structure of

substrate protein, 2) Cross-linking with mediators [30, 31] 3) Identification of cross-linked residues [14, 32–34], 4) The final (end use) functionality at the macro-scale, such as gelation [29, 35, 36]. Some generic conclusions from these studies are that random coil proteins (e.g. caseins) are enzymatically cross-linked to a higher extent than globular proteins (e.g. whey proteins). Globular proteins require pre-treatment, such as heating or breakdown of disulphide bonds in order to be cross-linked [29, 37]. In structural studies, α-lactalbumin (α-LA) turns out to be a favoured model protein since its tertiary structure can be decreased by removal of Ca^{2+} ion (apo form) bound to it by using chelating agents, such as ethylenediamine-tetraacetic acid (EDTA) [38], thereby avoiding the need of heat treatment. The apo form of bovine α-lactalbumin (α-LA) has been found to be more amenable to enzymatic cross-linking than the holo form [21, 39].The apo α-LA is known to polymerize and form particles when cross-linked using horseradish peroxidase (HRP) or microbial transglutaminase (mTG) (table 1.1) [26, 39–46]. Moreover, these two enzymes (HRP and mTG) are known to target different amino acids (described later) on substrate proteins [21, 40, 44, 47] . Amongst these studies on enzymatic cross-linking of the α-LA, only a few have attempted to investigate the mesoscale structure of the cross-linked protein particles ([43, 46] in table 1.1).

There are many experimental observations on size/structure function relations in the case of heat-induced protein particles [2, 5, 18, 48]. On the contrary, information available on the structure-function relation in the case of enzymatic cross-linking is rather limited (table 1.1). Hence, it is difficult to correlate the observed functionality to the constituent ingredients in the case of enzymatic cross-linking. For example, emulsion, foaming and gelling properties were shown to increase in some cases and to decrease in others when some food proteins were enzymatically cross-linked [49]. To understand the functionality of enzymatically cross-linked proteins, protein nanoparticles with controlled size and structure are needed in the intermediate scale (mesoscale). Further understanding can be obtained by linking the physical and chemical details at three hierarchical length-scales in the case of enzymatic cross-linking of proteins i.e. molecular scale, mesoscale and macroscale (figure 1.1). The focus of this thesis is on enzymatic cross-linking of bovine apo α-LA with HRP or mTG to form α-LA nanoparticles that can later be used as ingredients for achieving a desired techno-functionality. The hypothesis is that the techno-functional properties at macroscale are determined by the nanoparticle structures at mesoscale (figure 1.1). Further, it is hypothesized that formation and structure of nanoparticles at mesoscale is affected by the molecular scale details of the protein and the enzyme used for cross-linking (figure 1.1). More specifically, it is hypothesised that more cross-links per particle i.e. a higher cross-link density will result in improved functionality.

Table 1.1: *Enzymatic cross-linking of globular milk proteins. '+/−' indicates the presence or absence of the factor, DP is the degree of polymerization ($DP = M_w^{polymer}/M_w^{monomer}$, calculated from the reported M_w).*

Enzyme (EC number)	Source	Substrate	Special conditions	Degree of polymerization	R_g or R_h^* to M_w scaling	Functionality	Ref.
Laccase (1.10.3.2)	Fungal	WPI	± DTT	-	-	Gelation	[19]
	Fungal	α-LA	$-Ca^{2+}$	$\leqslant 3500$	0.5	Enhanced thermal-stability	[20]
Tyrosinase (1.14.18.1)	Fungal	α-LA	$-Ca^{2+}$	$\leqslant 140$	-	Enhanced thermal-stability	[20]
Peroxidase (1.11.1.7)	Microbial	WPI	-	-	-	Gelation	[19]
	Horseradish	α-LA	$\pm Ca^{2+}$	$\geqslant 2$	-	-	[21]
	HRP(type VI-a)	α-LA	$-Ca^{2+}$ T= 20, 37°C	$\geqslant 4$	-	Decrease of Foam-stability	[22]
	HRP(type VI-a)	α-LA	$-Ca^{2+}$	~ 100	0.4 *	Enhanced thermal-stability and gelation	[46]
Transglutaminase (2.3.2.13)	Microbial	WPI	DTT$\pm Ca^{2+}$	-	-	Gelation	[23, 24]
	Microbial	WPI	-	-	-	Enhanced thermal-stability	[25]
	Microbial	α-LA	-	> 4	-	Reduction of dilatational surface viscosity, reduced emulsion stability	[26]
	Microbial	β-LG	+DTT	$\sim 3 - 17$	-	Steep increase in viscosity, gelation	[27]
	Microbial	α-LA	+DTT $\pm Ca^{2+}$	$\gg 100$	0.44	-	[28]
	Guinea pig liver	α-LA	+DTT $\pm Ca^{2+}$	> 100	0.31	-	[28]
	Microbial	WPI	+heat shock	> 14	-	Enhanced thermal stability and increased precipitation at pH close to pI	[29]

WPI = whey protein isolate, DTT = dithiothreitol

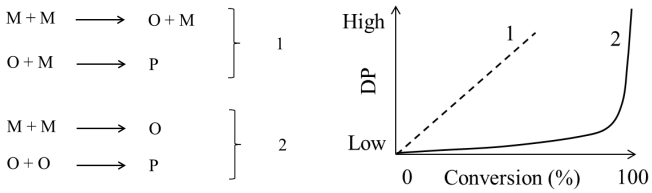

Figure 1.2: *Schematic illustration of 1) chain growth and 2) step growth mechanisms of nanoparticle formation. The evolution of degree of polymerization (DP) with conversion of monomers (M) in to oligomers (O) and polymers/particles (P) for two different ways of particle formation: 1) chain growth and 2) step growth.*

Mechanism of protein particle formation (polymerization)

A knowledge of the process of protein particle formation is required to control the size, mass and structure of the particles. In the simplest case, the polymerization (particle growth) of proteins during enzymatic cross-linking can follow either chain growth type (process 1) or step growth type (process 2) as depicted in figure 1.2. In a chain growth type of mechanism, a monomer is linked to existing oligomer and in this way polymers are formed while in step growth kind of mechanism, initially all the monomers react to form oligomers and then oligomers react in next step to form polymers. These two types of polymer growth mechanism can be distinguished from each other by monitoring the degree of polymerization ($= M_w^{\text{poly}}/M_w^{\text{mono}}$) as a function of monomer conversion. In the case of chain growth, the molar mass increases steadily with conversion while in the case of step growth high molar mass polymers are obtained only at very high conversions (figure 1.2). These are of course two extreme examples of growth mechanism and there could be mixed regimes in some cases.

The process of protein particle formation by heating involves a step growth type of mechanism [5]. When heated above their denaturation temperature, globular proteins unfold and that results in aggregation primarily through hydrophobic interactions, but may also involve di-sulfide exchange/shuffling and hydrogen bonding. In this first step, primary (smaller) particles are formed, which can later link with each other to form secondary (larger) particles [17]. The secondary particle growth depends on type of protein, solution pH and ionic strength and leads to formation of fibrils, fractal or compact particles [5, 17] (figure 1.3). In the case of fractal particles, the fractal dimension (d_f) of the secondary particles is determined by the limiting mechanism operational during the collision and linking of primary particles. If the process is limited only by the diffusion of primary particles and every collision results in formation of a link between them, then the resultant secondary particles are open type with low fractal dimension ($d_f \sim 1.8$). This is generally known as diffusion limited cluster aggregation (DLCA) [50], where the term cluster implies small primary particles. The process of formation of secondary particles can also be controlled by reactivity of

primary particles. In this case dense secondary particles are formed with $d_f \sim 2.1$ and the process is known as reaction limited cluster aggregation (RLCA) [50].

Characterization of nanoparticles: molecular scale

The functionality of protein particles is expected to depend on their structure. There are two aspects of the particle structure: physical and chemical. The chemical details that are important for particle properties are the number of cross-links (cross-linking density), distribution of cross-links (inter-molecular or intra-molecular) and the length of these cross-links. For example, in the case of protein cross-linking by oxidative enzymes, such as HRP, cross-links are formed between tyrosine residues to form a di-tyrosine (Y_2). Identification of the formed Y_2 is usually performed by measuring increase in absorbance around UV 318 nm (pH $\geq$ 7) [51] or by fluorescence emission peak at 420 nm after excitation at 315 nm (pH $\geq$ 7) [52, 53]. It has been suggested that UV 318 nm could also be used for quantification of Y_2 [41]. But, if Y_2 is present in a mixture with Y_n ($n > 2$, oligo-tyrosine), there could be artefacts in quantification using UV 318 or fluorescence. Previous studies have reported that covalent crosslinks, such as Y_2 and Y_3, are stable under the acid hydrolysis conditions (6 M HCl, 110 °C, 20 − 24 h) [33]. Hence, acid hydrolysis followed by LC-MS seems to be a robust method for quantification of mixtures containing Y_2 and oligo/poly-Tyr [54, 55]. So, identification and quantification of cross-links formed in proteins by oxidative enzymes such as HRP can be done by using a combination of all the above techniques for detection of Y_2 and acid hydrolysis followed by LC-MS for quantification of Y_2. In the case of an enzyme such as mTG, a different strategy can be used. The amount of ammonia released during the formation of a Lys-Gln cross-link can be used for quantification. Alternatively, the number of cross-links can easily be quantified using a spectrophotometric method for quantifying free lysine. The results of ammonia release are typically well correlated with the estimation of free lysine using trinitrobenzenesulfonate (TNBS) [56] or o-phtaldialdehyde (OPA) assay [57, 58].

Characterization of nanoparticles: mesoscale

The use of the term structure with respect to particles is ambiguous, since it may cover many different aspects of the particle, such as static or dynamic structures. Here, the term static structure is used for describing the structure of nanoparticles under Brownian motion in a solvent. This may include parameters, such as size, shape, density, and secondary/tertiary structure of the protein (monomer) in the particle [59]. The shapes can be sphere, rod, coil or a branched chains (figure 1.3) [5]. The branched chains varies in size and density depending on the degree of branching and distribution of branches [60]. The term dynamic is used for implying that the structure of particles change when they are subjected to external mechanical, hydrodynamic or physico-chemical conditions. For example, this occurs when; 1) They are compressed at an interface in a Langmuir trough, 2) During area change of drops/bubbles as they

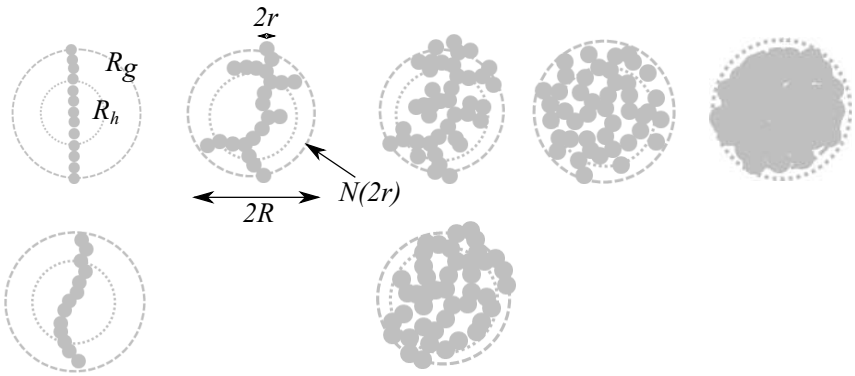

Chain type	Single (linear)	Branched	Single/Branched	Branched	Single/Branched
Common names	Rigid/ Semi-flexible rod/ Fibrils/ Fibres	Fractal	Fractal/ Random coil	Microgel	Spherical/ Globular/ Compact
R_g/R_h	>> 2	1 - 2.5	1 - 2	< 0.78	0.78
d_f	1	1.67 - 1.8	1.67 - 2.1	1.67 - 2.7	2.7 - 3
ν	1	0.5 - 0.6	0.33 - 0.6	~ 0.33	0.36 - 0.33

Figure 1.3: *Overview of various possible mesoscale structures of a single chain / branched polymer/particle.*

undergo Ostwald ripening in emulsions/foams, 3) They are subjected to shear flow, 4) If the pH/ionic strength of the solution are changed, 5) If the solvent quality is changed. The response of particles to these dynamic situations can be combined in the term softness. The softness of the particles is expected to depend on the cross-link density. Hence, particles with similar size, shape and density may still show different properties, if the number of internal cross-links is varied. The secondary structure of monomeric protein molecules in the nanoparticles may also change as a result of extensive cross-linking and that could affect their dynamic structure. Hence, the structure of nanoparticles is required to be studied at different levels; at the level of monomeric protein and at the level of particles.

The mesoscale structure (size, shape, conformation, etc.) of protein particles are often characterised using scattering or imaging techniques. Examples are small angle x-ray scattering (SAXS), small angle neutron scattering (SANS), multi-angle light scattering (MALS), scanning electron microscopy (SEM), transmission electron microscopy (TEM) and atomic force microscopy (AFM). Often there are three main challenges for these characterisations: 1) Polydispersity, 2) The modification of structures during sample preparation e.g. in SEM, TEM and AFM, and 3) Accessibility for routine analysis e.g. SAXS and SANS. Multi-angle light scattering (MALS) con-

nected in-line to a separation technique, such as size exclusion chromatography (SEC) or asymmetrical flow field flow fractionation (AF4), can be used for routine analysis. The advantages are in-line separation into monodispersed fractions and no artefacts related to structural modifications.The parameters that can be obtained from AF4-MALS and used to describe the protein nanoparticles are molar mass (M_w), radius of gyration (R_g), fractal dimension (d_f), and size to mass scaling ($R_g \sim M_w^{\nu}$). The hydrodynamic radius (R_h) can be obtained from dynamic light scattering (DLS). Typically, $\nu = 0.33$ for solid spheres, 1 for rods, 0.5 for flexible polymers in a theta solvent and around 0.6 for polymers in good solvent (figure 1.3) [60]. A R_g/R_h ratio of 0.77 indicates a compact sphere, $R_g/R_h \gg 2$ indicates an rod and $1 < R_g/R_h < 2$ indicates random coil or branched macromolecule (figure 1.3) [61,62]. AF4 is a relatively new separation technique and is gaining interest in pharmaceutical industry for separation and characterization of protein based formulations. So far, there are relatively only a few examples of the use of AF4 for characterization of food proteins.The separation in AF4 takes place by a balance of hydrodynamic drag on particles and diffusivity (figure 1.4). In the normal mode of elution, small particles are eluted first and then the large particles elute later since they are retained more close to the membrane (figure 1.4) [60]. The advantages of AF4 over SEC are that in AF4 pre-filtration or centrifugation of samples is not required and the pressures in channel are low, so the soft nanoparticles are not deformed that much [60]. This helps in getting rid of artefacts typically observed in the analysis of high molar mass branched polymers [63]. When these high molar mass branched polymers were separated by SEC, an upturn in the conformation plot of M_w versus R_g was observed. It was speculated that this was due to poor separation of branched polymers in SEC resulting from trapping of side chains in bead pores. These artefacts were not observed when the samples were separated and analysed by AF4 [63]. In AF4, typically, a trapezoidal channel is used for maintaining a constant cross-flow rates across the membrane (figure 1.4). The AF4 is generally coupled to concentration detectors, such as UV and RI and a static light scattering detector (MALS) [60]. The M_w and R_g for each separated fraction are fitted from the measured concentration (UV or RI) and the intensities of the scattered light at various angles (figure 1.4d) using Rayleigh-Gans-Debye approximation [60]. The intensity of the scattered light is plotted against the angle of observation for a single or variable concentration of particles. To neglect the concentration dependence, extrapolation of the scattered light intensity to zero angle can be done at a fixed particle concentration and this procedure is called a Debye plot [60]. Various light scattering formalisms are employed to make Debye plots, such as Zimm, Debye, or Berry formalism [60]. For Rayleigh (isotropic) scatterers ($2R_g < \lambda/20$), all the formalisms provide similar fits. But for larger particles ($2R_g > \lambda/20$), there are deviations between the fits from various formalisms and appropriate models must be chosen for estimations of M_w and R_g. For example, the Berry formalism has been found to be very robust for particles with size in the range $\lambda > 2R_g > \lambda/20$ [64].

The fractal dimension, d_f, is estimated from the angular dependence of the scattered light intensity i.e. from the slope of the power law regime in the plot of particle scattering factor, $P(q)$ *versus* the scattering wave vector (q) normalized

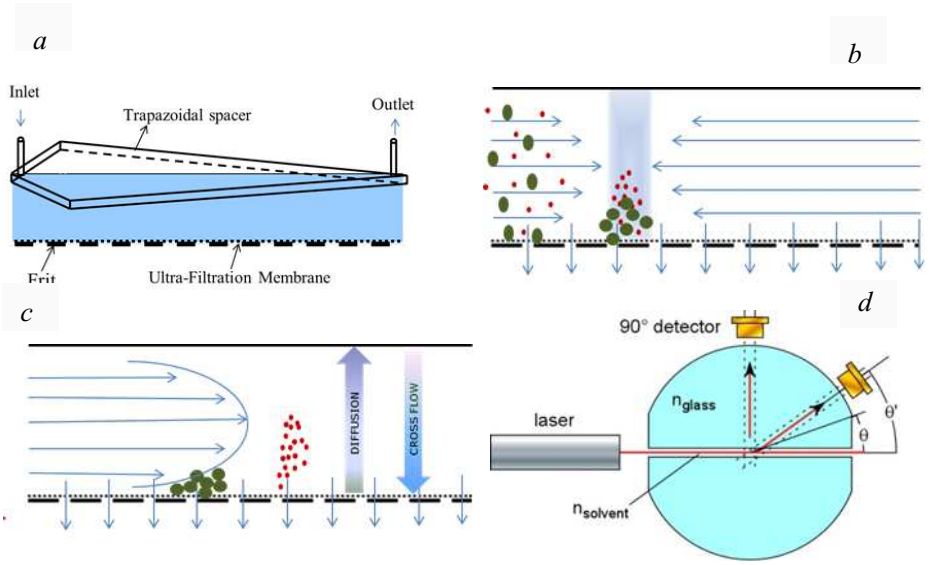

Figure 1.4: *Schematic of the AF4 flat channel flow cell (a). The first step in Af4 separation is the focusing of particles at the beginning of a channel (b), followed by elution where particles are separated based on hydrodynamic size (c). The in-line separated particles are then characterised by MALS (d). In (d), only two detectors are depicted but in reality there are 18 detectors surrounding the flow cell (picture taken from Google images).*

with R_g , i.e. $P(q) \sim (qR_g)^{-d_f}$ for $qR_g > 1$ [60, 61]. The true fractals are scale invariant and the structure is similar at large range of magnifications (self-similar). In food systems, typically the self-similarity is satisfied only for a certain range of length scales since these are stochastic fractals [65]. The scaling relations apply to both types of fractal structures. The number of primary particles within a secondary particle (N) have a scaling relation with the size of the secondary particle (R) and the size of the primary particles (r) as shown in figure 1.3, as given by $N = (R/r)^{d_f}$. There are two ways to obtain d_f ; one from high q as described above and the other from low q ($d_f = 1/\nu$). The low q data mainly reflects the nanoparticle structure at the dimensions $\sim R$, while high q data shows the zoomed in structure at the dimensions $\sim r$ (figure 1.3). These two numbers would be similar for a true fractal, however for a stochastic fractal particles these can vary.

Influence of conditions, substrate and enzymes on cross-linked structures

The physico-chemical conditions of the protein solutions such as temperature, ionic strength and pH have a huge effect on the products obtained after enzymatic cross-

linking. For example, the cross-linking of apo α-LA using HRP at 37 °C led to formation of more higher molar mass particles ($>$ 60 kDa, assessed from size exclusion chromatography, SEC) than that of 20°C for the same extent of cross-linking [39]. Moreover, the variation of ionic strength and pH was reported to be an important parameter to direct the molar mass distribution of protein particles [39]. For the same conversion of monomeric α-LA, almost two times more dimers of α-lactalbumin were formed at low ionic strength (0.1 mM ammonium acetate) than at high ionic strength (100 mM ammonium acetate) [39]. Similarly, approximately two times larger ($>$ 60 kDa) particles were formed at pH 5.9 than at pH 6.8 and ionic strengths of $0.1 - 10$ mM ammonium acetate, while there was no major difference at 100 mM ammonium acetate [39]. It was proven that dimerization of α-LA using HRP takes place between two tyrosine residues (Tyr18-Tyr50) [40]. It was speculated that formation of a di-tyrosine cross-link could lead to opening up of α-LA structure that would expose other tyrosine residues to water. However, involvement of all the four tyrosines of α-LA in cross-linking was not proved. Particles of R_h up to 25 nm were produced by sequential dosage of H_2O_2. Higher degrees of polymerization (DP) of apo α-LA can be achieved with HRP by employing a strategy of sequential dosage of H_2O_2 to prolong the active life-time of HRP [21, 22, 46]. The sequential H_2O_2 dosage methodology is also applied in this work to produce α-LA particles with high DP. The scaling exponent between R_h and M_w of 0.4 was found [46]. When this reaction was continued, two distinct phases were observed in the increase of R_h with time. This suggested that small particles formed initially were further cross-linked to form larger particles (two stage process).The mTG is one of the most researched enzymes for cross-linking globular proteins. It has been speculated that many Lys and Gln residues in a globular protein might be inaccessible to mTG despite being the fact that they are present on surface. It was suggested that glutamine residues in α-helices are difficult to be attacked by mTG [66]. Furthermore, the steric hindrance from adjacent side chains has been suggested to reduce the reactivity of target amino acids in native globular proteins [42]. A comparative study on cross-linking of α-LA with either guinea pig liver transglutaminase (gTG) or with mTG has revealed that the initial cross-linking rate was higher for gTG. However, on extensive reaction, mTG was found to form higher molar mass protein particles. These particles were analysed by SEC coupled to multi-angle light scattering (MALS) and a R_g to M_w scaling exponent was found to be around 0.31 for gTG and 0.44 for mTG. Hence, the structures obtained after enzymatic cross-linking are dependent on the solution conditions, substrate protein and the type of enzyme used. The enzymatic aspects are discussed next with a comparison of HRP and mTG (figure 1.5).

Horseradish peroxidase (HRP)

Horseradish peroxidase (HRP) is a heme (Fe^{3+}) containing glycoprotein of $M_w \pm 44$ kDa and has been widely studied in the past [67–71] (figure 1.5a). It contains two Ca^{2+} ions and the enzyme activity is known to be reduced by $\sim 25\%$ if one of them

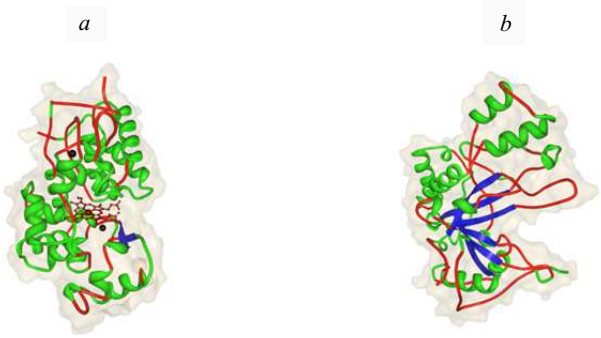

Figure 1.5: *Crystal structure of HRP (isozyme C, PDB accession code 1H58) depicting the heme centre and two calcium ions (black spheres) (a) and crystal structure of mTG (PDB accession code 1IU4) depicting the cleft at the active site (b).*

is removed [67]. There are at least seven known isozymes of HRP but they have the same catalytic mechanism. In presence of oxidizing substrates, such as hydrogen peroxide (H_2O_2), HRP can catalyze the oxidation of electron donors, such as phenolic moieties of tyrosine to form di-tyrosine covalent cross-links in proteins. The reaction involves different oxidation states of the enzyme and the reactions mechanisms are well reported [67]. It involves three distinct catalytic steps. First, HRP is oxidized by H_2O_2 leading to cleavage of H_2O_2 into water and incorporation of the oxygen atom into compound I (first HRP intermediate). The compound I contains an oxoferryl group ($Fe^{4+} = O$) and a porphyrin π-cation radical. Next, compound I oxidises the reducing substrate molecule by transfer of a single-electron. The discharge of π-cation radical leads to the formation of the compound II (second HRP intermediate, $Fe^{4+} = O$). Finally, the compound II is reduced back to the native form HRP (Fe^{3+}) by a second substrate molecule. The ferryl iron returns to its ferric state during this one-electron reduction and the oxygen accepts two protons to form a water molecule and is released from the heme. In summary, one mole of HRP in presence of one mole of H_2O_2 can generate two moles of free radicals (stoichiometrically equal to one covalent cross-link). The concentration of H_2O_2 and the enzyme exposure time are known to inactivate the enzyme through two different pathways i.e. one in presence and other in absence of donor substrate [72]. This inactivation caused by higher concentrations of H_2O_2 limits the extent of conversion and degree of cross-linking during the reaction. Hence, a strategy of sequential dosage of H_2O_2 was developed to prolong the active life-time of HRP [21,22,46]. HRP induced oxidation of tyrosine (Y), tyrosine containing peptides or proteins is known to lead to formation of the di-tyrosine (Y_2) [14,40,73–75]. In biological systems, oxidation with peroxidase results in Y_2, tri-tyrosine (Y_3) and tetra-tyrosine (Y_4) [40,54,55]. Two isomers of Y_2 and three isomers of Y_3 have been found so far in natural systems (figure 1.6). The Y_2 can be either a iso-Y_2 (3,O$'$) or a ortho-ortho-Y_2 (3,3$'$) [76,77]. The Y_3 can be iso-trityrosine, pulcherosine and ortho-trityrosine [21]. When low molar mass phenolic substrates are

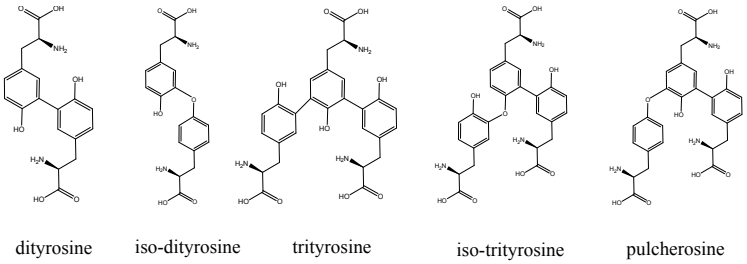

Figure 1.6: *Isomers of dityrosine and trityrosine.*

cross-linked with peroxidase, they polymerize to high molar mass. For example, cross-linking of L-tyrosine (Y) or N-acetyltyrosine with horseradish peroxidase (HRP) led to formation of high molar mass polymers [78]. Based on the reported molar mass of these polymers, the degree of polymerisation (DP) of Tyr can be estimated to be around 25. It is unknown if oligo-tyrosine cross-links could also be formed during extensive cross-linking of proteins with peroxidase.

Microbial transglutaminase (mTG)

Microbial transglutaminase (mTG) derived from *Streptoverticillium mobaraense* has a M_w of 37.86 kDa [79, 80]. The mTG is known to be active over a wide pH range between pH 4.0 and 9.0 but is most active between 6.0 and 7.0 [81–83]. The enzyme adopts a disk-like shape with a deep cleft at the edge of the disk, where a single cysteine residue (Cys-64) is located in the active site and is involved in the cross-linking mechanism [80] (figure 1.5b). MTG catalyses an acyl transfer reaction between γ-carboxyamide groups of glutamine residues (acyl donor) and the ϵ-amino groups of lysine residues (primary amino groups, acyl acceptor) (reaction-a in figure 1.7). This results in cross-linking of glutamine and lysine residues through $\epsilon - (\gamma$-glutamyl) lysine iso-peptide bond [84] (reaction-b in figure 1.7). There is a side reaction possible in the absence of an amine substrate [84]. When the reaction system does not contain free lysine residues or primary amines, water becomes the acceptor of acyl groups. This results in deamidation of the carboxyamide groups of glutamine residues and glutamic acid and ammonia are formed (reaction-c in figure 1.7) [81, 85]. A hypothetical catalytic mechanism of mTG was postulated [80], which is based on the ping pong mechanism of guinea pig liver TG proposed earlier [86], comprising the following steps. First, a glutamine substrate binds to catalytic cysteine residue in a binary complex as thioester. Next, ammonia is dissociated with the formation of an acyl enzyme intermediate. Finally, the acyl enzyme intermediate reacts with a second substrate i.e. an acyl acceptor (primary amine) to form a γ-glutamyl-amine product. The enzyme intermediate can also react with water to form glutamic acid. The enzyme looses its activity within a few minutes at 70 °C [82, 83].

Many studies on protein cross-linking with mTG show that cross-linking of Lys-

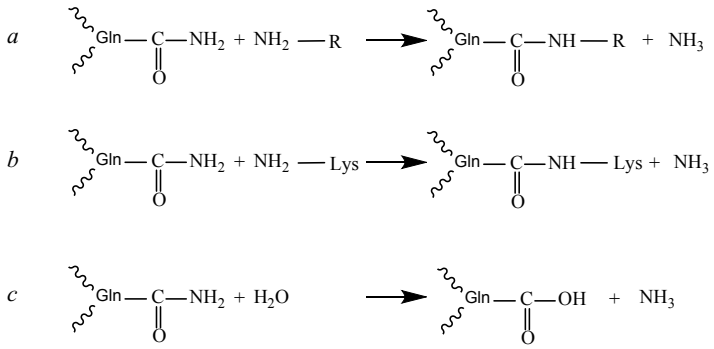

Figure 1.7: *Various reactions catalysed by mTG: (a) and (b) Acyl transfer and cross-linking reactions, respectively and (c) deamidation.*

Gln is most dominant reaction leading to formation of protein particles. Apparently, other side reactions that have been suggested e.g. deamidation do not take place when there are sufficient amount of proteins with accessible lysine residues. Compared to other types of TG, mTG has been reported to have little deamidation activity [87,88]. Deamidation reaction occurred only when the lysine residue was blocked. It was reported that mTG deamidated 7.7% of the Gln residue in citraconylated α_{s1}-casein (i.e. when the lysine residues were blocked) and there was no polymerization in this case, while almost all the intact α_{s1}-casein was polymerized (when lysine was not blocked) [87]. When the cross-linking of casein components (α_{s1}-, β- and κ-casein) using guinea pig liver TG was followed by trinitrobenzenesulfonate (TNBS) method, as well as by measurement of the ammonia released after reaction, the moles of lysines reacted were same as the moles of ammonia released per mole of the protein [56]. These studies indicate that deamidation will not occur as long as there are accessible free lysine residues in the protein.

Comparison of HRP with mTG

An important point regarding the action of HRP is that enzymatic action on substrate is limited only to the formation of a free radical. The collision of two such free radicals residues leads to formation of a cross-link between them and this second step is a non-enzymatic process. The difference between the action of mTG and HRP is that cross-link formation in the case of mTG takes place in the active site of the enzyme. So, the cross-linking step is a enzymatic process in the case of mTG as opposed to HRP. Moreover, mTG contains only one free sulfhydryl group and no di-sulfide bridges (table 1.2), so it can be used to cross-link globular proteins in presence of a reducing agent such as dithiothreitol (DTT). In the case of HRP, use of DTT might alter its structure and hence its activity. So, the structural modifications of the substrate globular proteins in the case of HRP has to be done by other methods. At present there is not much information available on various methods to make the structure

Table 1.2: *Molar mass (M_w), secondary sructure, free sulfhydryl, disulphide links, metal ions present and pI of α-LA, HRP and mTG.*

Protein	M_w (kDa)	Amino acids	Secondary structure (%)	Ligands and links	pI	Ref.
α-LA	14.18	123	α-Helix + 3_{10}Helix = 7 β-sheet = 3	S-S= 4 S-H= 0 Ca^{2+} = 1	4.6	www.uniprot.org (entry: P00711)
HRP	43.99	308	α-Helix + 3_{10}Helix = 13 β-sheet = 2	S-S = 4 S-H= 0 Ca^{2+} = 2 Fe^{3+} = 1 Glyc-osylation $\leq$ 20%	3.0-9.0 ($\geq$ 7 isozymes)	[67,69-70]
mTG	37.86	331	α-Helix + 3_{10}Helix = 11 β-sheet = 8	S-S = 0 S-H= 1	8.9	[80]

of the globular proteins more flexible for enzymatic cross-linking. One other option is pre-heat-shock of the substrate protein. In the case of α-LA, another option is to remove the bound calcium ion can be removed by chelating to make it more reactive. In this case, cross-linking of α-LA can be performed with mTG in the presence of a chelating agent, such as EDTA, since the enzyme does not contain any metal ions. But, the same cannot be done for HRP since it contains two bound calcium ions and EDTA would also remove them. So, in the case of HRP removal of metal ligands from the substrate protein would have to be done separately and then HRP must be introduced. The most important difference between the two enzymes is that they target different amino acid residues on the proteins. So, if the substrate protein contains different number of these target amino acids, probably different cross-linking densities (i.e. number of cross-links per particle) could be obtained by using these two enzymes. In this regard, apo form of bovine α-LA is an ideal substrate protein to be cross-linked by HRP and mTG and details of it are provided below.

α-Lactalbumin (α-LA)

α-LA is a calcium binding protein [89,90] (table 1.2). It is the second major whey protein in bovine milk [91]. It has widely been used as a model system for protein folding studies since it has a stable molten globule state [92]. A molten globule is folding intermediate of globular protein in between the native and denatured state [93]. Hence, a molten globule has a native-like secondary structure and a fluctuating tertiary structure [94]. Molten globule state of α-LA is observed under various conditions. For example, the acid-denatured state or as an equilibrium unfolding intermediate at a moderate concentration of guanidine hydrochloride or urea [92,93]. Removal of Ca^{2+}

ion also results in a partially unfolded state at pH $\sim$ 7 and low ionic strengths. The melting temperature of apo α-LA is 39 °C, while that of holo α-LA is 66 °C [95]. It has been suggested that the apo α-LA at low ionic strength and around melting temperatures has a conformation similar to a molten globule [93,96]. Apo α-LA has also been reported to be more sensitive to changes in pH and ionic strengths compared to the holo form and it shows a variety of conformational states [95]. A more flexible structure of apo α-LA at temperatures around 37 °C seems to be the reason for its high degree of polymerization by enzymatic cross-linking.

The bovine α-LA is a small globular protein of molar mass (M_w) around 14.2 kDa, hydrodynamic radius (R_h) = 1.88 − 2.5 nm [96] and radius of gyration (R_g) = 1.72 nm [97]. The hydrodynamic radii of holo form (+ Ca^{2+}), apo form (- Ca^{2+}), molten globule and unfolded α-LA are 1.88 nm, 1.91 nm, 2.0 nm and 2.5 nm, respectively. It has four tyrosine residues at position 18, 36, 50 and 103 in the amino acid sequence and these are the main targets of HRP (figure 1.8). These tyrosine residues are not equally solvent (water) exposed [98]. In the native state, only Tyr18 was found to be exposed, while Tyr 36 and Tyr50 also became exposed in molten globule state. Tyr103 did not become available even in molten globule state. The location of four tyrosine residues in the crystal structure of apo α-LA are roughly correlated with the solvent exposure measured with NMR. Hence, the position (exposure) in crystal structures can approximately indicate the reactivity of amino acid residues.The solvent exposure of these tyrosine moieties is very important since the cross-linking probability would be related to the accessibility of these groups. α-LA has six glutamines (positions: 2, 39, 43, 54, 65, 117) and 12 lysines (position: 5, 13, 16, 58, 62, 79, 93, 94, 98, 108, 114, 122) (figure 1.8a and 8b) [99,100] and these are the targets of mTG. All of the Lys and Gln residues are exposed to water molecules (figure 1.8b).

Functionality of protein particles: macroscale

Bulk rheology

Cross-linking of proteins can lead to a different rheological behavior [45], for example, an increase of viscosity or formation of a gel, which are often desired in food applications [2]. For protein solutions, this can be achieved by heat treatment or by enzymatic cross-linking of proteins [1, 5, 10]. The techno-functional properties such as gelation of whey proteins is usually achieved by heating them to produce protein particles of increasing size [5]. The gels made by heating are called heat-set protein gels [101]. In addition, gels can also be obtained by change of pH and ionic strength after cooling down to room temperature leading to cold-set gels [18]. Rheological properties of whey proteins were reported to be modified by heating them to make particles of various sizes and density [102]. A particle size of 50 nm led to 10 fold increase of solution shear viscosity (η). When the particle size was increased further to 63 nm, another 10 fold increase of η was found. However, a 33 % decrease of storage modulus ($G^{'}$) was also observed. This was attributed to the open structure of 63 nm

a

1 10 20
H–Glu–**Gln**–Leu–Thr–**Lys**–Cys–Glu–Val–Phe–Arg–Glu–Leu–**Lys**–Asp–Leu–**Lys**–Gly–**Tyr**–Gly–Gly–
21 30 40
Val–Ser–Leu–Pro–Glu–Trp–Val–Cys–Thr–Ala–Phe–His–Thr–Ser–Gly–**Tyr**–Aap–Thr–**Gln**–Ala–
41 50 60
Ile–Val–**Gln**–Asn–Asn–Asp–Ser–Thr–Glu–**Tyr**–Gly–Leu–Phe–**Gln**–Ile–Asn–Asn–**Lys**–Ile–Trp–
61 70 80
Cys–**Lys**–Asp–Asp–**Gln**–Asn–Pro–His–Ser–Ser–Asn–Ile–Cys–Asn–Ile–Ser–Cys–Asp–**Lys**–Phe–
81 90 100
Leu–Asp–Asp–Asp–Leu–Thr–Asp–Asp–Ile–Met–Cys–Val–**Lys**–**Lys**–Ile–Leu–Asp–**Lys**–Val–Gly–
101 110 120
Ile–Asn–**Tyr**–Trp–Leu–Ala–His–**Lys**–Ala–Leu–Cys–Ser–Glu–**Lys**–Leu–Asp–**Gln**–Trp–Leu–Cys–
123
Glu–**Lys**–Leu–OH

b

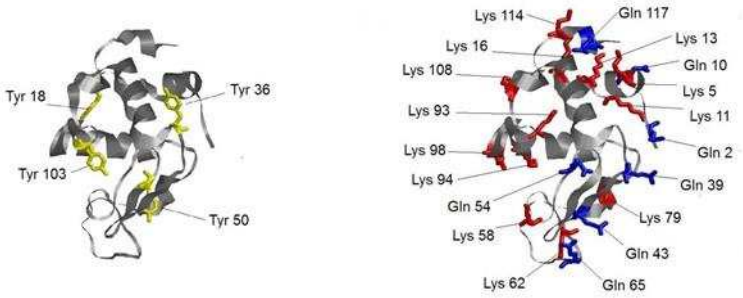

Figure 1.8: *Amino acid sequence of bovine α-LA [www. uniprot.org (entry: P00711)] (a). Crystal structure of α-LA with lysines, glutamines and tyrosines marked (PDB accession code 1F6R) (b).*

particles as compared to 50 nm and it was concluded that size and structure of protein particles affect the rheological properties. For cold-set gelation of whey proteins or ovalbumin, the gel microstructure was found not to depend on the characteristics of the particles [18]. But the small deformation properties of these protein gels were found to be influenced by the differences in shape and size of these particles. Hence, the rheological properties of the protein particles are believed to be correlated both to their size and structure. One approach used for studying heat-set or cold-set gels is to analyze rheological data using the scaling and fractal models. The dependence of storage modulus ($G^{'}$) on particle volume fraction (ϕ) in the case of heat-set or cold-set gelation of many proteins could be well described by scaling and fractal models [103,104]. Two distinct regimes (strong-link or weak-link) are considered based on the relative contribution of inter-particle or intra-particle interactions [103]. Wu and Morbidelli [104] further extended the model of Shih et al. [103] and developed a new scaling relation (equation 1.1 and equation 1.2) between $G^{'}$ and ϕ, which included an additional parameter α (see equation 1.2) i.e an effective microscopic elastic constant

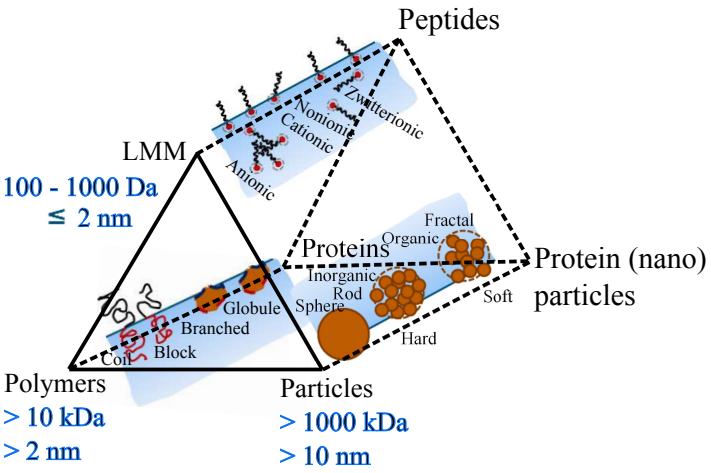

Figure 1.9: *Classification of monomeric protein, peptides and protein nanoparticles (polymers) based on size and mass in analogy with other types of surface active agents (surfactants; low molar mass (LMM), polymers and particles) generally used for stabilisation of interfaces.*

(equation 1.2). This parameter accounts for the elastic contributions of inter- and intra-particle links.

$$G^{'} \sim \phi^{\frac{\beta}{d-d_f}} \tag{1.1}$$

$$\beta = (d-2) + (2+x)(1-\alpha) \tag{1.2}$$

Where, d is the Euclidean dimension, d_f is the fractal dimension of the particle and x is the fractal dimension of the (gel) aggregate cluster backbone ($1 \leq x < d_f$). In the strong-link regime, $\alpha = 0$ and in the weak-link regime, $\alpha = 1$. The intermediate values of α indicate a transition regime. The scaling exponents in the fractal aggregation theory describe the strand structure as a function of secondary particle size and are related to the number of junctions/links per strand and the type of deformation mechanism of strand. The microscopic deformation of the strand structure could be bending or stretching. In this regard, the exponent, β has been used to differentiate the gel types based on the length and elastic constant of the stress carrying strands. The typical values of β observed for various regimes are; $\beta \geq 4$ for fractal strands, $\beta = 3$ for hinged strands, $\beta = 2$ for stretched strands and $\beta = 1$ for weak links [65]. For example, casein gels formed by slow acidification show $\beta = 3$, rennet casein gels exhibit $\beta = 2$ [65]. Values of $\beta \geq 4$ have also been observed in many heat-set protein gels [101, 105]. The rheological modifications at macro-scale are also described extensively for enzymatic cross-linking. It is hypothesized that in the case of enzymatic cross-linking, the size and meso-scale structure of the intermediate protein nanoparticles would determine their final macro-scale techno-functional properties.

Foaming properties

There are two aspects to foam. One is the foam-ability and the second is foam-stability. Surfactants are required for making and stabilizing foams. One of the main difference between various types of surfactants used for making foams is their size (figure 1.9). Depending on size, surfactants can generally be classified as low molar mass (LMM), polymeric or particles (figure 1.9). The foaming properties are very different for LMM surfactants, proteins and particles. Typically, foam-ability reduces, while foam-stability improves with increasing size. In other words, even though there are many types of surfactants, foaming properties of a LMM surfactant is never same as that of a protein, and that of a protein is never same as that of a particle. For foam-ability, the mass transport of monomeric protein or protein nanoparticles to the newly created interface is crucial. This is specially related to the type of method used for foaming. For example, diffusion is more important in sparging method than in whipping. In a diffusion controlled process, the translational diffusion coefficient (D) of proteins or protein particles is important, which depends on their size, i.e., $D = k_B T/6\pi\eta R_h$, where k_B is the Boltzmann constant, T and η are temperature and viscosity, respectively. Once the surfactant reaches the interface, the next step is to adsorb. However, the adsorption step can be of low affinity type or high affinity type (spontaneous adsorption). The reasons for low affinity can be certain repulsion e.g. electrostatic, steric or unfavorable contact of hydrophobic patch due to incorrect orientation. Once, a foam is generated its stability is determined by a combination of various hydrodynamic factors (drainage), gas diffusion (Ostwald ripening), thin film stability (DLVO type interactions [106]). Again, the size and electrostatic interactions become important for determining the film stability.

Foam-ability

With respect to foam-ability (expressed as volume of foam formed at the end of a foaming process), the differences between the surfactants of different molar masses or sizes arise from the dynamics of transport of these surfactants at an interface as well as their interaction with the interface and the inter-molecular interactions. In terms of mass transport, size mainly affects the diffusion rate (although in presence of convection e.g. in whipping, relative role of this is difficult to address). The diffusion rate determines the time a surfactant needs to adsorb at an interface (assuming adsorption to be high affinity type). Typically, a faster diffusion and a high affinity adsorption are considered to increase the foam-ability. In the other extreme, when mass transport is not limiting (e.g. in presence of significant convection and high concentrations), the foam-ability is governed by adsorption, which in turn is determined by adsorption energies (high or low affinity). Consequently, the foam-ability is not only influenced by the type of surfactant, but also by the concentration and the foaming method. In the sparging method, the time scale of bubble surface generation and time scale of surfactant transport and adsorption will determine its stability.The larger surfactants diffuse slower to the interface. If transport is slow then adsorption

may be negligible at low surface ages even in high affinity case and the surface tension is that of the pure solvent. This results in unstable bubbles and they collapse (low foam-ability).The next step to diffusion is the adsorption of these surfactants at interface. This step can be limiting in case of low affinity adsorption. The low affinity can arise from electrostatic repulsion. If the protein/nanoparticle is charged i.e. pH $>$ pI or pH $<$ pI, an electrostatic surface potential will be present and influence the further adsorption of monomers. The high affinity can arise from increased surface hydrophobicity. An example of changing the adsorption affinities is chemical modifications on native proteins such as succinylation or caprylation to either increase the net charge or to increase the surface hydrophobicity, respectively [107, 108]. In the whipping method, the foam is made by first the formation of large bubbles and secondly breaking these down into smaller bubbles. Deformation will cause a large stress gradient over the bubble surface that overcomes the internal pressure gradient and the bubble will break up. Depending on the magnitude of hydrodynamic stresses, surfactant adsorption kinetics and their stabilization mechanism, the following stages could occur during whipping; 1) Shear or longitudinal stresses lead to bubble breakup into smaller sizes, 2) Mass transport and adsorption of the surfactant at the newly created interfacial area, 3) The bubbles colloid with other bubbles, stable bubbles repel each other, while unstable bubbles coalesce back to bigger bubble. The main differences between the two types of foaming methods are; 1) Residence time of bubbles in the solution, and 2) Secondary break-up of large bubbles in to smaller ones. In whipping method, the bubble residence times are as long as the energy input continues and the process invovles secondary bubble break-ups. In sparging method, the bubble residence times are determined by the size of the bubbles generated and the depth of the liquid pool. Moreover, secondary break-ups are rare in the bulk under the laminar flow conditions. So, in a sparging test, we can expect larger drop size in the case of protein nanoparticles as compared to the monomeric protein since the nanoparticles cannot reduce the air-water interfacial tension as fast as monomeric protein at similar weight concentrations (in the case when size dominates over the adsorption affinities).

Foam-stability

Particles, when used as surfactant, are known to produce very stable foams [9, 109–114]. For example, the bubbles covered with hard colloidal particles are stable against disproportionation for days to weeks. In contrast, bubbles stabilized by proteins or low molar mass (weight averaged molar mass, $M_w < 1$ kDa) surfactants collapse within few minutes or hours [115]. This phenomena of enhanced stablisation of interfaces by particles is also referred as Pickering-Ramsden type stablisation [116] or in the case of foams, simply a Pickering foam. The high stability of the foams stabilized by inorganic or organic particles (10 nm $< R_h <$ 100μm), in comparison to foams stabilized by native proteins (2 nm $< R_h <$ 10 nm), is often attributed to their size. The foam stabilised by hard particles (table 1.3) is more stable than that of monomeric proteins or soft heat-induced protein particles. This is usually explained

based on the large desorption energies required for the particles once adsorbed at the interface as given by, $W = \pi R^2 \gamma \left(1 \pm cos\theta\right)^2$, where, W is adsorption energy, R is the particle radius, γ is the interfacial tension and θ is the contact angle made by the particle at the interface [109]. It is usually argued that for colloidal particle stabilized foams, the disproportionation or Ostwald ripening can be completely stopped if the condition, $E > \gamma/2$, where E is the surface elastic modulus and γ is the surface tension is satisfied [109]. So, the enhanced stability of hard particle stabilized foam can be hypothesized to be either due to strongly adsorbed particles at the interface which cannot be easily displaced or due to thicker foam films. In the case of protein particles, especially if they are soft and of nano-size, the wetting properties e.g. the contact angle may not be important. A more important parameter for protein nanoparticles might be their softness, which can be varied by changing the cross-linking density in the case of enzymatic cross-linking. The instability of a foam starts with drainage, which brings the bubbles closer. Most of the early stage drainage takes place through Plateau border and the node, and only in later stages the film contributions become significant. A reduction in initial stage drainage implies blockage of Plateau border, which can be due to accumulation of particles. The drainage is inversely related to the bulk viscosity and can be slowed down by increasing it. Also the disjoining pressure and the film thickness are important. There is a large effect of ionic strength on the foam stability. This can be explained based on the disjoining pressure arguments based on DLVO theory [106]. Adsorption of charged proteins establishes a surface potential at the air-liquid interface, which is balanced by the diffuse double layer (Debye length) extending into the bulk film. The double layers of opposing interfaces repel each other in a thinning film resulting in a repulsive potential, which stabilizes the film. The range and the magnitude of the double layer repulsion decrease with increasing ionic strength. The increased ionic strength compresses or shrinks the Debye length; hence the range of electrostatic potential becomes shorter as predicted by the Poisson-Boltzmann and Debye-Hückel equations [106]. The total interaction energy is given by the sum of the electrical double layer repulsion, the attractive van der Waals interactions, and the steric forces. The combination of the van der Waals attraction and the repulsive potentials can lead to stability or instability depending upon the separation of gas bubbles and on the ionic strength.

In the case of protein particles, sometimes an enhanced foam stability is observed, whereas in other cases the aggregates seem to act as destabilisers (table 1.3). The foam stability of protein particles is never as high as inorganic or organic particle stabilized Pickering foams (table 1.3). It is interesting to note that the heat-induced protein particles of $R_h > 100$ nm by themselves are not able to produce foams with enhanced stability (table 1.3). Generally, the relation between mesoscale structure and functionality (e.g. Pickering stabilisation is explained only based on size and contact angle, but the structural details of particle are not considered). It can be hypothesized that, for open/weakly cross-linked protein nanoparticles, the adsorption would be similar to the flexible polymer, with some fraction of protein nanoparticles in contact with the interface. The remaining nanoparticle fraction (layer) in the aqueous phase may enhance stabilization. The adsorption of compact/highly cross-

Table 1.3: *Examples of Pickering foam stabilization with different types of particles.*

Particle	R_h	Mesoscale structure	Foaming method	C (%,w/v)	Foamability	$t_{0.5}$	Ref.
Silica (coated with CTAB)	7.5 ±1 nm	-	Hand-shaking	1	Silica + CTAB > Silica	> 30 days	[108]
zirconium phosphate (exfoliated by propylamine)	261 ±36 to 1142 ±305 nm	Nano-sheet: aspect ratio = 97 ± 13 to 426 ±114	Hand-shaking	2	Increases with nano-sheet concentration and aspect ratio	> 30 days	[109]
Ethyl cellulose	50-100 nm	-	Hand-shaking, Low shear and high shear whipping	2	Low in absence of surface active component	$\gg$ 30 days	[110]
Hydrophobin (class II)	-	-	Low shear whipping (aero-latte)	0.1	-	> 5 days	[111]
β-LG aggregates (made by heating)	35-197 nm	Fractal ($d_f = 2 \pm 0.2$)	Sparging	0.1	Aggregates < Native	[Aggregates < Native]; [Aggregates (35, 71 nm)+ Native > Native]; [Aggregates (117, 197 nm) + Native < Native]	[112]
Whey protein aggregates (made by heating)	Soluble: 6193 nm Insoluble: 660μm	Insoluble: highly branched and very cohesive	Sparging	2	Aggregates < Native	Native: 145 ±4.5 s Aggregates: 77 ±10 s	[113]
Whey protein aggregates (made by heating)	Soluble: $\sim$ 200 nm Insoluble: > 1μm	-	Whipping	2	Aggregates $\approx$ Native	Native: 360 ±55 s Aggregates: 590 ± 75 s to 1410 ± 130 s	[4]

linked protein nanoparticles may be similar to the hard colloidal particle (Pickering-Ramsden stabilization) [117,118]. The adsorbed state of protein nanoparticles would depend on the surface charge density and the exposed hydrophobicity. The contact angles may not be very important in the case of nanoparticles as compared to micron sized particles where it determines the capillary interactions [119]. Hence, mainly the size, structure, hydrophobicity and charge aspects are important in studying the foaming properties of monomeric protein and protein nanoparticles.

Aim of the thesis

The aim of this thesis is to understand the functionality of enzymatically cross-linked protein at macroscale by linking it to the physico-chemical properties of the protein nanoparticles at mesoscale.

Approach and outline of the thesis

A range of enzymatically cross-linked protein particles that vary in size and structure are required to understand the macroscale functionality of enzymatically cross-linked poteins. To achieve this, different protein particles were produced by cross-linking the same protein using two different enzymes.The two enzymes were selected to target different amino acid residues on same protein and obtain nanoparticles with different structures. The bulk rheology and foaming properties of these different types of nanoparticles can then be compared with that of monomeric protein. The approach used in this thesis is to make α-LA nanoparticles by cross-linking them with HRP and mTG and study their formation process, mesoscale structure and functionality. The objective is to develop a set of tool-box for meso-scale structure characterisation (physical and chemical) at different length scales and in the end to link mesoscale properties to macroscale functionality. To this end, the research conducted for this thesis is outlined as follows. The characterisation of mesoscale structures that are formed during cross-linking of α-LA with HRP are presented in chapter 2 followed by characterisation of chemical details in chapter 3 such as the identification of amino acids involved in the cross-links and length of these covalent cross-links. Chapter 4 describes the mesoscale structure of α-LA cross-linked with mTG and its comparison with that of HRP system. The differences between the bulk rheological properties of the α-LA nanoparticles made with either HRP or with mTG are given in chapter 5. This chapter compares their bulk rheological properties such as storage modulus and shear viscosity as a function of nanoparticle concentration. The foaming properties of these two types of α-LA nanoparticles are described in chapter 6. The foams were generated by whipping and sparging method and nanoparticles were foamed at different ionic strengths. Finally, the general outcomes of this thesis and their comparison with other systems in literature are summarised in chapter 7 (general discussion). General discussion is followed by summary in english and dutch at the end of the thesis.

Bibliography

[1] E. A. Foegeding and J. P. Davis. Food protein functionality: A comprehensive approach. *Food Hydrocolloid*, 25(8):1853–1864, 2011.

[2] S. Banerjee and S. Bhattacharya. Food gels: Gelling process and new applications. *Crit. Rev. Food Sci. Nutr.*, 52(4):334–346, 2011.

[3] P. J. Hailing and P. Walstra. Protein-stabilized foams and emulsions. *CRC Crit. Rev. Food Sci. Nutr.*, 15(2):155–203, 1981.

[4] G. Matheis and J. R. Whitaker. A review: Enzymatic cross-linking of proteins applicable to foods. *J. Food Biochem.*, 11(4):309–327, 1987.

[5] T. Nicolai and D. Durand. Controlled food protein aggregation for new functionality. *Curr. Opin. Colloid Interface Sci.*, 18(4):249–256, 2013.

[6] J. Yguerabide and Yguerabide. E. E. Light-scattering submicroscopic particles as highly fluorescent analogs and their use as tracer labels in clinical and biological applications: I. Theory. *Anal. Biochem.*, 262(2):137–156, 1998.

[7] E. Dickinson. Food emulsions and foams: Stabilization by particles. *Curr. Opin. Colloid Interface Sci.*, 15(1–2):40–49, 2010.

[8] B. S. Murray and R. Ettelaie. Foam stability: Proteins and nanoparticles. *Curr. Opin. Colloid Interface Sci.*, 9(5):314–320, 2004.

[9] I. Nicorescu, A. Riaublanc, C. Loisel, C. Vial, G. Djelveh, G. Cuvelier, and J. Legrand. Impact of protein self-assemblages on foam properties. *Food Res. Int.*, 42(10):1434–1445, 2009.

[10] J. Buchert, D. E. Cura, H. Ma, C. Gasparetti, E. Monogioudi, G. Faccio, M. Mattinen, H. Boer, R. Partanen, E. Selinheimo, R. Lantto, and K. Kruus. Crosslinking food proteins for improved functionality. *Annu. Rev. Food Sci. Technol.*, 1:113–138, 2010.

[11] T. Heck, G. Faccio, M. Richter, and L. Thöny-Meyer. Enzyme-catalyzed protein crosslinking. *Appl. Microbiol. Biotechnol.*, 97(2):461–475, 2013.

[12] S. S. Wong and L-J C. Wong. Chemical crosslinking and the stabilization of proteins and enzymes. *Enzyme Microb. Tech.*, 14(11):866–874, 1992.

[13] R. Aboumahmoud and P. Savello. Cross-linking of whey-protein by transglutaminase. *J. Dairy Sci.*, 73(2):256–263, 1990.

[14] R. Aeschbach, R. Amado, and H. Neukom. Formation of dityrosine cross-links in proteins by oxidation of tyrosine residues. *Biochim. Biophys. Acta - Protein Structure*, 439(2):292–301, 1976.

[15] S. N. Anuradha and V. Prakash. Altering functional attributes of proteins through cross linking by transglutaminase - a case study with whey and seed proteins. *Food Res. Int.*, 42(9):1259–1265, 2009.

[16] M. Vert, Y. Doi, K. H. Hellwich, M. Hess, P. Hodge, P. Kubisa, M. Rinaudo, and F. Schué. Terminology for biorelated polymers and applications (IUPAC recommendations 2012). *Pure Appl. Chem.*, 84(2):377–410, 2012.

[17] T. Nicolai, M. Britten, and C. Schmitt. β-Lactoglobulin and WPI aggregates: Formation, structure and applications. *Food Hydrocolloid*, 25(8):1945–1962, 2011.

[18] A. C. Alting, M. Weijers, E. H. A. De Hoog, A. M. Van De Pijpekamp, M. A. Cohen Stuart, R. J. Hamer, C. G. De Kruif, and R. W. Visschers. Acid-induced cold gelation of globular proteins: Effects of protein aggregate characteristics and disulfide bonding on rheological properties. *J. Agric. Food Chem.*, 52(3):623–631, 2004.

[19] M. Fargemand, J. Otte, and K. B. Qvist. Cross-linking of whey proteins by enzymatic oxidation. *J. Agric. Food Chem.*, 46(4):1326–1333, 1998.

[20] Y. Saricay. *New insight into enzymatic cross-linking of globular proteins: from nanostructure to functionality*. PhD thesis, Wageningen University, Wageningen, The Netherlands, 2014.

[21] G. Oudgenoeg. *Peroxidase Catalyzed Conjugation of Peptides, Proteins and Polysaccharides Via Endogenous and Exogenous Phenols*. PhD thesis, Wageningen University, Wageningen, The Netherlands, 2004.

[22] W. H. Heijnis. *Peroxidase-mediated cross-linking of bovine α-lactalbumin*. PhD thesis, Wageningen University, Wageningen, The Netherlands, 2010.

[23] V. D. Truong, D. A. Clare, G. L. Catignani, and H. E. Swaisgood. Cross-linking and rheological changes of whey proteins treated with microbial transglutaminase. *J. Agric. Food Chem.*, 52(5):1170–1176, 2004.

[24] C. P. Wilcox and H. E. Swaisgood. Modification of the rheological properties of whey protein isolate through the use of an immobilized microbial transglutaminase. *J. Agric. Food Chem.*, 50(20):5546–5551, 2002.

[25] W. Wang, Q. Zhong, and Z. Hu. Nanoscale understanding of thermal aggregation of whey protein pretreated by transglutaminase. *J. Agric. Food Chem.*, 61(2):435–446, 2012.

[26] R. Sharma, M. Zakora, and K. B. Qvist. Characteristics of oil-water emulsions stabilised by an industrial α-lactalbumin concentrate, cross-linked before and after emulsification, by a microbial transglutaminase. *Food Chem.*, 79(4):493–500, 2002.

[27] S. X. Liu, J-T. Kim, S. Kim, and M. Singh. The effect of polymer surface modification via interfacial polymerization on polymer-protein interaction. *J. Appl. Polym. Sci.*, 112(3):1704–1715, 2009.

[28] Y. Matsumura, D. S. Lee, and T. Mori. Molecular weight distributions of α-lactalbumin polymers formed by mammalian and microbial transglutaminases. *Food Hydrocolloid*, 14(1):49–59, 2000.

[29] S. Damodaran and K. K. Agyare. Effect of microbial transglutaminase treatment on thermal stability and pH-solubility of heat-shocked whey protein isolate. *Food Hydrocolloid*, 30(1):12–18, 2013.

[30] M. A. Stahmann, A. K. Spencer, and G. R. Honold. Cross linking of proteins in vitro by peroxidase. *Biopolymers*, 16(6):1307–1318, 1977.

[31] C. R. Thalmann and T. Lötzbeyer. Enzymatic cross-linking of proteins with tyrosinase. *Eur. Food Res. Technol.*, 214(4):276–281, 2002.

[32] P. J. Coussons, N. C. Price, S. M. Kelly, B. Smith, and L. Sawyer. Transglutaminase catalyzes the modification of glutamine side-chains in the c-terminal region of bovine beta-lactoglobulin. *Biochemical Journal*, 283:803–806, 1992.

[33] F. Fenaille, V. Parisod, J. Vuichoud, J-C Tabet, and P. A. Guy. Quantitative determination of dityrosine in milk powders by liquid chromatography coupled to tandem mass spectrometry using isotope dilution. *J. Chromatogr. A*, 1052(1–2):77–84, 2004.

[34] M. Griffin, J. Wilson, and L. Lorand. High-pressure liquid-chromatographic procedure for the determination of epsilon-(gamma-glutamyl)lysine in proteins. *Anal. Biochem.*, 124(2):406–413, 1982.

[35] C. Y. Gan, A. A. Latiff, L. H. Cheng, and A. M. Easa. Gelling of microbial transglutaminase cross-linked soy protein in the presence of ribose and sucrose. *Food Res. Int.*, 42(10):1373–1380, 2009.

[36] C. Gauche, P. L. M. Barreto, and M. T. Bordignon-Luiz. Effect of thermal treatment on whey protein polymerization by transglutaminase: Implications for functionality in processed dairy foods. *LWT-Food Sci. Technol.*, 43(2):214–219, 2010.

[37] C. V. L. Giosafatto, N. M. Rigby, N. Wellner, M. Ridout, F. Husband, and A. R. Mackie. Microbial transglutaminase-mediated modification of ovalbumin. *Food Hydrocolloid*, 26(1):7–7, 2012.

[38] E. Ibanoglu and S. Ibanoglu. Foaming behaviour of EDTA-treated α-lactalbumin. *Food Chem.*, 66(4):477–481, 1999.

[39] W. H. Heijnis, P. A. Wierenga, W. J. H. van Berkel, and H. Gruppen. Directing the oligomer size distribution of peroxidase-mediated cross-linked bovine α-lactalbumin. *J. Agric. Food Chem.*, 58(9):5692–5697, 2010.

[40] W. H. Heijnis, H. L. Dekker, L. J. de Koning, P. A. Wierenga, A. H. Westphal, C. G. de Koster, H. Gruppen, and W. J. H. van Berkel. Identification of the peroxidase-generated intermolecular dityrosine cross-link in bovine α-lactalbumin. *J. Agric. Food Chem.*, 59(1):444–449, 2010.

[41] W. H. Heijnis, P. A. Wierenga, A. E. M. Janssen, W. J. H. van Berkel, and H. Gruppen. In-line quantification of peroxidase-catalyzed cross-linking of α-lactalbumin in a microreactor. *Chem. Eng. J.*, 157(1):189–193, 2010.

[42] Y. Matsumura, Y. Chanyongvorakul, Y. Kumazawa, T Ohtsuka, and T. Mori. Enhanced susceptibility to transglutaminase reaction of α-lactalbumin in the molten globule state. *Biochim. Biophys. Acta - Protein Structure and Molecular Enzymology*, 1292(1):69–76, 1996.

[43] Y. Matsumura, D-S Lee, and T Mori. Molecular weight distributions of α-lactalbumin polymers formed by mammalian and microbial transglutaminases. *Food Hydrocolloid*, 14(1):49–59, 2000.

[44] W. F. Nieuwenhuizen, H. L. Dekker, L. J. de Koning, T. Groneveld, C. G. de Koster, and G. A. H. de Jong. Modification of glutamine and lysine residues in holo and apo α-lactalbumin with microbial transglutaminase. *J. Agric. Food Chem.*, 51(24):7132–7139, 2003.

[45] Y. Saricay, S. K. Dhayal, P. A. Wierenga, and R. de Vries. Protein cluster formation during enzymatic cross-linking of globular proteins. *Farad. Discuss.*, 158(1):51–63, 2012.

[46] Y. Saricay, P. A. Wierenga, and R. de Vries. Nanostructure development during peroxidase catalysed cross-linking of α-lactalbumin. *Food Hydrocolloid*, 33(2):280–288, 2013.

[47] W. F. Nieuwenhuizen, H. L. Dekker, T. Gróneveld, C. G. de Koster, and G. A. H. de Jong. Transglutaminase-mediated modification of glutamine and lysine residues in native bovine β-lactoglobulin. *Biotechnology and Bioengineering*, 85(3):248–258, 2004.

[48] A. Moro, G. D. Baez, G. A. Ballerini, P. A. Busti, and N. J. Delorenzi. Emulsifying and foaming properties of β-lactoglobulin modified by heat treatment. *Food Res. Int.*, 51(1):1–7, 2013.

[49] B. Hiller and P. C. Lorenzen. Functional properties of milk proteins as affected by enzymatic oligomerisation. *Food Res. Int.*, 42(8):899–908, 2009.

[50] P. Aymard, D. Durand, T. Nicolai, and J. C. Gimel. Fractality of globular protein aggregates: From the molecular to the microscopic level. *Fractals*, 05(supp02):23–43, 1997.

[51] T. Michon, W. Wang, E. Ferrasson, and J. Guéguen. Wheat prolamine crosslinking through dityrosine formation catalyzed by peroxidases: Improvement in the modification of a poorly accessible substrate by indirect catalysis. *Biotechnol. Bioeng.*, 63(4):449–458, 1999.

[52] S. O. Andersen. The cross-links in resilin identified as dityrosine and trityrosine. *Biochim. Biophys. Acta- General Subjects*, 93(1):213–215, 1964.

[53] T. DiMarco and C. Giulivi. Current analytical methods for the detection of dityrosine, a biomarker of oxidative stress in biological samples. *Mass Spectrom. Rev.*, 26(1):108–120, 2007.

[54] D. Fujimoto, K. Horiuchi, and M. Hirama. Isotrityrosine, a new crosslinking amino acid isolated from ascaris cuticle collagen. *Biochem. Biophys. Res. Commun.*, 99(2):637–643, 1981.

[55] L.V. Lopez-Llorca and S.C. Fry. Dityrosine, trityrosine and tetratyrosine, potential cross-links in structural proteins of plant-parasitic nematodes. *Nematologica*, 35(2):165–179, 1989.

[56] F.-X. Schmid. *Biological Macromolecules: UV-visible Spectrophotometry*. John Wiley & Sons,, 2001.

[57] C. Dinnella, M. T. Gargaro, R. Rossano, and E. Monteleone. Spectrophotometric assay using o-phtaldialdehyde for the determination of transglutaminase activity on casein. *Food Chem.*, 78(3):363–368, 2002.

[58] J. Flanagan and R. J. FitzGerald. Characterisation and quantification of the reaction(s) catalysed by transglutaminase using the o-phthaldialdehyde reagent. *Food-Nahrung*, 47(3):207–212, 2003.

[59] L. O. Narhi, J. Schmit, K. Bechtold-Peters, and D. Sharma. Classification of protein aggregates. *J. Pharm. Sci.*, 101(2):493–498, 2012.

[60] S. Podzimek. *Light scattering, size exclusion chromatography and asymmetric flow field flow fractionation*. John Wiley & Sons, Hoboken, NJ, USA, 2011.

[61] W. Burchard. *Light scattering in Physical techniques for the study of food biopolymers*. S.B. Ross-Murphy (Ed.), Blackie, Glasgow/London, UK, 1994.

[62] L. Nilsson. Separation and characterization of food macromolecules using field-flow fractionation: A review. *Food Hydrocolloid*, 30(1):1–11, 2013.

[63] T. Otte, H. Pasch, T. Macko, R. Brúll, F. J. Stadler, J. Kaschta, F. Becker, and M. Buback. Characterization of branched ultrahigh molar mass polymers by asymmetrical flow field-flow fractionation and size exclusion chromatography. *J. Chromatogr. A*, 1218(27):4257–4267, 2011.

[64] M. Andersson, B. Wittgren, and K. G. Wahlund. Accuracy in multiangle light scattering measurements for molar mass and radius estimations. model calculations and experiments. *Anal. Chem.*, 75(16):4279–4291, 2003.

[65] P. Walstra. *Physical Chemistry of Foods*. Marcel Dekker, NY, USA, 2002.

[66] P. J. Coussons, S. M. Kelly, N. C. Price, C. M. Johnson, B. Smith, and L. Sawyer. Selective modification by transglutaminase of a glutamine side-chain in the hinge region of the histidine-388 glutamine mutant of yeast phosphoglycerate kinase. *Biochem. J.*, 273:73–78, 1991.

[67] A. M. Azevedo, V. C. Martins, D. M. F. Prazeres, V. Vojinovic, J. M. S. Cabral, L. P. Fonseca, and M. R. El-Gewely. *Horseradish peroxidase: A valuable tool in biotechnology*, volume 9. Elsevier, 2003.

[68] M. Gajhede, D. J. Schuller, A. Henriksen, A. T. Smith, and T. L. Poulos. Crystal structure of horseradish peroxidase c at 2.15 angstrom resolution. *Nat. Struct. Mol. Biol.*, 4(12):1032–1038, 1997.

[69] L. M. Shannon, E. Kay, and J. Y. Lew. Peroxidase isozymes from horseradish roots. i. Isolation and physical properties. *J. Biol. Chem.*, 241(9):2166–2172, 1966.

[70] N. C. Veitch. Horseradish peroxidase: A modern view of a classic enzyme. *Phytochem.*, 65(3):249–259, 2004.

[71] K. G. Welinder. Amino acid sequence studies of horseradish peroxidase. *FEBS J.*, 96(3):483–502, 1979.

[72] J. Hernandez-Ruiz, M. B. Arnao, A. N. Hiner, F. Garcia-Novas, and M. Acosta. Catalase like activity of horseradish peroxidase: Relationship to enzyme inactivation by H2O2. *Biochem. J.*, 354(3):107–114, 2001.

[73] T. Michon, M. Chenu, N. Kellershon, M. Desmadril, and J. Gueguen. Horseradish peroxidase oxidation of tyrosine-containing peptides and their subsequent polymerization: A kinetic study. *Biochemistry*, 36(28):8504–8513, 1997.

[74] K. Minamihata, M. Goto, and N. Kamiya. Site-specific protein cross-linking by peroxidase-catalyzed activation of a tyrosine-containing peptide tag. *Bioconjugate Chem.*, 22(1):74–81, 2010.

[75] C. Steffensen, M-L. Mattinen, H. Andersen, K. Kruus, J. Buchert, and J. Nielsen. Cross-linking of tyrosine-containing peptides by hydrogen peroxide-activated Coprinus cinereus peroxidase. *Eur. Food Res. Technol.*, 227(1):57–67, 2008.

[76] G. Oudgenoeg, E. Dirksen, S. Ingemann, R. Hilhorst, H. Gruppen, C. G. Boeriu, S. R. Piersma, W. J. H. Van Berkel, C. Laane, and A. G. J. Voragen. Horseradish peroxidase-catalyzed oligomerization of ferulic acid on a template of a tyrosine-containing tripeptide. *J. Biol. Chem.*, 277(24):21332–21340, 2002.

[77] G. Oudgenoeg, R. Hilhorst, S. R. Piersma, C. G. Boeriu, H. Gruppen, M. Hessing, A. G. J. Voragen, and C. Laane. Peroxidase-mediated cross-linking of a tyrosine-containing peptide with ferulic acid. *J. Agric. Food Chem.*, 49(5):2503–2510, 2001.

[78] T. Fukuoka, Y. Tachibana, H. Tonami, H. Uyama, and S. Kobayashi. Enzymatic polymerization of tyrosine derivatives. peroxidase- and protease-catalyzed synthesis of poly-tyrosines with different structures. *Biomacromolecules*, 3(4):768–774, 2002.

[79] T. Kanaji, H. Ozaki, T. Takao, H. Kawajiri, H. Ide, M. Motoki, and Y. Shimonishi. Primary structure of microbial transglutaminase from Streptoverticillium sp. strain-s-8112. *J. Biol. Chem.*, 268(16):11565–11572, 1993.

[80] T. Kashiwagi, K. Yokoyama, K. Ishikawa, K. Ono, D. Ejima, H. Matsui, and E. Suzuki. Crystal structure of microbial transglutaminase from Streptoverticillium mobaraense. *J. Biol. Chem.*, 277(46):44252–44260, 2002.

[81] H. Ando, M. Adachi, K. Umeda, A. Matsuura, M. Nonaka, R. Uchio, H. Tanaka, and M. Motoki. Purification and characteristics of a novel transglutaminase derived from microorganisms. *Agric. Biol. Chem.*, 53(10):2613–2617, 1989.

[82] K. Seguro, N. Nio, and M. Motoki. Some characteristics of a microbial protein cross-linking enzyme: Transglutaminase. *ACS SYM SER*, 650:271–280, 1996.

[83] K. Yokoyama, N. Nio, and Y. Kikuchi. Properties and applications of microbial transglutaminase. *Appl. Microbiol. Biotechnol.*, 64(4):447–454, 2004.

[84] J. E. Folk. Mechanism and basis for specificity of transglutaminase-catalyzed epsilon-gamma-glutamyl lysine bond formation. *Adv Enzymol Relat Areas Mol Biol*, 54:1–56, 1983.

[85] G. A. H. DE Jong and S. J. Koppelman. Transglutaminase catalyzed reactions: Impact on food applications. *J. Food Sci.*, 67(8):2798–2806, 2002.

[86] J. E. Folk and P. W. Cole. Mechanism of action of guinea pig liver transglutaminase .i. purification and properties of enzyme - identification of a functional cysteine essential for activity. *J. Biol. Chem.*, 241(23):5518–5525, 1966.

[87] S. Kumar. Spectroscopy of organic compounds. *Cosmic Rays*, 10:4, 2006.

[88] T. Ohtsuka, Y. Umezawa, N. Nio, and K. Kubota. Comparison of deamidation activity of transglutaminases. *J. Food Sci.*, 66(1):25–29, 2001.

[89] P. J. Anderson, C. L. Brooks, and L. J. Berliner. Functional identification of calcium binding residues in bovine α-Lactalbumin. *Biochemistry*, 36(39):11648–11654, 1997.

[90] Y. Hiraoka, T. Segawa, K. Kuwajima, S. Sugai, and N. Murai. α-lactalbumin: a calcium metalloprotein. *Biochem. Biophys. Res. Commun.*, 95(3):1098–1104, 1980.

[91] G. Mukhopadhyay, J. Khanam, A. Nanda, and A. Sarkar. Quantitative Characterization of Bovine Serum Albumin, α-lactalbumin and β-lactoglobulin in commercial whey sample by RP-LC. *Chromatographia*, 71(7):699–702, 2010.

[92] K. K. Kuwajima. The molten globule state of α-lactalbumin. *The FASEB Journal*, 10(1):102–109, 1996.

[93] K. Kuwajima. The Molten globule state as a clue for understanding the folding and cooperativity of globular-protein structure. *Proteins*, 6(2):87–103, 1989.

[94] D. A. Dolgikh, R. I. Gilmanshin, E. V. Brazhnikov, V. E. Bychkova, G. V. Semisotnov, S. Y. Venyaminov, and O. B. Ptitsyn. α-Lactalbumin - compact state with fluctuating tertiary structure. *FEBS Lett.*, 136(2):311–315, 1981.

[95] Y. V. Griko and D. P. Remeta. Energetics of solvent and ligand-induced conformational changes in α-lactalbumin. *Protein Sci.*, 8(3):554–561, 1999.

[96] K. Gast, D. Zirwer, M. Muller-Frohne, and G. Damaschun. Compactness of the kinetic molten globule of bovine α-lactalbumin: A dynamic light scattering study. *Protein Sci.*, 7(9):2004–2011, 1998.

[97] M. Kataoka, F. Tokunaga, K. Kuwajima, and Y. Goto. Structural characterization of the molten globule of α-lactalbumin by solution x-ray scattering. *Protein Sci.*, 6(2):422–430, 1997.

[98] C. E. Lyon, E. S. Suh, C. M. Dobson, and P. J. Hore. Probing the exposure of tyrosine and tryptophan residues in partially folded proteins and folding intermediates by cidnp pulse-labeling. *J. Am. Chem. Soc.*, 124(44):13018–13024, 2002.

[99] Jr. Farrell, H. M., R. Jimenez-Flores, G. T. Bleck, E. M. Brown, J. E. Butler, L. K. Creamer, C. L. Hicks, C. M. Hollar, K. F. Ng-Kwai-Hang, and H. E. Swaisgood. Nomenclature of the proteins of cows milk - sixth revision. *J. Dairy Sci.*, 87(6):1641–1674, 2004.

[100] E. D. Chrysina, K. K. Brew, and K. R. Acharya. Crystal structures of apo- and holo-bovine α-lactalbumin at 2.2 angstrom resolution reveal an effect of calcium on inter-lobe interactions. *J. Biol. Chem.*, 275(47):37021–37029, 2000.

[101] M. M. Ould Eleya, S. Ko, and S. Gunasekaran. Scaling and fractal analysis of viscoelastic properties of heat-induced protein gels. *Food Hydrocolloid*, 18(2):315–323, 2004.

[102] N. Purwanti, M. Smiddy, A. J. van der Goot, R. de Vries, A. Alting, and R. Boom. Modulation of rheological properties by heat-induced aggregation of whey protein solution. *Food Hydrocolloid*, 25(6):1482–1489, 2011.

[103] W-H. Shih, W. Y. Shih, S.-II Kim, J. Liu, and I. A. Aksay. Scaling behavior of the elastic properties of colloidal gels. *Phys. Rev. A*, 42(8):4772–4779, 1990.

[104] H. Wu and M. Morbidelli. A model relating structure of colloidal gels to their elastic properties. *Langmuir*, 17(4):1030–1036, 2001.

[105] A. Maltais, G. E. Remondetto, and M. Subirade. Mechanisms involved in the formation and structure of soya protein cold-set gels: A molecular and supramolecular investigation. *Food Hydrocolloid*, 22(4):550–559, 2008.

[106] J. N. Israelachvili. *Intermolecular and Surface Forces (Third Edition)*. Academic Press, San Diego, CA, USA, 2011.

[107] P. A. Wierenga, M. B. J. Meinders, M. R. Egmond, A. G. J. Voragen, and H. H. J. de Jongh. Quantitative description of the relation between protein net charge and protein adsorption to air-water interfaces. *J. Phys. Chem. B*, 109(35):16946–16952, 2005.

[108] P. A. Wierenga, M. B. J. Meinders, M. R. Egmond, F. A. G. J. Voragen, and H. H. J. de Jongh. Protein exposed hydrophobicity reduces the kinetic barrier for adsorption of ovalbumin to the air-water interface. *Langmuir*, 19(21):8964–8970, 2003.

[109] A. Maestro, E. Rio, W. Drenckhan, D. Langevin, and A. Salonen. Foams stabilised by mixtures of nanoparticles and oppositely charged surfactants: relationship between bubble shrinkage and foam coarsening. *Soft Matter*, 10:6975–6983, 2014.

[110] J. S. Guevara, A. F. Mejia, M. Shuai, Y-W. Chang, M. S. Mannan, and Z. Cheng. Stabilization of pickering foams by high-aspect-ratio nano-sheets. *Soft Matter*, 9(4):1327–1336, 2013.

[111] H. Jin, W. Zhou, J. Cao, S. D. Stoyanov, T. B. J. Blijdenstein, P. W. N. de Groot, L. N. Arnaudov, and E. G. Pelan. Super stable foams stabilized by colloidal ethyl cellulose particles. *Soft Matter*, 8(7):2194–2205, 2012.

[112] A. R. Cox, D. L. Aldred, and A. B. Russell. Exceptional stability of food foams using class II hydrophobin HFBII. *Food Hydrocolloid*, 23(2):366–376, 2009.

[113] B. Rullier, B. Novales, and M. A. V. Axelos. Effect of protein aggregates on foaming properties of β-lactoglobulin. *Colloids Surf. A Physicochem. Eng. Asp.*, 330(2–3):96–102, 2008.

[114] I. Nicorescu, C. Loisel, C. Vial, A. Riaublanc, G. Djelveh, G. Cuvelier, and J. Legrand. Combined effect of dynamic heat treatment and ionic strength on the properties of whey protein foams part ii. *Food Res. Int.*, 41(10):980–988, 2008.

[115] Z. P. Du, M. P. Bilbao-Montoya, B. P. Binks, E. Dickinson, R. Ettelaie, and B. S. Murray. Outstanding stability of particle-stabilized bubbles. *Langmuir*, 19(8):3106–3108, 2003.

[116] S. U. Pickering. CXCVI.-emulsions. *J. Chem. Soc. Faraday Trans.*, 91(0):2001–2021, 1907.

[117] R. G. Alargova, D. S. Warhadpande, V. N. Paunov, and O. D. Velev. Foam superstabilization by polymer microrods. *Langmuir*, 20(24):10371–10374, 2004.

[118] M. G. Basavaraj, G. G. Fuller, J. Fransaer, and J. Vermant. Packing, flipping, and buckling transitions in compressed monolayers of ellipsoidal latex particles. *Langmuir*, 22(15):6605–6612, 2006.

[119] M. Destribats, V. Lapeyre, M. Wolfs, E. Sellier, F. Leal-Calderon, V. Ravaine, and V. Schmitt. Soft microgels as pickering emulsion stabilisers: role of particle deformability. *Soft Matter*, 7(17):7689–7698, 2011.

Chapter 2

Controlled formation of protein nanoparticles by enzymatic cross-linking of α-lactalbumin with horseradish peroxidase *

Inorganic and organic colloidal particles are known to impart much higher stability to foams and emulsions than proteins, heat-induced protein aggregates or low molar mass surfactants. In this study we show that α-lactalbumin can be enzymatically cross-linked by horse-radish peroxidase to produce nanoparticles with controlled size and meso-scale structure. Furthermore, the effects of process parameters, such as the protein concentration (10 - 30 g L^{-1}), total dosed amount of hydrogen peroxide (0–10 mM), the time gap between each dosage of hydrogen peroxide (120–600 s) and ionic strength (100–200 mM), on the sizes of the nanoparticles have been investigated. The cross-linked protein nanoparticles varied in size (radius of gyration, R_g) and weight averaged molar mass (M_w), ranging between monomeric protein ($\sim$ 2 nm, 14.2 kDa) and nanoparticles (200 nm, 100 MDa). The speed of particle formation increased with increasing ionic strength, but their meso-scale structure remained similar. The R_g of these nanoparticles scaled as $M_w^{0.6}$, indicating similar meso-scale structure (conformation) at all length scales but variation of density with size. The apparent density (internal protein concentration) of the nanoparticles was between 104 and 10 kg m^{-3} for $R_g \sim 20$ nm and $R_g > 100$ nm respectively.

*This chapter is published as: Surender K. Dhayal, Harry Gruppen, Renko de Vries, Peter A. Wierenga, Food Hydrocolloids 36, (2014) 53-59.

Introduction

In recent years, particle stabilised (Pickering) foams [1] are gaining interest because of their high stability. For example, bubbles covered with particles are stable against disproportionation for weeks, while bubbles stabilized by proteins or low molar mass ($M_w < 1$ kDa) surfactants collapse within a few minutes or hours [2, 3]. This phenomenon of enhanced stablisation of interfaces by particles is referred to as Pickering-Ramsden type stabilisation [4,5]. The high stability of the foams stabilized by particles is often attributed to their size [1, 2, 6]. However, protein aggregates of the size similar to hard colloidal particles are not known to impart such high stability to the foams [7–9]. Hence, it seems that in the case of protein aggregates, in addition to size there are other properties, for example density and deformability which are determining the foam stability. The density and deformability of an aggregate in turn can be related to its meso-scale structure. The meso-scale in this paper is defined as the length scale between a monomeric protein, typically $\approx 2 - 5$ nm and its aggregates smaller than 1 μm. The role of meso-scale structure of aggregates in Pickering stabilisation is not yet well understood since most researchers so far have focused on the role of size. There are some initial indications that the meso-scale structure also determines the interfacial properties, albeit only under certain conditions for example when electrostatic interactions have been screened [9–12]. To understand the correlation between the meso-scale structure of a particle and its interfacial and foaming properties, two factors are needed. First, a process / system is needed to produce particles of a well-defined (controlled) size and structure. The second, is a technique to characterize the structure of such particles with minimum artefacts due to poly-dispersity and sample processing. So far, effect of protein aggregates on interfacial properties has been studied mostly using heat-induced aggregation [7–9, 13, 14]. Enzymatic cross-linking of monomeric proteins could be an alternative method to make protein aggregates (nanoparticles) with the advantages of mild reaction conditions and high specificity i.e well defined covalent cross-links. Various techniques have been used to analyse the meso-scale structure of protein aggregates, e.g. light/x-ray/neutron scattering, atomic force microscopy and cryo-transmission/scanning electron microscopy [9–12]. Amongst these, light scattering is a very versatile technique for the following two reasons. 1) It can be coupled to a separation device, such as size exclusion chromatography and asymmetric flow field flow fractionation (AF4), to separate the poly-disperse mixtures of particles. 2) It can be used to simultaneously measure the size i.e radius of gyration (R_g) or hydrodynamic radius (R_h), molar mass (M_w) and fractal dimension, d_f [15] in solution conditions. The meso-scale structure of the aggregates can be described by its d_f, which can be determined in two ways i.e. either from the scaling of size and mass, $R_g \sim M_w^{1/d_f}$, [15], or from the angular dependence of the scattered light intensity, $P(q) \sim (qR_g)^{-d_f}$, where $P(q)$ is the particle scattering factor and q is the scattering wave vector [15, 16]. The shape/structure of an aggregate in solution can also be predicted from the ratio of geometrically defined radius of gyration to hydrodynamic radius i.e. R_g/R_h [16]. For example, $R_g/R_h = 0.77$ indicates a compact homogeneous sphere, $R_g/R_h > 0.77$ indicates anisotropic shape

and $1 < R_g/R_h < 2$ indicates random coil or branched macromolecule [16,17]. In this paper, we explore the possibility of using enzymatic cross-linking to produce protein nanoparticles of controlled size and structure. Studies dealing with enzymatic cross-linking of proteins use various types of enzymes such as transglutaminase [14,18,19], peroxidase [18,20,21], tyrosinase [18,19] or laccase [18,22]. The advantage of using peroxidase is that the reaction is dependent on the supply of co-substrate, hydrogen peroxide (H_2O_2). Hence, the cross-linking can be relatively easily controlled by the addition of H_2O_2. However, too high concentrations of H_2O_2 can lead to inactivation of the enzyme [23]. In previous work [21] it has been shown that multiple dosages of small amounts of H_2O_2 can result in increased sizes of protein aggregates. It was further shown that the ionic strength seemed to influence the size distribution of the oligomers [21]; whether it also effects the meso-scale structure is not known. Later, the idea of multiple H_2O_2 additions was extended for high number of H_2O_2 dosages, resulting in the formation of cross-linked particles of R_h up to 30 nm [24,25]. The R_h of these particles scaled as $M_w^{0.4}$, indicating that these particles were highly branched (compact) [25] . The aim of the present work is to determine the extent to which the conditions used during enzymatic crosslinking of protein affects the types of aggregates that are formed. To this end apo α-lactalbumin (α-LA) and horseradish peroxidase (HRP) were used. The formed aggregate size, mass and structure are analysed using asymmetric flow field flow fractionation (AF4) followed by multi-angle laser light scattering.

Materials and methods

Materials

α-Lactalbumin (α-LA) was obtained from Davisco Foods International Inc. (Le Sueur, MN, USA, $\sim$ 85% of α-LA in calcium free apo form, as per supplier information). The total protein content ($N \times 6.25$) of the powder was 85.6 % (w/w, wet basis). Approximately 90 % of all proteins were α-LA as determined using the UV peak area at 280 nm in the AF4 fractogram. The other proteins were $\beta-$ lactoglobulin and bovine serum albumin as confirmed by SDS PAGE (no further details shown). Horseradish peroxidase (HRP) was obtained from Sigma (P6782, Peroxidase type VIA). The iron content of HRP, as given by the Reinheitszahl (R_Z) index i.e. A_{403}/A_{275} , was determined spectrophotometrically to be $\sim$ 3. All other chemicals used were of analytical grade.

Sample preparation

Milli-Q water (18.2 MΩ cm) was used for all solutions. The α-LA was dissolved in 0.1 M ammonium acetate solution (pH 6.8) to obtain concentrations of 10 or 20 or 30 g L^{-1}. The protein solution was stirred for 2 h, after which the visually clear solution was left overnight at 4 °C. Next it was centrifuged (40000 g, 1 h, 20 °C) and the supernatant was filtered over a 0.2 μm polyethersulfone membrane syringe

filter (type: SY25PL-S, Advanced Microdevices, Ambala, India) to remove small amounts of aggregates already present in the powder. The HRP was dissolved in 0.1 M ammonium acetate solution (pH 6.8). The concentration of proteins was determined with a UV spectrophotometer using the reported molar extinction coefficients of the proteins, i.e. $\varepsilon_{280} = 28460\ M^{-1}\ cm^{-1}$ for α-LA (www. uniprot.org, entry: P00711) and $\varepsilon_{403} = 112000\ M^{-1}\ cm^{-1}$ for HRP([26]) . A 50 mM stock solution of hydrogen peroxide in Milli-Q water was prepared and used for the controlled dosage using a syringe pump. The concentration was measured using the reported molar extinction coefficient of $\varepsilon_{240} = 43.6\ M^{-1}\ cm^{-1}$ ([26]). For cross-linking reaction in any other buffer e.g. sodium phosphate or Tris-HCl, the protein and enzyme solutions were made at pH 7.0.

HRP activity

The activity of HRP was measured using the 2,2-azino-bis-3-ethylbenzthiazoline-6-sulfonic acid (ABTS) assay [21] at pH 7.0 ± 0.2 and 37 °C. The activity in the 0.1 M ammonium acetate buffer,pH 7.0 ± 0.2 was found to be 10.9 ± 0.6 μkat mg^{-1}.

Cross-linking reaction

The cross-linking experiments were done at two different scales i.e. 5 or 10 mL (small scale) and 40 mL (large scale). Small-scale experiments were done to test the effect of different solution conditions on the kinetics of nanoparticle formation using online dynamic light scattering (DLS). From the results, certain conditions were chosen and cross-linking reactions were performed at large scale to produce a set of particles with well-defined sizes. These were stored by freeze-drying and subsequently used to analyse the structure by multi-angle static light scattering. In all cases the pH of the reaction mixtures was maintained at 7.0 ± 0.2.

Small-scale preparation

The small-scale (5 or 10 mL) crosslinking experiments were performed in a home built set up and monitored online using DLS (for details see [25]). Crosslinking was performed by sequential dosage of H_2O_2 (table 1.1) into the protein solution, thermostated at 37 °C. The number of H_2O_2 additions is indicated by n_{H2O2} in table (2.1) and figure 2.1b. Hydrogen peroxide (H_2O_2, 50 mM) solution was added at set intervals (Δt) by a computer controlled syringe pump, programmed to dose 2μL per mL of the reaction volume. At the end of each H_2O_2 addition, the solution was stirred for 30 s, followed by a period of rest for 60 s. Then the intensity fluctuations in the scattered light were measured at 90° for 60 s and six such scans were averaged to obtain the z-average R_h. These measurements were recorded at set intervals till the end of the reactions. Time intervals (Δt) of 120, 210 and 600 s were used to see the effect of addition rate on particle formation and decide which Δt to use for large-scale reaction. The lower particle size at any given number of H_2O_2 additions is lower for a

Table 2.1: *Conditions used for various cross-linking reactions and the resultant hydrodynamic radius slope (dR_h/dt) and plateau (R_h^{final}). The pH in all cases is 7.0 ±0.2, I is the calculated ionic strength and κ is measured electrical conductivity. The number of hydrogen peroxide additions is abbreviated as n_{H2O2} and the interval between each addition of H_2O_2 is given by Δt_{H2O2}.*

α-LA (g/L)	HRP (g/L)	buffer type	buffer conc. (M)	NaCl (M)	κ* (mS/cm)	I** (M)	HRP Activity*** (μkat/mg)	Δt_{H2O2} (s)	n_{H2O2} (-)	dR_h/dt (nm/h)	R_h^{final} (nm)
10	0.5	ammonium acetate	0.1	0	9.3	0.1	10.9	600	80	3.2	25
20	1	ammonium acetate	0.1	0	9.3	0.1	10.9	300	160	6.5	50
30	1.5	ammonium acetate	0.1	0	9.3	0.1	10.9	210	229	11.1	109
40	2	ammonium acetate	0.1	0	9.3	0.1	10.9	210	250	-	gel
30	3	ammonium acetate	0.1	0	9.3	0.1	10.9	210	250	13.4	164
30	1.5	ammonium acetate	0.1	0	18.8	0.2	10.1	210	114	16.7	156
30	1.5	sodium phosphate	0.1	0	10.2	0.21	5.5	210	250	6.8	59
30	1.5	sodium phosphate	0.01	0.1	10.8	0.12	-	210	250	7.8	69
30	1.5	Tris-HCl	0.1	0	7.3	0.1	4.7	210	250	7.8	73
30	1.5	-	-	0.1	10.4	0.1	-	210	250	5.7	55

*Conductivity of only salt/buffer solutions measured at 26 ±1 °C.

**Ionic strength is calculated assuming full dissociation, as $I = 1/2\Sigma_i C_i z_i^2$, where C is the molar concentration of an ion of valence z.

***Activity measured in absence of α-LA using ABTS assay with a standard deviation of 0.6 μkat mg^{-1}.

Table 2.2: *Hydrodynamic size, molar mass, radius of gyration and apparent weight averaged densities for α-LA nanoparticles cross-linked to varying extents.*

Ionic Strength	Sample (hour)	R_h (nm)	R_g (nm)	M_w (MDa)	R_g/R_h	ρ_{app} (kg m^{-3})	DP
0.1 M NH_4OAc	2	20	20	2.1	1	104	148
	4	34	66	13.8	2	19	973
	7	65	165	108	2.5	9.5	7613
	10	89	180	154	2	10.5	10856
0.1 M NH_4OAc + 0.1 M NaCl	1	16	-	0.4	-	-	30
	2	26	37	5.6	1.4	42.8	392
	5	75	213	211	2.8	8.7	14874
	10	113	194	221	1.7	12	15579

Δt of 120 s, suggesting a faster enzyme inactivation (figure 2.1b). This was not found to be the case for Δt of 210 s or greater and hence for further studies, a Δt of ≥ 210 s was used. For the study of the effect of α-LA concentration, the ratio of α-LA to HRP was kept constant at 20 (w/w). To keep a similar ratio of HRP and H_2O_2 the Δt used was 600, 300 and 210 s for 10, 20 and 30 g L^{-1} α-LA respectively. These Δt values were also based on the enzyme activation studies done by [25].

Large-scale preparation

Two different sets of α-LA nanoparticles were made at large-scale. First set consisted of nanoparticles made by varying the bulk concentration of α-LA (10, 20 or 30 g L^{-1}) as described above.

The second set consisted of nanoparticles made with 30 g L^{-1} of α-LA at two different ionic strengths i.e. 0.1 M ammonium acetate (NH_4OAc) and 0.1 M NH_4OAc $\pm$0.1 M NaCl, using Δt of 210 s for both experiments. For each ionic strength, the samples were made by varying the reaction time from 1 to 10 h (table 2.1), while keeping all other parameters constant as given in table 1.1. Protein solutions (35 mL) were incubated at 37 °C in a jacketed glass vessel with continuous stirring and HRP (5 mL) was added to it. A 50 mM H_2O_2 solution was added at set intervals by a computer controlled syringe pump, programmed to dose 2 μL per mL of the reaction volume. Protein nanoparticles of sizes (R_h) ranging between approximately 25 and 100 nm were produced by varying the protein bulk concentration, or ionic strength, or the total number of H_2O_2 additions (equivalent to the total reaction time) (table 1.1). The pH was checked at the end of the reaction and was found to be 6.8, hence there was no change in the pH during the cross-linking reaction. The reaction mixtures were not treated to inactivate the enzyme, since typically all the H_2O_2 was reacted before the addition of next step. Furthermore, the enzyme was found to be inactivated after this long-time incubation. The final reaction mixtures were mixed with 1 M sucrose

solution in 1:1 volume ratio, to avoid aggregation during freezing and freeze-drying. Next, they were then frozen at -80 °C and freeze-dried. The dried powders were stored at -20 °C. Prior to use, the freeze-dried powder was reconstituted in a 10 mM sodium phosphate buffer (pH = 7.0) at a concentration close to the desired protein concentration. Next, solutions (20 mL) were dialysed extensively with a 300 kDa cellulose ester membrane (SpectraPor, Spectrum Laboratories, Rancho Dominguez, CA, USA) at 4 °C against around 20 L of distilled water (pH $\sim$ 7) and in the final step against a 10 mM sodium phosphate buffer, pH 7.0. The dialysis was monitored by measuring the conductivity and UV spectra of the outer solution. It was stopped when the conductivity of outer solution was the same as distilled water and no proteins could be detected by UV 280 nm absorbance. The final protein concentration of the dialysed solutions was calculated as % N $\times$6.25, where % N is the nitrogen content as determined by Dumas method using a Flash EA 1112 NC Analyzer (Thermo Fischer Scientific, Waltham, MA, USA). The conversion factor of 6.25 was calculated based on the primary sequence of α-LA obtained from www. uniprot.org (entry P00711).

Dynamic light scattering

For large-scale sample preparation, the R_h directly after the reaction, and after the dialysis was measured using a nano-zetasizer (Nano-ZS, model: ZEN 3600, Malvern Instruments, Worcestershire, UK) equipped with 633 nm laser. The samples were put in a 1 mL quartz cuvette with 10 mm path length. The measurements were performed at 25 °C in the automatic mode, in which the attenuator and the measurement position were selected automatically. The intensity fluctuations in the scattered light were measured at 173° for 30 s. Ten such scans were averaged to obtain the correlation curve. Next, intensity based size distributions were calculated using the standard software of Malvern.

Asymmetric Flow Field Flow Fractionation (AF4)

AF4 was used to fractionate the polydisperse nanoparticles and followed by online multi-angle static light scattering (MALS) and concentration measurement using UV and RI to determine their size and mass. The AF4 instrumentation comprised of a HPLC unit (Ultimate 3000, Dionex/Thermo Fisher Scientific, Sunnyvale, CA, USA) containing a pump, auto-sampler, column compartment and a UV cell with diode array detector. The other units such as Eclipse Dual tech, which contains the flow control valves, MALS (Dawn Heleos-II, $\lambda = 658$ nm, 130 mW Laser, vertically polarised), RI detector (Optilab T-rEX), flow cell and its various parts (spacer, membrane, porous support plate etc) were from Wyatt Technology (Santa Barbara, CA, USA). The pump flow rate was controlled by the Eclipse separation system using the Chromeleon software. Data collection and analysis were done with ASTRA-6 software (Wyatt Technology) The flow cell comprised of a short channel (145 mm length), fitted with a spacer of 350 μm gap (350W) and a 10 kDa regenerated cellulose membrane. The flow rates, focusing time and the amount of sample to be injected were

optimised to achieve a good separation of polydisperse samples, no overlapping peaks of the un-fractioned samples along with the void peak, and no peak shifts or band broadening due to sample overloading. The total sample amounted to 10-30 μg of injected protein using a 50 μL loop in partial inject mode. The detector flow rate was kept constant at 1 mL min^{-1}. The sample was injected at a flow rate of 0.2 mL min^{-1} and focused for 8 min. Elution was done under varying cross flow rate (V_x). At the start of elution, V_x was kept constant at 2 mL min^{-1} for 5 minutes and then exponentially decreased [27,28] from 2 to 0.1 mL min^{-1} with a decay time constant of 5 min. The exponential decay was achieved by eight linear decays of one min duration, followed by seven linear decays of two minute duration. V_x was then kept constant at 0.1 mL min^{-1} for 5 minutes and finally decreased to 0 mL min^{-1} and kept at that for 10 min. Light scattering signals from 53° to 100° were used for the extrapolation using 1st order fits [29] with Berry formalism [29, 30] ($\sqrt{KC}/R_\theta$) *vs.* ($sin^2(\theta/2)$). From the fitted weight averaged molar masses (M_w) and R_g, the apparent density can be calculated using equation 2.1.

$$\rho_{\text{app}} = \frac{M_w}{N_A \frac{4}{3}\pi R_g^3} \tag{2.1}$$

Where, ρ_{app} is the apparent density, M_w is the weight averaged molar mass, R_g is the $z-$averaged radius of gyration, and N_A is the Avogadros number. The M_w and R_g were averaged using consecutive online separated fraction (slice) in the chromatogram, i.e. the data was collected every 0.5 s. The M_w was calculated using the refractive index chromatograms as the concentration source, using a dn/dC of 0.185, a typical value for proteins. A blank was run before the actual measurements and subsequently subtracted from the sample spectra to obtain the refractive index chromatogram corresponding to protein nanoparticles only. The correction for axial dispersion (band broadening), normalization and peak alignment were done as described in the ASTRA manual (Wyatt Technology). The fractal dimension of the nanoparticles can be obtained from the slope of the power law regime in the plot of the angular (q) dependence of the scattered light intensity. This can generally be described by [16, 30]

$$R(q) \propto I(q) = KCM_wP(q)S(q) \tag{2.2}$$

Where, $R(q)$ is the excess Rayleigh ratio, $I(q)$ is the intensity of the scattered light, K is an optical constant and C is the concentration. $P(q)$ is the particle scattering factor (function) and describes the intra-particle scattering from the elementary scattering units. The structure factor, $S(q)$ is related to the inter-particle interactions. After fractionation, the typical protein concentration in the light scattering cell is of the order of 0.01 to 0.1 g L^{-1}. Under these dilute conditions the inter-particle interactions and hence the contribution from the structure factor or second virial coefficient on scattering can be neglected. The $P(q)$ as a function of the scattering wave vector q has been used to obtain the fractal dimension (d_f) of the large nanoparticles. The slices from the fractograms of the separated nanoparticles were taken at the peak. For

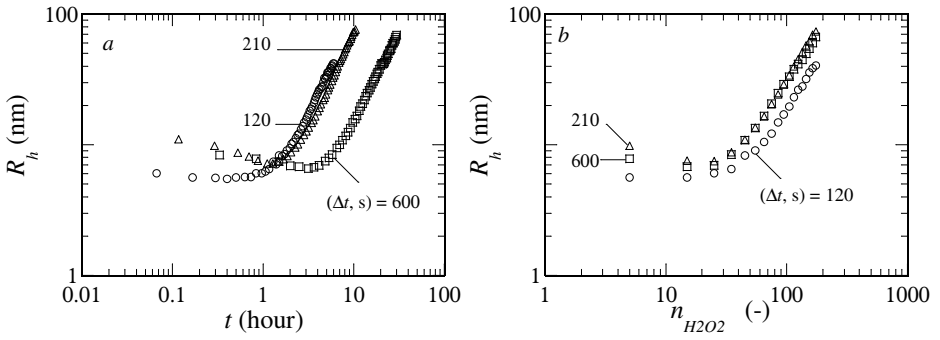

Figure 2.1: *z-Averaged hydrodynamic radius for 30 g L^{-1} α-LA cross-linked with 1.5 g L^{-1} HRP in 0.1 M NH_4OAc at pH 6.8 and under variable dosing rates of H_2O_2, indicated by Δt of 120, 210 and 600 s as a function of time (a) and the number of additions of hydrogen peroxide, n_{H2O2} (b). For clarity, only 30 % and 10 % of the data points are shown in a and b, respectively.*

each of these slices, the R_g was normalised with $R_{q\to 0}$ (similar to the $I(q)$ normalised with the fitted M_w and plotted against qR_g (q normalised with the fitted R_g).

Results and discussion

Preparation of protein nanoparticles

The effect of the addition rate of H_2O_2 on the size and speed of nanoparticle formation is shown in figure 2.1a. The reaction was performed by the step-wise addition of H_2O_2 to the solution containing α-LA and HRP. The interval between each addition (Δt) was varied to arrive at three different rates of H_2O_2 addition i.e 120, 210 and 600 s.

Figure 2.1a shows two steps in the nanoparticle formation process; 1) a constant period during which there is no change of the particle size and 2) a power law region in which the R_h increases with the total reaction time. The slope of R_h versus time gives the rate of nanoparticle formation (table 2.1). The curves corresponding to Δts of 210 and 600 s collapse onto one single curve (figure 2.1b) when the R_h is plotted as a function of the number of H_2O_2 additions (n_{H2O2}). The curve of $\Delta t = 120$ s does not collapse onto the other curves which indicates that the enzyme was inactivated. This was due to higher bulk concentration of H_2O_2 resulting from the fact that the H_2O_2 was added faster than it was consumed. It also shows that the amount of H_2O_2 added in each step is utilized within 210 s. Hence, a $\Delta t \geq 210$ s was used to prepare the α-LA nanoparticles as given in table 2.1. For pure, monomeric α-LA, the R_h is around 2 nm (data not shown), as expected. However, in the presence of HRP a very small amount of small oligomers is formed. This results in an initial z-average $R_h \geq 6$ nm (figure 2.1). These oligomers are formed by electrostatic interaction between α-

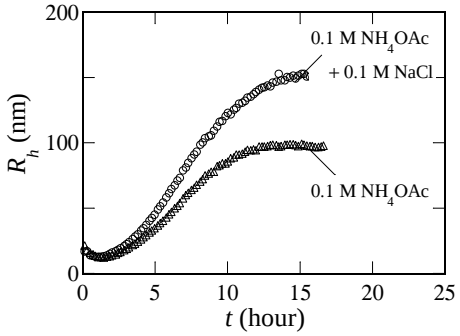

Figure 2.2: *z-Averaged hydrodynamic radius for enzymatic cross-linking reaction of 30 g L^{-1} α-lactalbumin in 0.1 M ammonium acetate (NH_4OAc) with and without additional 0.1 M NaCl.*

LA and HRP, which is a mixture of several (at least seven) isozymes with pI ranging from 3 to 9. Using size exclusion chromatography it was confirmed that most of the α-LA was still present as monomeric protein (data not shown).

The enzymatic crosslinking of 30 g L^{-1} α-LA (table 2.1) with HRP at Δt of 210 s and two different ionic strengths was monitored using online DLS (figure 2.2). For both cases, the z-averaged hydrodynamic radius (R_h) remained constant for the initial 1 hour and then started to increase with the subsequent additions of H_2O_2. The R_h increased linearly between the time interval of 4–8 hours and leveled off after 14 hours of reaction at $\approx$ 100 nm for 0.1 M NH_4OAc and $\approx$ 150 nm for 0.1 M NH_4OAc + 0.1 M NaCl. As we have shown previously, the plateau corresponds to the complete inactivation of HRP [25] . This was confirmed by adding a fresh batch of enzyme at this point (plateau), after which the R_h was found to increase further [25](no further data given). The SDS-PAGE under reducing conditions revealed that covalent crosslinks were formed between the proteins in both cases (data not shown).

The effects of protein bulk concentration, buffer type and ionic strength on the reaction kinetics (the slope of R_h *vs.* t and plateau indicative of final R_h) are shown in table 2.1. An increase of protein concentration from 10 g L^{-1} to 30 g L^{-1} resulted in an increase of final size from 25 nm to 100 nm. At 40 g L^{-1} a gel was formed. For the reaction in 30 g L^{-1} and pH 7.0 $\pm$0.2, the final R_h in case of 0.1 M sodium phosphate, Tris-HCl buffer, or NaCl solution ranged from 55$-$73 nm (table 2.1). In NH_4OAc with or without NaCl higher values for R_h were obtained (109 to 156 nm), as well as higher slopes. Since the ABTS assay showed a lower activity of HRP in sodium phosphate and Tris-HCl buffers, this explains the smaller size of the nanoparticles obtained in these two cases. Similar observations have been reported previously [31]. An increase in ionic strength (additional 0.1 M NaCl) further increased the reaction speed in the second regime, even though the speed of formation in the lag time regime remained the same. The kinetics and final R_h observed during the cross-linking reaction depend

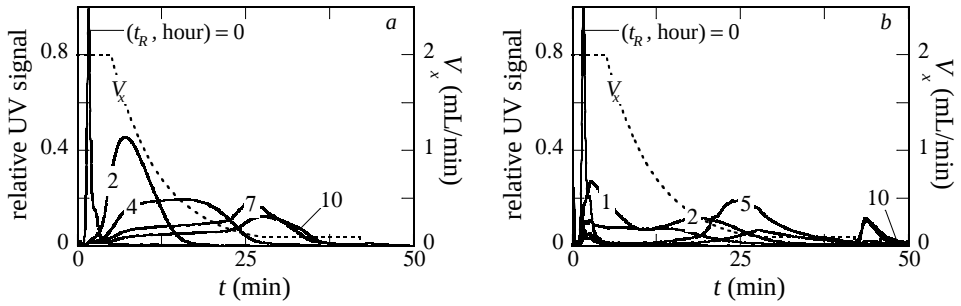

Figure 2.3: *AF4 fractograms depicting the cross-flow rate profile, programmed to exponentially decay with a t-half of 5 minutes. The fractograms are based on the absorbance at UV 280 nm. α-LA nanoparticles cross-linked to varying extents in presence of 0.1 M ammonium acetate (a) and with additional 0.1 M NaCl (b).*

on the enzyme activity and on the efficiency with which activated proteins form cross-links. To distinguish between these two effects, enzyme activity was tested with the ABTS assay. These results showed a significantly lower activity ($< 50\%$) in sodium phosphate or Tris-HCl, than in ammonium acetate. In contrast, the increase of ionic strength by addition of NaCl to the ammonium acetated buffer had no significant effect. Therefore, the effect of NaCl addition is most probably related to the screening of charge around α-LA molecules.

Characterization of protein nanoparticles by AF4

The protein nanoparticles obtained after different times of incubation (30 g L^{-1}, 0.1 M NH_4OAc, with or without 0.1 M NaCl) with R_h of 25, 50, 75 and 100 nm were injected and separated using AF4. The area under the curve of the absorbance at the UV-280 nm shows that apo α-LA was initially converted into oligomers ($t = 2$h and $t = 1$h in figure 2.3a and 2.3b, respectively). The oligomer in this paper is defined as cross-linked apo α-LA in the range of 28.4 kDa to 1 MDa, (DP 2–70) and a polymer as $M_w > 1$ MDa. These oligomers further cross-linked with themselves to form higher mass polymers or nanoparticles ($t = 4$, 7, 10 h and $t = 2$, 5, 10 h in figure 2.3a and figure 2.3b, respectively.

This suggests that protein molecules were first cross-linked to form oligomers followed by the crosslinking between oligomers to form polymers. This two-step mechanism of nanoparticle formation has also been previously suggested by us [25]. Finally ultra-high molar mass ($\gg 1$ MDa) nanoparticles are formed towards the end of the crosslinking reaction. The same mechanism applies to the reaction at low ionic strength, implying that the ionic strength probably changes only the kinetics. As expected, the average elution time of the nanoparticles increase with increasing time of cross-linking (figure 2.3).

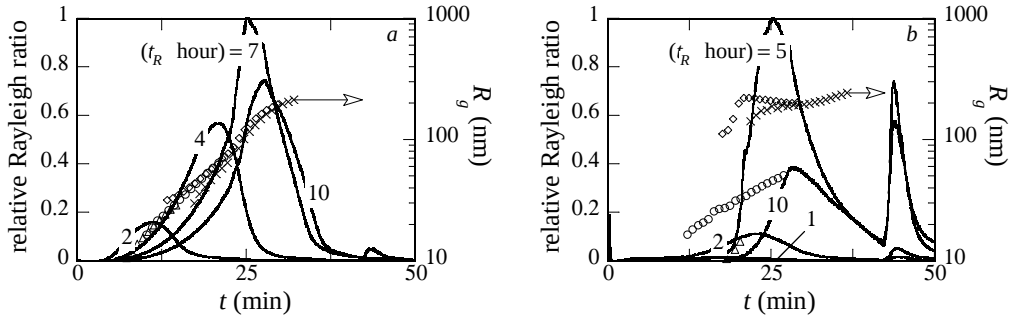

Figure 2.4: *AF4 fractograms depicting the Rayleigh ratio and the fitted R_g for 30 g L^{-1} α-LA cross-linked with 1.5 g L^{-1} HRP at pH 6.8 in 0.1 M NH_4OAc (a) and 0.1 M NH_4OAc + 0.1 M NaCl (b) at different time points. The legends for R_g represent the samples collected after cross-linking for 2 h (○), 4 h (△), 7 h (◊) and 10 h (×) in (a) and 2 h (○), 5 h (◊) and 10 h (×) in (b). For clarity, only 1 % of the data points are shown for R_g.*

The fractograms using the scattered light intensity (expressed as the Rayleigh ratio, R_g), for the four samples shown in figure 2.3 fractogram are depicted in figure 2.4. The large nanoparticles scatter more light compared to the small ones, and hence, the light scattering curves showed a peak, which is shifted in time. The fitted R_g for the separated samples at a given elution time increased from $\approx$ 10 nm up to $\approx$ 200 nm with the extent of reaction (figure 2.4).

The M_w distributions showed an increase of the average M_w from 0.2 to 300 MDa (figure 2.5) and table 2.2). The weight average molar mass (M_w), z-average R_g and R_h, apparent density and poly-dispersity are summarized in table 2.2. The apparent density decreases from around 104 kg m^{-3} for $R_g \approx 20$ nm to around 10 kg m^{-3} for $R_g > 100$ nm. These observations show that R_g increases faster than the molar mass, indicating that the nanoparticles get progressively less dense with the extent of cross-linking.

The information on the structural details (architecture) was obtained from the conformation plot (figure 2.5) showing the scaling of size (R_g) and mass (M_w). The slope of such a curve gives an indication of the meso-scale structure of the particle. The conformation plots of various nanoparticles (figure 2.5) show that the scaling exponent of all nanoparticles is between 0.5 and 0.6. This shows that the scaling of mass with the size is similar to a reaction or diffusion limited cluster aggregation [15]. This indicates that the nanoparticles formed under various conditions have similar conformation (meso-structure) in solution, and 2) that they have a fractal (self-similar) structure. Still, it is important to note that even though the scaling is similar, the density of the particles does decrease with the increasing particle size.

Apparent density is used as a parameter to describe the meso-scale structure of nanoparticles in addition to the other types of analysis such as scaling of size and mass, ratio of R_g/R_h, and the slope of power law regime in $P(q)$ *vs.* qRg. It is

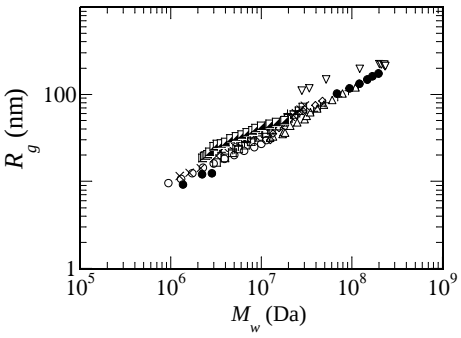

Figure 2.5: *Conformation plot indicating the scaling of size (R_g) to mass (M_w) of nanoparticles made at pH 6.8 in 0.1 M NH_4OAc using an α-LA concentration of 10 g L^{-1} (×), 20 g L^{-1} (+) and 30 g L^{-1}, for which the samples were collected after cross-linking for 2 h (○), 4 h (□), 7 h (△) and 10 h (◊). The other samples were made in 30 g L^{-1} of α-LA, 0.1 M NH_4OAc + 0.1 M NaCl and collected after 2 h (●), 5 h (⊠) and 10 h (▽). The curves have a slope of between 0.5 to 0.6. For clarity, only 1 % of the data points are shown.*

used to calculate the internal concentration of the nanoparticles and to distinguish between dilute / open type or concentrated / dense type nanoparticles [17]. The apparent density of these nanoparticles can be calculated based on the geometric volume inscribed by the sphere of radius equal to R_g according to equation 2.1. R_g scales as $M_w^{0.6}$, hence the apparent density scales with the size as $\rho \approx R_g^{-1.3}$. This indicates that the nanoparticles get progressively diluted with increasing size i.e. they are tenuous. The R_h is always smaller than the R_g for larger nanoparticles (table 2.2), indicating that the drainage of solvent through the outer dilute region is different from the inner denser regions during the diffusion of particles in solution. The R_g/R_h ratio is around 1 for 20 nm particles and increases to around or greater than 2 for the large nanoparticles (table 2.2). These values are also typical of poly-dispersed, branched or open type macromolecules [16, 17].

In addition, the structure was also analysed from the angular dependence of the scattered light (figure 2.6) expressed by the particle scattering factor $P(q)$. The scaling of $P(q)$ with qR_g shows a slope of 2.1 ±0.1 and 2.0 ±0.1 for high and low ionic strength, respectively. This again indicates that the large nanoparticles, formed at any ionic strength or bulk protein concentration, are self-similar with a fractal dimension of ≈ 2. The data points can be described well by the Ornstein-Zernike type relation ($P(q) \approx qR_g^{-2}$) [32]. The fact that the data points for the nanoparticles of various sizes, produced under various reaction conditions, collapses onto a single master curve, indicates that these nanoparticles have similar structures at various length scales.

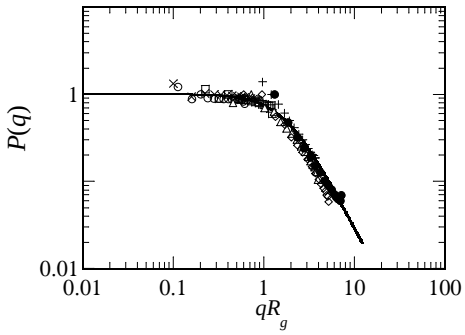

Figure 2.6: *Scaling of particle scattering factor with scattering wave vector, same symbols as in figure 2.5.*

Conclusion

Peroxidase mediated crosslinking can be used to produce protein nanoparticles of controlled size and meso-structure. The dosing rate and total dosed amount of the added hydrogen peroxide is an effective ways to control the size (mass) of protein nanoparticles prepared by enzymatic cross-linking with HRP. The nanoparticles made by enzymatic cross-linking are self- similar with a fractal dimension of ≈ 2. These nanoparticles seem to be similar in structure to most of the heat-induced protein particles made at pH around 7. However, in contrast to heat-induced protein aggregates, the peroxidase cross-linked protein nanoparticles are not much affected by the solution ionic strengths at the time of formation.

Bibliography

[1] J. S. Guevara, A. F. Mejia, M. Shuai, Y-W. Chang, M. S. Mannan, and Z. Cheng. Stabilization of Pickering foams by high-aspect-ratio nano-sheets. *Soft Matter*, 9(4):1327–1336, 2013.

[2] A. Cervantes Martinez, E. Rio, G. Delon, A. Saint-Jalmes, D. Langevin, and B. P. Binks. On the origin of the remarkable stability of aqueous foams stabilised by nanoparticles: link with microscopic surface properties. *Soft Matter*, 4(7):1531–1535, 2008.

[3] E. Dickinson. Food emulsions and foams: Stabilization by particles. *Curr. Opin. Colloid Interface Sci.*, 15(1–2):40–49, 2010.

[4] S. U. Pickering. CXCVI.-Emulsions. *J. Chem. Soc. Faraday Trans.*, 91:2001–2021, 1907.

[5] W. Ramsden. Separation of solids in the surface-layers of solutions and suspensions sbservations on surface-sembranes, bubbles, emulsions, and mechanical coagulation. - preliminary account. *Proc. R. Soc. Lond.*, 72(477–486):156–164, 1903.

[6] T. N. Hunter, R. J. Pugh, G. V. Franks, and G. J. Jameson. The role of particles in stabilising foams and emulsions. *Adv. Colloid Interface Sci.*, 137(2):57–81, 2008.

[7] A. Moro, G. D. Báez, G. A. Ballerini, P. A. Busti, and N. J. Delorenzi. Emulsifying and foaming properties of β-lactoglobulin modified by heat treatment. *Food Res. Int.*, 51(1):1–7, 2013.

[8] B. Rullier, B. Novales, and M. A. V. Axelos. Effect of protein aggregates on foaming properties of β-lactoglobulin. *Colloids Surf., A*, 330(2–3):96–102, 2008.

[9] C. Schmitt, C. Bovay, M. Rouvet, S. Shojaei-Rami, and E. Kolodziejczyk. Whey protein soluble aggregates from heating with NaCl: Physicochemical, interfacial, and foaming properties. *Langmuir*, 23(8):4155–4166, 2007.

[10] M. Destribats, V. Lapeyre, M. Wolfs, E. Sellier, F. Leal-Calderon, V. Ravaine, and V. Schmitt. Soft microgels as pickering emulsion stabilisers: role of particle deformability. *Soft Matter*, 7(17):7689–7698, 2011.

[11] N. Mahmoudi, M. A. V. Axelos, and A. Riaublanc. Interfacial properties of fractal and spherical whey protein aggregates. *Soft Matter*, 7(17):7643–7654, 2011.

[12] N. Mahmoudi, C. Gaillard, F. Boué, M. A. V. Axelos, and A. Riaublanc. Self-similar assemblies of globular whey proteins at the airwater interface: Effect of the structure. *J. Colloid Interface Sci.*, 345(1):54–63, 2010.

[13] D. A. Kim, M. Cornec, and G. Narsimhan. Effect of thermal treatment on interfacial properties of β-lactoglobulin. *J. Colloid Interface Sci.*, 285(1):100–109, 2005.

[14] A. Moro, G. D. Bez, P. A. Busti, G. A. Ballerini, and N. J. Delorenzi. Effects of heat-treated β-lactoglobulin and its aggregates on foaming properties. *Food Hydrocolloid*, 25(5):1009–1015, 2011.

[15] P. Aymard, D. Durand, T. Nicolai, and J. C. Gimel. Fractality of globular protein aggregates: from the molecular to the microscopic level. *Fractals*, 05(supp02):23–43, 1997.

[16] W. Burchard. *Light Scattering in Physical techniques for the study of food biopolymers*. S.B. Ross-Murphy (Ed.), Blackie, Glasgow/London, UK, 1994.

[17] L. Nilsson. Separation and characterization of food macromolecules using field-flow fractionation: A review. *Food Hydrocolloid*, 30(1):1–11, 2013.

[18] J. Buchert, Dilek Ercili C., H. Ma, C. Gasparetti, E. Monogioudi, G. Faccio, M. Mattinen, H. Boer, R. Partanen, E. Selinheimo, R. Lantto, and K. Kruus. Crosslinking food proteins for improved functionality. *Annu. Rev. Food Sci.*, 1(1):113–138, 2010.

[19] D. Ercili-Cura, R. Partanen, F. Husband, M. Ridout, A. Macierzanka, M. Lille, H. Boer, R. Lantto, J. Buchert, and A. R. Mackie. Enzymatic cross-linking of β-lactoglobulin in solution and at airwater interface: Structural constraints. *Food Hydrocolloid*, 28(1):1–9, 2012.

[20] W. H. Heijnis, H. L. Dekker, L. J. de Koning, P. A. Wierenga, A. H. Westphal, C. G. de Koster, H. Gruppen, and W. J. H. van Berkel. Identification of the peroxidase-generated intermolecular dityrosine cross-link in bovine α-lactalbumin. *J. Agric. Food Chem.*, 59(1):444–449, 2010.

[21] W. H. Heijnis, P. A. Wierenga, W. J. H. van Berkel, and H. Gruppen. Directing the oligomer size distribution of peroxidase-mediated cross-linked bovine α-lactalbumin. *J. Agric. Food Chem.*, 58(9):5692–5697, 2010.

[22] R. Lantto, E. Puolanne, N. Kalkkinen, J. Buchert, and K. Autio. Enzyme-aided modification of chicken-breast myofibril proteins: Effect of laccase and transglutaminase on gelation and thermal stability. *J. Agric. Food Chem.*, 53(23):9231–9237, 2005.

[23] K. J. Baynton, J. K. Bewtra, N. Biswas, and K. E. Taylor. Inactivation of horseradish peroxidase by phenol and hydrogen peroxide: a kinetic investigation. *Biochim. Biophys. Acta - Protein Structure and Molecular Enzymology*, 1206(2):272–278, 1994.

[24] Y. Saricay, S. K. Dhayal, P. A. Wierenga, and R. de Vries. Protein cluster formation during enzymatic cross-linking of globular proteins. *Farad. Discuss.*, 158(0):51–63, 2012.

[25] Y. Saricay, P. A. Wierenga, and R. de Vries. Nanostructure development during peroxidase catalysed cross-linking of α-lactalbumin. *Food Hydrocolloid*, 33(2):280–288, 2013.

[26] H. Pichorner, D. Metodiewa, and C. C. Winterbourn. Generation of superoxide and tyrosine peroxide as a result of tyrosyl radical scavenging by glutathione. *Arch. Biochem. Biophys.*, 323(2):429–437, 1995.

[27] J. J. Kirkland, C. H. Dilks Jr, S. W. Rementer, and W. W. Yau. Asymmetric-channel flow field-flow fractionation with exponential force-field programming. *J. Chromatogr. A*, 593(1–2):339–355, 1992.

[28] M. Leeman, K-G. Wahlund, and B. Wittgren. Programmed cross flow asymmetrical flow field-flow fractionation for the size separation of pullulans and hydroxypropyl cellulose. *J. Chromatogr. A*, 1134(1–2):236–245, 2006.

[29] M. Andersson, B. Wittgren, and K-G. Wahlund. Accuracy in multiangle light scattering measurements for molar mass and radius estimations. model calculations and experiments. *Anal. Chem.*, 75(16):4279–4291, 2003.

[30] S. Podzimek. *Light Scattering, Size Exclusion Chromatography and Asymmetric Flow Field Flow Fractionation: Powerful Tools for the Characterization of Polymers, Proteins and Nanoparticles*. John Wiley & Sons, Hoboken, NJ, USA, 2011.

[31] B. Hiller and P.-C. Lorenzen. Effect of buffer systems on the extent of enzymatic oligomerisation of milk proteins. *LWT-Food Sci. Technol.*, 41(6):1140–1144, 2008.

[32] T. Nicolai, C. Urban, and P. Schurtenberger. Light scattering study of turbid heat-set globular protein gels using cross-correlation dynamic light scattering. *J. Colloid Interface Sci.*, 240(2):419–424, 2001.

Chapter 3

Peroxidase induced oligo-tyrosine cross-links during polymerization of α-lactalbumin *

Abstract

Horseradish peroxidase (HRP) induced cross-linking of proteins has been reported to proceed through formation of di-tyrosine cross-links. In the case of low molar mass phenolic substrates, the enzymatic oxidation is reported to lead to polymerisation of the phenols. The aim of this work was to investigate if during oxidative cross-linking of proteins oligo-tyrosine cross-links are formed in addition to dityrosine. To this end, α-lactalbumin (α-LA) was cross-linked using horseradish peroxidase (HRP) and hydrogen peroxide (H_2O_2). The reaction products were acid hydrolysed, after which the cross-linked amino acids were investigated by LC-MS and MALDI-MS. To test the effect of the size of the substrate, the cross-linking reaction was also performed with L-tyrosine, N-acetyl L-tyrosinamide and angiotensin. These products were analysed by LC-MS directly, as well as after acid hydrolysis. In the acid hydrolysates of all samples oligo-tyrosine (Y_n, $n = 3 - 8$) was found in addition to di-tyrosine (Y_2). Two stages of cross-linking of α-LA were identified: a) $1 - 2$ cross-links were formed per monomer until the monomers were converted into oligomers, and b) subsequent cross-linking of oligomers formed in the first stage to form nanoparticles containing $3 - 4$ cross-links per monomer. The transition from first stage to the second stage coincided with the point where di-tyrosine started to decrease and more oligo-tyrosines were formed. In conclusion, extensive polymerization of α-LA using HRP via oligo-tyrosine cross-links

*S. K. Dhayal, S. Sforza, P. A. Wierenga and H. Gruppen.

is possible, as is the case for low molar mass tyrosine containing substrates.

Introduction

Enzymatic cross-linking of proteins results in modification of the techno-functional properties of native protein. In addition to transglutaminase, different oxidative enzymes such as laccase, tyrosinase and peroxidase have been used to cross-link food proteins [1,2]. These oxidative enzymes are known to induce oxidation and cross-links on tyrosine (Tyr, Y), cysteine or tryptophan [1,3]. A chemical characterization of the cross-linked proteins is important to compare the products obtained using different enzymes, or under different conditions. The chemical details include aspects such as the nature, type and average number of covalent cross-links formed per monomer. For peroxidase cross-linking of proteins, typically researchers have focussed on di-tyrosine (Y_2) cross-links. The detection of Y_2 is usually done by appearance of an absorbance peak around UV 318 nm (pH $>$ 7) or by fluorescence emission peaks around 420 nm after excitation at 315 nm [4, 5]. In the case of cross-linking of apo form of the bovine whey α-lactalbumin (α-LA) with HRP only Y_2 links have been found and considered [6–8]. However, for low molar mass substrates, such as L-tyrosine or N-acetyltyrosine, higher polymers were observed after crosslinking with horseradish peroxidase (HRP) [9]. Based on the reported molar mass of these polymers, the highest observed degree of polymerisation (DP) of Tyr is around 25. In some natural systems, cross-linking of structural proteins, such as resilin and elastin, with peroxidase leads to a DP of $2 - 4$ [10–12]. Since mass spectrometry (MS) analysis on large protein polymers does not work, there is no clear direct way to determine the cross-links *in situ*. Hence, a different approach is needed. Therefore, acid hydrolysis, followed by MS seems to be an alternate method for quantification of mixtures containing oligo/poly-Tyr [13–15]. Previous studies have reported that covalent cross-links, such as Y_2 and Y_3, are stable under the acid hydrolysis conditions (6 M HCl, 110 °C, 24 h) [13]. However, the use of acid hydrolysis has so far never been used for quantifying the cross-links formed after extensive oxidation of proteins. To obtain more insight into the structure of oxidatively cross-linked proteins, an investigation is made of the degree of polymerisation of tyrosin in cross-linked apo α-lactalbumin. In addition, a comparison is made with substrates of different molecular mass to see how the polymerisation reaction depends on the substrate size.

Materials and method

Materials

Bovine α-lactalbumin (α-LA) commercially sold in apo form was obtained from Davisco Foods International (Le Sueur, MN, USA). The protein content (N $\times$6.25) was 95 % (w/w) dry basis [16]. The conversion factor of 6.25 was calculated based on the primary sequence of α-LA. Approximately 90 % of the total proteins was α-LA [16],

of which around 80 % (mol/mol) was in calcium free apo form [17]. Horseradish peroxidase (HRP), (P6782, peroxidase type VIA), L-tyrosine, N-acetyl-L-tyrosinamide and 2,2-azino-bis-3-ethylbenzothiazoline-6-sulfonic acid (ABTS) were obtained from Sigma. Angiotensin (sequence: DRVYIHPF) was obtained from Abcam Biochemicals (Cambridge, UK). All other chemicals used were of analytical grade (Sigma or Merck).

Enzyme activity

HRP was used as received and its activity was measured in duplicate in 0.1 M ammonium acetate solution (pH 7.0 ± 0.2) and 37 °C using the ABTS assay [17]. The rate of product formation was determined from the absorbance measured at 405 nm (= 36.8 $mmol^{-1}$ cm^{-1}). The activity of the enzyme preparation was 10.9 ± 0.6 μkat mg^{-1}.

Preparative production of cross-linked samples

All solutions were prepared in Milli-Q water (18.2 MΩ cm). All the reactions were performed in a 0.1 M ammonium acetate solution set at pH 7.0 ± 0.2. The conditions and procedure of cross-linking were same as described before for α-LA/HRP/H_2O_2 system [16]. The substrate and their concentrations used in this study were L-tyrosine (2 mM), N-acetyl-L-tyrosinamide (2 mM), angiotensin (2 mM; equivalent to 2 mM of tyrosine) and α-LA (2.1 mM; equivalent to 6.72 mM of tyrosine in apo α-LA). The cross-linking was performed at 37 °C using a molar substrate to enzyme ratio of 60. The initial substrate concentrations were verified spectrophotometrically using the molar extinction coefficients of ϵ_{280} = 28460 M^{-1} cm^{-1} for α-LA (www. uniprot.org, entry: P00711), ϵ_{403} = 112000 M^{-1} cm^{-1} for HRP [18], ϵ_{274} = 1400 M^{-1} cm^{-1} for L-tyrosine [19], $\epsilon_{274.5}$ = 1340 M^{-1} cm^{-1} for N-acetyl L-tyrosinamide [20] and ϵ_{214} = 25162 M^{-1} cm^{-1} for angiotensin [19]. The mixture (10 mL) of substrate and HRP was incubated at 37 °C in a jacketed glass vessel with continuous stirring and equilibrated for 15 minutes. A computer controlled syringe pump was programmed to dose 2 μL of a 50 mM H_2O_2 solution per mL of the reaction volume at set intervals (Δt = 210 s). The polymerization of L-tyrosine and α-LA was monitored during the reaction by measuring the absorbance at UV 318 nm and fluorescence measurement (λ_{ex} = 315 nm and λ_{em} = 350 − 500 nm). Samples were taken after different numbers of H_2O_2 additions (n_{H2O2} = 1, 3, 5, 10, 20, 35, 85, 120, 150 and 180). For UV 318 nm absorbance and fluorescence experiments, 100 mL scale samples (n_{H2O2} = 35, 85, 120, 180) were prepared and mixed (1:1) with 1 M sucrose and freeze-dried as described previously [16]. Before analysis, the α-LA nanoparticles were extensively dialysed to remove unreacted monomers and sucrose as described elsewhere [16]. All reactions were performed in duplicate.

Measurement of conversion, size, mass and structure of α-LA nanoparticles

To monitor the rate of α-LA nanoparticle formation, the crosslinking experiments were performed in a home built set-up at 5 mL scale and monitored inline using dynamic light scattering (DLS) as described previously [8]. The scattered light intensity was measured at 90° and the distribution of hydrodynamic radius (R_h) was obtained using the regularization method utilizing CONTIN routine and Stokes-Einstein equation [21]. The mesoscale structure of the nanoparticles was determined from scaling of the radius of gyration (R_g) to molar mass (M_w) and the apparent density, which were obtained from asymmetric flow field flow fractionation (AF4) followed by multi-angle light scattering (MALS) and refractive index (RI) detectors. The AF4-MALS instrumentation and the analysis method was similar as described before [16]. The RI fractograms were divided in to three sections to quantify the monomers (0.75 to 2.1 min.), oligomers (2.1 to 10 min.) and polymers (10 to 45 min.). The integrated area in each section was subsequently normalised with the total area to obtain the amount of protein in each section. The AF4 separation was performed under normal (10 mM sodium phosphate buffer, pH 7.0) and dissociating/reducing conditions (10 mM sodium phosphate buffer, pH 7.0 in presence of 2 % (w/v) sodium dodecyl sulphate (SDS) and 0.1 M dithiothreitol (DTT)). The measurements were performed in duplicate and the average of duplicates in each case was used for analysis.

Acid hydrolysis

A volume of 2.4 mL of the cross-linked samples collected after certain time of reaction (concentration same as that used for reaction) were put into a 12 mL Pyrex glass tube fitted with teflon-lined screw caps. Next, 3.6 mL of 10 M HCl was added to the solution. The tubes were flushed with nitrogen for 2 minutes. The hydrolysis was carried out at 110 °C for 24 h. After evaporating the acid for 24 hours under nitrogen, the samples were reconstituted with 1 mL of eluent A and used for ultra high-performance liquid chromatography-electrospray ionization-mass spectrometry (UHPLC-ESI-MS) as explained below. The acid hydrolysis was performed in duplicate.

UHPLC-ESI-MS

Acid hydrolysed and dried samples were reconstituted in 1 mL of eluent A (1% (v/v) acetonitrile (ACN), 0.1% (v/v) trifluoroacetic acid (TFA) in UPLC grade water). Next, the solutions were centrifuged (15,000 g ; 5 minutes ; 20°C). The samples were analysed by LC/UV/ESI-MS using an ACQUITY UPLC separation system (Waters, Milford, MA, USA) equipped with a C4-reversed phase column (UPLC BEH C4 1.7μm, 2.1 × 100mm, Waters) coupled to a PLC LG 500 PDA detector (Waters) and to a SYNAPT G2-Si High Definition Mass Spectrometer (Waters). Eluents used were A (H_2O + 1% (v/v) ACN + 0.1% (v/v) TFA) and eluent B (ACN + 0.1% (v/v) TFA). The eluent profile was 0 to 2 min isocratic 90% A, from 2 to 12 min linear

gradient from 90% A to 25% A, from 12 to 15 min linear gradient from 25% A to 100% B, from 12 to 15 min isocratic at 100% B, then re-equilibration to the initial conditions. The flow rate was set at 0.35 mL min^{-1} and a volume 4 μL was injected. The PDA detector is operated at a sampling rate of 40 points s^{-1} in the range 200-400 nm, resolution 1.2 nm. The SYNAPT mass spectrometer was operated in the positive ion mode (resolution mode), capillary voltage 3 kV, sampling cone 30 V, source temperature 150 °C, desolvation temperature 500 °C, cone gas flow (N_2) 200 L h^{-1}, desolvation gas flow (N_2) 800 L h^{-1}, acquisition in the Full Scan mode, scan time 0.3 sec, interscan time 0.015 sec, acquisition range 150-4000 m/z. The MS was calibrated using NaI (m/z range: $200 - 2000$). The MS data were processed using the sofware MassLynx v 4.1 (Waters).

MALDI-TOF MS

Matrix-assisted laser desorption/ionization time-of flight mass spectrometry (MALDI-TOF MS, Bruker Daltonics, Bremen, Germany) was used for detecting oligo-tyrosine cross-links in the acid hydrolysed α-LA nanoparticles. The MALDI-TOF MS was equipped with a laser of $\lambda = 355$ nm (Bruker smartbeam-II laser) and it was used at a laser power of 50 %. The analysis was performed in positive mode and the ions were detected using reflector mode. A peptide calibration standard ($0.7 - 3$ kDa, Bruker Daltonics) was used to calibrate the instrument. The samples (5 μL, 1 g L^{-1}, 0.1% (v/v) TFA) were mixed with 5 μL of matrix solution. The matrix solution comprised of a saturated solution of cyano-4-hydroxycinnamic acid in a solvent made by mixing 100 μL (0.1 % (v/v) TFA + 1 % (v/v) ACN + water) and 50 μL (0.1 % (v/v) TFA + ACN). One μL of each solution was applied on a stainless steel metal plate. The samples were crystallized and analysed on an Ultraflextreme workstation which was controlled using Flex Control software (Bruker Daltonics). The data were analysed using Flex Analysis software.

Results and discussion

Polymerization of small substrates with HRP/H_2O_2

For N-acetyl-L-tyrosinamide (222.24 Da) clear narrow peaks and a broader peak of larger products are observed in the UV 214 nm chromatogram for the reaction product formed after 10 additions of H_2O_2 (figure 3.1a). The narrow peaks were identified using MS to belong to the dimers ($n = 2$; 442.48 Da) and trimers ($n = 3$; 662.72 Da). There were two separate peaks of dimers (retention time = 1.55 and 1.80 minutes, respectively) indicating that at least two isomers of dimers were formed (figure 3.1a). In the broad peak, a range of oligomers ($n = 4 - 12$; $882.96 - 2644.88$ Da) were identified.

Also for angiotensin, the dimer ($n = 2$; 2090.36 Da) and a broad peak of oligomers ($n = 3 - 10$; $3134.54 - 10443.8$ Da) were formed after crosslinking (figure 3.1b). The ESI-MS spectrum of the oligomer peak ($n_{H2O2} = 10$) in the figures 3.1c

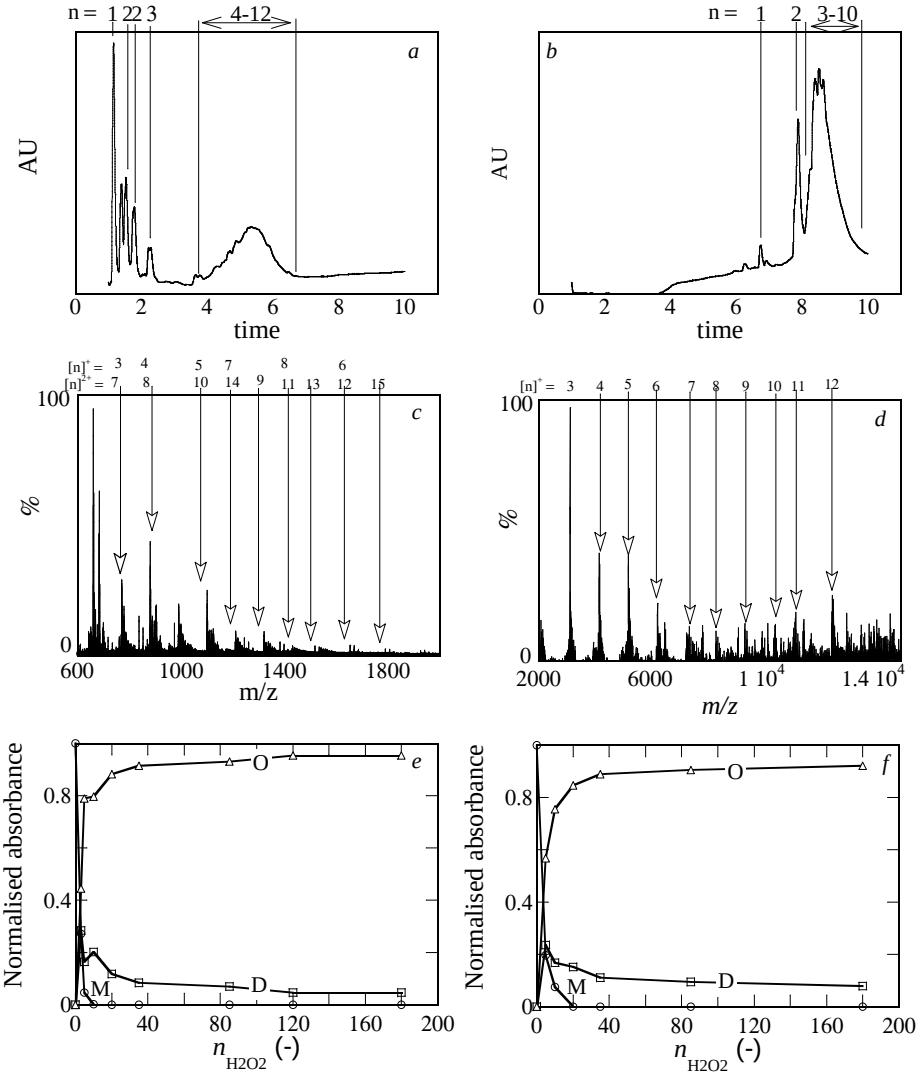

Figure 3.1: *Polymerization of N-acetyl-L-tyrosinamide (a, c, e) and Angiotensin (b, d, f) after cross-linking with HRP/H_2O_2. The UV 214 nm chromatogram of the samples recorded after $n_{H2O2} = 10$ during the cross-linking (a, b). ESI-MS spectra of the intact oligomers (c, d). The area under the curve of UV 214 nm chromatogram of monomers (M), dimers (D) and oligomers (O) for various additions of H_2O_2 (e, f). n indicates the DP and $[n]^+$ / $[n]^{2+}$ indicates the charged state i.e. +1 or +2 of the ions.*

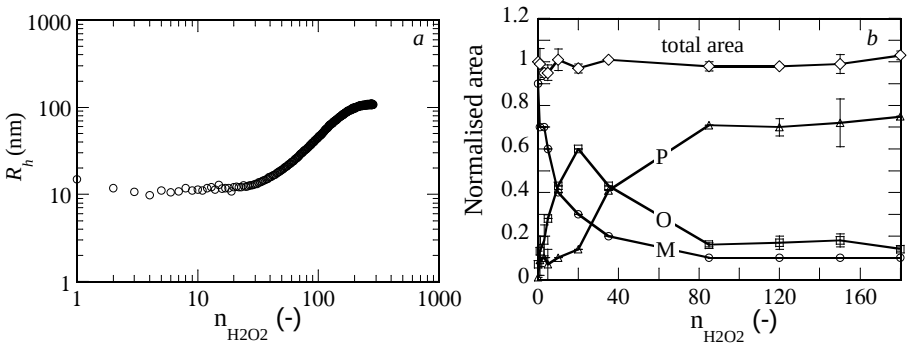

Figure 3.2: *Increase in hydrodynamic radius (R_h) of apo α-LA when it is cross-linked using HRP and sequential dosage of H_2O_2 (n_{H2O2}), monitored online with DLS (a). The AF4-RI area under the curve of monomers (M), oligomers (O) and particles (P) for various additions of H_2O_2 (b).*

and 3.1d depicts that a degree of polymerization (DP) up to 15 and 12 was achieved for N-acetyl-L-tyrosinamide and angiotensin, respectively. The MS spectrum of the intact polymers of N-acetyl-L-tyrosinamide (figure 3.1c) depicts the presence of protonated (single charged, $[n]^+$) trimer (662.28 Da) to octamer (1763.92 Da). Protonated (double charged, $[n]^{2+}$) oligomers (DP = 7 − 15, 1543.68 − 3525.84 Da) of N-acetyl-L-tyrosinamide are also seen in figure 3.1c. The MS of the intact oligomers of angiotensin showed single charged oligomers (figure 3.1d). Trimer (3134.54 Da) and larger oligomers ($DP = 4 - 12$, 4178.72 − 12532.16 Da) of angiotensin were formed. From the UV absorbance, the relative abundance of dimers and oligomers for various extents of cross-linking reaction ($n_{H2O2} = 0 - 180$) of N-acetyl-L-tyrosinamide and angiotensin were determined (figures 3.1e and 3.1f). For both substrates formation of dimers is observed after 5 dosages of H_2O_2. Upon further reaction, the amount of dimers decreased, with a corresponding increase in larger oligomers. For the cross-linking of free amino acid L-tyrosine (Y), similar formation and subsequent decrease of dimers (Y_2) was seen (data not shown). However, in the case of tyrosine, the decrease of dimers was not equalled by a corresponding increase in the amount of oligomers. This may have been due to that fact that oligomers larger than DP 8 were not detected, indicating that oligo-tyrosine is not as soluble as the intact oligomers of N-acetyl-L-tyrosinamide and angiotensin.

Polymerization of α-LA with HRP/H_2O_2

The polymerization of α-LA is evident from the increase of hydrodynamic radius (R_h) when H_2O_2 is added into the solution (figure 3.2a). Moreover, similar as for the low molar mass substrates, the formation and further conversion of dimers and oligomers of α-LA can be obtained from the integrated area in AF4-RI fractograms (figure 3.2b).

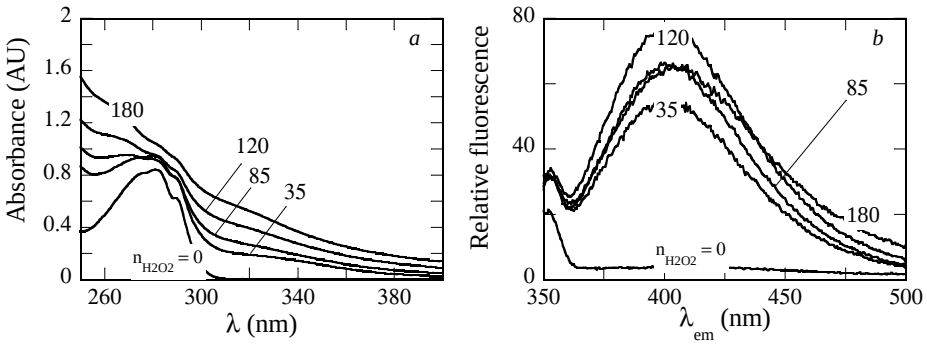

Figure 3.3: *Absorbance spectra depicting increase at UV 318 nm (a) and fluorescence spectra depicting emission around 400 nm (b) for α-LA samples cross-linked using HRP and* $n_{H2O2} = 0$*, 35, 85, 120 and 180.*

The polymerization of α-LA involved tyrosine cross-links as indicated by an increase of absorbance around 318 nm (figure 3.3a) and increase of fluorescence emission peak around 405 nm (figure 3.3b). The fluorescence emission peak did not increase for the largest α-LA nanoparticles ($n_{H2O2} = 180$) but the curve was found to broaden towards higher wavelengths. But, the 318 nm absorbance for $n_{H2O2} = 180$ was higher than that of $n_{H2O2} = 120$ indicating that tyrosine cross-links were formed, but the fluorescence was probably quenched for the large ($R_h \approx 100$ nm) nanoparticles. The UV absorbance and fluorescence measurements have typically been used under the assumption that in protein cross-linking only dityrosine is formed. To analyse the crosslink products in more detail, the samples were acid hydrolysed, and then analysed by LC-MS.

Detection of (oligo)tyrosine cross-links

Since poymers of α-LA could not be directly analysed by LC-MS, the cross-linked proteins were acid hydrolysed to yield free amino acids and cross-linked tyrosines, which are stable in the conditions of the hydrolysis. After acid hydrolysis of α-LA nanoparticles, the UV 214 chromatograms indicate a loss of tyrosine (Y, 3−4 minutes) and formation of di-tyrosine (Y_2, $4-5$ minutes, figure 3.4a). Surprisingly, even in the case of α-lactalbumin, clear MS signals are obtained that show the formation of larger oligomers of tyrosine (Y_{3-8}, $8-11$ minutes) which is similar to the case of the low molar mass compounds (figure 3.4b). In addition to the LC-MS, MALDI-TOF-MS was used to confirm the presence of oligotyrosine with a different technique (figure 3.4c). With that technique the presence of the oligomers were confirmed. Up to octa-tyrosine cross-links were detected for extensively cross-linked samples and are summarized in table 3.1.

The conversion of Y in to Y_2 and Y_{3-8} is evident from the decrease of the amount

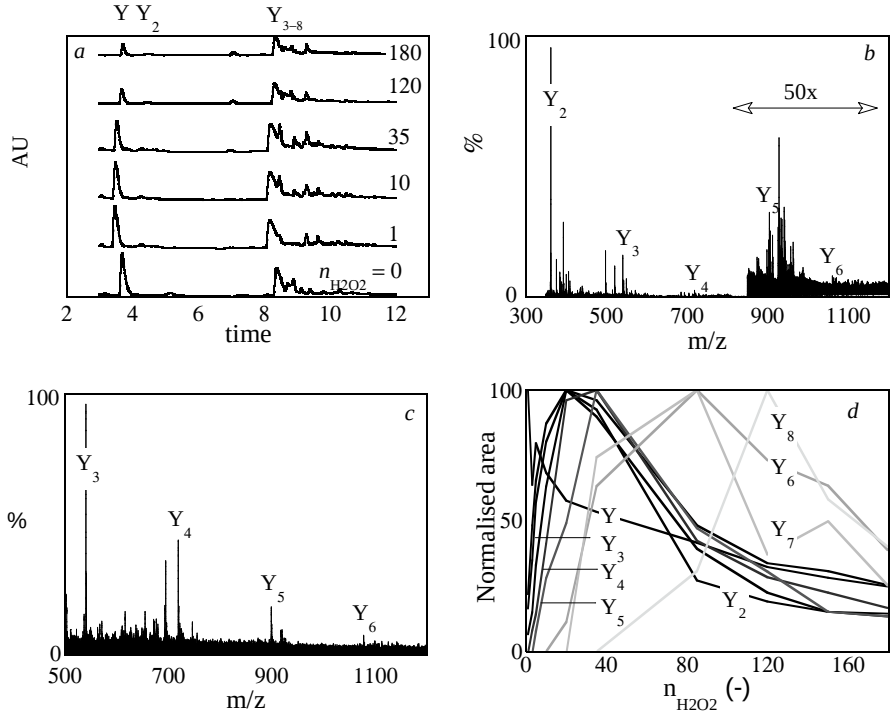

Figure 3.4: *The UV 214 nm chromatograms of acid hydrolysed α-LA nanoparticle (a). ESI-MS spectra from 8 to 16 minutes for $n_{H2O2} = 10$ of acid hydrolysed α-LA nanoparticle (b). The MALDI-TOF MS spectra of acid hydrolysed α-LA nanoparticle formed after $n_{H2O2} = 10$ (c). The abundance of tyrosine (Y), di-tyrosine (Y_2), and oligo-tyrosine (Y_{3-8}), normalized to the maximum for every compound in acid hydrolysed α-LA nanoparticle for various additions of H_2O_2 (d).*

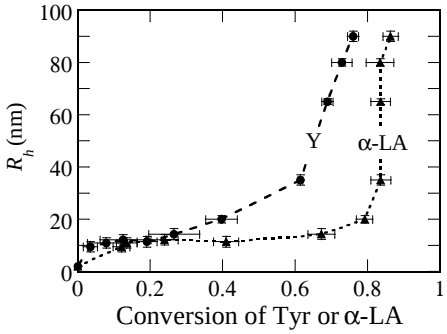

Figure 3.5: *Hydrodynamic radius (R_h) of cross-linked nanoparticles at various conversions of tyrosine (Y) and monomeric α-LA.*

of Y and an increase of Y_2 and Y_{3-8} with increasing dosage of H_2O_2 (figure 3.4d). The relative abundance of all different oligomers formed after various extents of cross-linking ($n_{H2O2} = 0 - 180$) was determined based on the MS intensity (figure 3.4d). After an initial increase, the amount of Y_2 started to decrease after 35 dosage of H_2O_2. This indicates that Y_2 were further cross-linked in to larger oligomers (Y_{3-8}) for α-LA/HRP system. After extended crosslinking, a DP of 8 is observed, but the relative abundance of this compound decreases upon further modification, indicating formation of even larger oligomers that were not detected by the LC-MS. This may be due to the insolubility of larger oligomers as indicated by the presence of pellets after centrifugation of the acid hydrolyzed samples and loss of total area under the curves of UV 214 nm chromatograms (figure 3.4a). The total peak area decreased from $100 - 36$ % with the extent of polymerization. The UV 214 nm chromatograms after acid hydrolysis of N-acetyl-L-tyrosinamide, angiotensin and L-tyrosine were similar to the chromatograms of α-LA nanoparticles (figure 3.4a). The polymerization of N-acetyl-L-tyrosinamide, angiotensin and L-tyrosine takes place by formation of tyrosine-tyrosine cross-links. This was proved by acid hydrolysis of theses samples and detection of oligo-tyrosine (Y_{2-8}) cross-links (table 3.1).

Hence, cross-linking of tyrosine containing substrates with HRP/H_2O_2 leads to polymerization of that substrate through formation of not only di-tyrosine but also oligo-tyrosine cross-links. It can be ascertained that oligo-tyrosine cross-links are formed even in the case of complex substrates such as proteins. Moreover, in the case of α-LA/HRP nanoparticles, no other cross-links involving amino acids other than tyrosine were detected in the acid hydrolysates.

Model of α-LA polymerization with HRP/H_2O_2

The online DLS and AF4 results indicate that polymerization of α-LA takes place in two stages. The conversion of tyrosine into oligotyrosine was seen in the acid

Table 3.1: *Oligo-tyrosine cross-links detected in various samples after acid hydrolysis.*

	Tyr			Ac-Tyr-amide		Angiotensin		α-LA	
	Theoretical mass [M] (Da)	Observed m/z $[M + nH]^{n+}$(Da)	Calculated* mass [M] (Da)	Observed m/z $[M + nH]^{n+}$(Da)	Calculated* mass [M] (Da)	Observed m/z $[M + nH]^{n+}$ (Da)	Calculated* mass [M] (Da)	Observed m/z $[M + nH]^{n+}$(Da)	Calculated* mass [M] (Da)
Tyrosine (Y)	181.0739	182.0845 $[H]^+$	181.0767	182.0786 $[H]^+$	181.0708	182.1151 $[H]^+$	181.1073	182.0814 $[H]^+$	181.0736
Di-tyrosine (Y_2)	360.1321	361.1441 $[H]^+$	360.1363	361.1358 $[H]^+$	360.1280	361.1810 $[H]^+$	360.1732	361.1429 $[H]^+$	360.1351
Tri-tyrosine (Y_3)	539.1904	540.2123 $[H]^+$	539.2045	540.2021 $[H]^+$	539.1943	540.2495 $[H]^+$	539.2417	540.1660 $[H]^+$	539.1582
Tetra-tyrosine (Y_4)	718.2486	719.2783 $[H]^+$	718.2705	719.2665 $[H]^+$	718.2587	719.3242 $[H]^+$	718.3164	719.2560 $[H]^+$	718.2482
Penta-tyrosine (Y_5)	897.3069	898.3397 $[H]^+$	897.3319	898.3266 $[H]^+$	897.3188	898.3943 $[H]^+$	897.3865	898.3372 $[H]^+$	897.3294
Hexa-tyrosine (Y_6)	1076.3651	1077.3969 $[H]^+$	1076.3891	1077.3969 $[H]^+$	1076.3891	1077.4453 $[H]^+$	1076.4375	1077.3760 $[H]^+$	1076.3682
Hepta-tyrosine (Y_7)	1255.4234	628.7277 $[2H]^{2+}$	1255.4398	628.7277 $[2H]^{2+}$	1255.4398	628.7802 $[2H]^{2+}$	1255.5448	1256.4100 $[H]^{2+}$ 628.7088 $[2H]^{2+}$	1255.402
Octa-tyrosine (Y_8)	1434.4816	718.2487 $[2H]^{2+}$	1434.4818	718.2604 $[2H]^{2+}$	1434.5052	718.1425 $[2H]^{2+}$	1434.2694	718.1329 $[2H]^{2+}$	1434.2502

* calculated based on the observed data.

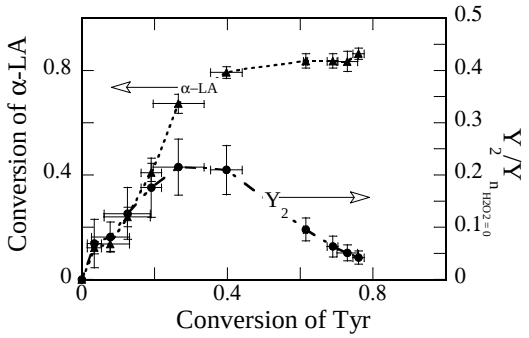

Figure 3.6: *The conversion of monomeric α-LA obtained from AF4 fractograms and the conversion of tyrosine (Y) and di-tyrosine (Y_2) obtained from UV 214 nm chromatograms of LC-MS runs of acid hydrolysates.*

hydrolysates of the α-LA particles. These two different sets of information, obtained at molecular ($\sim$ 2 nm) and mesoscale ($5 - 500$ nm) can be combined together to obtain further insight in to the mechanism of α-LA polymerization. For example, the conversion of monomeric α-LA (obtained from AF4-RI) and the conversion of tyrosine in acid hydrolysates obtained from LCMS can be plotted against R_h for each addition of H_2O_2 (figure 3.5). The two stages are clearly evident from the fact that a significant increase of R_h is obtained only at higher conversion of tyrosine or monomeric α-LA (figure 3.5). As confirmed by AF4 (figure 3.2b), the monomeric α-LA is mostly converted during the initial additions of H_2O_2. More than 50 % of the monomeric α-LA was converted into oligomers after 10 additions of H_2O_2. The conversion reaches a value around 85 % after 35 additions and remains unchanged after that. The fact that the monomeric apo α-LA is fully converted after $n_{H2O2} = 35$ while the R_h remains constant and its gradual increase for the subsequent additions indicate that the polymerization of α-LA takes place in two stages. In the first stage, small oligomers of α-LA are formed and in a later stage these oligomers cross-link with each other to form large particles of α-LA (nanoparticles).

The conversion of monomeric protein can also be plotted against the conversion of tyrosine in the acid hydrolysate (figure 3.6). This combined information can then be used to estimate the average number of tyrosine cross-links per molecule of α-LA in the nanoparticles. The molar concentration of tyrosine is four times that of α-LA since each molecule of α-LA contains four tyrosine residues. For upto 35 additions of H_2O_2, around 80 % of the α-LA is converted while only $25 - 50$ % of tyrosine is reacted. This indicates that on an average one to two tyrosine are cross-linked per molecule during this first stage. During this stage, tyrosine is mainly converted into di-tyrosine (figure 3.6). After 35 additions of H_2O_2, the amount of di-tyrosine started to decrease and as shown earlier (figure 3.4d), larger oligomers started to increase.

In the second stage, these oligomers of α-LA are further cross-linked with each

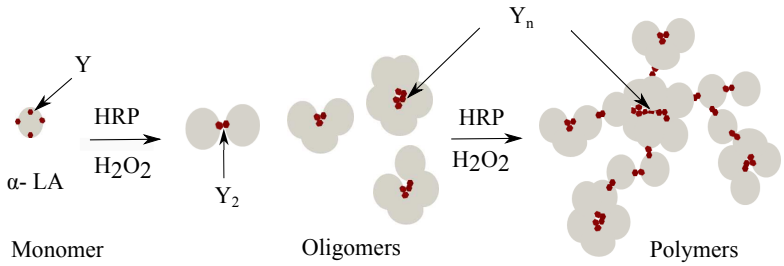

Figure 3.7: *The proposed two-stage process of polymerization of α-LA by oligo-Tyr cross-links. The α-LA molecule in the cartoon is represented as grey circle and tyrosine as red hexagons on it. The polymerization is depicted by highlighting only the cross-linked tyrosine residues in red.*

other to form nanoparticles. During this stage, more tyrosines are cross-linked per molecule and for the extensively polymerized samples, three to four tyrosines are estimated to be reacted per molecule of α-LA (figure 3.6). Formation of α-LA nanoparticles in two stages is schematically depicted in figure 3.7. Since, not all tyrosines were equally exposed in α-LA, the data implies that eventually all tyrosines become available for reaction. It is speculated that this can happen if the fluctuating tertiary structure of apo α-LA is completely lost after the formation of initial cross-link on the most exposed tyrosine.

Conclusion

Similar to the HRP induced cross-linking of low molar mass tyrosine containing substrates, oxidative cross-linking of proteins that contain accessible tyrosine can lead to formation of protein nanoparticles that contain oligo-tyrosine cross-links. Hence, the possibility of oligo-tyrosine cross-links should always be considered in addition to di-tyrosine cross-links for the case of oxidative enzymatic cross-linking of proteins.

Bibliography

[1] J. Buchert, D. E. Cura, H. Ma, C. Gasparetti, E. Monogioudi, G. Faccio, M. Mattinen, H. Boer, R. Partanen, E. Selinheimo, R. Lantto, and K. Kruus. Crosslinking food proteins for improved functionality. *Annu. Rev. Food Sci. Technol.*, 1:113–138, 2010.

[2] E. Özrenk. The use of transglutaminase in dairy products. *Int. J Dairy Technol.*, 59(1):1–7, 2006.

[3] T. Heck, G. Faccio, M. Richter, and L. Thöny-Meyer. Enzyme-catalyzed protein crosslinking. *Appl. Microbiol. Biotechnol.*, 97(2):461–475, 2013.

[4] T. DiMarco and C. Giulivi. Current analytical methods for the detection of dityrosine, a biomarker of oxidative stress, in biological samples. *Mass Spectrom. Rev.*, 26(1):108–120, 2007.

[5] D. A. Malencik and S. R. Anderson. Dityrosine formation in calmodulin: Cross-linking and polymerization catalyzed by arthromyces peroxidase. *Biochemistry*, 35(14):4375–4386, 1996.

[6] W. H. Heijnis, H. L. Dekker, L. J. de Koning, P. A. Wierenga, A. H. Westphal, C. G. de Koster, H. Gruppen, and W. J. H. van Berkel. Identification of the peroxidase-generated intermolecular dityrosine cross-link in bovine α-lactalbumin. *J. Agric. Food Chem.*, 59(1):444–449, 2010.

[7] G. Oudgenoeg. *Peroxidase Catalyzed Conjugation of Peptides, Proteins and Polysaccharides Via Endogenous and Exogenous Phenols*. PhD thesis, Wageningen University, Wageningen, The Netherlands, 2004.

[8] Y. Saricay, P. Wierenga, and R. de Vries. Nanostructure development during peroxidase catalysed cross-linking of α-lactalbumin. *Food Hydrocolloid*, 33(2):280–288, 2013.

[9] T. Fukuoka, Y. Tachibana, H. Tonami, H. Uyama, and S. Kobayashi. Enzymatic polymerization of tyrosine derivatives. peroxidase- and protease-catalyzed synthesis of polytyrosines with different structures. *Biomacromolecules*, 3(4):768–774, 2002.

[10] S. O. Andersen. The cross-links in resilin identified as dityrosine and trityrosine. *Biochim. Biophys. Acta - General Subjects*, 93(1):213–215, 1964.

[11] F. LaBella, F. Keeley, S. Vivian, and D. Thornhill. Evidence for dityrosine in elastin. *Biochem. Biophys. Res. Commun.*, 26(6):748–753, 1967.

[12] L.V. Lopez-Llorca and S.C. Fry. Dityrosine, trityrosine and tetratyrosine, potential cross-links in structural proteins of plant-parasitic nematodes. *Nematologica*, 35(2):165–179, 1989.

[13] F. Fenaille, V. Parisod, J. Vuichoud, J-C Tabet, and P. A. Guy. Quantitative determination of dityrosine in milk powders by liquid chromatography coupled to tandem mass spectrometry using isotope dilution. *J. Chromatogr. A*, 1052(1–2):77–84, 2004.

[14] D. Fujimoto, K. Horiuchi, and M. Hirama. Isotrityrosine, a new crosslinking amino acid isolated from ascaris cuticle collagen. *Biochem. Biophys. Res. Commun.*, 99(2):637–643, 1981.

[15] F. Hanft and P. Koehler. Quantitation of dityrosine in wheat flour and dough by liquid chromatography-tandem mass spectrometry. *J. Agric. Food Chem.*, 53(7):2418–2423, 2005.

[16] S. K. Dhayal, H. Gruppen, R. de Vries, and P. A. Wierenga. Controlled formation of protein nanoparticles by enzymatic cross-linking of α-lactalbumin with horseradish peroxidase. *Food Hydrocolloid*, 36:53–59, 2014.

[17] W. H. Heijnis, P. A. Wierenga, W. J. H. van Berkel, and H. Gruppen. Directing the oligomer size distribution of peroxidase-mediated cross-linked bovine α-lactalbumin. *J. Agric. Food Chem.*, 58(9):5692–5697, 2010.

[18] H. Pichorner, D. Metodiewa, and C. C. Winterbourn. Generation of superoxide and tyrosine peroxide as a result of tyrosyl radical scavenging by glutathione. *Arch. Biochem. Biophys.*, 323(2):429–437, 1995.

[19] B. J. H. Kuipers and H. Gruppen. Prediction of molar extinction coefficients of proteins and peptides using UV absorption of the constituent amino acids at 214 nm to enable quantitative reverse phase high-performance liquid chromatographymass spectrometry analysis. *J. Agric. Food Chem.*, 55(14):5445–5451, 2007.

[20] T. Michon, M. Chenu, N. Kellershon, M. Desmadril, and J. Gueguen. Horseradish peroxidase oxidation of tyrosine-containing peptides and their subsequent polymerization: A kinetic study. *Biochemistry*, 36(28):8504–8513, 1997.

[21] S. Podzimek. *Light scattering, size exclusion chromatography and asymmetric flow field flow fractionation,*. John Wiley & Sons, Hoboken, NJ, USA, 2011.

Chapter 4

Comparison of mesoscale structures of α-lactalbumin nanoparticles cross-linked with microbial transglutaminase and horseradish peroxidase *

Abstract

Enzymatic crosslinking of proteins may be a useful tool to modify the protein techno-functional properties. Since the different enzymes use different substrate amino acids, they are expected to form protein nanoparticles with different mesoscale structure. For instance, HRP induces crosslinks between tyrosine (4 in α-LA), and mTG between lysine and glutamine (12 and 6 respectively in α-LA). These differences in the number and their location in the crystal structure of target amino acids (Lys/Gln vs. Tyr) are expected to result in differences in the mechanism of growth (formation), as well as the mesoscale properties of the cross-linked α-LA particles made with either mTG or HRP. Differences in mesoscale structure are expected to be important for techno-functional properties such as water holding capacity. For both enzymes, the nanoparticle growth followed a step growth mechanism. Initially, oligomers ($0.0142 < M_w < 1$ MDa) were formed, which were further cross-linked in later stage to form polymers ($M_w > 1$ MDa). Still, significant differences were observed in the mesoscale structure. The density of nanoparticles of $R_h \approx 100$ nm was almost two times higher for α-LA/mTG (22 kg m^{-3}) than the α-LA/HRP. The denser structure was also confirmed by the

*S. K. Dhayal, R. J. de Vries, H. Gruppen, P. A. Wierenga.

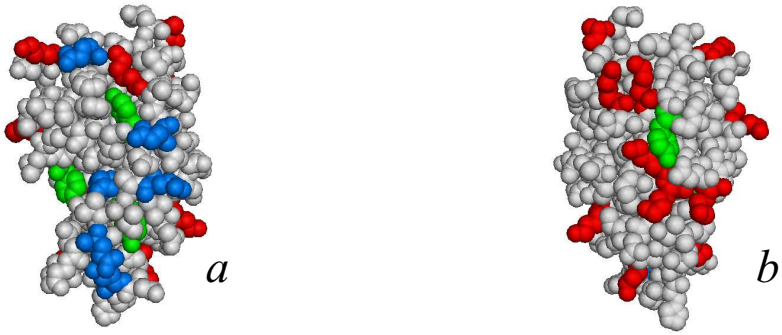

Figure 4.1: *Crystal structure of bovine apo α-LA visualised with PyMol (PDB accession code: 1F6R). Highlighted amino acids are Tyr (green), Lys (red) and Gln (blue). The front (a) and back (b) views are shown.*

power law scaling exponent between R_g and M_w, which was 0.38 $\pm$ 0.05 and 0.57 $\pm$ 0.05 for α-LA/mTG and α-LA/HRP nanoparticles, respectively. The difference in density was also reflected by difference in water holding capacity, thermal stability as well as by different swelling behavior of nanoparticles at ionic strengths < 1 mM.

Introduction

Food proteins have been cross-linked by different enzymes, to modify the protein techno-functional properties such as gelation, emulsion and foam stability etc. [1, 2]. The most commonly studied enzymes are the oxidative enzymes such as laccase, tyrosinase, peroxidase and the transferase enzyme, transglutaminase [2]. Since in these reactions covalent intermolecular bonds are formed, in essence it is similar to a polymerization reaction, where the protein is the monomeric unit of the finally formed cross-linked polymer. At the same time, intramolecular bonds (within each protein monomer) can also be formed. Consequently, the properties of the polymers (nanoparticles) will depend on the size, the shape, but also other structural properties, such as the number (and distribution) of inter- and intramolecular cross-links. This will depend on the combination of enzyme and substrate. For instance, α-lactalbumin (α-LA) has 12 Lys and 6 Gln, which are the substrates for cross-linking by mTG [3,4]. At the same time, it has only 4 Tyr, which are the substrates for HRP [5]. In addition, Lys and Gln are typically more accessible (solvent exposed) than Tyr (figure 4.1), even in the molten globule state of the apo α-lactalbumin. Transglutaminase induced cross-linking was shown to improve the water holding capacity of acid milk gels and was linked to the differences of gel micro-structure [6]. It may consequently be expected that using mTG and HRP for the cross-linking, different structures are obtained, which in turn will lead to differences in the techno-functional properties, such as water holding capacity. Most of the work on enzymatic cross-linking of pro-

teins has so far focused on either the bio-chemical details at molecular scale or the final (end use) functionality at the macroscale such as gelation. However, the details at the intermediate scale i.e. mesoscale ($5 - 500$ nm) are not extensively described and hence the link between molecular and macroscale is also not well understood. For example, in the case of α-LA, it is not known if the differences in the accessibility and number of substrate amino acids would lead to a similar or a different process of polymerization. Further, it is also not known if the process of polymerization influences the mesoscale structures that are formed. In the case of heat induced protein aggregation, the macro-scale functionality was found to be linked to the meso-scale structural details [7]. It remains to be seen if a similar correlation also exists for the case of enzymatically cross-linked protein polymers (particles). The polymerization in the case of enzymatic cross-linking could either proceed as chain growth or as step growth. In chain growth, a monomer is linked to an existing oligomer and grows to form polymers. While, in step growth kind of mechanism, initially all the monomers react to form oligomers and then oligomers react in next step to form polymers. The knowledge of the reaction mechanism can then be used for controlling the molar mass (M_w) of the nanoparticles. The mechanism of a reaction is identified from the degree of polymerization ($= M_w^{\text{poly}}/M_w^{\text{mono}}$) as a function of the monomer conversion. In the case of chain growth, the molar mass increases steadily with conversion while in the case of step growth high molar mass polymers are obtained only at very high conversions.

When considering the structure of the protein nanoparticles, it is important to realise that term structure may cover different aspects of the particle. Firstly, a distinction can be made between the static properties (e.g. when in solution), and the dynamic properties (e.g. compressibility). The static properties may include parameters, such as size, shape, density, or secondary/tertiary structure of the protein (monomer) in the particle [8]. The shapes can be sphere, rod, coil or a branched coil [7]. The branched coils can vary in size and density depending on the degree of branching and distribution of branches [9]. The dynamic properties describe how the structure of particles varies when they are subjected to external stresses. For example, when they are compressed at an interface during area change in a Langmuir trough. The change in particle structure when subjected a change of pH or ionic strength of the solution describes their softness. The dynamic structure (softness) of the particles is expected to depend on the details of cross-link density i.e. the number of cross-links per particle. The secondary structure of α-LA molecules in the nanoparticles may also change as a result of extensive cross-linking and that could affect their dynamic structure. Hence, the structure of nanoparticles is studied at different levels in this chapter. Furthermore, the mesoscale structure of α-LA/mTG nanoparticles will be compared with that of α-LA/HRP.

Materials and methods

Materials

α-Lactalbumin (α-LA) was obtained from Davisco Foods International, (Le Sueur, MN, USA). The protein content was 95 % (w/w) dry basis, as determined by DUMAS (N $\times$6.25) [10]. The conversion factor of 6.25 was calculated based on the primary sequence of α-LA obtained from the uniprot database (www.uniprot.org; entry P00711). Of the total proteins, 90 % was α-LA [10], of which 80 % (mol/mol) was in calcium free apo form [11]. Microbial transglutaminase (mTG), sold as ActivaR-YG was procured from Ajinomoto Foods (Paris, France). It is derived from *Streptoverticillium mobaraense* and is supplied as a powdered mixture containing approximately 99% maltodextrin + lactose and 1% mTG (suppliers information). Horseradish peroxidase (HRP) was obtained from Sigma (P6782, Peroxidase type VIA). Dithiothreitol (DTT), N-carbobenzoxy-L-glutaminyl-glycine (Nα-CBZ-Gln-Gly), 2,2-azinobis-3-ethylbenzothiazoline-6-sulfonic acid (ABTS), and hydroxylamine hydrochloride were procured from Sigma. All other chemicals used were of analytical grade.

Purification of mTG

To remove maltodextrin, lactose and other minor impurities, commercial mTG was purified by ion-exchange using a method adapted from [12]. The main differences in the method and conditions were that purification was done at 4 °C using StreamlineTM, SP XL in a batch mode and the enzyme was eluted using a 500 mM sodium acetate buffer (pH 8.0) which also contained 1M sodium chloride (NaCl). The eluted enzyme was diafiltered (Amicon Millipore, MA, USA) to remove excess salts using a regenerated cellulose membrane of 10 kDa cut-off (Millipore) and 100 mM sodium phosphate buffer, pH 7.0; 4 °C. The concentration of the purified enzyme (37.8 kDa) was determined spectrophotometrically using $\epsilon_{280} = 74025$ M^{-1} cm^{-1} [13].

Enzyme activity

The activity of purified mTG was measured at pH 7.0 and 37 °C following a modified colorimetric hydroxamate procedure [14]. The substrate, Nα-CBZ-Gln-Gly was used at a concentration of 3 mM. The product (CBZ-Gln-Gly-hydroxamate) formed was determined from the absorbance measured at 525 nm ($\epsilon = 0.47$ μmol^{-1} cm^{-1}). HRP was used as received and its activity was measured in 0.1 M ammonium acetate at pH 7.0 $\pm$ 0.2 and 37 °C using the ABTS assay [11]. The formed product (oxidised ABTS) was determined from the absorbance measured at 405 nm ($\epsilon = 36.8$ $mmol^{-1}$ cm^{-1}). The specific catalytic activity of both enzyme preparations is expressed as kat mg^{-1}, where one katal (kat) is one mole of product formed per second under specified conditions [15]. The enzyme activities were found to be 4.7 $\pm$ 0.4 nkat mg^{-1} and 10.9 $\pm$ 0.6 μkat mg^{-1} for mTG and HRP, respectively.

Cross-linking reaction

Sample preparation

All solutions were prepared in Milli-Q water (18.2 MΩ cm). For all the reactions, α-LA solutions of 30 g L^{-1} were prepared by mild stirring followed by centrifugation (40,000 g, 1 h, 20 °C) and filtration of supernatant over a 0.2 μm polyethersulfone membrane syringe filter (type: SY25PL-S, Advanced Microdevices, Ambala, India). For both enzyme systems, the pH of the reaction mixtures was maintained at 7.0 ± 0.2 using 0.1 M sodium phosphate buffer for mTG and 0.1 M ammonium acetate for HRP reactions. The cross-linking of α-LA with mTG or HRP was performed at 37 °C using an α-LA : enzyme ratio of 20:1 (w/w) corresponding to a molar ratio of 62 α-LA : HRP and 53 α-LA : mTG. Since α-LA has 12 Lys, 6 Gln and only 4 Tyr, the molar ratio of enzyme to total substrate amino acids is around 4 mmole HRP/mole Tyr and 1 mmole mTG/mole (Lys+Gln). The protein concentration was determined using the reported molar extinction coefficients of the proteins, i.e. ϵ_{280} = 28460 M^{-1} cm^{-1} for α-LA (www. uniprot.org, entry: P00711), ϵ_{280} = 74025 M^{-1} cm^{-1} for mTG [13] and ϵ_{403} = 112000 M^{-1} cm^{-1} for HRP [16].

α-LA/mTG cross-linking reaction

Cross-linking of α-LA with mTG was performed in 100 mL capped glass bottles that were kept in an oven maintained at 37 °C. The solutions were mixed using a magnetic stirrer. Samples were taken out at various time points (1, 5, 20, 30, 40, 50 and 72 h). The mTG was inactivated by heating the solution at 95 °C for 5 minutes. It was verified using dynamic light scattering (DLS) and asymmetrical flow field flow fractionation (AF4) that the heat treatment at 95 °C for 5 minutes did not result in changes in hydrodynamic radius (R_h) or radius of gyration (R_g) or M_w.

α-LA/HRP cross-linking reaction

The cross-linking of α-LA with HRP was performed as described before [10]. A solution of α-LA and HRP was incubated at 37 °C in a jacketed glass vessel with continuous stirring. A computer controlled syringe pump was programmed to dose 2 μL of a 50 mM H_2O_2 solution per mL of the reaction volume at set intervals (t = 210 s). Samples were taken after different numbers of H_2O_2 additions (n_{H2O2} = 1, 3, 5, 10, 20, 35, 85, 120 and 180).

Storage and use of α-LA nanoparticles

At the end of cross-linking, the large scale (100 mL) samples were mixed with equal volumes of 1 M sucrose and frozen. The frozen sample was subsequently freeze-dried and stored at -20 °C [10]. Before use, the freeze-dried powder was reconstituted in 10 mM sodium phosphate buffer, pH 7.0 and then extensively dialysed with a 300 kDa regenerated cellulose membrane [10]. The protein concentration of the dialysate (% N ×6.25), was determined by the Dumas method [17]. These samples were used for

CD, AF4, swelling, water holding capacity and thermal stability experiments. The samples collected at various time points were not freeze-dried and used directly in AF4 to determine the conversion, molar mass and size.

Dynamic light scattering (DLS)

To follow the rate of nanoparticle formation, the crosslinking experiments were also performed in a home built set-up at 5 mL scale and monitored online using DLS (for details see [18]). The scattered light intensity was measured at 90° and the R_h distribution was obtained using the regularization method utilizing CONTIN routine and Stokes-Einstein equation [9]. All other DLS measurements were performed using a zeta sizer (λ = 633 nm, Nano ZS, Malvern Instruments, Malvern, UK) following the method described previously [10]. Samples were diluted in a 10 mM phosphate buffer at pH 7.0 to yield a concentration of around 0.1 g L^{-1} and the intensity of scattered light was measured at 173°. The z-average R_h was obtained from the intensity weighted size distributions using the zeta sizer software (Malvern).

Asymmetric flow field flow fractionation (AF4)

Cross-linked nanoparticle mixtures were separated using an asymmetric flow field flow fractionation (AF4) as described before [10] . The AF4 instrumentation comprised of an Eclipse Dual tech (Wyatt Technology, Santa Barbara, CA, USA) linked to a HPLC unit (Ultimate 3000, Dionex/Thermo Fisher Scientific, Sunnyvale, CA, USA) with UV diode array detector and a multi-angle light scattering (MALS, Dawn Heleos-II, λ = 665 nm, 130 mW Laser), RI detector (Optilab T-rEX), flow cell (short flat channel, 145 mm length). The flat channel was fitted with a spacer (type W, 350 μm) and a membrane (10 kDa regenerated cellulose, Millipore PLGC), procured from Wyatt Technology. The pump flow rate was controlled by the Eclipse separation system using the Chromeleon software. Data collection and analysis were done with ASTRA-6 software (Wyatt Technology). The detector flow rate was kept constant at 1 mL min^{-1}, while elution was done under varying cross flow rate (V_x). At the start of elution, V_x was kept constant at 2 mL min^{-1} for 5 min and then exponentially decreased from 2 to 0.1 mL min^{-1} with a decay time constant of 5 min. The exponential decay was achieved by 22 linear decays of 1 min duration each. Then, V_x was kept constant at 0.1 mL min^{-1} for 5 minutes, and then at 0 mL min^{-1} for 10 minutes. The refractive index (RI) was used to fit the molar mass distribution using a dn/dC value of 0.185 mL g^{-1} [19]. Light scattering signals from the most precise angles between 29.6° to 140° were used for the extrapolation using 1^{st} order fits with Berry formalism to obtain M_w and R_g [9, 20]. The data for R_g of the monomeric α-LA was taken from [21]. Further, the apparent density (ρ_{app}) was calculated using fitted M_w and R_g. The fractal dimension (d_f) [22, 23] was obtained in two different ways. First, from the scaling of M_w and R_g (referred to as low q) i.e. $d_f = 1/\nu$, where ν is the scaling exponent obtained from $R_g \sim M_w^{\nu}$. Second, from the angular dependence of scattered light intensity when $qR_g > 1$ (referred to as high q) [10]. The

RI fractograms were integrated between 1 to 40 minutes to obtain the total amount of protein eluting from the flow cell. Based on the elution profile and molar mass of the formed nanoparticles, a distinction is made between oligomers and polymers. The fractograms were further divided into three sections i.e monomers (1 to 2 min., 0.0142 MDa), oligomers (2 to 10 min., $0.0142 MDa < M_w < 1$ MDa) and polymers (10 to 40 min., $M_w > 1$ MDa). The integrated area in each section was then divided by the total area to obtain the fraction of protein in each section. The fraction of monomeric protein left after certain time of reaction with the original (starting) amount of monomeric protein is defined as conversion (%). The conversion of monomeric α-LA into oligomers and polymers is used to quantify the extent of the reaction. To indicate the number of α-LA monomers cross-linked per nanoparticle, the degree of polymerisation (DP) is calculated by dividing the M_w of α-LA nanoparticles by the M_w of monomeric α-LA (14.2 kDa). The samples were analysed in duplicates and the average of these is reported with standard deviations. The standard deviation in d_f was obtained from the variation of d_f in nanoparticles obtained at various conversions.

Circular Dichroism (CD)

The secondary and tertiary structure of monomeric and crosslinked α-LA were determined using far and near ultraviolet (UV) circular dichroism (CD), respectively and the analysis method was adapted from [11]. The mean residue ellipticity at wavelength λ ($[\theta]_{MRE,\lambda}$) was calculated from the measured ellipticity at that wavelength (θ_λ, degrees) using the equations described in [24]. The secondary structure was quantified by using Dichroweb online server [25]. The data were fitted using various algorithms such as CONTIN, CDSSTR, SELCON 3, K2D [26–28]. For each algorithm, the reference protein data used were set 4, 7 and SP175 [28, 29]. Spectra were not corrected for scattering artefacts; the normalized root-mean-square deviations (NRMSD) were between 0.04 and 0.3. The near UV spectra in the wavelength range $290 - 305$ and $275 - 282$ nm are due to Trp and Tyr, respectively [24]. A change in spectra around 294 and 275 nm indicates a change in the mobility or dielectric environment of Trp and Tyr [24]. The secondary structure content shown is the average ($\pm$ standard deviation) of all the analyses. The maximum error in the estimation of secondary structure is around 20 %, hence, a change in secondary structure content is statistically significant only if it is > 20 %.

Swelling, water holding capacity, thermal stability

To test if some bulk techno-functional properties are affected by the differences in the mesoscale structure, the swelling, water holding capacity and thermal stability of α-LA/mTG ($R_h = 60$ nm) and α-LA/HRP ($R_h = 65$ nm) nanoparticles were investigated. Swelling was studied by measuring the changes in R_h when the ionic strength was varied. The nanoparticle samples were dialysed against MQ water and then diluted to a concentration of 0.1 g L^{-1} with MQ-water (ionic strength, I $\approx$ 0.001 mM), sodium phosphate buffer (I = 0.001, 0.25. 2.5 and 25 mM) and sodium phosphate

buffer + NaCl (I = 125, 500 and 1000 mM) at pH 7.0. Then the R_h at a given ionic strength was measured using DLS.The dialysed samples were diluted to a concentration of 1 g L^{-1} using a 10 mM sodium phosphate buffer, pH 7.0 for water holding capacity and thermal stability measurements. For water holding capacity experiment, 15 mL of solution was transferred to an Amicon-Ultra15 tubes fitted with regenerated cellulose membrane of 100 kDa cut-off (Merck Millipore, Cork, Ireland). The tubes were centrifuged (4000 g; 20 °C). The centrifuge was stopped at different time points to weigh the filtrate. The differences in the filtrate volume versus time curves are used as indicators of the differences in water holding capacity of the nanoparticles. For thermal stability, 1 mL of solution was heated at 90 °C in a glass cuvette placed inside the DLS. Simultaneously, change in R_h over a period of one hour was measured. No change in the R_h indicates high thermal stability of nanoparticles i.e. they do not undergo any major structural change upon heating.

Results and discussion

Nanoparticle formation

The radius of gyration (R_g) and hydrodynamic radius (R_h) of monomeric apo α-LA are similar and around 2 nm (table 4.1). After the longest time of incubation with mTG, the R_g and R_h increase up to 146 nm and 100 nm, respectively (table 4.1). The AF4 under dissociating and reducing conditions (data not shown) also proves that the nanoparticle formation takes place solely by covalent cross-linking in both enzyme systems. The AF4 fractograms (figures 4.2a, 4.2b) indicate that monomers are lost during the course of cross-linking, reaching a conversion of around 95 % at the end of reaction for the α-LA/mTG system.

Until a conversion of 80 % mainly oligomers were formed. The polymeric peaks start to appear only at conversions beyond 85 %. For the α-LA/HRP system, the AF4 fractograms (figure 4.2c, 4.2d) indicate that monomers reach a conversion of around 85 % at the end of cross-linking reaction. Similar as for mTG, initially the oligomers were formed until a conversion of 80 % and the polymeric peaks start to appear only at conversions beyond 80 %. The values of conversion at the end of cross-linking are different for the two systems, indicating that mTG also cross-links a significant fraction of the 20 % holo α-LA present in the starting mixture. During the initial stage of cross-linking, the decrease of monomeric α-LA corresponds to an increase of oligomers ($0.0142 < M_w < 1$ MDa) (figure 4.3a). There are no large molar mass nanoparticles present during this stage. In the second stage (conversion > 80 %) there is a decrease in the area under the curve of oligomers and an increase of high molar mass polymers ($M_w > 1$ MDa). For conversion up to 80%, the degree of polymerisation is not more than 100, while DP > 10000 is reached for conversion between 80 to 95 % (figure 4.3b). The formation of ultra-high molar mass polymers only towards very high conversions (> 80 %) indicates a mechanism similar to step-growth polymerization.

Two distinct stages in the process of α-LA/mTG nanoparticle formation were also

Table 4.1: *Comparison of $\alpha-LA/mTG$ and $\alpha-LA/HRP$ nanoparticles made from 30 g L^{-1} $\alpha-LA$ at pH 7. The parameters described are hydrodynamic radius (R_h), radius of gyration (R_g), weight averaged molar mass (M_w), apparent density (ρ_{app}) based on R_g, degree of polymerisation (DP), R_g to M_w scaling exponent (ν) and fractal dimension (d_f).*

	R_h (nm)	M_w (MDa)	R_g (nm)	ρ_{app} (kg/m^3)	R_g/R_h (-)	DP	ν (-)	d_f (low q)	d_f (high q)
Apo α−LA	2 ±0.1	0.0142	1.72 *	1106	0.86	1	-	-	-
α−LA/mTG	30 ±1 44.5 ±1 60 ±1.8 77 ±1.5 100 ±2.5	3.2 ±0.1 31.7 ±1.1 65.7 ±1.9 102 ±3.5 168.6 ±5.1	39.8 ±0.7 81.8 ±2.3 105 ±1 117.2 ±1.6 145.6 ±1.7	20 ±0.7 22.4 ±1.2 22.5 ±0.5 25 ±0.8 21.6 ±0.6	1.3 1.8 ±0.1 1.7 1.5 1.5	227 ±6 2227 ±68 4617 ±116 7167 ±214 11846 ±312	0.38 ±0.05	2.7 ±0.5	2.2 ±0.1
α−LA/HRP	20 ±1 35 ±1.3 65 ±1 90 ±2	2.1 ±0.01 13.8 ±0.04 111.8 ±3.8 161.7 ±7.7	20.8 ±0.8 66.4 ±0.4 167 ±2 182.3 ±2.3	88.4 ±5.6 18.6 ±0.2 9.5 ±0.3 10.6 ±0.4	1.0 1.9 ±0.1 2.6 2.0	149 ±1 975 ±2 7855 ±236 11345 ±476	0.57 ±0.05	1.8 ±0.2	2 ±0.1

* Data taken from reference [21].

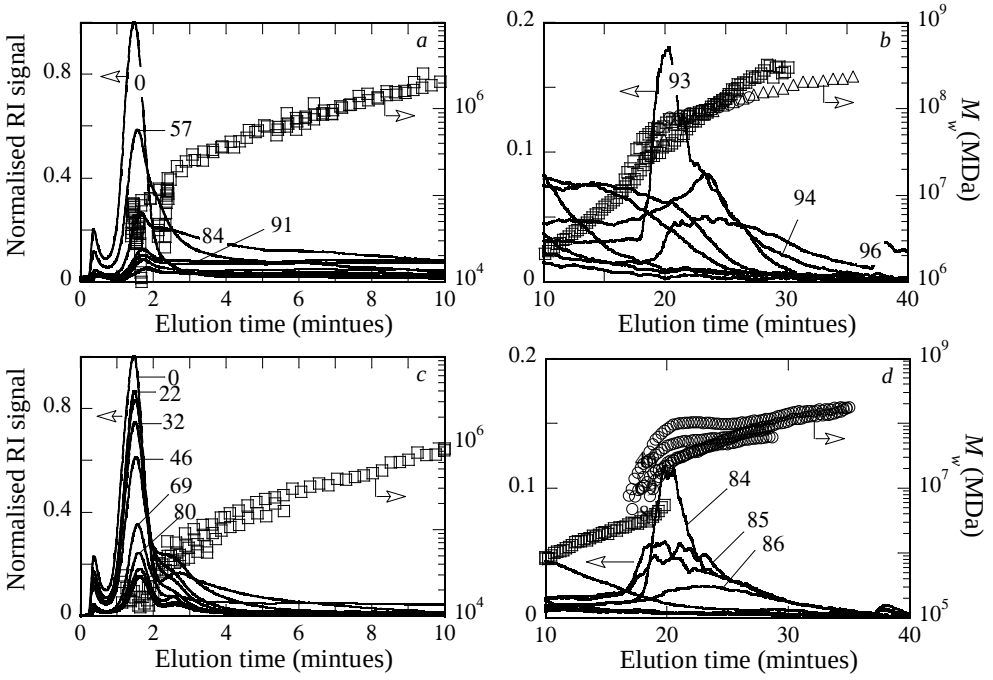

Figure 4.2: *AF4 fractograms of α-LA/mTG nanoparticles (a, b) and α-LA/HRP nanoparticles (c, d). The markers represent the fitted M_w for sample with increasing conversion of monomeric α-LA (% conversion is labelled for each curve).*

observed in DLS (figure 4.4a). In the first stage ($0 - 40$ h), the R_h of nanoparticles increases to around 45 nm and in the second stage ($40 - 72$ h), the increase in R_h is much faster and it reaches a value of 110 nm. The intensity weighted size distribution for the selected points (a-e) from figure 4.4a can be seen in figure 4.4b. A similar two-stage mechanism of nanoparticle formation in DLS was observed for cross-linking of α-LA with HRP (chapter 2). Crosslinking of α-LA with HRP led to a small increase of R_h to around 10 nm during the initial 1 hour (20 H_2O_2 additions) and then the R_h started to increase rapidly with the subsequent additions of H_2O_2 and reached a value around 100 nm after 10 hours of reaction (180 H_2O_2 additions). The overall mechanism of nanoparticle formation (growth) as monitored by DLS seems to be similar for both enzyme systems. The two step polymerization process concluded from AF4 matches earlier conclusions [18] on cross-linking of α-LA with HRP, where size exclusion chromatography was used for separating the early stage nanoparticles.

The R_h versus time curves obtained from DLS in the case of enzymatic cross-linking seem similar to that of heat-induced aggregation of β-lactoglobulin [30]. The AF4 and DLS results clearly indicate that for both enzymes the nanoparticle form-

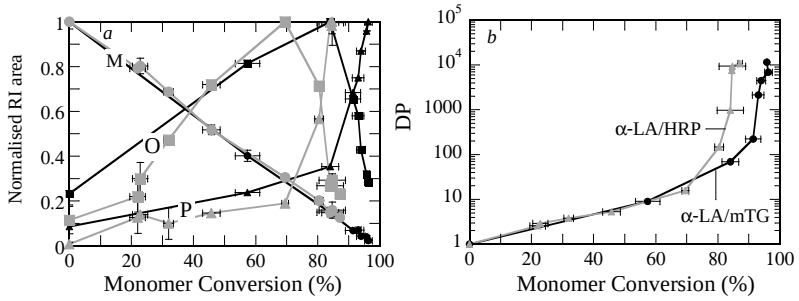

Figure 4.3: *Conversion curve of monomers (M), oligomers (O) and polymers (P) of α-LA /mTG (black) and α-LA /HRP (grey) samples (a). Degree of polymerisation (DP = M_w/ M_w,α-LA) versus conversion of monomeric α-LA for α-LA /mTG (black) and α-LA /HRP (grey) nanoparticles (b).*

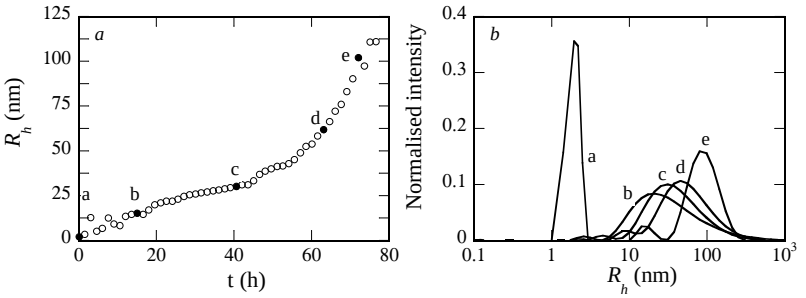

Figure 4.4: *Kinetics of α-LA/mTG nanoparticle formation depicted by increase of hydrodynamic radius (R_h) with time (a). The intensity weighted R_h distribution of selected data points (a-e) i.e. the filled symbols (b).*

ation proceeds in same way despite the fact that both enzymes induce cross-linking by different biochemical mechanisms and are known to target different amino acids. This shows that the nanoparticle growth mechanism is not dependent on the number and accessibility of target amino acids.

Mesoscale structure

The mesoscale structure of nanoparticles is evaluated at two different levels i.e. at monomer level and at the particle level. The near UV CD spectra of apo α-LA (monomeric) before and after enzymatic cross-linking are given in figure 4.5a. The α-LA monomer in the HRP and mTG nanoparticles shows a decrease of the mean residue ellipticity (MRE) from 250 to less than 100 deg cm^2 $dmol^{-1}$ at wavelength around 275 nm, and the peak at 294 nm is absent. This indicates absence of tertiary

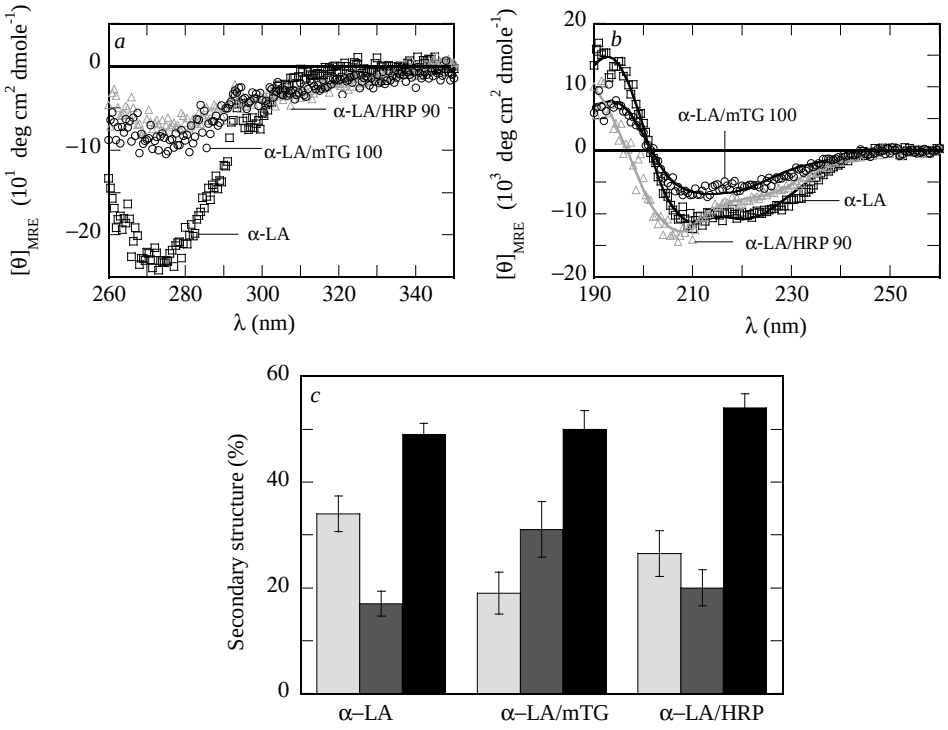

Figure 4.5: *Near UV (a) and far UV (b) CD spectra indicating variations in tertiary and secondary structure for α-LA (□) and α-LA /mTG (R_h = 100 nm, ○), α-LA /HRP (R_h = 90 nm, △) nanoparticles. The solid curves in (b) are the CONTIN fit. The secondary structure composition obtained from fitting the far UV CD spectra is given in (c); α-helix (light grey), β-sheet (dark grey) and turns + unordered (black).*

structure in α-LA monomer in the nanoparticles after enzymatic cross-linking. The far UV CD spectra of apo α-LA, α-LA/mTG and α-LA/HRP nanoparticles and the secondary structure fits are given in figures 4.5a and figure 4.5b, respectively. The fraction of α-helix after cross-linking with mTG is reduced by 44 % while in the case of HRP it decreased by only 23 %. The fraction of β-sheets after cross-linking with mTG increased by 82 % while there was no significant change in the case of HRP. The unordered fraction did not change significantly in both cases. Hence, two things were concluded from CD data; 1) even after extensive cross-linking, there is a significant amount of secondary structure present in both cases but it is different from the composition of α-LA before cross-linking and 2) the unordered content in α-LA/HRP nanoparticles is slightly more than that of α-LA/mTG.

At nanoparticle level, the structure was described by the power law exponent of scaling of R_g with M_w and the apparent density of the nanoparticles. The size to mass scaling exponent (ν) for α-LA/HRP and α-LA/mTG nanoparticles is 0.57 $\pm$ 0.05 and 0.38 $\pm$ 0.05, respectively (table 4.1 and figure 4.6a). This indicates that the α-LA/mTG nanoparticles are more branched (dense) than α-LA/HRP nanoparticles. This was also confirmed by the d_f (low q) obtained from size to mass scaling, which was 1.8 $\pm$ 0.2 and 2.7 $\pm$ 0.5 for α-LA/HRP and α-LA/mTG nanoparticles, respectively (table 4.1). The d_f (high q) obtained from the angular dependence of light scattering were 2.0 $\pm$ 0.1 and 2.2 $\pm$ 0.1 for α-LA/HRP and α-LA/mTG nanoparticles, respectively (table 4.1, figure 4.6b). It can be concluded that both type of nanoparticles have a fractal structure. But, the differences between d_f obtained from low and high q indicate that they are not self-similar at all length scales. The size to mass scaling exponent is very sensitive to branching and the exponent can approach values around 0.33 with increasing degree of branching. Typically, the exponent of 0.33 indicates a solid sphere with d_f of 3, yet a highly branched fractal aggregate with $d_f < 3$ can also exhibit the same exponent. The fractal nature of the nanoparticles is also evident from the ratio of R_g/R_h, which changes from around 1 for small to around 2.5 for large nanoparticles (table 4.1). The $R_g/R_h > 1$ is typically displayed by many fractal aggregates ([31]).

Another parameter for differentiating the two types of nanoparticles is their apparent density. The α-LA/HRP nanoparticles have an apparent density of around 10 kg m^{-3} for $R_g > 100$ nm (table 4.1). The apparent density of α-LA/mTG nanoparticles of $R_g > 100$ nm is on an average around 22 kg m^{-3}. In conclusion, the mesoscale structure of both types of nanoparticles can be described as fractal type but with the differences in the degree of branching (density). The α-LA/mTG nanoparticles are denser than α-LA/HRP nanoparticles. The number and accessibility of target amino acids seem to be correlated with the apparent density of the nanoparticles.

Link between structure and nanoparticle properties

The α-LA/mTG and α-LA/HRP nanoparticles exhibit a constant R_h for regular ionic strengths (> 0.01 mM). Surprisingly, at very low ionic strength there is a significant increase in R_h, which is much higher for α-LA/HRP than for α-LA/mTG nanoparticles

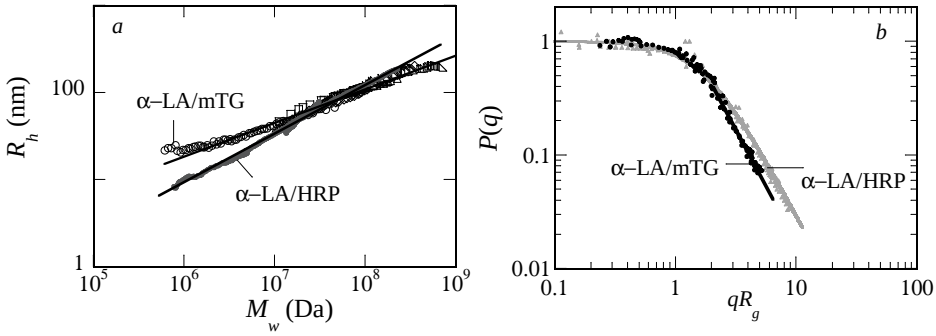

Figure 4.6: *Scaling of size versus mass for the α-LA/mTG (black, power law scaling exponent, $\nu = 0.38$, $R^2 = 0.98$) and α-LA/HRP (grey, $\nu = 0.57$, $R^2 = 0.99$) nanoparticles described in table 4.1 . Particle scattering factor, $P(q)$ versus qR_g for the samples described in table 4.1. The thin lines are power law fit for α-LA/mTG ($n = 2.2$, $R^2 = 0.99$) and α-LA/HRP ($n = 2.0$, $R^2 = 0.99$) nanoparticles and the thick grey line is a fit represented by $P(q) = \left(1 + \left(qR_g^2\right)/3\right)^{-1}$.*

(figure 4.7a). The R_h of both types of nanoparticles remains unchanged at around 60 nm in the ionic strength range of 10 to 1000 mM, while it increases below 10 mM. When the ionic strength is < 0.001 mM, the R_h of α-LA/HRP nanoparticles increases much more than that of α-LA/mTG nanoparticles. At ionic strength of around 0.001 mM, the R_h is 140 and 90 nm for α-LA/HRP and α-LA/mTG nanoparticles, respectively. Hence, the α-LA/HRP nanoparticles swell more than α-LA/mTG nanoparticles and this is correlated with more open type of structure for the former.

There was also a significant difference in the water holding capacity of these two types of nanoparticles as indicated by the amount of buffer centrifuged out as a function of centrifugation time for the two types of nanoparticles at the same ionic strength (25 mM) (figure 4.7b). In the case of buffer (without protein) and monomeric α-LA, all the water is centrifuged out within 2 and 5 minutes, respectively. For the same centrifugal force, much less water is centrifuged out in the case of nanoparticle solutions. In first two minutes, around 2 g of water was centrifuged out of nanoparticle solutions as compared to 14 g in the case of only buffer. When the two types of nanoparticles are compared, the amount of water centrifuged out of α-LA/mTG solution at any given point of time is more than that of α-LA/HRP solution. For example, after 5 minutes of centrifugation, 10 g of water was centrifuged out of α-LA/mTG solution as compared to only 7 g for α-LA/HRP solution. The differences in the water holding capacity seems correlated with the open versus compact mesoscale structure of the α-LA/HRP and α-LA/mTG nanoparticles, respectively. When heated at 90 °C for one hour, the R_h of α-LA/mTG nanoparticles remains constant while it decreases by 20 nm for α-LA/HRP nanoparticles (figure 4.7c). Hence, rigid (more dense) mesoscale structures may prevent the changes in nanoparticle structure

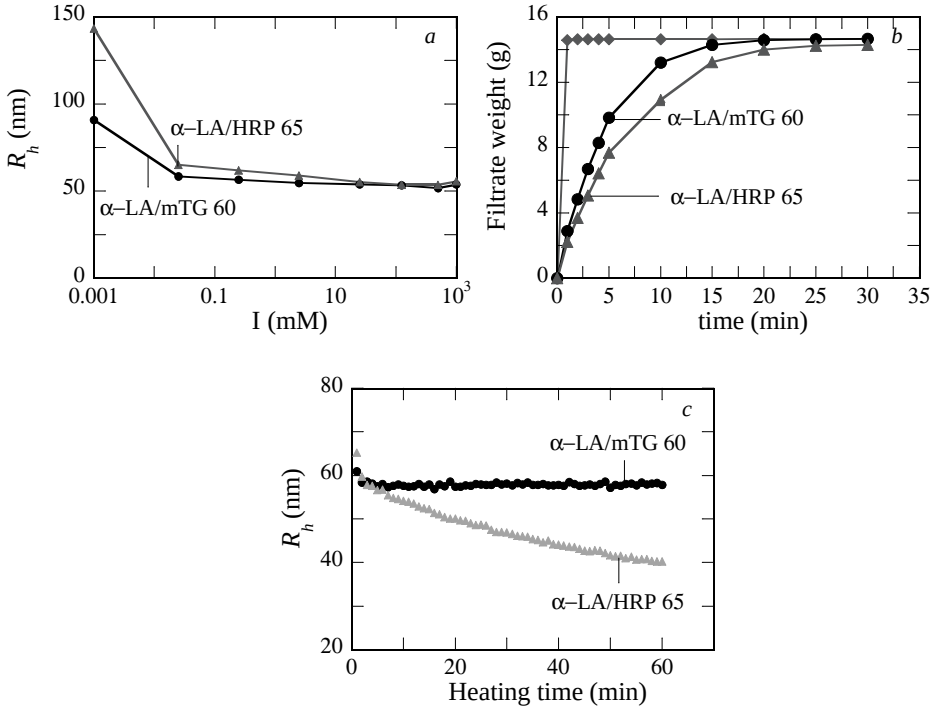

Figure 4.7: *Z-average R_h as a function of ionic strength (a), water holding capacity as indicated by the amount of water that can be centrifuged out at a fixed rotational speed from a solution of 1 g L^{-1} nanoparticles (b) and thermal stability at 90 °C (c) for α-LA/mTG ($R_h = 60$ nm) and α-LA/HRP ($R_h = 65$ nm) nanoparticles. Only 10 mM sodium phosphate buffer ($pH = 7.0$) is represented by filled diamond in b.*

at high temperatures and this can partly explain the stability of α-LA/mTG nanoparticles. In conclusion, the R_h decrease during heating of open type of α-LA/HRP nanoparticles indicates that the cross-link network is weaker in this case, while more dense type of α-LA/mTG nanoparticles have a stronger network. Hence, there also seems to be a correlation between the mesoscale structure and the thermal stability of nanoparticles. The difference in structure seems to correlate with a difference in water holding capacity. In summary, both types of α-LA nanoparticles have a fractal nature but cross-linking with mTG results in more denser particles. It is important to note that the term denser is relative to the nanoparticles made with HRP and as such both types of nanoparticles are very dilute compared to some heat-induced protein particles. The structure/size of the nanoparticles changes a lot with low ionic strength. Upon short time heating, the particle size seem to be stable, although for extended heating, the α-LA/mTG nanoparticles are more stable. The differences in the mesoscale structure of the α-LA nanoparticles made with mTG and HRP are expected to lead to different techno-functional properties.

Conclusion

The mesoscale structure of protein nanoparticles can be controlled and modulated by enzymatic cross-linking. Protein nanoparticles with different mesoscale structures can be obtained from same protein by using enzymes that target different amino acids on that protein. The apparent density in combination with scaling of size and mass can be used for quantification of differences in mesoscale structure of protein nanoparticles. In enzymatic cross-linking of proteins, the mesoscale structure can be different despite a similar way in which the polymerization (nanoparticle formation) proceeds. There seems to be a strong correlation between the number/accessibility of target amino acids and the mesoscale structure of protein nanoparticles. The number and location of the target (substrate) amino acids in the protein can lead to varying density of these nanoparticles. There are indications that the functional properties of the protein nanoparticles are affected by the mesoscale structures of the nanoparticles.

Bibliography

[1] J. Buchert, D. Ercili Cura, H. Ma, C. Gasparetti, E. Monogioudi, G. Faccio, M. Mattinen, H. Boer, R. Partanen, E. Selinheimo, R. Lantto, and K. Kruus. Crosslinking food proteins for improved functionality. *Ann. Rev. Food Sci. Technol.*, 1(1):113–138, 2010.

[2] T. Heck, G. Faccio, M. Richter, and L. Thöny-Meyer. Enzyme-catalyzed protein crosslinking. *Appl. Microbiol. Biotechnol.*, 97(2):461–475, 2013.

[3] W. F. Nieuwenhuizen, H. L. Dekker, L. J. de Koning, T. Gröneveld, C. G. de Koster, and G. A. H. de Jong. Modification of glutamine and lysine residues in holo and apo α-Lactalbumin with microbial transglutaminase. *J. Agric. Food Chem.*, 51(24):7132–7139, 2003.

[4] R. Sharma, P. C. Lorenzen, and K. B. Qvist. Influence of transglutaminase treatment of skim milk on the formation of ϵ-(γ-glutamyl)lysine and the susceptibility of individual proteins towards crosslinking. *Int. Dairy J.*, 11(10):785–793, 2001.

[5] W. H. Heijnis, H. L. Dekker, L. J. de Koning, P. A. Wierenga, A. H. Westphal, C. G. de Koster, H. Gruppen, and W. J. H. van Berkel. Identification of the peroxidase-generated intermolecular dityrosine cross-link in bovine α-lactalbumin. *J. Agric. Food Chem.*, 59(1):444–449, 2010.

[6] D. Ercili-Cura, M. Lille, D. Legland, S. Gaucel, K. Poutanen, R. Partanen, and R. Lantto. Structural mechanisms leading to improved water retention in acid milk gels by use of transglutaminase. *Food Hydrocolloid*, 30(1):419–427, 2013.

[7] T. Nicolai and D. Durand. Controlled food protein aggregation for new functionality. *Curr. Opin. Colloid Interface Sci.*, 18(4):249–256, 2013.

[8] L. O. Narhi, J. Schmit, K. Bechtold-Peters, and D. Sharma. Classification of protein aggregates. *J. Pharm. Sci.*, 101(2):493–498, 2012.

[9] S. Podzimek. *Light Scattering, Size Exclusion Chromatography and Asymmetric Flow Field Flow Fractionation: Powerful Tools for the Characterization of Polymers, Proteins and Nanoparticles*. John Wiley & Sons, Hoboken, NJ, USA, 2011.

[10] S. K. Dhayal, H. Gruppen, R. de Vries, and P. A. Wierenga. Controlled formation of protein nanoparticles by enzymatic cross-linking of α-lactalbumin with horseradish peroxidase. *Food Hydrocolloid*, 36:53–59, 2014.

[11] W. H. Heijnis, P. A. Wierenga, W. J. H. van Berkel, and H. Gruppen. Directing the oligomer size distribution of peroxidase-mediated cross-linked bovine α-lactalbumin. *J. Agric. Food Chem.*, 58(9):5692–5697, 2010.

[12] R. Lantto, E. Puolanne, N. Kalkkinen, J. Buchert, and K. Autio. Enzyme-aided modification of chicken-breast myofibril proteins: Effect of laccase and transglutaminase on gelation and thermal stability. *J. Agric. Food Chem.*, 53(23):9231–9237, 2005.

[13] C. N. Pace, F. Vajdos, L. Fee, G. Grimsley, and T. Gray. How to measure and predict the molar absorption coefficient of a protein. *Protein Sci.*, 4(11):2411–2423, 1995.

[14] J. E. Folk and P. W. Cole. Mechanism of action of guinea pig liver transglutaminase .i. purification and properties of enzyme - identification of a functional cysteine essential for activity. *J. Biol. Chem.*, 241(23):5518–5525, 1966.

[15] Units of enzyme activity. *Eur. J. Biochem.*, 97:319–320, 1979.

[16] H. Pichorner, D. Metodiewa, and C. C. Winterbourn. Generation of superoxide and tyrosine peroxide as a result of tyrosyl radical scavenging by glutathione. *Arch. Biochem. Biophys.*, 323(2):429–437, 1995.

[17] H. A. Kosters, P. A. Wierenga, R. de Vries, and H. Gruppen. Characteristics and effects of specific peptides on heat-induced aggregation of β-lactoglobulin. *Biomacromolecules*, 12(6):2159–2170, 2011.

[18] Y. Saricay, P. Wierenga, and R. de Vries. Nanostructure development during peroxidase catalysed cross-linking of α-lactalbumin. *Food Hydrocolloid*, 33(2):280–288, 2013.

[19] H. Y. Zhao, P. H. Brown, and P. Schuckt. On the distribution of protein refractive index increments. *Biophysical J.*, 100(9):2309–2317, 2011.

[20] M. Andersson, B. Wittgren, and K-G. Wahlund. Accuracy in multiangle light scattering measurements for molar mass and radius estimations. Model calculations and experiments. *Anal. Chem.*, 75(16):4279–4291, 2003.

[21] M. Kataoka, F. Tokunaga, K. Kuwajima, and Y. Goto. Structural characterization of the molten globule of α-lactalbumin by solution x-ray scattering. *Protein Sci.*, 6(2):422–430, 1997.

[22] P. Aymard, D. Durand, T. Nicolai, and J. C. Gimel. Fractality of globular protein aggregates: From the molecular to the microscopic level. *Fractals*, 05(supp02):23–43, 1997.

[23] W. Burchard. *Light scattering in Physical techniques for the study of food biopolymers*. S.B. Ross-Murphy (Ed.), Blackie, Glasgow/London, UK, London, UK, 1994.

[24] S. M. Kelly, T. J. Jess, and N. C. Price. How to study proteins by circular dichroism. *Bba-Proteins Proteom.*, 1751(2):119–139, 2005.

[25] L. Whitmore and B. A. Wallace. DICHROWEB, an online server for protein secondary structure analyses from circular dichroism spectroscopic data. *Nucleic Acids Res.*, 32(suppl 2):668–673, 2004.

[26] M. A. Andrade, P. Chacon, J. J. Merelo, and F. Moran. Evaluation of secondary structure of proteins from uv circular dichroism spectra using an unsupervised learning neural network. *Protein Eng.*, 6(4):383–390, 1993.

[27] S. W. Provencher and J. Gloeckner. Estimation of globular protein secondary structure from circular dichroism. *Biochemistry*, 20(1):33–37, 1981.

[28] N. Sreerama and R. W. Woody. Estimation of protein secondary structure from circular dichroism spectra: Comparison of CONTIN, SELCON, and CDSSTR methods with an expanded reference set. *Anal. Biochem.*, 287(2):252–260, 2000.

[29] J. G. Lees, A. J. Miles, F. Wien, and B. A. Wallace. A reference database for circular dichroism spectroscopy covering fold and secondary structure space. *Bioinformatics*, 22(16):1955–1962, 2006.

[30] U. M. Elofsson, P. Dejmek, and M. A. Paulsson. Heat-induced aggregation of β-lactoglobulin studied by dynamic light scattering. *Int. Dairy J.*, 6(4):343–357, 1996.

[31] C. M. Sorensen. The mobility of fractal aggregates: A review. *Aerosol Sci. Technol.*, 45(7):765–779, 2011.

Chapter 5

Effect of mesoscale structure on rheological properties of enzymatically cross-linked α-lactalbumin nanoparticles *

Abstract

Cross-linking of α-lactalbumin (α-LA) with microbial transglutaminase (mTG) or horseradish peroxidase (HRP) was used to produce nanoparticles with different, i.e. compact and open, mesoscale structure. These protein nanoparticles were subsequently used to make a gel e.g. by concentrating the nanoparticle solutions (2-step gel). Alternatively, continuous enzymatic cross-linking of proteins would also lead to a gel if there is sufficient amount of protein present (1-step gel). The aim of this chapter is to investigate a) the effect of differences in mesoscale structure of protein nanoparticles on bulk rheology of 2-step gels. and b) the differences in rheological properties of 2-step versus 1-step gels (made by continuous mTG cross-linking). For both particles, the jamming concentration was determined by measuring the storage modulus ($G^{'}$), loss modulus ($G^{''}$) and shear viscosity (η) as a function of concentration. The differences in particle structure were reflected by their rheological properties. The jamming concentration for α-LA/mTG nanoparticles (R_h = 60 nm) was 50 $\pm$ 5 g L^{-1} as compared to 40 $\pm$ 5 g L^{-1} for α-LA/HRP (R_h = 65 nm). The power law exponent of $G^{'}$ versus concentration curve is much higher (n = 18.7) for α-LA/mTG while n = 5.26 for α-LA/HRP nanoparticles. Another difference between the α-LA/mTG and α-LA/HRP nanoparticles is that the former shows more hysteresis in flow curves. There were no major differences between the rheological properties

*S. K. Dhayal, Y. Saricay, R. J. de Vries, P. A. Wierenga, H. Gruppen.

of α-LA/mTG 1-step and 2-step gels.

Introduction

Rheological modifications of ingredients leading to improved techno-functional properties, such as an increase of viscosity or formation of a gel, are often desired in food applications [1]. The rheological properties of protein solutions can be changed e.g. by heating or by enzymatic cross-linking [2–4]. Heat aggregation of whey proteins to a size of 50 nm led to increase of solution shear viscosity (η) to around 200 mPa s as compared to 10 mPa s for native protein [5]. When the aggregate size was increased further to 63 nm, they found an increase of η to around 2 Pa s. However, a decrease of storage modulus ($G^{'}$) was also observed from $\sim$ 3000 Pa to $\sim$ 2000 Pa. This was attributed to the open structure of 63 nm aggregates as compared to the 50 nm aggregates. It was concluded that size and structure of aggregates affect the rheological properties. Gelation may be induced by heating of proteins at sufficiently high concentrations [6], or by a 2-step process, generally referred to as cold gelation [7]. In the latter method, proteins are first aggregated by heating at low concentrations, subsequently gelation is induced by a change in pH, ionic strength or concentration [7]. For cold-set gelation of whey proteins or ovalbumin at acidic pH, the gel microstructure was found to be independent on the characteristics of the aggregates [7]. On the other hand, the small deformation properties of these protein gels were found to be influenced by the differences in shape and size of these aggregates. Hence, the rheological properties of the protein aggregates are believed to be correlated both to their size and structure. This implies that a control over protein aggregate size and structure can be used for controlling their techno-functional properties, such as bulk rheology. Now, in the method of enzymatic cross-linking, the question is if indeed the different enzymes, through the different mechanism of cross-linking induce differences that are reflected in significant changes in rheology. In a way similar to heating, enzymatic cross-linking can be used to produce a gel directly (in 1-step) or to produce protein nanoparticles that are later used to make a gel (2-step). In most studies considering rheological properties resulting from enzymatic cross-linking, gels are formed in the 1-step process. The 1-step enzymatic gelation of proteins has been studied for different oxidases and transferase enzymes, for example laccase, tyrosinase, peroxidase and transglutaminase [8–10]. Extensive cross-linking of 40 g L^{-1} α-lactalbumin (α-LA) with horseradish peroxidase (HRP) leads to formation of a gel [11, 12]. With the same substrate and enzyme, nanoparticles of sizes 25, 50 and 100 nm were made, that were later concentrated. Above 30 g L^{-1} the nanoparticles formed gels [13]. In previous work, it was shown that nanoparticles of α-LA can be also be made with microbial transglutaminase (mTG) in a controlled manner [11]. When samples were compared at the similar particle size, it was found that there are significant differences in the structure. The α-LA/HRP nanoparticles were found to be of open type i.e. low apparent density ($\leq$ 10 kg m^{-3} for radius of gyration, R_g = 100 - 200 nm) [11]. In contrast, the α-LA/mTG nanoparticles were found to be of compact type with higher

apparent density ($\sim$ 20 kg m^{-3}) (chapter 4). The α-LA/mTG nanoparticles held less water than α-LA/HRP nanoparticles indicating some correlation between mesoscale structure and functionality (chapter 4). The aims of this chapter are to investigate 1) the effect of differences in mesoscale structure of α-LA nanoparticles made either with mTG or with HRP on the bulk rheology of 2-step gels and 2) the differences in rheological properties of 1-step versus 2-step gels of α-LA/mTG system.

Materials and methods

Materials

α-Lactalbumin (α-LA) was obtained from Davisco Foods International (Le Sueur, MN, USA). The protein content was 95 % (w/w) on dry basis, as determined by DUMAS (N $\times$6.25, a factor based on amino acid composition) [11]. Around 90 % of the total proteins was α-LA [11], of which around 80 % (mol/mol) was in calcium free apo form [14]. Microbial transglutaminase (mTG), commercially sold as ActivaR-YG was procured from Ajinomoto Foods (Paris, France). Horseradish peroxidase (HRP) was obtained from Sigma (P6782, Peroxidase type VIA). All other chemicals used were of analytical grade.

Enzyme activity

Commercial mTG was purified by cation-exchange using StreamlineTM, SP XL in a batch mode (chapter 4). The activity of purified mTG was measured at pH 7.0 and 37 °C following the colorimetric hydroxamate procedure [15] with some modifications (chapter 4). HRP was used as received and its activity was measured in 0.1 M ammonium acetate at pH 7.0 $\pm$ 0.2 and 37 °C using the ABTS assay [14]. The specific catalytic activity was found to be 29.1 $\pm$ 1.7 nkat mg^{-1} and 10.9 $\pm$ 0.6 μkat mg^{-1} for mTG and HRP, respectively.

Cross-linking reaction

All solutions were prepared in Milli-Q water (18.2 MΩ cm). Details of the cross-linking reactions were described previously (chapters 2 and 4) [11]. A mixture of 30 g L^{-1} α-LA and enzyme in a ratio of 20 (w/w) was incubated at 37 °C and pH 7.0 $\pm$ 0.2 using a 0.1 M sodium phosphate buffer for mTG and a 0.1 M ammonium acetate solution for HRP reactions. The α-LA/HRP reaction was terminated by stopping the addition of H_2O_2 after 120 additions, while mTG was inactivated after 17 h of reaction by heating the solution at 90 °C for 5 minutes. Next, the samples were mixed with equal volumes of 1 M sucrose and frozen. The frozen sample was subsequently freeze-dried and stored at -20 °C [11]. Before use, the freeze-dried powder was reconstituted in 10 mM sodium phosphate buffer, pH 7.0 and then extensively dialysed against de-mineralised water and finally against 10 mM sodium phosphate buffer (pH 7.0) with a 300 kDa regenerated cellulose membrane [11]. The protein concentration of the dialysate (% N

$\times$6.25), was determined by Dumas method. The α-LA/HRP nanoparticles obtained had a hydrodynamic radius (R_h) of 65 nm and the α-LA/mTG nanoparticles had a R_h of 60 nm.

Dynamic light scattering (DLS)

DLS measurements were performed using a Zeta sizer equipped with a laser at a wavelength of 633 nm (Nano ZS, Malvern Instruments, Malvern, UK). Samples were diluted in a 10 mM sodium phosphate buffer at pH 7 to yield a concentration of 0.1 g L^{-1}. The diluted sample (500 L) was transferred into a 1 mL quartz cuvette. The intensity of scattered light was measured at 173°. Each sample was equilibrated at 25 °C for 300 seconds, and each measured point consisted of the average of 10 individual measurements of 10 seconds each. Three such measured data points were further averaged to obtain z-average hydrodynamic radius R_h from the intensity weighted size distributions using the zeta sizer software (Malvern) following the regularization method and utilizing Stokes-Einstein equation [16].

Determination of molar mass and radius of gyration by AF4

Dialysed nanoparticles were separated using an asymmetric flow field flow fractionation (AF4) and characterized by multi-angle light scattering (MALS) in combination with RI detector, as described before [11] . The AF4 was performed on an Eclipse Dual tech (Wyatt Technology, Santa Barbara, CA, USA) linked to a HPLC unit (Ultimate 3000, Dionex/Thermo Fisher Scientific, Sunnyvale, CA, USA) with UV diode array detector and a MALS (Dawn Heleos-II, $\lambda = 665$ nm, 130 mW Laser, Wyatt), RI detector (Optilab T-rEX, Wyatt), flow cell (short flat channel, 145 mm length). The flat channel was fitted with a spacer (type W, 350 m) and a membrane (10 kDa regenerated cellulose, Millipore PLGC), procured from Wyatt Technology. The pump flow rate was controlled by the Eclipse separation system using the Chromeleon software. Data collection and analysis were done with ASTRA-6 software (Wyatt Technology). The refractive index (RI) was used to fit the molar mass distribution using a dn/dC value of 0.185 mL g^{-1} [17]. Light scattering signals from the angles with most precise signals between 29.6° to 140° were used for the extrapolation using 1st order fits with Berry formalism to obtain M_w and R_g [16,18]. The deviations in the fitted mass and size were less than 3 %. Further, the apparent density (ρ_{app}) was calculated using fitted M_w and R_g [11]. The data for R_g of the monomeric α-LA was taken from [19]. The fractal dimension (d_f) was obtained in two different ways. First, from the scaling of M_w and R_g (referred to as low q) i.e. $d_f = 1/\nu$, where ν is the scaling exponent obtained from $R_g \sim M_w^{\nu}$. Second, from the angular dependence of scattered light intensity when $qR_g > 1$ (referred to as high q) (Chapter 4).

Atomic Force Microscopy (AFM) imaging

The dialysed nanoparticles at pH 7.0 were used for AFM imaging. Sample preparation and imaging was done as described previously [12]. AFM imaging was done with a scanning probe microscope (NanoScope V Multimode, Bruker, Leiderdorp, The Netherlands), using a noncontact, ultra-sharp silicon cantilever (NT-MDTCSCS11) in the scan-assist imaging mode. The image processing and analysis were done using the Nanoscope analysis software (version 1.30, Bruker). The average dimensions of the nanoparticles were calculated from the analysis of around 50 nanoparticles clusters from different images. The height distribution was plotted with bin sizes of 4 nm, spread from 0 to 24 nm. The data was fitted to a log-normal function and the mean of the distribution was obtained from the fit.

Rheology experiments

Shear viscosity (η), storage ($G^{'}$) and loss ($G^{''}$) modulus were measured for various concentrations of the nanoparticles of a given size. All rheological measurements were performed in a stress-controlled rheometer (MRC 301 or 501, Anton Paar, St Albans, UK). The temperature in the rheometer was controlled by a Peltier system and kept constant at 20 °C for all experiments. Before the start of each experiment, samples were equilibrated at 20 °C for 10 minutes in the rheometer itself. In order to minimise the evaporation of water, a solvent trap was used for all measurements. Two types of rheological measurements i.e. oscillatory and steady state shear flow were performed for each sample with a resting period of 10 minutes between each type of measurement. A fixed sequence of rheological measurements was followed for all samples, starting with oscillatory frequency sweep and ending with shear flow measurements. For nanoparticle concentrations $\leqslant 40$ g L^{-1}, the measurements were done with a Couette (concentric cylinder) geometry with an inner diameter of 10.835 mm and a gap width of 0.832 mm. Samples at > 40 g L^{-1} were tested using a cone and plate geometry with a cone diameter of 24.969 mm and a cone angle of 0.993°. Plots of $G^{'}$ or $G^{''}$ as a function of the strain amplitude ($0.1 - 100$ %) for a given frequency (0.1 or 10 rad s^{-1}) were used to identify the linear visco-elastic regime (LVR). A strain amplitude of 1 % was chosen for further experiments since it was found to be well within the LVR. The oscillatory measurements were done by applying a sinusoidal strain with an amplitude of 1 % and measuring the sinusoidal stress in the frequency range of 0.1 and 10 rad s^{-1}. For each frequency sweep, 70 data points were acquired logarithmically and the acquisition time for each frequency was varied from 100 s for 0.1 rad s^{-1} to 0.1 s for 10 rad s^{-1}. The steady state flow measurements were done by applying a loop of shear rate gradient i.e. from 0.01 to 100 s^{-1} and then decreasing it back to 0.01 s^{-1}. The data was collected logarithmically and the acquisition time was varied from 100 s for 0.1 s^{-1} to 0.1 s for 100 s^{-1}. The flow measurements were also performed for the 2-step gels of nanoparticles to obtain an idea of the large deformation properties of these gels. The differences were quantified in terms of apparent shear viscosity (η_{app}) of these gels and the hysteresis in the flow

Table 5.1: *Nanoparticles used for rheological experiments. The parameters described are hydrodynamic radius (R_h), radius of gyration (R_g), weight averaged molar mass (M_w), apparent density (ρ_{app}) based on R_g, degree of polymerisation (DP), size (R_g) to mass (M_w) scaling exponent (ν) and fractal dimension (d_f).*

	R_h (nm)	M_w (MDa)	R_g (nm)	ρ_{app} (kg/m^3)	DP	ν (-)	d_f (low q)	d_f (high q)
Apo α−LA	2 ±0.1	0.0142	1.72 *	1106	1	-	-	-
α−LA/mTG	60 ±1.8	77.2 ±2.2	108.1 ±1.1	24.2 ±0.6	5427 ±136	0.38 ±0.05	2.7 ±0.5	2.2 ±0.1
α-LA/HRP	65 ±1	111.8 ±3.8	167 ±2	9.5 ±0.3	7855 ±236	0.57 ±0.05	1.8 ±0.2	2 ±0.1

* Data taken from reference [19].

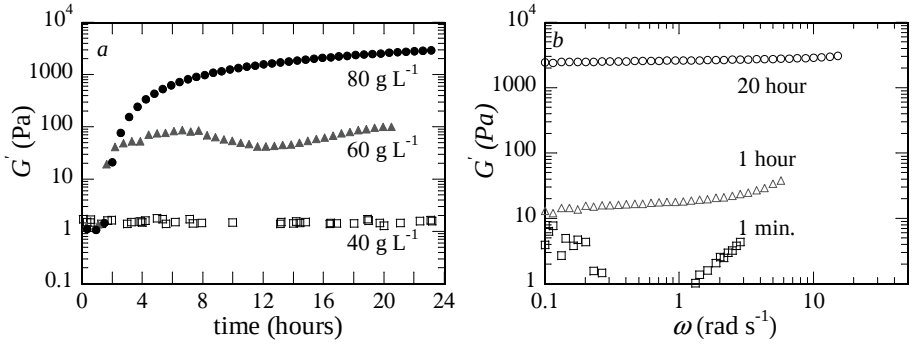

Figure 5.1: *Storage modulus ($G^{'}$), measured at an angular frequency (ω) of 1 rad s^{-1} during the course of mTG induced crosslinking of α-LA at concentrations of 40 (□), 60 (▲) and 80 (●) g L^{-1} (a), and $G^{'}$ measured at varying ω after 1 minute (□), 1 hour (△) and 20 (○) hours of reaction for 80 g L^{-1} sample (b).*

curves.

Rheology of 1-step gels

The cross-linking reaction of α-LA with mTG was performed directly in the Couette cell maintained at 37 °C to form a α-LA/mTG 1-step gels. Cross-linking was carried out in 0.1 M sodium phosphate buffer (pH 7.0) for three different concentrations (40, 60 and 80 g L^{-1}) of α-LA using α-LA : mTG ratio of 20 w/w. The cross-linking reaction was followed online by repeating the oscillatory measurement (frequency sweep) described in the rheology section over a period of 24 hours. At the end samples were cooled down and the rheological measurements were performed at 20 °C.

Rheology of concentrated solutions and 2-step gel

The protein concentration of the dialysed samples (10 mM sodium phosphate buffer, pH 7.0) was measured using DUMAS (N ×6.25) (chapter 4). The samples were then either diluted or further concentrated by filtration over a regenerated cellulose membrane of 100 kDa cut-off using Amicon-Ultra15 tubes (4000 g; 20 °C, Merck Millipore, Cork, Ireland) to obtain concentrations between 1 and 80 g L^{-1}. The final concentrations of the nanoparticles (retentate) were calculated using the weight of the filtrate. Samples were transferred into 2 mL eppendorf tubes and centrifuged (4,000 g ; 5 min ; 4 °C) to remove air bubbles and stored at 4 °C for 12 h. The $G^{'}$, $G^{''}$ and η versus concentration series data at selected angular frequency (1 rad s^{-1}) or shear rate (1 s^{-1}) is reported as average of duplicate samples.

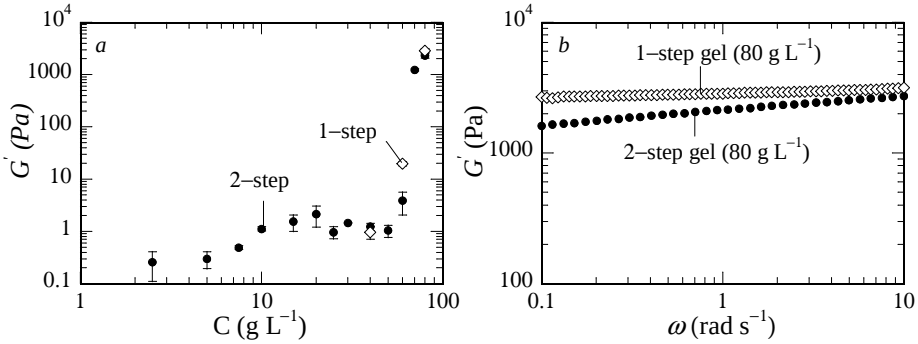

Figure 5.2: *Storage ($G^{'}$) modulus measured at an angular frequency of 1 rad s^{-1} as a function of increasing bulk concentrations of α-LA/mTG nanoparticles (2-step process) (a). The $G^{'}$ after 24 hours measured at 20 °C for α-LA/mTG 1-step reaction ($\diamond$) is also plotted in (a). The $G^{'}$ versus angular frequency (ω) for 1-step and 2-step α-LA/mTG gels (80 g L^{-1}) (b).*

Results and discussion

Rheology of 1-step versus 2-step gels of α-LA/mTG

The mTG crosslinking of α-LA was used to study the differences between the rheological properties of the gels obtained from 1-step and 2-step gelation process. This system was chosen since this cross-linking reaction can easily be performed inside the rheometer cell and monitored online. Online cross-linking with an α-LA concentration of 40 g L^{-1} did not lead to gelation as indicated by a very low value of the storage modulus ($G^{'}$). The $G^{'}$ was around 2 Pa and it did not change within 24 hours of reaction (figure 5.1a). When the online cross-linking was performed at a concentration of 60 and 80 g L^{-1}, the $G^{'}$ started to increase after about 1 hour of reaction and reached a plateau value of around 80 and 2000 Pa, respectively (figure 5.1a). The $G^{'}$ as function of frequency for the 80 g L^{-1} sample shows a transition from a solution to a gel (figure 5.1b). At the start of the cross-linking reaction (1 minute) scattered data is obtained. After around one hour of reaction the $G^{'}$ starts to increase and reaches a value around $10 - 20$ Pa and shows frequency dependence. In the final gel, $G^{'}$ is frequency independent(figure 5.1b).

To compare the 1-step gelation, $G^{'}$ of concentrated solutions of 60 nm nanoparticles was measured as function of concentration (figure 5.2a). Until a concentration of 50 g L^{-1}, no gelation was observed, but when α-LA/mTG nanoparticles were concentrated beyond 50 g L^{-1}, the $G^{'}$ increased by 1000 times (figure 5.2a). At comparable concentrations, values of $G^{'}$ are similar for the 1-step gel as for the 2-step gels. However, a small difference is observed in the frequency dependence (figure 5.2b).

For the 2-step gel, $G^{'}$ is weakly frequency dependent and ranges between 1000 and 2000 Pa. The $G^{'}$ of α-LA/mTG 1-step gel is frequency independent and is around

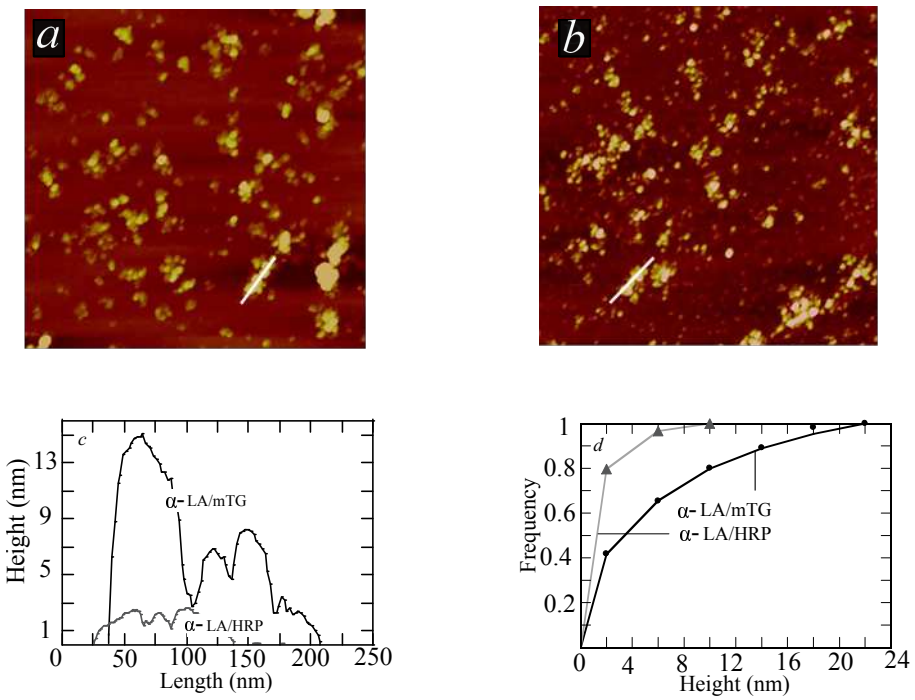

Figure 5.3: *AFM image depicting the cross-profiles of α-LA/mTG (a) and α-LA/HRP (b) nanoparticles. The images show a scanned area of 1 μm × 1μm and the section profile of α-LA/mTG (black curve) and α-LA/HRP nanoparticles across the white line in each image is shown in (c). The height distribution for α-LA/mTG and α-LA/HRP nanoparticles obtained by analysis of multiple images is depicted in (d) where the curves represent a cumulative log-normal fit.*

2000 Pa. This is almost similar to the 2-step gel made at same bulk concentration (80 g L^{-1}). Hence, rheological properties of 1-step and 2-step gels made by enzymatic cross-linking are almost similar. So, the effect of mesoscale structure of the nanoparticles on rheological properties can be studied for the 2-step gels made by concentrating two types of nanoparticles of R_h 60 and 65 nm made with mTG and HRP, respectively (table 5.1).

Rheology of α-LA/mTG versus α-LA/HRP 2-step gels

The two types of nanoparticles, made with mTG and HRP have similar values of R_h, but significantly different values for R_g (table 5.1). This is also reflected in their density, which for α-LA/mTG nanoparticles is two times higher (24 kg m^{-3}) than for α-LA/HRP (9.5 kg m^{-3}) (table 5.1). This structural difference is also reflected in a 50 % higher fractal dimension (low q) of α-LA/mTG nanoparticles (table 5.1).

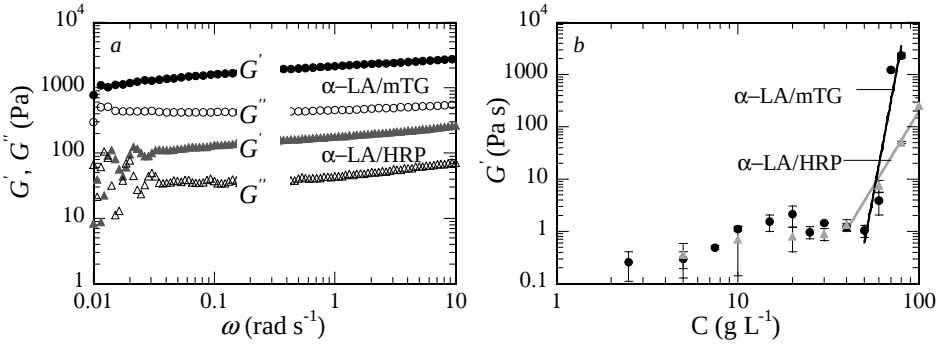

Figure 5.4: *Storage ($G^{'}$, filled symbols) and loss modulus ($G^{''}$, open symbols) versus angular frequency (ω) of α-LA/mTG and α-LA/HRP nanoparticles (a). $G^{'}$ at various bulk concentrations measured at an angular frequency of 1 rad s^{-1} (b). The solid lines represent power law fit with scaling exponents of 18.7 (R^2 0.92) for α-LA/mTG and 5.26 (R^2 0.97) for α-LA/HRP nanoparticles.*

In addition to the difference in structure in solution, it appears that the particles are different with respect to their rigidity. AFM analysis showed that the α-LA/mTG nanoparticles appear to be more rigid indicated by the fact that they flatten less (figure 5.3a, c) compared to α-LA/HRP nanoparticles on the surface (figure 5.3b, c). The nanoparticle height distribution could be well described by a log-normal function (figure 5.3d). The mean of the height distribution is 14 nm for α-LA/mTG nanoparticles as opposed to 4 nm for α-LA/HRP nanoparticles. The α-LA/mTG nanoparticles retain their shape much better upon drying, indicating that they are more rigid than α-LA/HRP nanoparticles. As the mesoscale structures of these two types of nanoparticles were significantly different. Next it was investigated if this affected their bulk rheological properties.

There were significant differences in the $G^{'}$ of gels made with both types of particles. At equal concentrations, $G^{'}$ of α-LA/mTG nanoparticle gels is much higher ($1000 - 2000$ Pa) than that of α-LA/HRP nanoparticle gels ($100 - 200$ Pa) (figure 5.4a). The $G^{'}$ is almost frequency independent in both cases. For both types of nanoparticles the $G^{'}$ showed a divergence beyond a critical concentration i.e. around 50 g L^{-1} and 40 g L^{-1} for α-LA/mTG and α-LA/HRP nanoparticles, respectively (figure 5.4b). The power law exponent of $G^{'}$ versus concentration curve is much higher ($n = 18.7$) for α-LA/mTG than for α-LA/HRP nanoparticles ($n = 5.26$). The exponent for α-LA/HRP nanoparticles is in the range typically observed in the case of heat-set protein gels [6, 19]. A rough estimation of the jamming volume fraction can be obtained from the ratio of critical concentration and apparent density based on R_h for the two types of nanoparticles. The jamming volume fraction calculated is around 0.4 and 0.3 for α-LA/mTG and α-LA/HRP nanoparticles, respectively. A lower jamming volume fraction of α-LA/HRP nanoparticles was expected due to their

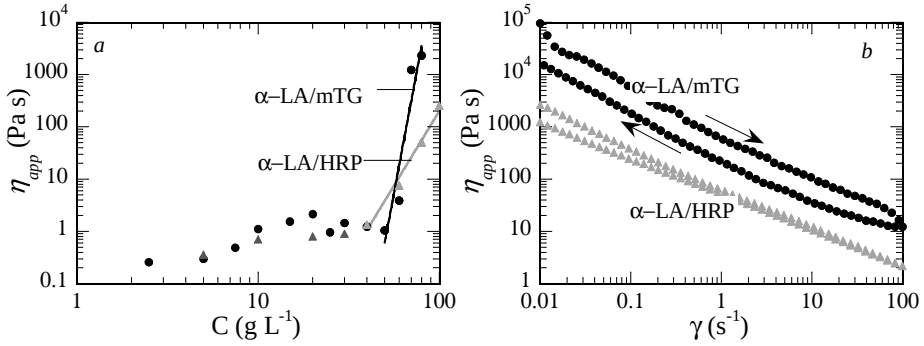

Figure 5.5: *Apparent shear viscosity (η_{app}) at various bulk concentrations measured at a shear rate (γ) of 1 s^{-1} for α-LA/mTG α-LA/HRP nanoparticles (a). The solid lines represent power law fit with scaling exponents of 14.06 (R^2 0.86) for α-LA/mTG and 4.26 (R^2 0.96) for α-LA/HRP. The η_{app} versus γ of 80 g L^{-1} nanoparticles in 10 mM sodium phosphate buffer at pH 7.0 (b).*

open structure.

Differences between the two types of nanoparticles were also evident in their shear viscosities. The shear viscosity (η) of water is around 1 mPa s at 20 °C and it is around 3 ± 0.5 mPa s for a 80 g L^{-1} solution of monomeric protein. The apparent shear viscosity (η_{app}) of nanoparticle solutions was much higher than that of monomeric protein. The η_{app} of the nanoparticle solution was in the range of 30 to 100 mPa s for the concentrations varying between 1 to 40 g L^{-1} (figure 5.5a). In this concentration range, the viscosity profiles are weakly shear thinning and there is no significant hysteresis during a shear rate cycle (increase followed by decrease) for both types of nanoparticles. However, beyond close packing ($\geq$ 40 g L^{-1}) the apparent viscosities increased by many decades and also showed more hysteresis. The hysteresis in the case of α-LA/mTG nanoparticles was much more pronounced than that of α-LA/HRP nanoparticles (figure 5.5b). The hysteresis is indicative of irreversibility of the network upon shear-induced breakage in α-LA/mTG case. This irreversibility indicates more attractive interactions in the concentrated solutions of α-LA/mTG nanoparticles as compared to repulsive interactions in the case of α-LA/HRP nanoparticles. In summary, the rheological properties of α-LA nanoparticles made by enzymatic cross-linking are strongly correlated to their mesoscale structure.

Conclusion

Enzymatically cross-linked protein nanoparticles above a critical concentration produces gels that have similar rheological properties as gels made by extensive (continuous) enzymatic cross-linking of that protein. Rheological properties of the protein

nanoparticles are affected by their meso-scale structure. Denser and more rigid nanoparticles can produce gels with higher storage modulus, while more softer particles appear to produce softer but self-healing type of gels. This indicates that bulk techno-functional properties of the protein nanoparticles can be modulated by varying the mesoscale structure of nanoparticles. Hence, protein nanoparticles can be used as ingredients for controlling the functionality in food systems. An advantage of using enzymatically cross-linked protein nanoparticles as food ingredient is that enzyme used for inducing the cross-links is not part of the food content.

Bibliography

[1] S. Banerjee and S. Bhattacharya. Food gels: Gelling process and new applications. *Crit. Rev. Food Sci. Nutr.*, 52(4):334–346, 2011.

[2] J. Buchert, D. Ercili Cura, H. Ma, C. Gasparetti, E. Monogioudi, G. Faccio, M. Mattinen, H. Boer, R. Partanen, E. Selinheimo, R. Lantto, and K. Kruus. Crosslinking food proteins for improved functionality. *Annu. Rev. Food Sci. Technol.*, 1(1):113–138, 2010.

[3] E. A. Foegeding and Jack P. Davis. Food protein functionality: A comprehensive approach. *Food Hydrocolloid*, 25(8):1853–1864, 2011.

[4] T. Nicolai and D. Durand. Controlled food protein aggregation for new functionality. *Curr. Opin. Colloid Interface Sci.*, 18(4):249–256, 2013.

[5] N. Purwanti, M. Smiddy, A. J. van der Goot, R. de Vries, A. C. Alting, and R. M. Boom. Modulation of rheological properties by heat-induced aggregation of whey protein solution. *Food Hydrocolloid*, 25(6):1482–1489, 2011.

[6] M. M. Ould Eleya, S. Ko, and S. Gunasekaran. Scaling and fractal analysis of viscoelastic properties of heat-induced protein gels. *Food Hydrocolloid*, 18(2):315–323, 2004.

[7] A. C. Alting, M. Weijers, E. H. A. De Hoog, A. M. Van De Pijpekamp, M. A. Cohen Stuart, R. J. Hamer, C. G. De Kruif, and R. W. Visschers. Acid-induced cold gelation of globular proteins: effects of protein aggregate characteristics and disulfide bonding on rheological properties. *J. Agric. Food Chem.*, 52(3):623–631, 2004.

[8] E. Dickinson and Y. Yamamoto. Rheology of milk protein gels and protein-stabilized emulsion gels cross-linked with transglutaminase. *J. Agric. Food Chem.*, 44(6):1371–1377, 1996.

[9] T. Heck, G. Faccio, M. Richter, and L. Thöny-Meyer. Enzyme-catalyzed protein crosslinking. *Appl. Microbiol. Biotechnol.*, 97(2):461–475, 2013.

[10] Y. Saricay, S. K. Dhayal, P. A. Wierenga, and R. de Vries. Protein cluster formation during enzymatic cross-linking of globular proteins. *Farad. Discuss.*, 158(0):51–63, 2012.

[11] S. K. Dhayal, H. Gruppen, R. de Vries, and P. A. Wierenga. Controlled formation of protein nanoparticles by enzymatic cross-linking of α-lactalbumin with horseradish peroxidase. *Food Hydrocolloid*, 36:53–59, 2014.

[12] Y. Saricay, P. A. Wierenga, and R. de Vries. Nanostructure development during peroxidase catalysed cross-linking of α-lactalbumin. *Food Hydrocolloid*, 33(2):280–288, 2013.

[13] Y. Saricay. *New insights into enzymatic cross-linking of globular proteins: From nanostructure to functionality*. PhD thesis, Wageningen University, Wageningen, The Netherlands, 2014.

[14] W. H. Heijnis, P. A. Wierenga, W. J. H. van Berkel, and H. Gruppen. Directing the oligomer size distribution of peroxidase-mediated cross-linked bovine α-lactalbumin. *J. Agric. Food Chem.*, 58(9):5692–5697, 2010.

[15] J. E. Folk and P. W. Cole. Mechanism of action of guinea pig liver transglutaminase .i. purification and properties of enzyme - identification of a functional cysteine essential for activity. *J. Biol. Chem.*, 241(23):5518–5525, 1966.

[16] S. Podzimek. *Light Scattering, Size Exclusion Chromatography and Asymmetric Flow Field Flow Fractionation: Powerful Tools for the Characterization of Polymers, Proteins and Nanoparticles.* John Wiley & Sons, Hoboken, NJ, USA, 2011.

[17] H. Y. Zhao, P. H. Brown, and P. Schuckt. On the distribution of protein refractive index increments. *Biophys. J.*, 100(9):2309–2317, 2011.

[18] M. Andersson, B. Wittgren, and K-G. Wahlund. Accuracy in multiangle light scattering measurements for molar mass and radius estimations. model calculations and experiments. *Anal. Chem.*, 75(16):4279–4291, 2003.

[19] M. Kataoka, F. Tokunaga, K. Kuwajima, and Y. Goto. Structural characterization of the molten globule of α-lactalbumin by solution x-ray scattering. *Protein Sci.*, 6(2):422–430, 1997.

Chapter 6

Enzymatic cross-linking of α-lactalbumin to produce nanoparticles with increased foam stability *

Abstract

Hard colloidal nanoparticles (e.g. partly hydrophobised silica), when used as surfactant are known to make foams with very high foam-stability. Nanoparticles can also be produced from proteins by enzymatic cross-linking of proteins. Such protein based particles are more suitable for food applications, but it is not know if they provide Pickering foam stabilisation and to what extent. α-Lactalbumin (α-LA) was cross-linked with either microbial transglutaminase (mTG) or horseradish peroxidase (HRP) to produce α-LA/mTG and α-LA/HRP nanoparticles. With both enzymes a range of nanoparticles were produced with hydrodynamic radii ranging from $20 - 100$ nm. The adsorption of nanoparticles to the air-water interface was probed by increase in surface pressure (Π) with time. In the beginning of the Π versus time curves, there was a lag time of $10 - 200$ s, for nanoparticles with R_h of $30 - 100$ nm, respectively. A faster increase of Π with time was observed by increasing the ionic strength ($I = 0 - 125$ mM). The foam-ability of the nanoparticles was also found to increase with increasing ionic strength. At a fixed I, the foam-ability of the nanoparticles decreased with increasing size while their foam-stability increased. Foams produced by low-shear whipping were found to be 2 to 6 times more stable for nanoparticles than for monomeric α-LA ($R_h \approx 2$ nm). At an ionic strength of 125 mM ionic strength and protein concentration $\geqslant 10$ g L^{-1}, the foam-stability of α-LA/mTG nanoparticles

*S. K. Dhayal, R.J.B.M. Delahaije, R. J. de Vries, H. Gruppen, P. A. Wierenga.

(R_h = 100 nm, ρ_{app} = 21.6 kg m^{-3}) was $2-4$ times higher than α-LA/HRP nanoparticles (R_h = 90 nm, ρ_{app} = 10.6 kg m^{-3}). This indicated that foam-stablity of nanoparticles is determined not only by size but also by differences in mesoscale structure. So, indeed enzymatic cross-linking of proteins to make nanoparticles is moving a step towards particle like behavior e.g. slower adsorption and higher foam stability. However, the cross-link density should be further increased to obtain hard particle-like rigidity and foam-stability.

Introduction

Particle stabilised foams and emulsions have received a lot of attention, due to their reported high stability (up to months) [1]. The mechanism of stabilisation by particles (referred to as Pickering-Ramsden stabilisation [2, 3]) is supposed to be due to their large size, resulting in high adsorption energies. For other surfactants, such as proteins and low molar mass surfactants, typically lower foam stabilities are observed. However, in analogy to hard colloidal particles, protein particles made by heating native proteins have increased foam stability, compared to the non-heated proteins [4–6]. Still, these heat-induced protein particles are not known to produce the same Pickering effect as that of hard colloidal particles. The foam half-life time ($t_{0.5}$) is only of the order of a few hours for protein particles as compared to many days or months for hard particles [7, 8]. There appear to be many factors that govern the foaming properties of protein particles, such as size, mesoscale structure [9, 10], and foaming method. For example, heat induced protein particles of $R_h \sim 35-197$ nm had a lower foam-stability than native protein in a sparging test [6]. But, when the protein particles of $R_h \sim 35$ and 71 nm were mixed with 5 % of native protein, the mixtures showed higher foam-stability than native protein alone. Protein particles of $R_h \sim 117$ and 197 nm showed lower foam-stability even in a mixture with native protein [6].These results indicate that foaming properties of protein particles are limited by mass transport of particles in a sparging test. In fact, lower mass transport fluxes of large particles typically results in lower foam-ability. Hence, typically, either higher concentrations of particles ($>$ 1% w/v) are required, or presence of a low molar mass surfactant with large particles is needed [6, 11–14]. The slow diffusion also causes different foam properties when the foam is made by whipping as compared to sparging. In the case of heat-induced protein particles, when foams have been produced by whipping, the foam-stability was higher than foams made by sparging [4]. In addition to the method of foaming, the foam-ability of particles is also determined by their wetting properties and surface charge density. A major bottle-neck in these studies is a lack of data on meso-scale structural details, such as shape [7], particle (aggregate) density [15, 16], softness [15], and charge [17]. Enzymatic cross-linking is an alternative method to heating for producing protein particles. The main advantage of enzymatic cross-linking is the possibility to control the cross-linking density of protein particles and therby to control their mesoscale structure. In chapters 2 and 4, it was shown that protein nanoparticles with controlled size and mesoscale structure

can be produced with enzymatic cross-linking. The apo α-LA was cross-linked with two different enzymes; horseradish peroxidase (HRP) and microbial transglutaminase (mTG), to produce nanoparticles in the size range 20 to 200 nm. The nanoparticles made with HRP were open type, whereas those made with mTG were denser (rigid) type. For example, the apparent density (ρ_{app}) of α-LA/mTG nanoparticles of R_h = 100 nm was 21.6 kg m^{-3}, which is twice than that of 90 nm α-LA/HRP nanoparticles (ρ_{app} = 10.6 kg m^{-3}). The α-LA/mTG nanoparticles were more rigid as indicated by the fact that they showed less swelling at lower ionic strengths and less collapse on modified silica as compared to α-LA/HRP nanoparticles. The goal of this chapter is to compare surface and foaming properties of these two sets of α-LA nanoparticles as a function of their size and to compare the typical foam half-life times ($t_{0.5}$) with those reported in literature for other types of protein aggregates and colloidal particles.

Materials and methods

Materials

α-Lactalbumin (α-LA) was obtained from Davisco Foods International (Le Sueur, MN, USA). The protein content was 95 % (w/w) on dry basis, as determined by DUMAS (N $\times$6.25, based on amino acid composition) [18]. Around 90 % of the total proteins was α-LA [18], of which around 80 mol % was in the calcium free apo form [19]. Microbial transglutaminase (mTG), commercially sold as ActivaR-YG, was procured from Ajinomoto Foods (Paris, France). Horseradish peroxidase (HRP) was obtained from Sigma (P6782, Peroxidase type VIA). All other chemicals used were of analytical grade.

Enzyme activity

Commercial mTG was purified by cation-exchange using StreamlineTM, SP XL in a batch mode (chapter 4). The activity of purified mTG was measured at pH 7.0 and 37 °C following colorimetric hydroxamate procedure [20] with some modifications (chapter 4). HRP was used as received and its activity was measured in 0.1 M ammonium acetate at pH 7.0$\pm$0.2 and 37 °C using the ABTS assay [19]. The specific catalytic activity was found to be 4.7 $\pm$ 0.4 nkat mg^{-1} and 10.9 $\pm$ 0.6 μkat mg^{-1} for mTG and HRP, respectively.

Cross-linking reaction

All solutions were prepared in Milli-Q water (18.2 MΩ cm). Details of the cross-linking reactions were described previously (chapter 4) [18]. In the case of α-LA/HRP reaction samples were taken after three different numbers of H_2O_2 additions (n_{H2O2} = 35, 85 and 180). For α-LA/mTG reaction, samples were collected at various time points (20, 40 and 72 h). The α-LA/HRP reaction was terminated by stopping the

addition of H_2O_2, while mTG was inactivated by heating the solution at 90 °C for 5 minutes. It was verified using dynamic light scattering (DLS) that the heat treatment of α-LA/mTG nanoparticles at 95 °C for 5 minutes did not result in changes in R_h. Next, the samples were mixed with equal volumes of 1 M sucrose and frozen. The frozen sample was subsequently freeze-dried and stored at -20 °C [18]. Before use, the freeze-dried powder was reconstituted in 10 mM sodium phosphate buffer, pH 7.0 and then extensively dialysed with a 300 kDa regenerated cellulose membrane against de-mineralised water and finally against 10 mM sodium phosphate buffer containing 0.1 M NaCl (pH 7.0) [18]. The protein concentration of the dialysate (% N $\times$6.25), was determined by Dumas method. The hydrodynamic radii (R_h) of the α-LA/HRP nanoparticles were 20, 35, 65 and 90 nm and the R_h of the α-LA/mTG nanoparticles were 30, 60 and 100 nm.

Dynamic light scattering (DLS)

The DLS measurements were performed using a Zeta Sizer (λ = 633 nm, Nano ZS, Malvern Instruments, Malvern, UK) following the method described previously [18]. Samples were diluted in a 10 mM sodium phosphate buffer at pH 7.0 to yield a concentration of around 0.1 g L^{-1} and the intensity of scattered light was measured at 173°. The z-average R_h was obtained from the intensity weighted size distributions using the zeta sizer software (Malvern).

Asymmetrical flow field flow fractionation (AF4)

Dialysed nanoparticles were separated using asymmetric flow field flow fractionation (AF4) and characterized by multi-angle light scattering (MALS) in combination with RI detector, as described before [18]. The AF4 instrumentation comprised of an Eclipse Dual tech (Wyatt Technology, Santa Barbara, CA, USA) linked to a HPLC unit (Ultimate 3000, Dionex/Thermo Fisher Scientific, Sunnyvale, CA, USA) with UV diode array detector and a MALS (Dawn Heleos-II, λ = 665 nm, 130 mW Laser, Wyatt), RI detector (Optilab T-rEX, Wyatt), flow cell (short flat channel, 145 mm length). The flat channel was fitted with a spacer (type W, 350 μm, Wyatt) and a membrane (10 kDa regenerated cellulose, Millipore, Wyatt). The pump flow rate was controlled by the Eclipse separation system using the Chromeleon software. Data collection and analysis were done with ASTRA-6 software (Wyatt Technology). The refractive index (RI) was used to fit the molar mass distribution using a dn/dc value of 0.185 mL g^{-1} [21]. Light scattering signals from the most precise angles between 29.6° to 140° were used for the extrapolation using 1st order fits with Berry formalism to obtain M_w and R_g [22, 23]. The data for R_g of the monomeric protein was taken from [24]. The deviations in the fitted mass and size were less than 3 %. Further, the apparent density (ρ_{app}) was calculated using fitted M_w and R_g [18]. The fractal dimension (d_f) was obtained in two different ways. First, from the scaling of M_w and R_g (referred to as low q) i.e. $d_f = 1/\nu$, where ν is the scaling exponent obtained from $R_g \sim M_w^{\nu}$. Second, from the angular dependence of scattered light intensity when

$qR_g > 1$ (referred to as high q) (Chapter 4).

Electrophoretic mobility

The electrophoretic mobility (nm^2 V^{-1} s^{-1}) of the α-LA or α-LA nanoparticles was determined using the Zetasizer 2000 (Malvern Instruments, Worcestershire, U.K.). Measurements were performed at 25 °C on α-LA (10 g L^{-1}) or α-LA nanoparticles (dialysed, 1 g L^{-1}) that were dissolved in 10 mM sodium phosphate buffer (pH 7.0, filtered through 0.1 μm membrane). The values reported are average of five measurements. The electrophoretic mobility of α-LA nanoparticles as compared to monomeric α-LA is used as an indication of changes in apparent charge density of nanoparticles. The electrophoretic mobility was not converted into zeta-potential since there is no model available for fractal nanoparticles which relates surface potential to mobility.

Exposed hydrophobicity by ANSA adsorption

The exposed hydrophobicity of α-LA nanoparticles relative to monomeric α-LA was determined at 25 °C using 8-anilino-1-naphthalenesulfonic acid (ANSA) as a fluorescent probe, following the method described in [25]. The measurements were performed at $\lambda_{ex} = 385$ nm and $\lambda_{em} = 400 - 650$ nm, using a Varian Cary Eclipse fluorescence spectrophotometer (Agilent Technologies, Santa Clara, CA, USA). The protein solutions (0.1 g L^{-1}) and ANSA solution (2.4 mM) were prepared in a 10 mM sodium phosphate buffer set at pH 7.0 with additional 0.1 M NaCl. Aliquots of 10 μL of ANSA solution were added to 1 mL of protein solution in a quartz cuvette ($l = 1$ cm). The integrated area under the emission spectrum was then corrected with the area of the buffer. The relative exposed hydrophobicity was calculated as the ratio of the area of the nanoparticles relative to that of monomeric α-LA.

Surface pressure

The rising bubble method coupled with software for drop shape analysis was used for the measurement of surface pressure (ADT, Teclis IT Concept, Longessaigne, France). A small bubble of around 10 μL volume was formed in a solution (thermostated at 20 °C) of monomeric α-LA or α-LA nanoparticles, under the following solution conditions: a) Protein concentration of 0.01, 0.1 and 1 g L^{-1} in 10 mM sodium phosphate buffer (pH 7.0) and b) Protein concentration 0.1 g L^{-1} in MQ water (ionic strength, $I \approx 0$ mM), 10 mM sodium phosphate buffer (pH 7.0, $I = 25$ mM) and 10 mM sodium phosphate buffer (pH 7.0) + 0.1 M NaCl ($I = 125$ mM). A constant bubble surface area of 22 ± 0.1 mm^2 was maintained and the change in surface tension with time (γ_t) was recorded. The surface tension was determined from the shape of drop via numerically fitting Young-Laplace-Gauss equation using Teclis software. This data was converted into surface pressure versus time by subtracting surface tension of water (γ_0) i.e. $\Pi_t = \gamma_0 - \gamma_t$. The surface tension of buffers was close to water, i.e. 72.8 $\pm$0.5 mN m^{-1}.

Surface excess

The amount of monomeric α-LA or α-LA nanoparticles adsorbed at the air-water interface was determined using a null ellipsometer (Multiskop, Optrel, Sinzing, Germany). Concentrated proteins were diluted in 10 mM sodium phosphate buffer (pH 7.0) containing 100 mM NaCl and 20 ppm NaN_3 to obtain a protein concentration of 1 g L^{-1}. The buffer was measured for 600 s prior to each measurement. Next, the protein solutions were transferred into a petri dish and the measurements were done at time zero and after 24 hours. Monochromatic laser light ($\lambda = 632.8$ nm) was used at an angle of incidence of 50° and the changes in the ellipsometric angles (Δ and ψ) were measured after reflection from the interface. Δ and ψ increase due to adsorption of protein at the air-water interface due to formation of a layer of thickness (δ_{ad}) and the resultant change of the refractive index (n_{ad}). The n_{ad} and δ_{ad} were obtained by fitting a three layer model, i.e. air, water and one adsorbed layer between them. The fitting parameters were: $n_{\mathrm{air}} = 1.000$, $n_{\mathrm{buffer}} = n_{\mathrm{water}}$ $(n_w) = 1.333$, $dn/dc = 0.185$ mL g^{-1} and the angle of incidence = 50°. The fitted n_{ad} and δ_{ad} were subsequently used to calculate the adsorbed amount (surface excess, Γ, mg m^{-2}) using equation 6.1 [26].

$$\Gamma = \frac{(n_{\mathrm{ad}} - n_w)\,\delta_{\mathrm{ad}}}{\frac{dn}{dc}} \tag{6.1}$$

Thin film thickness

Thickness of thin horizontal films containing monomeric α-LA orα-LA nanoparticles was measured using a Sheludko cell [27]. Protein solutions (1 g L^{-1} in 10 mM sodium phosphate buffer (pH 7.0) containing 100 mM NaCl and 20 ppm NaN_3) were equilibrated in the cell for 10 minutes. A thin film ($R \sim 100$ μm) was formed by suction of liquid form the circular film holder containing a thick liquid film. The equilibrium film thickness was calculated using the intensity of the reflected monochromatic light ($\lambda = 546$ nm). The average intensity of light (pixels) was recorded in the centre of the film in a circle of radius of around 25 μm. The thickness of the film was calculated as described in [28] using equation 6.2.

$$h = \frac{\lambda}{2\pi n} sin^{-1}\left(\sqrt{\frac{I - I_{min}}{I_{max} - I_{min}}}\right) \tag{6.2}$$

Where, n is the refractive index, I is the intensity of the reflected light, and I_{min} and I_{max} are the minimum and maximum intensities, respectively.

Foam-ability and foam-stability using whipping test

Foams were produced by using a mechanical low shear mixer (Aerolatte, Shanghai Dixi Electronic Company, People's Republic of China). Aerolatte is a hand held electric mixer which has a circular rotor (outer diameter = 22 mm) with a coiled wire along

the circumference, and a rotation speed of 12,000 rpm in air [29]. Solutions of α-LA or α-LA nanoparticles (20 mL) containing 20 ppm NaN_3 were used for measurement (0.1, 1, 5, 10 and 20 g L^{-1}, $I \approx 0$ mM (MQ-water, pH 6.3 ± 0.2), $I = 25$ mM and 125 mM, both at pH 7.0 ± 0.1). The solutions were placed inside plastic containers of inner diameter = 3.4 cm and height = 7.5 cm and the containers were graduated with a scale of 1 mm resolution. The foams were generated by placing the mixing head centrally and around one cm below the air-water surface. The whipping was done for a fixed time of 5 minutes at room temperature (23 ± 3 °C). Foam heights were recorded for various time points until more than half of the most stable foam had collapsed. The foam height was calculated as total height (liquid + foam i.e. the height of foam/air interface) minus the height of the drained liquid i.e. the liquid/foam interface. The time required for the foam height to reduce by half of its initial height ($t_{0.5}$) is used as an indicator of foam-stability. The foam height obtained just after whipping (H_0) is used as an indicator of foam-ability. Experiments were performed in duplicate with fresh solutions each time and the results are reported as average ± standard deviation of these measurements. A single experiment was also performed for α-LA/mTG nanoparticles (5 g L^{-1}, $I = 125$ mM at pH 7.0) in presence of 2 % (v/v) of ethanol to test the foam-stability of nanoparticles in presence of a low molar mass surface-active agent.

Foam properties using sparging test

The foam-stability of the protein nanoparticles by sparging method was measured using Foamscan (Teclis, Longessaigne, France). The foam formation and breakdown were monitored by combination of optical (CCD camera) and conductivity measurements. Conductivity electrodes were placed along the foam tube to monitor the liquid content of foam as well as the volume of liquid drained out of foam and collected at the bottom. Pressurised air was sparged at a flow rate of 200 mL min^{-1} through a metallic plate containing square grid of tapered holes of 30 μm diameter. The foaming tube had an inner diameter of 3.5 cm and the temperature was maintained at 22 ±1 °C by circulating the water from the water bath through outer jacket of the foam tube. A 40 mL of nanoparticle solution (1 20 g L^{-1}, 10 mM sodium phosphate buffer containing 0.1 M NaCl, pH 7.0) was used for testing. Nanoparticle sample preparation was same as in whipping test. Conductivity measurements were used for determining the drainage volume. The time required for 50 % of the liquid volume to drain is defined as $t_{0.5,drainage}$.The foam generation was programmed to produce a fixed volume (200 mL) of foam and if this was not possible then the sparging was stopped after five minutes and the decay of foam volume with time was monitored. The bubble size was measured at the middle of foam column using a CCD camera and a prism and lighting arrangement at the surface of foam tube. The time required for the foam volume to reduce to half of its initial volume ($t_{0.5}$) was used as indication of foam-stability. The data collection and analysis were done by the software supplied by Teclis. Experiments were performed in duplicate and the results are reported as average ± standard deviation of these measurements.

Table 6.1: *Charateristics of nanoparticles used for adsorption, thin film and foaming experiments. The parameters described are hydrodynamic radius (R_h), radius of gyration (R_g), weight averaged molar mass (M_w), apparent density (ρ_{app}) based on R_g, electrophoretic mobility (μ), exposed hydrophobicity relative to monomeric $\alpha-LA$ (H), size to mass scaling exponent, ν ($R_g \sim M_w^{\nu}$) and fractal dimension (d_f). The ν and d_f represent average of nanoparticles of various sizes.*

	R_h (nm)	M_w (MDa)	R_g (nm)	ρ_{app} (kg/m^3)	μ (nm/ Volt s)	H (±0.3)	ν (-)	d_f (low q)	d_f (high q)
Apo α-LA	2	0.0142	1.72 *	1106	16 ±1	1	-	-	-
α−LA/HRP	20 ±1	2.1 ±0.01	20.8 ±0.8	88.4 ±5.6	21 ±2	1.3	0.57 ±0.05	1.8 ±0.2	2.0 ±0.1
	35 ±1.3	13.8 ±0.04	66.4 ±0.4	18.6 ±0.2	25 ±1	0.8			
	65 ±1.1	111.8±3.8	167 ±2	9.5 ±0.3	27 ±1	0.7			
	90 ±2	161.7 ±7.7	182.3±2.3	10.6 ±0.4	27 ±1.5	0.6			
α−LA/mTG	30 ±1	3.2 ±0.1	39.8 ±0.7	20 ±0.7	22 ±1.5	4.7	0.38 ±0.05	2.7 ±0.5	2.2 ±0.1
	60 ±1.8	65.7 ±1.9	105 ±1	22.5 ±0.5	25 ±1	5.0			
	100 ±2.5	168.6 ±5.1	145.6 ±1.7	21.6 ±0.6	26 ±1	3.0			

* Data taken from reference [24].

Results and discussion

α-LA nanoparticles used for foaming study

The monomericα-LA has a hydrodynamic radius (R_h) of 2 nm (table 6.1). After cross-linking monomeric α-LA with HRP or mTG, α-LA/HRP or α-LA/mTG nanoparticles of R_h 20, 35, 65, 90 nm and 30, 60, 100 nm were obtained, respectively (table 6.1). The mesoscale structure of α-LA/mTG nanoparticles is different from that of α-LA/HRP nanoparticles (chapter 4). The nanoparticles made with HRP were open type (e.g. $\rho_{\text{app}} = 1.06\%$ (w/v) for $R_h = 90$ nm), whereas those made with mTG were rigid/denser type (e.g. $\rho_{\text{app}} = 2.16\%$ (w/v) for $R_h = 100$ nm). The term denser for α-LA/mTG nanoparticles is used relative to the density of α-LA/HRP nanoparticles. Otherwise, compared to some heat-induced protein particles, the density in both particles is $4-10$ times lower [16]. The exposed hydrophobicity of α-LA/mTG nanoparticles was $3-5$ times higher than that of monomeric α-LA, while it was similar to monomeric α-LA in the case of α-LA/HRP (table 6.1). This may have a significant effect on adsorption kinetics. For example, an increase of relative hydrophobicity of from 1 for native to 2.4 for modified (caprylated) ovalbumin showed a dramatic increase in adsorption kinetics where the lag time in native of around 600 s was reduced to less than 10 s [25]. Despite the differences in density and exposed hydrophobicity, the electrophoretic mobility (μ) of α-LA/HRP and α-LA/mTG nanoparticles was found to be similar, although for in both cases the charge increased with size. The electrophoretic mobility (μ) of monomeric α-LA is around 16 ± 1 nm V^{-1} s^{-1} (table 6.1). After enzymatic cross-linking the μ increased significantly with increasing nanoparticle size. For both types of nanoparticles, μ were around 22 ± 3 nm V^{-1} s^{-1} and 26 ± 2 nm V^{-1} s^{-1} for R_h of $20-35$ nm and $60-100$ nm, respectively (table 6.1). Increase of charge with size is not surprising and has been observed before for heat-shocked and mTG treated protein particles. An increase of charge (reflected by increase of zeta-potential) was observed in the case of preheating a WPI dispersion (at pH 7.5, $0-100$ mM NaCl, 80 °C for 15 min) and subsequent treatment with mTG (5.1 U g^{-1} WPI at pH 7.5 and 50 °C for 4 h) [30]. They observed an increase of size (d_{43}) from 9.8 nm for WPI dispersion to 31.7 after preheating and to 37 nm after preheating and mTG treatment. After pretreatment the zeta-potential increased from - 27 to -33.5 and -32.8 mV, respectively [30]. A subtle balance between size, mesoscale structure, surface potential and surface hydrophobicity is expected to affect the foaming properties and the results are described in the following sections.

Interfacial properties of α-LA nanoparticles used for foaming study

Adsorption at air-water interface

As expected, the adsorption of monomeric α-LA or α-LA nanoparticles at the air-water interface resulted in a decrease of air-water surface (interfacial) tension as indicated by the increase of surface pressure (Π) with time (figure 6.1). The rate of surface pressure change decreased with increasing size of the nanoparticles. For ex-

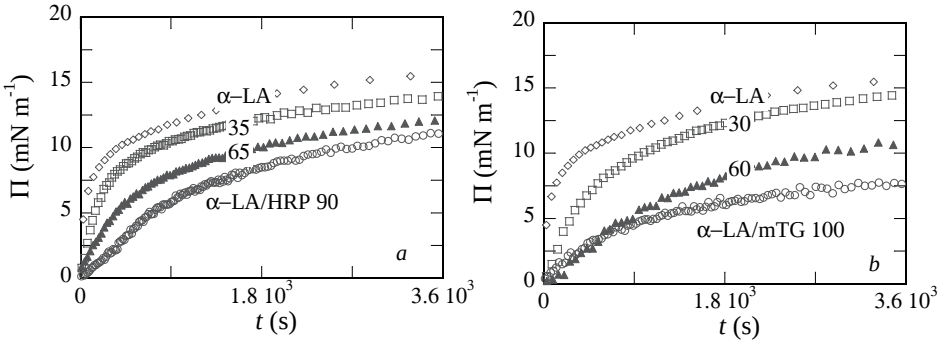

Figure 6.1: *Surface pressure of 0.1 g L^{-1} solutions of α-LA nanoparticles in 10 mM sodium phosphate buffer (pH 7.0): α-LA /HRP (a) and α-LA /mTG (b). Monomeric α-LA ($R_h = 2$ nm), α-LA/HRP ($R_h = 35$, 65 and 90 nm), α-LA/mTG ($R_h = 30$, 60 and 100 nm).*

ample, for the 100 nm α-LA/mTG nanoparticles, the surface pressure values reached after 1 hour of adsorption is less than half of the value reached for monomeric α-LA (figure 6.1b). Moreover, there was a lag-time of around 30 and 200 s observed for the α-LA/mTG and α-LA/HRP nanoparticles, respectively, at a bulk protein concentration of 0.1 g L^{-1}. The lag-time, as well as the rate of increase of Π with time were found to decrease with increasing bulk protein concentration (data not shown). The most striking observation was that almost no adsorption (increase of Π) was observed for both types of nanoparticles when the solution ionic strength (I) was ≈ 0 (MQ water). An example of this is shown for the largest nanoparticles in figure 6.2. In fact, for these nanoparticles, Π was ≥ 2 mN m^{-1} even after 20 hours. This extremely long lag-time was found to dramatically decrease with increasing ionic strengths ($I = 25$ and 125 mM) (figure 6.2).

The increase of ionic strength not only increases the speed of adsorption at short times, but also the magnitude of Π at longer time scales increased. The values of Π reached after 1 hour in the case of α-LA/HRP 90 nm particles were around 10 and 19 mN m^{-1} for $I = 25$ and 125 mM, respectively. The value of Π reached after 1 hour in the case of α-LA/mTG 100 nm particles was around 6 and 14 mN m^{-1} for $I = 25$ and 125 mM, respectively. The foam-ability of nanoparticles is well correlated to the dynamics of adsorption and explains the lower foam-ability of α-LA nanoparticles as compared to monomeric α-LA. The increase of adsorption speed with increasing ionic strength is correlated with the improvement in foam-ability of α-LA nanoparticles with increasing ionic strength. An important point in this regard is that the R_h of the nanoparticles depends on solution ionic strengths, especially when $I < 0.01$ mM (chapter 4). At $I < 0.01$ mM a high R_h (140 nm) was determined for α-LA/HRP, while in buffer solutions ($I = 25$ mM) the R_h decreased to 65 nm. This confirms electrostatic repulsion is a strong influence on the nanoparticle structure.

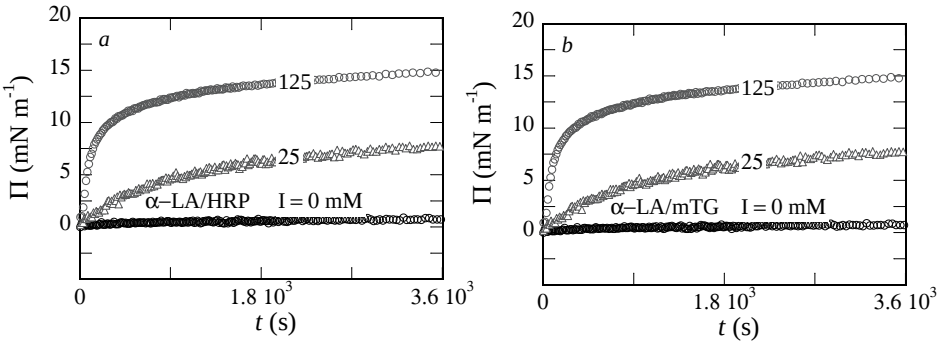

Figure 6.2: *Surface pressure as a function of time for varying ionic strengths ($I = 0$, 25 and 125 mM) for α-LA /HRP nanoparticles of $R_h = 90$ nm (a) and α-LA/mTG nanoparticles of $R_h = 100$ nm (b).*

The increase of R_h at low ionic strengths could contribute to slower mass transport rates toward the interface. In addition, the charge of the particles can also increase the electrostatic barrier for adsorption. An electrostatic barrier to adsorption in the case of modified proteins has been systematically studied by succinylation (i.e. increase in net charge) for ovalbumin [17]. It was also shown to lead to lower adsorption speeds with increasing charge. Since for the nanoparticles the adsorption speeds are increased with ionic strength, it seems that here also the adsorption kinetics are (in part) also affected by the increased net charge, as indicated by the higher electrophoretic mobility. Air-water interface has been experimentally proved to have a negative zeta potential (-65 mV for air bubbles in deionized water to about -20 mV for ionic strengths, $I = 0.1$ M with NaCl at pH $\sim$ 7) [31, 32]. An increased potential over the nanoparticle surface must then result in an increased electrostatic repulsive barrier towards air-water interface. The electrostatic barrier was reduced by increased ionic strengths due to charge screening (decrease of Debye lengths) and can be explained by the DLVO theory [33].

Thin films and single air/water interface

The thickness of thin films stabilized by monomeric α-LA was around 20 nm and appears to be a common black film (figure 6.3). The average thickness of the films formed with α-LA nanoparticles were about $2-3$ times higher than that of monomeric α-LA for both types of nanoparticles in the size range of R_h $20-65$ nm. The film made with 100 nm α-LA/mTG nanoparticles was around 140 nm thick, which is about 2.5 times more than that of 90 nm α-LA/HRP nanoparticles. Moreover, even while the cross-linked nanoparticles used to make thin films are quite large, the films for $30-60$ nm particles seem quite homogeneous. Only for the largest particles, clear heterogeneity in the films is visible (figure 6.3a). The higher stability of foams made

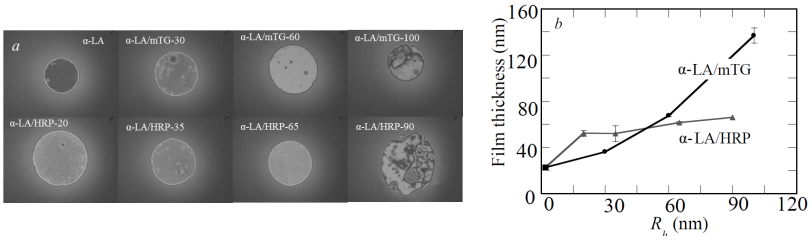

Figure 6.3: *Thin liquid films containing monomeric α-LA, α-LA/HRP and α-LA/mTG nanoparticles (a). Thickness of the thin films deduced from the intensities at the centre of the film for α-LA(■), α-LA/HRP (▲) and α-LA/mTG (●) (b).*

with α-LA nanoparticles as compared to monomeric α-LA are correlated with the thickness of the thin horizontal films.

Another indication of the thickness of the adsorbed layer was derived from ellipsometry experiments. The thickness of the adsorbed layer was around 10 nm for monomeric α-LA and it varied from $10-20$ nm for α-LA nanoparticles ($R_h = 20-35$ nm) (figure 6.4b). But, the adsorbed layer thickness of 60 and 100 nm α-LA/mTG nanoparticles was up to 30 nm i.e. almost twice than α-LA/HRP nanoparticles ($R_h =$ 65 and 90 nm). There is a good correlation between the thickness of single air/water interface and the thickness of thin films containing α-LA nanoparticles. At the same time, there was only a small increase in the surface excess (Γ) of adsorbed proteins after 24 hours of adsorption. For monomeric α-LA Γ was around 2.5 mg m^{-2} (figure 6.4a), and for α-LA/mTG and α-LA/HRP nanoparticles Γs were 2.75 and 3.25 mg m^{-2} respectively.

The film thicknesses are about twice that of adsorbed layer thickness at single air/water interface. This indicates that the thin films contain at least a monolayer of α-LA nanoparticles at each interface. An important point to note is that the thickness of nanoparticles at interface is smaller than their corresponding R_h in bulk. This indicates that they flatten at the interface, but α-LA/HRP nanoparticles flatten more than α-LA/mTG nanoparticles. This observation is similar to the differences in flattening of α-LA/mTG and α-LA/HRP nanoparticles observed on modified silica surfaces (AFM images, chapter 5). The interfacial and thin film properties of nanoparticles described above are considered to be relevant to foam-stability since they have a direct influence on the disjoining pressures in the foam-films.

Foam properties by whipping

Foam-ability

At low ionic strength ($I \leq 0.001$ mM), the monomeric α-LA could be foamed to a foam height of 1 to 3.5 cm for concentrations increasing from 0.1 to 20 g L^{-1}

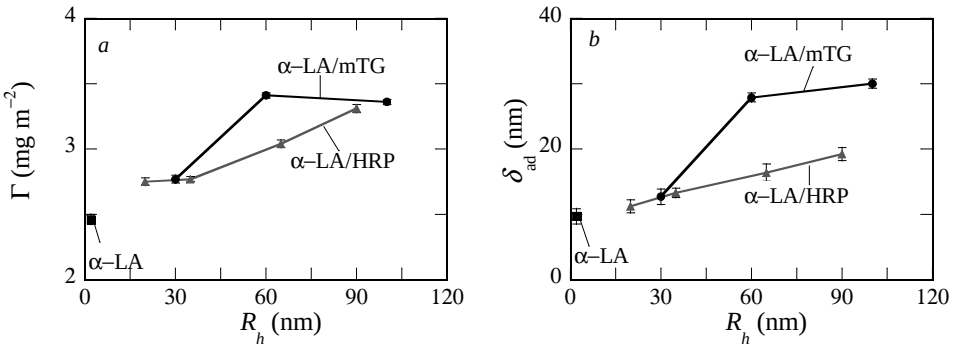

Figure 6.4: *Surface excess concentration (Γ) (a) and the thickness of the adsorbed layer (δ_{ad}) at air-water interface (b) of monomeric α-LA (■), α-LA/HRP (▲) and α-LA/mTG (●) nanoparticles after 24 hours.*

(figure 6.5). The α-LA nanoparticles could not be foamed at all for concentrations less than 1 g L^{-1} at low ionic strengths. At concentrations of 5 g L^{-1}, a foam height less than 1 cm was obtained with α-LA nanoparticles of $R_h = 20 - 35$ nm (figure 6.5a). For α-LA/mTG nanoparticles of $R_h = 60$ and 100 nm (at 5 g L^{-1}), the foam height was less than 0.5 cm (figure 6.5a). An increase in ionic strength to 25 and 125 mM led to an increase (of two to three times) in foam-ability (figure 6.5a). At the higher ionic strength a range of concentrations were tested, but only for the largest particles (α-LA/mTG 100 nm and α-LA/HRP 90 nm, $I = 125$ mM). For these nanoparticles an increase of protein concentration from 1 to 5 g L^{-1} led to increase of foam volume (height) at the end of whipping (figure 6.5b). For higher concentrations (10 and 20 g L^{-1}) the foam volume obtained at the end of whipping reached a plateau (figure 6.5b). Since the differences in foam-ability may affect the observed foam-stability, a test was done by foaming in presence of ethanol. The α-LA/mTG nanoparticle solutions were supplemented with 2 % (v/v) ethanol and indeed their foam-ability was comparable to that of monomeric protein in presence of ethanol (figure 6.5b). The reduction in foam-ability with size is similar to the case of heat-induced protein particles or hard colloidal particles. In those cases, typically, either higher concentrations of particles (> 1 % w/v) are used, or low molar mass surfactant is mixed with large particles [6,11–14]. So, the lower foam-ability of larger nanoparticles can be improved by mixing these nanoparticles with small amounts of a very surface-active material. There seems to be a direct correlation between the adsorption kinetics and foam-ability. The lower foam volumes of large α-LA nanoparticles at lower ionic strengths must be due the increased electrostatic repulsion between nanoparticles and air/water interface. The foam-ability of large nanoparticles at low ionic strengths is not caused by the lower diffusion coefficients of nanoparticles, since the mass transport in whipping is dominated by convection in the bulk and diffusion is only important in the boundary layer. Hence, larger nanoparticles results

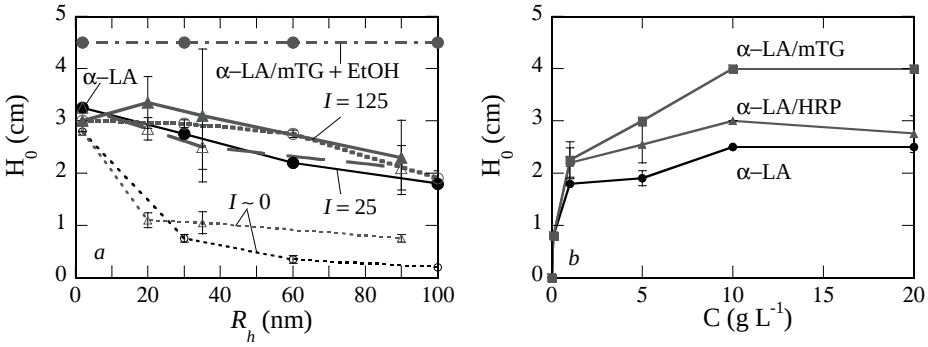

Figure 6.5: *Foam-ability as indicated by foam height at zero time (H_0, cm) produced in low shear whipping of solutions of α-LA (R_h = 2 nm), α-LA/HRP (R_h = 20, 35 and 90 nm) and α-LA/mTG (R_h = 30, 60 and 100 nm) at ionic strengths, I = 0, 25, 125 mM; α-LA/mTG + 2 % (v/v) EtOH nanoparticles at a bulk protein concentration of 5 g L^{-1} (a), and for increasing concentration at 125 mM ionic strength for monomeric α-LA (R_h = 2 nm), α-LA/HRP (R_h = 90 nm) and α-LA/mTG (R_h = 100 nm) (b).*

in lower foam volumes due to lower adsorption flux of nanoparticles towards the newly created air-water interface during whipping. In other words, the process of foam generation is controlled by the adsorption. The short time scale adsorption data in combination with the observed low foam-ability of larger nanoparticles indicate that the time-scale of adsorption in comparison to the timescale of creation of new interface determines the total amount of interfacial area initially generated (foam volume).

Foam-stability

Despite their lower foam-ability, foams produced with α-LA nanoparticles by low-shear whipping were found to be 2 to 6 times more stable as compared to monomeric protein (figure 6.6a). The foam-stability increased with increasing size of nanoparticles and increasing ionic strength. The half-life time ($t_{0.5}$) of the foam produced with α-LA nanoparticles was similar to monomeric α-LA when I 0.001 mM because the nanoparticles had a poor foam-ability at low I. The typical $t_{0.5}$ were less than 1 hour for all the samples at low I (figure 6.6a). The foam-stability was improved at I = 25 and 125 mM (figure 6.6a), although between these two conditions there was no significant difference. The $t_{0.5}$ were 1 to 3 times that of monomeric α-LA for α-LA/HRP 20, 35 nm and α-LA/mTG 30 nm particles at higher ionic strengths. The $t_{0.5}$ of α-LA/mTG 60, 100 nm and α-LA/HRP 90 nm particles increased further and were about 6 times higher than for monomeric α-LA (figure 6.6a). Although the absolute $t_{0.5}$ of foams made in various studies cannot be compared due to variations in concentrations, geometry of device, whipping times etc, an approximate literature comparison can be made with the increase of foam-stability of heat-induced protein

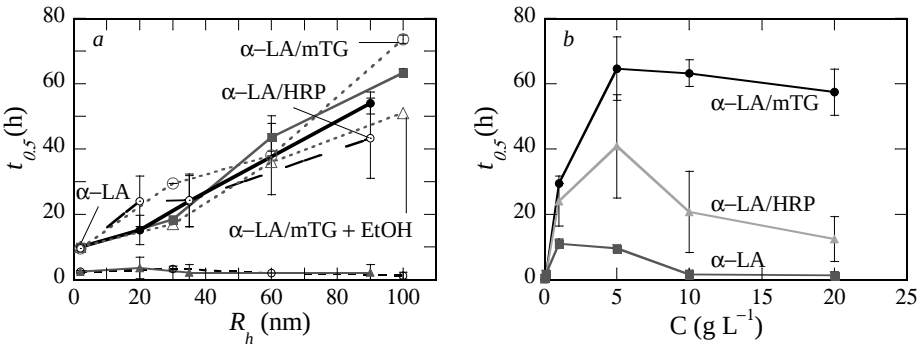

Figure 6.6: *Foam-stability as indicated by foam-life time ($t_{0.5}$) produced in low shear whipping of solutions of α-LA (R_h = 2 nm), α-LA/HRP (R_h = 20, 35 and 90 nm) and α-LA/mTG (R_h = 30, 60 and 100 nm). The ionic strengths are I = 0, 25, 125 mM and the protein concentration is 5 g L^{-1} in all the cases (a). The $t_{0.5}$ obtained for increasing concentration at 125 mM ionic strength for monomeric α-LA (R_h = 2 nm), α-LA/HRP (R_h = 90 nm) and α-LA/mTG (R_h = 100 nm) (b).*

particles with respect to monomeric proteins. For heat-induced protein particles of whey protein (R_h = 200 nm, 20 g L^{-1}), the $t_{0.5}$ was $1.5 - 4$ times higher than for unheated whey proteins [4]. The foam-stability of 5 g L^{-1} α-LA/mTG nanoparticles in presence of 2 % (v/v) ethanol was lower than that of nanoparticles alone (figure 6.6a). Nevertheless, the $t_{0.5}$ of α-LA/mTG 60 and 100 nm particles in presence of 2 % (v/v) ethanol was still $3 - 4$ times higher than that of monomeric α-LA in the presence of ethanol. So, the differences observed in foam-stability of nanoparticles and monomeric proteins were not due to differences in their foam-ability.

Until a concentration of 5 g L^{-1} there were no major differences between the foam-stability of the α-LA/mTG and α-LA/HRP nanoparticles. This indicates that the foam-stability at low protein concentrations is affected only by size of the nanoparticles and that the differences in their mesoscale structure are not particularly important in this regime. However, there was a significant difference between the foam-stability of α-LA/mTG and α-LA/HRP nanoparticles at higher concentrations (10 and 20 g L^{-1}). The foams produced with 100 nm α-LA/mTG nanoparticles were $2 - 4$ times more stable than that of 90 nm α-LA/HRP nanoparticles (figure 6.6b). Hence, in a concentrated regime, the foam-stability is affected not only by size, but also by the mesoscale structure of the nanoparticles. The more dense and rigid α-LA/mTG nanoparticles (as shown in chapters 4 and 5) are more effective Pickering foam stabilizers than open type of α-LA/HRP nanoparticles.

The enhanced stability of protein nanoparticles stabilized foam produced by whipping can be hypothesised to be due to strongly adsorbed particles at interface and thicker foam films. There are two regimes of foam-stabilization by α-LA nanoparticles, low and high concentration. It appears that the foam-stabilization at low concentra-

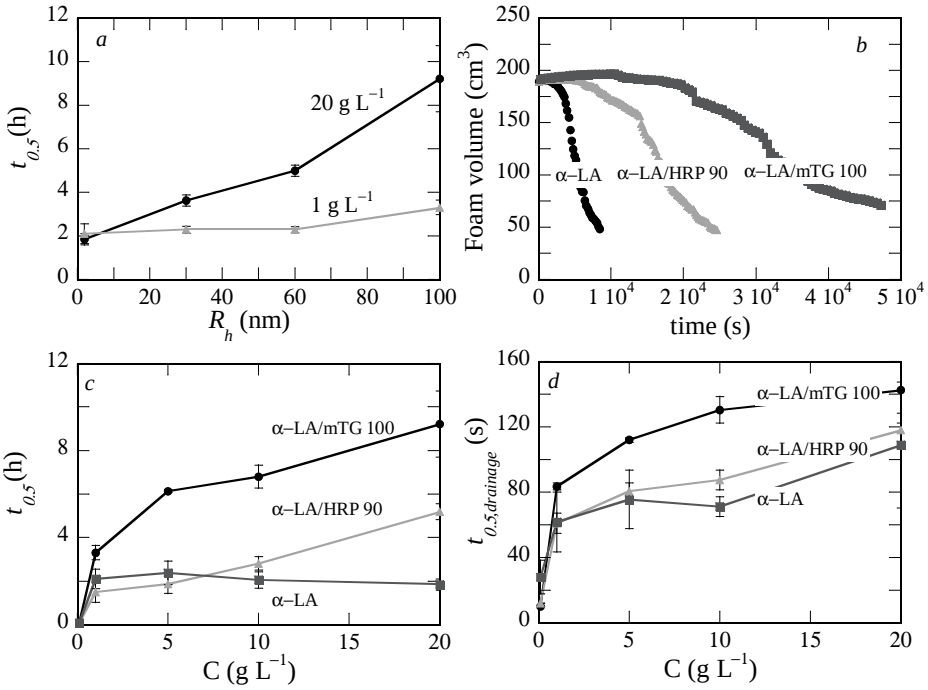

Figure 6.7: *Foam half life time ($t_{0.5}$) of (a) monomeric α-LA (R_h = 2 nm) and α-LA/mTG nanopaticles (R_h = 30, 60 and 100 nm) at I = 125 mM and pH 7.0, 1 and 20 g L^{-1}. (b) monomeric protein and HRP and mTG nanoparticles at 20 g L^{-1}. (c) The foam $t_{0.5}$ and (D) liquid drainage $t_{0.5,drainage}$ (d) of monomeric α-LA, α-LA/HRP nanopaticles (R_h = 90 nm) and α-LA/mTG nanopaticles (R_h = 100 nm) at increasing concentration.*

tion ($0.1-5$ g L^{-1}) regime is mainly determined by the size of the nanoparticles. But, at concentration $\geqslant$ 10 g L^{-1} the mesoscale structure of nanoparticle in the foam films becomes more important for the foam-stability. For the case of α-LA/mTG nanoparticles, the foam-stability at concentrations above 5 g L^{-1} could be related to jamming of nanoparticles in the foam film. It is speculated that at high concentrations, the real concentration in the foam film may be above the critical jamming concentration and the bulk rheological properties after jamming contribute to the foam stability. The differences in the rheological behaviour beyond jamming (chapter 5), in combination with higher surface hydrophobicity of α-LA/mTG as compared to α-LA/HRP nanoparticles appears to result in higher foam-stability of the former.The behaviour of α-LA/HRP nanoparticles is more like monomeric α-LA. For both of them, the foam-stability increases with concentration, reaches a maximum and then starts to decrease at higher concentrations. Decrease of foam-stability at higher concentrations is not typical for protein stabilized foams. It was suspected that the decrease of

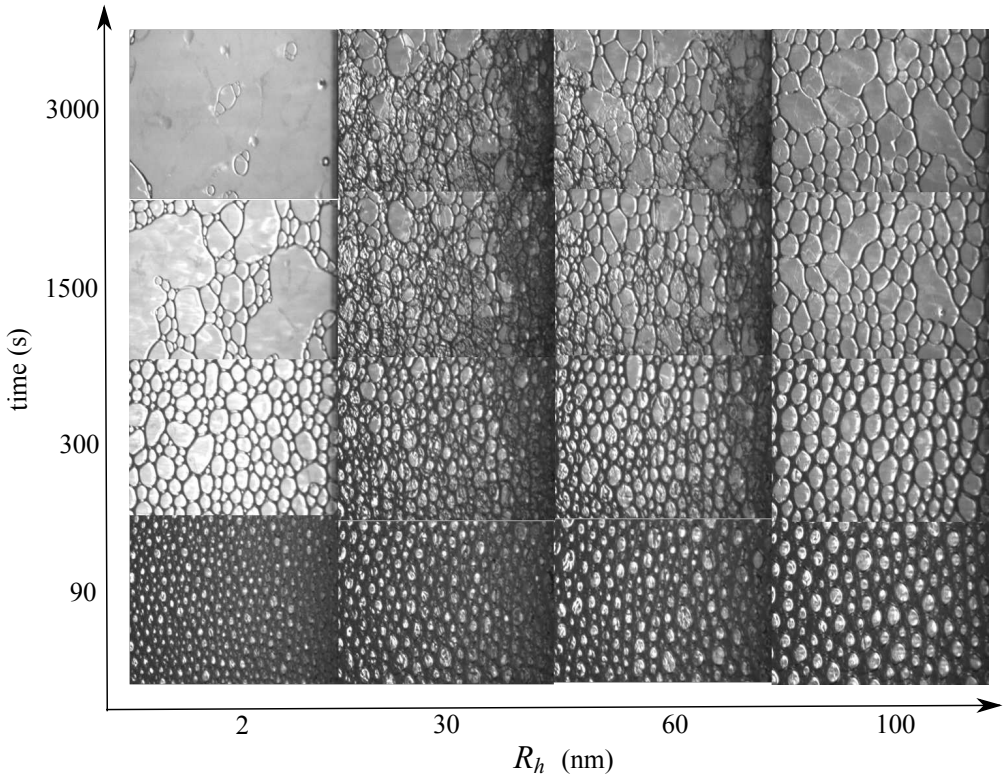

Figure 6.8: *Bubble sizes of monomeric α-LA (R_h = 2 nm) and α-LA/mTG nanopaticles (R_h = 30, 60 and 100 nm) at different times and at I = 125 mM, pH 7.0 and C = 20 g L^{-1}. The magnification is same for all images.*

monomeric α-LA foam-stability could be due to the presence of fat particles (triglycerides or fatty acids) as contaminants. But, ultra centrifugation and pre-filtration of α-LA solutions did not change the foam-stability profile. Therefore, it seems that this decrease in foam stability with increasing protein(-nanoparticle) concentration is not due to impurities, but a property of the protein.

Foam properties by sparging

Since for the nanoparticles, very long adsorption times (lag-times) were observed in the adsorption kinetics, it may be assumed that the method of foaming can affect the observed foam properties. In the whipping test, the air bubbles are continuously remixed into the solution, while in a sparging test, the bubbles directly go to the top of the solution. Therefore, in addition to the whipping, a sparging test was performed. Again, for monomeric α-LA and larger α-LA/mTG nanoparticles, a strong effect of concentration is observed (figure 6.7a). At 1 g L^{-1}, the foam-stability of all samples is

quite similar (increased only from $2-3$ h). At 20 g L^{-1} the differences become much more apparent, since the foam $t_{0.5}$ increases ~ 4 fold ($2-9$ h) from monomeric α-LA to α-LA/mTG nanoparticle ($R_h = 100$ nm). This indicates that indeed in the sparging experiment, the slow adsorption kinetics need to be taken into account by performing experiments at higher concentrations to allow sufficient adsorption of the protein nanoparticles within the time of the bubble rise. Moreover, the α-LA/mTG 100 nm nanoparticles (at 20 g L^{-1}) have a much higher foam-stability than the α-LA/HRP 90 nm nanoparticles i.e. roughly two times (figure 6.7b). In fact the foam-stability of α-LA/mTG 100 nm particles was higher than α-LA/HRP 90 nm particles for all the concentrations greater than 1 g L^{-1} (figure 6.7c). For α-LA/HRP 90 nm particles, the sparging shows continuous foam-stability with increasing concentration, while in whipping actually a decrease is observed at higher concentrations. At 20 g L^{-1}, both types of nanoparticles have higher foam-stability than monomeric α-LA.This higher foam stability can be due to delayed drainage, or due to Pickering stabilisation. From the drainage curves (figure 6.7d), there is indeed a small difference between the two types of HRP and mTG particles. However, at 20 g L^{-1}, for monomeric α-LA drainage curve is almost identical to that of the α-LA/HRP 90 nm particles, while the foam stability is almost two times higher for the α-LA/HRP 90 nm particles. So, the foam-stability is most probably determined by Pickering stabilisation.

The drainage half-life times ($t_{0.5,drainage}$) were correlated with the transition of the bubbles shapes from spherical to polyhedral (figure 6.8). For all samples the bubbles were spherical just after the end of sparging. The liquid volume drained by more than 90 % in around 300 s, which is roughly $\sim 3 \times t_{0.5,drainage}$. At the same time, bubbles appear to be polyhedral, confirming that indeed the liquid drainage is fast even for a concentration of 20 g L^{-1}. An interesting observation is that, even in a sparging test with 20 g L^{-1} the bubble size increases with size of the surfactant i.e. smallest bubble for monomeric α-LA and largest bubble for the α-LA/mTG 100 nm nanoparticle (figure 6.8). So, there are specific differences between the whipping and sparging test, but in general the foam-stability is found to increase $2-4$ times with increasing size of the nanoparticles. The total foam-stability ($t_{0.5}$) cannot be compared between whipping and sparging test since there are differences in the bubble size and foam height. In general, the foaming properties of α-LA nanoparticles appear to be governed by a subtle balance between size, mesoscale structure, surface potential and surface hydrophobicity. The enhancement in foam-stability by enzymatically cross-linked protein nanoparticles is comparable to heat induced protein aggregates of similar size range [4]. But, the foam half-life times are much less than that of hard colloidal particles ($t_{0.5} > 30$ days [1]). Moreover, at a protein concentration of ≥ 5 g L^{-1}, the denser and more rigid α-LA/mTG nanoparticles (table 6.1, chapters 4 and 5) give higher stability than softer α-LA/HRP nanoparticles. The foam-stability of α-LA/HRP nanoparticles is close to monomeric α-LA, while foam-stability of α-LA/mTG nanoparticles is towards the hard particles. Hence, it appears that size and softness are both important for Pickering foam stabilization. Soft protein nanoparticles can effectively reduce the interfacial tension, but they cannot completely arrest the process of Ostwald ripening due to various relaxation processes originat-

ing from their flexible structure. The softness of protein nanoparticles seems to be as important as the contact angles for micron-sized particles. Hence, protein nanoparticles with higher cross-linking density are required to observe the Pickering foam stabilization similar to hard colloidal particles. The enzymatically cross-linked protein nanoparticles have potential to be used in food applications where either a reduction of foam-ability is desired or an enhancement of foam-stability is desired. In combination with a suitable low molar mass surfactant (monomeric/native protein) they can provide both good foam-ability as well as high foam-stability.

Conclusion

The enzymatic cross-linking of a protein was succesfully used to produce a set of protein nanoparticles with increasing size and two different mesoscale structures. The foaming properties of protein nanoparticles can be controlled by varying their size, concentration and solution ionic strengths.The increase in size corresponded to a change in adsorption and foaming behaviour from a typical protein to more nanoparticle behaviour. As such, the approach seems to be promising. With increasing density (mTG) particles, the highest foam stabilities were observed, even though still lower than for inorganic nanoparticles. A main difference seems to be the softness (rigidity) of protein particles. Soft protein particles seem to provide only soft-Pickering stabilisation. Therefore, other modifications, or enzymes may be considered to obtain cross-linked protein nanoparticles with even more rigid/dense structures.

Bibliography

[1] A. Maestro, E. Rio, W. Drenckhan, D. Langevin, and A. Salonen. Foams stabilised by mixtures of nanoparticles and oppositely charged surfactants: relationship between bubble shrinkage and foam coarsening. *Soft Matter*, 10(36):6975–6983, 2014.

[2] S. U. Pickering. CXCVI.-Emulsions. *J. Chem. Soc., Trans.*, 91:2001–2021, 1907.

[3] W. Ramsden. Separation of solids in the surface-layers of solutions and suspensions (observations on surface-membranes, bubbles, emulsions, and mechanical coagulation). – preliminary account. *Proc. R. Soc. Lond.*, 72(477–486):156–164, 1903.

[4] I. Nicorescu, C. Loisel, C. Vial, A. Riaublanc, G. Djelveh, G. Cuvelier, and J. Legrand. Combined effect of dynamic heat treatment and ionic strength on the properties of whey protein foams part ii. *Food Res. Int.*, 41(10):980–988, 2008.

[5] I. Nicorescu, A. Riaublanc, C. Loisel, C. Vial, G. Djelveh, G. Cuvelier, and J. Legrand. Impact of protein self-assemblages on foam properties. *Food Res. Int.*, 42(10):1434–1445, 2009.

[6] B. Rullier, B. Novales, and M. A. V. Axelos. Effect of protein aggregates on foaming properties of β-lactoglobulin. *Colloids Surf., A*, 330(2–3):96–102, 2008.

[7] J. S. Guevara, A. F. Mejia, M. Shuai, Y.-W. Chang, M. S. Mannan, and Z. Cheng. Stabilization of Pickering foams by high-aspect-ratio nano-sheets. *Soft Matter*, 9(4):1327–1336, 2013.

[8] A. Stocco, W. Drenckhan, E. Rio, D. Langevin, and B. P. Binks. Particle-stabilised foams: an interfacial study. *Soft Matter*, 5(11):2215–2222, 2009.

[9] N. Mahmoudi, M. A. V. Axelos, and A. Riaublanc. Interfacial properties of fractal and spherical whey protein aggregates. *Soft Matter*, 7(17):7643–7654, 2011.

[10] N. Mahmoudi, C. Gaillard, Fran¸cois Boué, M. A. V. Axelos, and A. Riaublanc. Self-similar assemblies of globular whey proteins at the air-water interface: Effect of the structure. *J. Colloid Interface Sci.*, 345(1):54–63, 2010.

[11] D. A. Kim, M. Cornec, and G. Narsimhan. Effect of thermal treatment on interfacial properties of β-lactoglobulin. *J. Colloid Interface Sci.*, 285(1):100–109, 2005.

[12] A. Moro, G. D. Báez, G. A. Ballerini, P. A. Busti, and N. J. Delorenzi. Emulsifying and foaming properties of β-lactoglobulin modified by heat treatment. *Food Res. Int.*, 51(1):1–7, 2013.

[13] A. Moro, G. D. Báez, P. A. Busti, G. A. Ballerini, and N. J. Delorenzi. Effects of heat-treated β-lactoglobulin and its aggregates on foaming properties. *Food Hydrocolloid*, 25(5):1009–1015, 2011.

[14] C. Schmitt, C. Bovay, M. Rouvet, S. Shojaei-Rami, and E. Kolodziejczyk. Whey protein soluble aggregates from heating with NaCl: Physicochemical, interfacial, and foaming properties. *Langmuir*, 23(8):4155–4166, 2007.

[15] M. Destribats, V. Lapeyre, M. Wolfs, E. Sellier, F. Leal-Calderon, V. Ravaine, and V. Schmitt. Soft microgels as Pickering emulsion stabilisers: role of particle deformability. *Soft Matter*, 7(17):7689–7698, 2011.

[16] D. Saglam, P. Venema, E. van der Linden, and R. J. de Vries. Design, properties, and applications of protein micro- and nanoparticles. *Curr. Opin. Colloid Interface Sci*, 19(5):428–437, 2014.

[17] P. A. Wierenga, M. B. J. Meinders, M. R. Egmond, A. G. J. Voragen, and H. H. J. de Jongh. Quantitative description of the relation between protein net charge and protein adsorption to air-water interfaces. *J. Phys. Chem. B*, 109(35):16946–16952, 2005.

[18] S. K. Dhayal, H. Gruppen, R. de Vries, and P. A. Wierenga. Controlled formation of protein nanoparticles by enzymatic cross-linking of α-lactalbumin with horseradish peroxidase. *Food Hydrocolloid*, 36(0):53–59, 2014.

[19] W. H. Heijnis, P. A. Wierenga, W. J. H. van Berkel, and H. Gruppen. Directing the oligomer size distribution of peroxidase-mediated cross-linked bovine α-lactalbumin. *J. Agric. Food Chem.*, 58(9):5692–5697, 2010.

[20] J. E. Folk and P. W. Cole. Mechanism of action of guinea pig liver transglutaminase .i. Purification and properties of enzyme - identification of a functional cysteine essential for activity. *J. Biol. Chem.*, 241(23):5518–5525, 1966.

[21] H. Y. Zhao, P. H. Brown, and P. Schuckt. On the distribution of protein refractive index increments. *Biophysical J.*, 100(9):2309–2317, 2011.

[22] M. Andersson, B. Wittgren, and K. G. Wahlund. Accuracy in multiangle light scattering measurements for molar mass and radius estimations. model calculations and experiments. *Anal. Chem.*, 75(16):4279–4291, 2003.

[23] S. Podzimek. *Light scattering, size exclusion chromatography and asymmetric flow field flow fractionation,*. John Wiley & Sons, Hoboken, NJ, USA, 2011.

[24] M. Kataoka, F. Tokunaga, K. Kuwajima, and Y. Goto. Structural characterization of the molten globule of α-lactalbumin by solution X-ray scattering. *Protein Sci.*, 6(2):422–430, 1997.

[25] P. A. Wierenga, M. B. J. Meinders, M. R. Egmond, F. A. G. J. Voragen, and H. H. J. de Jongh. Protein exposed hydrophobicity reduces the kinetic barrier for adsorption of ovalbumin to the air-water interface. *Langmuir*, 19(21):8964–8970, 2003.

[26] J. A. De Feijter, J. Benjamins, and F. A. Veer. Ellipsometry as a tool to study the adsorption behavior of synthetic and biopolymers at the air-water interface. *Biopolymers*, 17(7):1759–1772, 1978.

[27] A. Scheludko and D. Exerowa. Über den elektrostatischen druck in schaumfilmen aus wsserigen elektrolytlösungen. *Colloid Polym. Sci.*, 165(2):148–151, 1959.

[28] R. J. B. M. Delahaije, P. A. Wierenga, N. H. van Nieuwenhuijzen, M. L. F. Giuseppin, and H. Gruppen. Protein concentration and protein-exposed hydrophobicity as dominant parameters determining the flocculation of protein-stabilized oil-in-water emulsions. *Langmuir*, 29(37):11567–11574, 2013.

[29] A. R. Cox, D. L. Aldred, and A. B. Russell. Exceptional stability of food foams using class ii hydrophobin HFBII. *Food Hydrocolloid*, 23(2):366–376, 2009.

[30] W. Wang, Q. Zhong, and Z. Hu. Nanoscale understanding of thermal aggregation of whey protein pretreated by transglutaminase. *J. Agric. Food Chem.*, 61(2):1–60, 435–446.

[31] A. Graciaa, G. Morel, P. Saulner, J. Lachaise, and R. S. Schechter. The ζ-potential of gas bubbles. *J. Colloid Interface Sci.*, 172(1):131–136, 1995.

[32] C. Yang, T. Dabros, D. Li, J. Czarnecki, and J. H. Masliyah. Measurement of the zeta potential of gas bubbles in aqueous solutions by microelectrophoresis method. *J. Colloid Interface Sci.*, 243(1):128–135, 2001.

[33] J. N. Israelachvili. *Intermolecular and Surface Forces (Third Edition)*. Academic Press, San Diego, CA, USA, 2011.

Chapter 7

General Discussion

In this thesis, enzymatic cross-linking by microbial transglutaminase (mTG) and horseradish peroxidase (HRP) was used to produce α-lactalbumin (α-LA) nanoparticles (polymers). The mesoscale structure of the nanoparticles is determined by the type of enzymes and substrate protein. Different amino acid sequences in substrate proteins will affect the number, and the protein structure will affect the accessibility of amino acids that can be used by the enzyme. Therefore, a particular enzyme substrate combination can lead to variations not only in the number of cross-links but also on the length of the linkages. Most cross-links are thought to be between two individual amino acids. For instance, HRP induced cross-linking of proteins has so far been believed to induce di-tyrosine cross-links. But, oligo-tyrosine cross-links can also be formed in proteins. These could potentially have an effect on the rigidity of the nanoparticles. In terms of functionality, protein particles of size similar to other hard colloidal particles i.e. $R_h \sim 100$ nm can be produced by enzymatic cross-linking. But, enzymatic cross-linking results in soft protein particles which do not provide Pickering stability as high as that of hard particles. We do see the effects of mesoscale structure e.g. size and rigidity of protein nanoparticles on functionality. But, higher cross-link densities and rigidities are required for higher Pickering effect.

Clearly, currently used methods are not easy to study and quantify aspects such as softness. So, first we will discuss some issues with the methods of characterisation of mesoscale structure and stability of the nanoparticle structures. Then we will reflect on identification/quantification of cross-links and relation between mesoscale structure and functionality. Finally, an outlook will be presented towards the substrate protein systems other than α-LA.

Table 7.1: *Summary of various aspects of protein nanoparticle structure, its impact on functionality and method to quantify them (used in this thesis).*

	Structure/Functionality	Characterization	Chapters
Molecular scale	2° and 3° structure	CD	4
	cross-links/monomer	AF4 and LC-MS/OPA	3,7
	Inter/intra molecular cross-links	Conversion of monomer versus conversion of amino acid	3,7
	Length of cross-links	Acid hydrolysis/LC-MS	3
Mesoscale	Exposed hydrophobicity	ANSA	6
	Hydrodynamic radius (R_h)	DLS	2-6
	Radius of gyration (R_g)	MALS	2, 4-6
	R_g/R_h ratio	MALS, DLS	2, 4-6
	Molar mass (M_w)	MALS	2-7
	Apparent density (ρ_{app})	MALS	2, 4-6
	Degree of polymerization (DP)	AF4 MALS	2-6
	d_f	AF4 MALS	2, 4-6
	μ	Zetasizer	6
	Adsorbed layer thickness	Ellipsometer, Scheludko cell, AFM	6
	Swelling (δR_h)	δI in DLS	4
Macroscale	Bulk rheology	Rheometer	5
	Foam properties	Low shear whipping (Aerolatte), Sparging (low shear whipping)	6
	Adsorption/surface rheology	ADT	6
	Water holding capacity	Centrifugal filtration	4
	Thermal stability	Heating in DLS	4

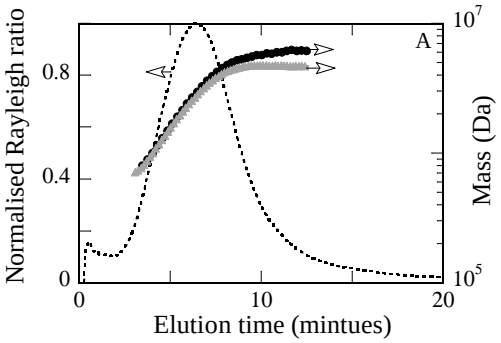

Figure 7.1: *Differences between the M_w fitted using UV (grey) and RI (black) as concentration detector.*

Use of AF4-MALS-UV/RI for characterisation of mesoscale structure

To describe the meso-scale structure of (protein-)nanoparticles, several different parameters can be used (table 7.1). Out of the 15 identified parameters, 8 were obtained directly or derived from the asymmetrical flow field flow fractionation (AF4) in combination with multi-angle light scattering (MALS) (table 7.1). As such, this technique proved to be a powerful technique for a fast and coherent analysis of the protein nanoparticles (table 7.1). One main advantage of AF4 over for instance size-exclusion chromatography, was that no pre-treatment of sample (e.g. filtration /centrifugation) was required. Also, more than 95 % of the injected material was detected and analysed in the AF4 (based on the mass balance done with RI). However, it was also found that one should take care in choosing the correct membrane, since the regenerated cellulose (RC) membrane showed some non-specific interaction at low ionic strength ($<$ 1 mM). In the eluent containing 10 mM sodium phosphate buffer (pH 7.0), the non-specific interactions of nanoparticles with membrane were not detectable.

Another issue in the AF4-MALS analysis was the determination of the concentration of the eluting compounds. For proteins, typically the UV detector would be chosen, since it is specific for proteins and less sensitive to pressure variations than the RI detector. However, the use of UV detector leads to under-estimation of molar mass for larger particles (7.5 to 12.5 min, figure 7.1) as compared to RI detector. The question is which detector to use for the estimation of molar masses (M_w).

Most likely, the under-estimation of the M_w based on using the UV detector is due to the light scattering induced by the particles in the UV detector. We attribute this to light scattering since the difference in M_w indicate an increase in the molar extinction coefficient of the protein nanoparticles by around 25 %. Upon crosslinking, a maximum difference of 5 % is expected, assuming either complete loss of tyrosine signal, or change of the tyrosine molar absorption coefficient from exposed to buried.

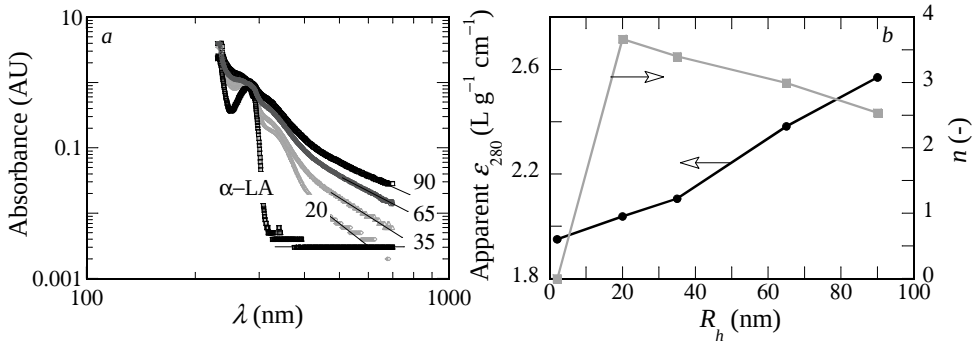

Figure 7.2: *Scaling of UV absorbance measured at various wavelengths, depicted in logarithmic scale (a). The various symbols are, native α-LA, nanoparticles of z-averaged hydrodynamic radius; 20, 35, 65 and 90 nm. Various dotted lines are the power law fit to data between 500 and 700 nm. The apparent extinction coefficient of nanoparticles as determined using the concentration measured with DUMAS and then measuring absorbance as a function of various dilutions (b). The power law exponents from 2a are shown on second y-axis in 2b.*

Therefore, most likely the under-estimation in M_w is due to scattering contributions. It is well known that the intensity of light scattering by a solid particle scales as the size R^6. So, we may expect the scattering contributions to increase with the size. In the simplest case of isotropic or Rayleigh scattering [1,2], the absorbance should scale as λ^{-n} ($n = 4$). For HRP induced nanoparticles of increasing size, the UV spectra were plotted on a log-log scale in figure 7.2a, and a power law was fitted between 500 and 700 nm to obtain the scaling exponent, n. The λ was chosen in a region where the measured absorbance is solely due to the light scattering, i.e. in our case $\lambda > 500$ nm. At those wavelengths conjugated aromatic molecules with chromophores similar to di-tyrosine, do not show any absorbance [3]. The exponent n changes from approximately 3.7 to $\sim$ 2.5 (figure 7.2b), indicating that the nanoparticles formed at the end of the reaction are so large that the mechanism of light scattering is changing from the Rayleigh to the Mie type [1]. This results in an apparent increase of extinction coefficient (figure 7.2b). Hence, measurement of nanoparticle concentration with UV by using extinction coefficient of monomeric protein would lead to errors in measurement of concentration. In the RI detector, the effect of scattering is much less important. The intensity of scattered light varies inversely with wavelength i.e λ^{-n} and the λ used in RI detector is 660 nm as compared to 280 nm in UV detector. In addition, the dn/dC of protein nanoparticles is not influenced by cross-linking of amino acids, such as the presence of di-tyrosine/oligo-tyrosine. Consequently, dn/dC is the same as for the native protein as long as the size of the nanoparticle is smaller than the λ used in the RI detector. For particles larger than λ of RI, the RI detector could be used after determination of dn/dC for those particles.

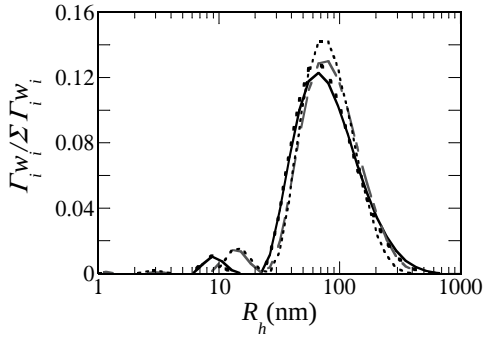

Figure 7.3: *Distribution of hydrodynamic radii determined from DLS for various cryo-protectants; protein nanoparticle mixture before freeze drying (solid continuous black line), and after freeze drying with sucrose (dashed black line), trehalose (dotted black), sorbitol (dahsed-dotted grey line). Y-axis is the weighted intensity.*

Stability of nanoparticle structure

Most often in the studies involving protein particles, the particles are preserved and stored by freeze-drying. It was shown in chapter 4 that the α-LA nanoparticles made using mTG and HRP are rather dilute i.e. their apparent densities are < 10 % (w/v). Hence, stability of the nanoparticle structures during freezing and drying might change and this issue should always be considered. Else, there could be a serious artefact in the analysis of structure-function relations. Indeed, when the α-LA/HRP nanoparticles were freeze dried directly as such without any stabiliser, the freeze dried powder could not be re-dissolved completely. After filtration of the suspension of freeze-dried particles (over a 0.45 μm filter) it was found that more than 50 % of the protein nanoparticles were irreversibly changed to insoluble aggregates. The insoluble aggregates could not be dissolved even in presence of 1 % (w/w) sodium dodecyl sulphate, SDS (i.e. around 10 times its critical micellar concentration, CMC) or 0.1 M sodium hydroxide.

A possible explanation is the freeze concentration of protein nanoparticles as a result of ice crystallization. The cold denaturation of proteins, analogous to heat induced denaturation, has also been described in literature [4]. So, when the denatured protein nanoparticles are being pushed into each other due to freeze concentration, probably they are stuck into primary minima, leading to irreversible aggregation. This phenomenon has been observed often during the freeze drying of antibody formulations [5, 6]. There are a number of different hypotheses reported in literature to explain this phenomena, such as adsorption of proteins at ice-solution interface and subsequent change in structure [7] disruption of the hydration water hydrogen bonding [8] and changes in the solution pH due to partial crystallization of the buffering salt [7]. A typical solution to this problem is to freeze dry proteins in presence of a

molecule containing hydroxyl groups, such as disaccharides [7]. Sugars are believed to form H-bonds with proteins and form a glassy mixture on freeze concentration, which is believed to preserve the structure [9]. At the start of the thesis, different low molecular weight compounds were tested for their effect on the freeze-thaw stability of protein nanoparticles The phase separation could not be completely prevented with glycerol or Tween-80. Tween-80 was tried at the CMC (= 0.1 mM), and 10 times below and above CMC. For enzymatically cross-linked α-LA nanoparticles, sucrose, trehalose and sorbitol (tested at 0.5M concentration for 15 g L^{-1} protein nanoparticles) were found to be most effective. However, the powder obtained after freeze drying was found to be more free flowing and easy to handle in case of sucrose and trehalose as compared to sorbitol. Hence, it was decided to use sucrose for the further work (chapters $2-6$) as a cryo-protectant for enzymatically cross-linked protein nanoparticles. The size distribution of the protein nanoparticles before and after freeze drying with sugars, as measured by DLS is depicted in figure 7.3. It proves that the cryo-protectants are indeed very effective in stabilising the structure of protein nanoparticles during freezing and subsequently during drying steps.

Identification/Quantification of cross-links

While it seems straightforward to claim to study a link between structure and (techno-) functionality, it became apparent in this study that a full, quantitative description of the structure of protein nanoparticles is not easy to achieve. Yes, different methods exist and have been used. However, in most studies in literature, only a few methods are used simultaneously. In addition, even particles with a similar topological structures may behave differently if the internal structure, or cross-links are different. Indications of softness were obtained by atomic force microscopy (AFM) (chapter 4) and ellipsometric measurements (chapter 6). In both techniques, the α-LA/HRP nanoparticles are more soft than α-LA/mTG, as indicated by more extensive flattening of the particles at solid/water and air/water interface. The origin of this softness could be the flexibility for internal rearrangement due to lower number of cross-links per molecule. Hence, it is important to quantify the cross-links per molecule and the length of the cross-links.

Cross-links per molecule: HRP vs mTG

Differences in the mesoscale structure of α-LA/mTG and α-LA/HRP nanoparticles seems to be correlated with the fact that there is a significant difference in the number and accessibility of target amino acids (Tyr versus Lys/Gln). This most probably leads to a difference in the average number of cross-links per monomeric protein in the nanoparticles.The plot of conversion of monomeric protein versus the conversion of target amino acid seems to be a reliable method to estimate the average number of cross-links per protein molecule (monomer) (chapter 3). The conversion of monomeric α-LA plotted against the conversion of Tyr (in the case of HRP) and against conversion of Lys (in the case of mTG) indicates that more cross-links are formed per

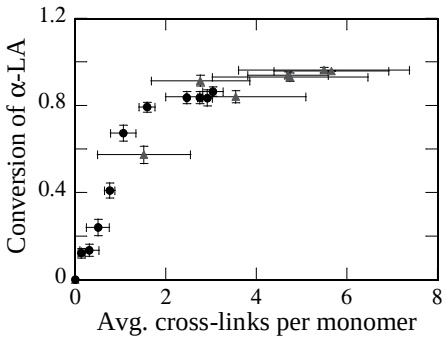

Figure 7.4: *Conversion of monomeric α-LA as a function of the average number of cross-links per monomer in α-LA/HRP (●) and α-LA/mTG (▲) nanoparticles.*

molecule with mTG in both the stages of nanoparticles formation (figure 7.4). The conversion of Lys was obtained using OPA assay [10]. In the first stage (conversion of α-LA $\sim$ 80 %), there were only $1-2$ cross-links formed in α-LA/HRP as compared to $1-3$ cross-links in α-LA/mTG nanoparticles. In the second stage (conversion of oligomers to polymers), the average number of cross-links increased to $3-4$ for α-LA/HRP and it was $4-7$ for α-LA/mTG.

Tyrosine cross-links induced by HRP

While most studies on protein crosslinking by HRP focus on the reactivity of tyrosine, the possible side-reactions towards other amino acids, or the oxidizing effect of the H_2O_2 has not been discussed at great length in literature. Oxidative enzymes are known to oxidise a variety of amino acid residues in proteins, such as methionine, cysteine, tryptophan, histidine [11] .On the contrary, we observed cross-linking of only tyrosine residues (chapter 3). To delineate the effect of oxidation of amino acids versus their cross-link ability, various model reactions were performed. For example, apo α-LA was incubated with H_2O_2 in absence of HRP, various single amino acids such as tyrosine, tryptophan, cysteine, histidine were incubated with HRP and H_2O_2 separately as well as in the presence of tyrosine at an equal molar ratio. It was found that in absence of HRP, incubation of α-LA with H_2O_2 results in oxidation of the methionine. This was inferred from the increase of the molar mass of α-LA by16 Da (in ESI-MS), but no cross-linking was observed in this case. The absence of cross-linking was concluded from the absence of peaks other than that of monomeric α-LA in RP-HPLC-MS. Upon incubation of single amino acids in the presence of HRP and H_2O_2, oxidation of tryptophan was observed, only tyrosine was cross-linked (oligomerize). These results indicate that tyrosine is most reactive amino acid in presence of oxidative enzymes. The next questions are, which methods are most suitable for quantification of tyrosine cross-links and are all the tyrosines reactive?

Table 7.2: *Tyrosine containing peptides and di-tyrosine cross-linked di-peptides identified using LC-MS in the hydrolysates of α-LA nanoparticles made with BLP.*

Tyrosine present	Sequence	Theoretical mass [M] (Da)	Observed m/z $[M+nH]^{n+}$	Observed mass [M] (Da)
Y18	[17-31] [G**Y**GGVSLPEWVCTTF]	1614.74	808.4 $[M+2H]^{2+}$	1614.8
Y36	[32-48] [HTSG**Y**DTQAIVQNNDSTE]	1978.85	990.4 $[M+2H]^{2+}$	1978.8
Y50	[50-53] [**Y**GLF]	498.25	499.3 $[M+H]^{+}$	498.3
Y103	[99-103] [VGIN**Y**]	564.29	565.3 $[M+H]^{+}$	564.3
Y18-Y50	[17-31] + [50-53]	2110.99	1056.48 $[M+2H]^{2+}$	2110.96
Y18-Y36	[17-31] + [32-48]	3591.59	1198.21 $[M+3H]^{3+}$	3591.63
Y103-Y103	[99-103] + [99-103]	1126.58	564.45 $[M+2H]^{2+}$	1126.9

It has been suggested that absorbance at UV 318 can be used for quantifying the tyrosine cross-links [12]. For the larger particles, this may be complicated by two factors. Firstly, the molar extinction coeffcients of di-tyrosine and higher oligomers of tyrosine are not known. Secondly, as discussed above, the UV absorbance is affected by the light scattering of larger particles. In addition, there is a problem in quantification by UV for the larger particles due to scattering (as discussed in the AF4 section). Therefore, the quantification of di-tyrosine/oligo-tyrosine was done in this thesis after separation of acid hydrolysates in the UHPLC. In this method (acid hydrolysis followed by LC-MS) oligomers up to DP 8 could be analysed. However, higher oligomers could not be analysed due to insolubility (chapter 3). Hence, it became evident that the only way to quantify the total amount of reacted tyrosine is to estimate it from the amount of tyrosine reacted. Three methods were tested to quantify the amount of tyrosine reacted (figure 7.5). These were tyrosine fluorescence [12], the Folin−Ciocalteu assay [13] (performed on intact protein nanoparticles) and acid hydrolysis followed by LC-MS [14].There was a good correlation found between all three of them (figure 7.5). While there was a good correlation between the relative decrease of Tyr, in absolute levels we may still be hindered by the scattering artefacts during Folin Ciocalteu and fluorescence measurements.

In the first stage of cross-linking, on average $1-2$ tyrosine residues are cross-linked per α-LA molecule and $3-4$ in the second stage (chapter 3, figure 7.4). As explained above, this was estimated based on the relative conversion of monomeric α-LA (from AF4) and conversion of tyrosine (acid hydrolysis, LC-MS). As a confirmatory experiment, a partial enzymatic hydrolysis of α-LA nanoparticles with *Bacillus*

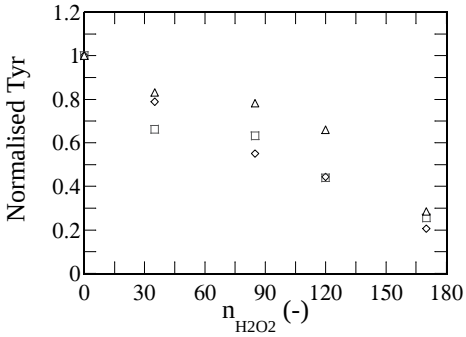

Figure 7.5: *Tyrosine conversion obtained relative to the unmodified monomeric α-LA by various methods: Tyrosine fluorescence (□), Folin − Ciocalteuassay(△), acid hydrolysis followed by LC-MS (◇).*

licheniformis protease (BLP) was performed. After hydrolysis, peptides containing each of the four tyrosines, separately as well as di-peptides linked by di-tyrosine cross-links were identified. The experimental approach was partly as described in [15] and the details of BLP and hydrolysis conditions were same as used for some other proteins [10]. The α-LA nanoparticles were hydrolysed with BLP until 5 % degree of hydrolysis (DH). This resulted in the formation of peptides of various molar masses as seen in figure 7.6a. These peptide mixtures were further analysed by LC-MS following a method similar to [15]. Four different peptides containing the Tyr18, 36, 50 and 103 were identified (table 7.2). Furthermore, combinations of these peptides linked by a di-tyrosine cross-link were also found (table 7.2). Cross-links were found between Tyr18 and Tyr50, Tyr18 and Tyr36, Tyr103 and Tyr103 (figure 7.6b).

The Y18-Y50 cross-link was also previously found in the α-LA dimer [15]. They probably did not find the other cross-links since only the dimer was isolated by ion-exchange after one addition of H_2O_2. In our experiment, we did not hydrolyse a purified dimer, but a heterogeneous sample of large nanoparticles was used i.e. $n_{H2O2} = 1 - 170$. These results indicate that all the four tyrosine residues in α-LA are reactive.

It is known that not all the four tyrosine residues in α-LA are equally exposed to the solvent [16]. It had earlier been speculated that during enzymatic cross-linking, the α-LA structure might open up leading to exposure of all tyrosines [17]. In this work, we conclusively prove this by combining the CD data (chapter 4) on monomeric α-LA and α-LA nanoparticles of $R_h = 90$ nm with the fact that we find all the four tyrosines to be reactive. The tertiary structure of the α-LA is completely lost and this most probably leads to exposure of all tyrosine residues. In addition, the regions around tyrosine residues seem to be flexible enough (minimum steric hindrance) to enable the formation of oligo-tyrosine cross-links. It is interesting to note that glycine (Gly) is present next to three of the tyrosine residues in α-LA sequence. Tyr18 is in

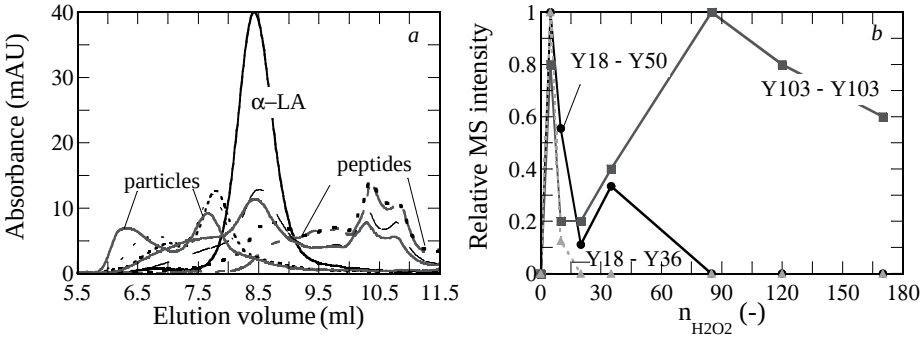

Figure 7.6: *SEC profile of samples $n_{H2O2} = 0$, 5, 10, 35 (black to light grey) before (full) and after (dashed) enzymatic hydrolysis (a). The sum of the major peak areas corresponding to Y18-Y50 crosslinked di-peptides, Y18-Y36, Y103-Y103, respectively in MS chromatogram, normalised to maximum of each di-peptide at various dosage of n_{H2O2} (b).*

between Gly17 and Gly19, Gly20. Tyr36 is next to Gly35 and Tyr50 is next to Gly51. In natural systems where tri-tyrosine and tetra-tyrosine have been detected, Tyr was also found to be present next to Gly [18]. Based on this we speculate that formation of oligo-tyrosine is favoured if Tyr is located next to a low molar volume amino acid such as Gly due to minimum steric hindrance.

Link between mesoscale structure and functionality

Enzymatic digestibility of α-LA nanoparticles

For the identification of the tyrosine residues involved in cross-linking (as described above), the α-LA/HRP nanoparticles were hydrolysed with BLP until DH of 5 %. Also, experiments were performed where the hydrolysis was carried out until a plateau was observed in the degree of hydrolysis (DH) and we refer to this as end point hydrolysis (figure 7.7). An interesting observation during this study was that the end point DH was inversely related to the nanoparticle molar mass (size). The DH was around $12-16$ % for monomeric α-LA and the early stage α-LA/HRP oligomers. But, it decreases to around 4 % for α-LA/HRP polymers (nanoparticles). This indicates that the enzymatic digestibility of α-LA nanoparticles is decreased after cross-linking. This effect is similar to that seen for reduction of enzymatic digestion of cross-linked (enzymatically) casein polymers [19].

Bulk rheological properties

If there is a relation between the rheology of the gels and the structure of the nanoparticles used for making that gel, then a scaling analysis should lead to different fractal dimensions (d_f) of the nanoparticles. These d_f can then be compared with

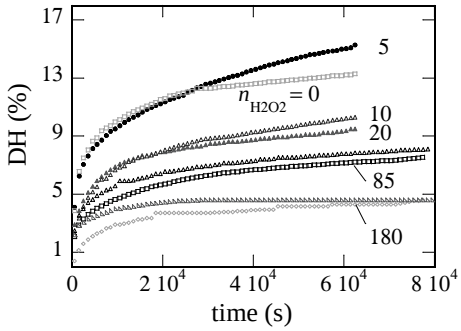

Figure 7.7: *Degree of hydrolysis achieved with BLP of monomeric α-LA ($n_{H2O2} = 0$) and α-LA nanoparticles of increasing degree of polymerization indicated by $n_{H2O2} = 5 - 180$.*

Table 7.3: *The structural parameters obtained by fitting the scaling model of Wu and Morbidelli [20] to the $G^{'}$ versus concentration data. The fitting was performed by setting $d = 3$ and $x = [1, 1.3]$ and solving for the d_f subject to the constraints: $0 \leqslant \alpha \leqslant 1$, $1 \leqslant d_f \leqslant 3$, and $1 \leqslant x < d_f$ [20]. The n_{exp}, n_{fit} and d_f stand for power law scaling exponent obtained from the $G^{'}$ versus C experiment, the fitted exponent and the fractal dimension, respectively. The β and α are the parameters in equations 1.1 and 1.2 (chapter 1), respectively.*

	n_{exp}	n_{fit}	d_f	β	α at $x = 1.3$	Regime
α-LA/mTG	18.7	18.7	2.79 ±0.003	3.97 ±0.05	0.112	Transition gel
α-LA/HRP	5.26	5.26	2.24±0.001	4.00 ±0.01	0.094	Transition gel

those obtained from light scattering. Scaling analysis then becomes an alternative way to link the rheology of the gels with the structure of the constituent particles.The rheological behaviour of the gels made by concentrating a solution of nanoparticles beyond jamming concentration was found to be related to mesoscale structure of the nanoparticles (chapter 5). The double logarithmic plots of storage modulus ($G^{'}$) versus concentration, beyond close packing concentration were fitted with power law and the exponent (n) was obtained from the fit (n_{exp}. in table 7.3). Now, the scaling model of Wu and Morbidelli [20] (equations 1 and 2 in chapter 1) is used and the best fit parameters are obtained by minimization of the squared difference between the experimental and the fitted n (n_{fit} in table 7.3).

Based on the fitted values of α (table 7.3), it can be concluded that gel in both cases is a transition gel. A transition gel is in between the strong-link and weak-link regime i.e. the inter-particle interactions are of the same order as intra-particle interactions (see chapter 1). For comparison, soy protein cold-set gels made in presence of 10 mM calcium concentration are of filamentous type and are characterised as transition gel [21]. Also, egg white gels made in the pH range $3-11$ are in the transition regime [22]. The exponent for α-LA/HRP nanoparticles is in the range typically observed in the case of heat-set or cold-set protein gels [21,22]. The interesting part is that while these

basic properties were similar, the gels formed with enzymatically cross-linked protein particles were found to be thermoreversible [23], while typicaly heat-induced protein gels are not. The values of exponent β can be used to gain information about the structure of the stress-bearing backbones in the gels as the magnitude of β is related to the number of junctions/links per strand and the type of deformation mechanism of strand. The value of β observed for both cases is around 4 (table 7.3). A value of $\beta \geqslant 4$ is typical for the fractal strands which are randomly curved and flexible and the strands mainly deform by bending [24, 25]. Values of $\beta \geqslant 4$ have also been observed in many heat-set protein gels [21, 22]. In summary, the $G^{'}$ versus concentration data could be well described by the scaling model. The gels formed by concentrating solutions of α-LA/HRP and α-LA/mTG nanoparticles are similar type i.e. in both cases gels appear to be filamentous with fractal starnds. The main difference in the rheology of the gels comes from the differences in the structure of the nanoparticles used for making the gels. The differences between the mesoscale structure of α-LA/HRP and α-LA/mTG nanoparticles is reflected in the fractal dimension (d_f) obtained by fitting rheological data. The α-LA/mTG nanoparticles have a $d_f = 2.79$ as compared to 2.24 for α-LA/HRP nanoparticles. These values are reasonably similar to the values obtained from low q. Hence, the rheological behaviour of protein nanoparticles is indeed linked to the mesoscale structure of the particles.

Foaming and surface properties

Enzymatic crosslinking had significant effects on the foam properties. Indeed, as was hoped at the start of the project, the enzymatic crosslinking changed the properties from typical protein to more particle-like behavior. This was reflected in a low adsorption kinetics, and consequent low foam-ability with increasing size of the nanoparticles. While, at the same time the foam-stability (when formed at sufficient concentration, or high ionic strength) was significantly improved (chapter 6).The foams made with α-LA nanoparticles were two to six times higher than that of monomeric α-LA. Foam-stability of rigid α-LA/mTG nanoparticles of R_h 100 nm was two to three times higher than that of diluter and softer α-LA/HRP nanoparticles of R_h 90 nm. An interesting feature of the foams made with protein nanoparticles was that the drainage kinetics of the liquid from the foam was not significantly different for monomeric protein and the nanoparticles (chapter 6). All the foams drained to more than 90 % in about five minutes and the bubbles changed from spherical (wet foam) to polyhedral (dry foam). So, the higher stability of foams stabilised by nanoparticles is not due to the slowing down of drainage. It is either due to jamming of nanoparticles in the bulk of the foam films or due to reduction of Ostwald ripening due to thicker interfacial layers. The reduction of Ostwald ripening by nanoparticles is evident from figure 7.8a. The foams were made with 1 g L^{-1} monomeric α-LA and α-LA/HRP nanoparticles in 100 mM ammonium acetate buffer (pH 6.8) by whipping method (same as in chapter 6). Next, the bubbles from the dry foam were diluted with 0.5 % xanthan solution to a volume fraction of less than 50 % air phase. This strategy results in very thick films of xanthan between the bubbles and due to yield

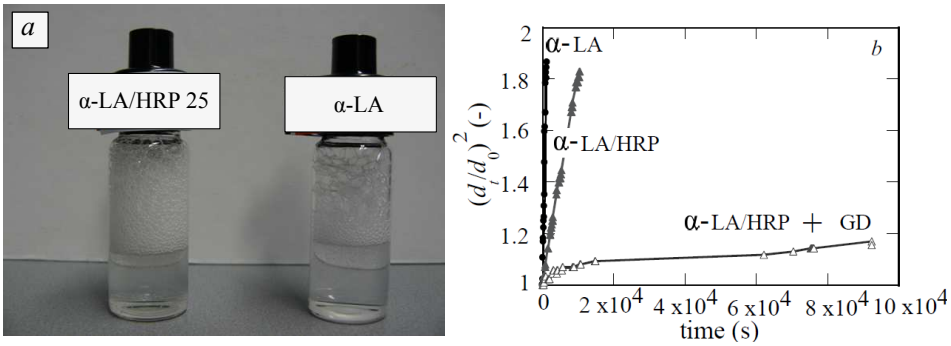

Figure 7.8: *Ostwald ripening of bubbles covered with α-LA/HRP nanoparticles of $R_h = 25$ nm versus monomeric protein in xanthan solution (a). Relative change in bubble diameter with time according to [26] (b).*

stress of the xanthan, coalescence is completely prevented [26] The only mechanism operational is Ostwald ripening. The Ostwald ripening in the case of nanoparticles was significantly slower than that of monomeric protein as indicated by the slope of the plot of time variation of the squared bubble diameter at any time with the initial bubble diameter (figure 7.8b). The Ostwald ripening was completely arrested when the dilute bubbles covered with nanoparticles were further cross-linked with gluteraldehyde (GD) (figure 7.8b). These results indicate that enzymatically cross-linked protein nanoparticles form thicker interfacial layers and that slows down the process of Ostwald ripening. However, the cross-link density in the case of enzymatic cross-linking is not sufficiently high to completely arrest the foam collapse.

So, it is very clear that Pickering foam stabilisation by hard particles is much higher than soft protein particles. But, in terms of the theoretical explanations for this effect, there are few contradictions and these are discussed next. First, a typical argument for Pickering stabilisation is based on size. Typically, it is argued that, the adsorption energies (W) at an interface scales as square of the particle size (R), i.e. $W = \pi R^2 \gamma \left(1 \pm cos\theta\right)^2$, where, γ is the interfacial tension and θ is the contact angle. Once adsorbed, it is impossible to detach a particle of $R > 10$ nm and $\theta \sim 90^\circ$ at room temperature, since $W \gg 100$ k_BT. Hence, use of particles as surfactants leads to ultra-stable foams and emulsions [27]. Here, it is assumed that a solid particle of radius R is adsorbed at the interface. In the case of soft protein nanoparticles, we showed in chapter 6 that only a part of the nanoparticles is attached to the interface. So, the size to put in the above equation would be size of the primary particle or size of the monomer and not the size of the secondary (large) nanoparticle. So, the origin of stability with soft protein particles as compared to monomeric protein is most probably related to the fact that desorption of such an fractal particle from interface would require simultaneous detachment from multiple points. Moreover, the contact angle in such a scenario where only a few primary particle of size < 100 nm are attaching to interface is probably not so important. Hence, new theoretical model is

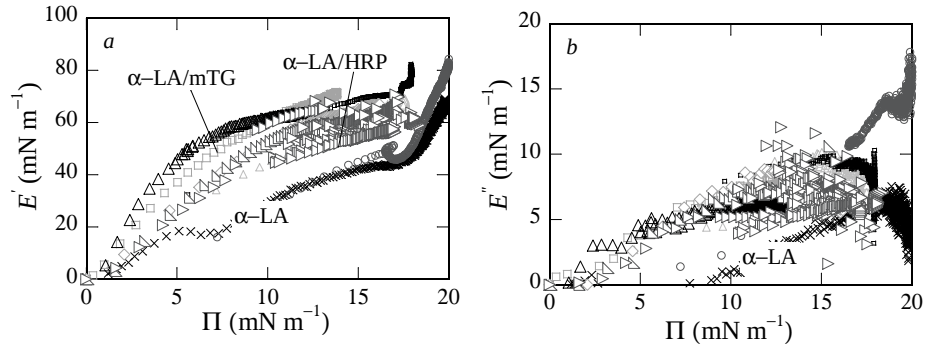

Figure 7.9: *Surface dilatational elastic modulus (a) and loss modulus (b) as a function of surface pressure for α-LA /HRP and α-LA/mTG nanoparticles.*

required to explain the enhanced stability obtained with fractal protein particles.

Secondly, another argument typically used for explaining Pickering stabilisation of foam is based on the surface elastic modulus (E). It is argued that Ostwald ripening can be completely arrested if $E > \gamma/2$, where γ is the surface tension [27]. As described below, the foam made with protein nanoparticles are unstable depite meeting this criterion based on surface elastic modulus. A typical argument used to explain foam stability is based on the surface rheological properties [27–31]. On the contrary, some researchers have shown that there is no direct relation between the surface properties and foam stability [32]. In our system, we found that the difference between the foaming properties of monomeric protein and protein nanoparticles is correlated with the thickness of interfacial layers and thin films. But, there was no clear correlation between foaming properties and the dilatational surface elastic modulus (figure 7.9a). For all the cases, surface elastic modulus ($E^{'}$) was higher than viscous modulus ($E^{''}$) (figures 7.9). At low surface pressures ($\Pi = 1 - 2.5$ mN m^{-1}), $E^{'}$ increased up to 20 mN m^{-1} and was similar for all the proteins. At intermediate surface pressures ($\Pi = 2.5 - 15$ mN m^{-1}), $E^{'}$ of protein nanoparticles was higher than monomeric protein. At $\Pi > 15$ mN m^{-1} there was no difference between monomeric protein and the nanoparticles. The foams were stable up to many hours in the case of protein nanoparticles and around two hours in the case of monomeric protein, so the actual Π in the film should be > 15 mN m^{-1}. The $E^{'}$ at high surface pressures is in the range 60 ± 10 mN m^{-1} for all the cases. The values of $E^{'}$ observed for α-LA nanoparticles are similar to the typical values of other globular proteins under similar experimental and measurement conditions. For example, non-modified/modified patatin has an $E^{'}$ approximately in the range $60 - 80$ mN m^{-1} for $\Pi > 15$ mN m^{-1} [33]. Typical compression elastic modulus obtained obtained with silica particles at bubble surfaces is around 70 mN m^{-1} [27]. So, in all the cases, monomeric globular proteins, protein particles and hard particles, apparently

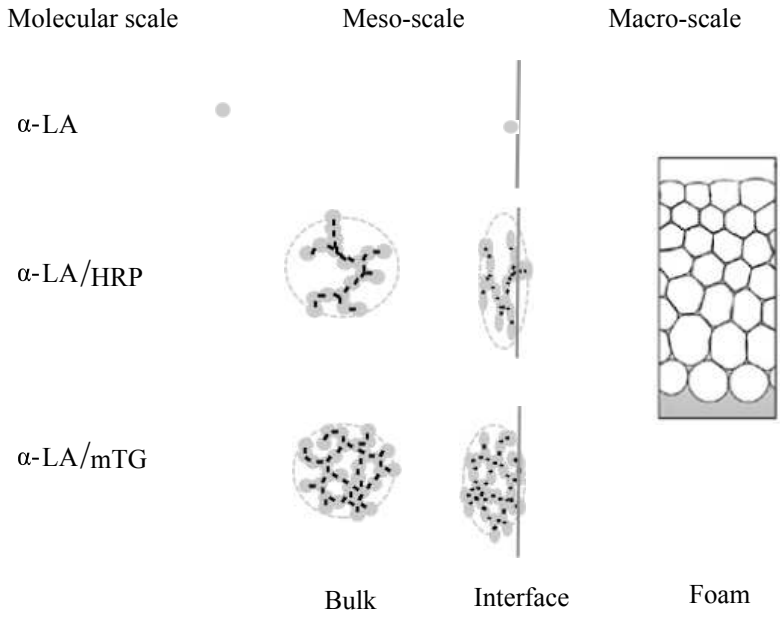

Figure 7.10: *Soft protein nanoparticles in bulk and at interface.*

the criterion of $E > \gamma/2$ is met. Still, they exhibit different Pickering effects. Hence, it seems that various relaxatation processes associated with soft particles, lead to $E < \gamma/2$ under the conditions prevalent realistically in the foam films. So, we conclude that the range of frequencies and amplitudes employed for measuring the surface rheological properties are probably not relevant to the real situation in a foam. Instead film thicknesses are better indicators of the observed foaming properties.

In conclusion, the foam-stability of the foams made with soft α-LA nanoparticles of size around 100 nm is much less than that of hard nanoparticles of similar size such as silica i.e. days versus months [31], respectively. This indicates that Pickering stabilization with protein nanoparticles is determined not only by their size but also by their softness. The softness of the enzymatically cross-linked protein nanoparticles was clearly evident from the collapse of the particles when deposited on to modified silica surface (chapter 5) or when adsorbed at air/water interface (chapter 6). The change in thickness of interfacial layer was correlated to the differences in the mesoscale structure of the nanoparticles (figure 7.10).

The above shows that there is a Pickering stabilization observed with enzymatically cross-linked protein particles, albeit not as strong as for solid inorganic nanoparticles. The Pickering effect seems to be related not only to the size, but also to the structure of the protein particles. With regard to size, the largest size of the protein particles obtained by enzymatic cross-linking ($R_h \sim 100$ nm) can be compared to typical heat-induced soluble protein particles [29, 34, 35]. Hard (inorganic, colloidal)

particles in the size range $10 - 1000$ nm provide Pickering stabilisation on the order of many months [26, 28, 31, 36]. There was a linear relation observed between the foam $t_{0.5}$ and protein nanoparticle size (chapter 6). So, based on this relation we can speculate that if the size of the protein nanoparticles is increased from $R_h \sim 100$ nm to $R_h \sim 1000$ nm, the foam $t_{0.5}$ should also becomes 10 times higher. Even in that case the foam-stability of protein nanoparticles will not be as high as hard particles. So, the softness of the protein nanoparticles seems to be the main reason for soft Pickering stabilisation. As described before, softness however is not so easy to quantify in the solution (bulk). There are indirect indications that it must be linked to the cross-link density (number of cross-links per particle) and must be reflected in the apparent density of the particles. Enzymatically cross-linked protein particles have a typical apparent density in the range $1 - 10$ % (w/v) (chapters 2 and 4). Dense heat-induced protein particles have a typical apparent densities in the range $10 - 40$ % (w/v) [37]. On the other hand, silica particles have a density of 220 % (w/v) [38]. So, it can be speculated that, $10 - 20$ times higher densities of the enzymatically protein nanoparticles are required to achieve the Pickering stabilisation similar to hard particles. An important point in this regard is the distinction between density and rigidity. These two factors can contribute different differently to Pickering stability. Low density but highly rigid particles may also be as effective Pickering stabilisers as dense particles. There could be many ways to increase the cross-link density or mass density of enzymatically cross-linked protein particles. For example: 1) By heating them after enzymatic cross-linking, 2) By making primary particles with one enzyme and then further cross-linking with a different enzyme to obtain denser secondary aggregates, or 3) Chemical cross-linking of protein particles e.g with gluteraldehyde (GD). A speculative example on the option 2 is formation of primary protein particles with high density using HRP, and then subsequent cross-linking of these primary particles with mTG to form also denser large particles. For option 3, an indirect example of achieving hard particle- like Pickering behaviour after cross-linking protein particles with GD was described above.

Outlook

Moving forward from the model (α-LA) system to other globular proteins

In chapters 2 and 4, it was shown that the formation of cross-linked apo α-LA nanoparticles can be controlled by using two different enzymes. But, α-LA is only the second major globular protein in the bovine milk. So, to move forward to whey protein mixtures, cross-linking properties of β -lactoglobulin (β-LG) are required to be investigated. The reason we focussed on globular proteins is that caseins seem to be good with regard to susceptibility to enzymatic crosslinking. So, in addition to β-LG, we also performed cross-linking of lysozyme (Lyz) and ovalbumin (Ova) with mTG (table 7.4). The effect of structural modifications of these globular proteins on

mTG-induced cross-linking was investigated. It is well known that globular proteins in their native form are hardly susceptible to microbial transglutaminase (mTG) induced reaction. Certain modification on the molecular structure can improve their susceptibility to be cross-linked by mTG [39, 40]. The most described method for improvement of the accessibility of glutamines and lysines is addition of a reducing agent, such as DTT [41]. DTT was found to cleave disulde bonds, leading to unfold the protein and resulting in a flexible structure of the substrate and a better susceptibility toward the mTG [42]. In addition, mTG does not contain di-sulfide bonds itself [43], this makes it unaffected by the treatment of DTT. Other methods such as heating or changing pH, can lead to conformational change of substrate proteins, but they also have an impact on the activity of mTG.

α-LA has only 12 Lys and 6 Gln as compared to 15 Lys and 9 Gln residues for β-LG. Still, low DP was obtained for holo α-LA and native β-LG with mTG (table 7.4). On the other hand, apo α-LA and DTT treated β-LG showed high cross-linking activity with mTG (table 7.4). CD measurements (data not shown) illustrated that the tertiary structure of β-LG decreased after incubation with DTT and this significantly improved the cross-linking activity with mTG. The measurement of the degree of cross-linking by OPA method showed that around 40 % of lysine groups in the DTT treated β-LG were involved in cross-linking. Cross-linked β-LG nanoparticles of different mass and size were obtained by incubating it with mTG under different substrate concentration, pH and ionic strength (table 7.4). Higher M_w nanoparticles were obtained with increasing β-LG concentration. The largest β-LG nanoparticles were obtained at a concentration of 20 g L^{-1} and a gel was obtained at 30 g L^{-1} (table 7.4). The mass and size of the cross-linked β-LG nanoparticles increased with addition of 0.1 M NaCl. Decreasing the pH to 6 and 5 did not lead to an increase of M_w but the R_g was higher. In conclusion, it was possible to produce β-LG nanoparticles by cross-linking DTT treated β-LG with mTG. But, the size and mass of the β-LG/mTG nanoparticles is much lower than that obtained in the case of apo α-LA/mTG. The β-LG/mTG nanoparticles appear to have a more open structure as compared to α-LA/mTG. This is also apparent from the fact that a gel was obtained at a concentration of 30 g L^{-1}. Lower reactivity of DTT treated β-LG as compared to apo α-LA, despite the fact that β-LG has larger number of target amino acids indicates that structural flexibility of substrate protein is as important as the total number. Bovine β-LG is a relatively small protein (M_w = 18.3 kDa) and contains 2 di-sulfide bonds per molecule [44]. As shown above and also in literature, the reactivity of β-LG to mTG catalysed reaction can be enhanced by treatment with DTT [41, 45]. Lysozyme from egg white (M_w = 14.5 kDa) has 4 disulfide bonds [46]. Ovalbumin from egg white (M_w = 45 kDa) has four sulphydryl groups with a single disulfide bridge [47]. In the case of α-LA and Lyz, a turbid solution was obtained after incubation with DTT, indicating a significant exposure of hydrophobic amino acids leading to aggregation. Howevere, incubation with DTT had no effect on solubility of Ova and β-LG. There are two main conclusions from these studies; 1) aggregation after pre-treatment is clearly a roadblock in the studies of whey protein mixtures, 2) structural flexibility of globular proteins is a limiting step in their enzymatic cross-

Table 7.4: *Effect of solution conditions on polymerization (cross-linking) of various globular proteins with mTG: α-lactalbumin (α-LA), β-lactoglobulin (β-LG), lysozyme (Lyz) and ovalbumin (Ova). NaP is sodium phosphate, DTT is dithiothreitol and - indicates that pre-treatment/analysis was not be perfomed.*

Protein	C (g L^{-1})	Buffer	NaCl (mM)	pH	Pretreatment	Visual observation	Monomer conversion (%)	M_w (MDa)	R_g (nm)	R_h (nm)
α-LA	10	NaP	100	7.0	$+Ca^{2+}$	Clear	33	8.7	49.5	37.2
	10	NaP	100	7.0	$-Ca^{2+}$	Clear	85	15.5	61.9	42.9
	10	NaP	100	7.0	$-Ca^{2+}$ + DTT	Turbid before cross-linking	-	-	-	-
β − LG	10	NaP	100	7.0	+ DTT	Clear		1.4	26.1	11.55
	20	NaP	100	7.0	+ DTT	Clear		50.6	97.7	41.3
	30	NaP	100	7.0	+ DTT	Clear		-	-	Gel
	10	NaP	100	5.0	+ DTT	Clear		1	33.6	12
	10	NaP	100	6.0	+ DTT	Clear		0.8	31.8	11.65
	10	NaP + NaCl	100 + 100	7.0	+ DTT	Clear	91	1.7	27.7	14.35
	10	NaP + NaCl	100 + 100	7.0	-	Clear	8	-	-	-
Lyz	10	NaP	100	7.0	-	Clear	0	-	-	-
	10	NaP	100	7.0	+DTT	Turbid befre cross-linking	-	-	-	-
Ova	10	NaP	100	7.0	-	Clear	5	-	-	
	10	NaP	100	7.0	+ DTT	Clear	7	-	-	

linking and 3) a method of making globular protein more flexible e.g. reducing S-S with DTT will not work for all proteins (e.g. Ova). Ova did not polymerize with mTG but β-LG on the other hand polymerized significantly. This is most probably due to the fact that the structure of Ova was not flexible enough, which can be expected since almost 50 % of the amino acids in Ova are hydrophobic. So, different strategies are required for specific globular proteins. In this respect, a different point of view can be that instead of focussing on the flexibility of the substrate protein, flexibility of the enzyme is required to be modified. For example, typically trypsin (also active on lysine) has no problem with native proteins. So, the direction in the future may also be to find other cross-linking enzymes e.g. genetically modified TG with less problems on the globular proteins.

Concluding remarks

The approach used for characterisation of the mesoscale structure of enzymatically cross-linked protein particles can easily be extended to protein particles made by non-enzymatic method also. To compare protein nanoparticles obtained by enzymatic crosslinking with different enzymes, or by heat induced aggregation, several parameters should be considered. In general, only few parameters are considered, which hinders a clear comparison of results from different studies. The AF4-MALS with subsequent data analysis provides access to at least eight different structural parameters. However, additional information on the extent of crosslinking, distribution of crosslinks and the resulting softness (rigiditiy) of the nanoparticles can not be derived from this technique. The softness of the protein nanoparticles seems to be an important parameter in relation to (techno-)functionality. Therefore, methods to quantify this parameters, and its dependence on cross-link density needs to be further explored. The hypothesis at the start of this thesis was that the functionality of protein particles is determined by the particle structure. The term functionality, more epecifically techno-functionality is very clear. It refers to the use of protein particles for the pupose of making a gel or an emulsion or a foam for some food application. However, the term structure is usually not well defined and many different aspects are covered by different researchers. We have shown that combination of AF4-MALS can be used to determine many aspects of particle structure simulateneously. It can certainly be concluded that the macroscale tecno-functional properties such as bulk rheology and foam stability are indeed determined by the mesoscale structure of the protein nanoparticles used for imparting that functionality.

Bibliography

[1] P.C. Hiemenz and R. Rajagopalan. *Principles of Colloid and Surface Chemistry, 3rd ed., (revised and expanded)*. Marcel Dekker, NY, USA, 1997.

[2] J. Yguerabide and E. E. Yguerabide. Light-scattering submicroscopic particles as highly fluorescent analogs and their use as tracer labels in clinical and biological applications: I. theory. *Anal. Biochem.*, 262(2):137–156, 1998.

[3] S. Kumar. Spectroscopy of organic compounds. *Cosmic Rays*, 10:4, 2006.

[4] P. L. Privalov. Cold denaturation of protein. *Crit. Rev. Biochem. Mol.*, 25(4):281–306, 1990.

[5] J. Carpenter, M. Pikal, B. Chang, and T. Randolph. Rational design of stable lyophilized protein formulations: some practical advice. *Pharm. Res.*, 14(8):969–975, 1997.

[6] Y. Li, W. F. Weiss, and C. J. Roberts. Characterization of high-molecular-weight nonnative aggregates and aggregation kinetics by size exclusion chromatography with inline multi-angle laser light scattering. *J. Pharm. Sci.*, 98(11):3997–4016, 2009.

[7] W. Wang. Lyophilization and development of solid protein pharmaceuticals. *Int. J. Pharm.*, 203(1–2):1–60, 2000.

[8] L. Chang, D. Shepherd, J. Sun, D. Ouellette, K. L. Grant, X. Tang, and M. J. Pikal. Mechanism of protein stabilization by sugars during freeze-drying and storage: Native structure preservation, specific interaction, and/or immobilization in a glassy matrix? *J. Pharm. Sci.*, 94(7):1427–1444, 2005.

[9] N. K. Jain and I. Roy. Effect of trehalose on protein structure. *Protein Sci.*, 18(1):24–36, 2009.

[10] C. I. Butre, P. A. Wierenga, and H. Gruppen. Effects of ionic strength on the enzymatic hydrolysis of diluted and concentrated whey protein isolate. *J. Agric. Food Chem.*, 60(22):5644–5651, 2012.

[11] J. Buchert, D. E. Cura, H. Ma, C. Gasparetti, E. Monogioudi, G. Faccio, M. Mattinen, H. Boer, R. Partanen, E. Selinheimo, R. Lantto, and K. Kruus. Crosslinking food proteins for improved functionality. *Annu. Rev. Food. Sci. Technol.*, 1:113–138, 2010.

[12] T. DiMarco and C. Giulivi. Current analytical methods for the detection of dityrosine, a biomarker of oxidative stress, in biological samples. *Mass Spectrom. Rev.*, 26(1):108–120, 2007.

[13] J. E. Noble and M. J. A. Bailey. Chapter 8 Quantitation of Protein. In R. R. Burgess and M. P. Deutscher, editors, *Guide to Protein Purification, 2nd Edition*, volume 463 of *Methods in Enzymology*, pages 73–95. Academic Press, 2009.

[14] F. Hanft and P. Koehler. Quantitation of dityrosine in wheat flour and dough by liquid chromatography-tandem mass spectrometry. *J. Agric. Food Chem.*, 53(7):2418–2423, 2005.

[15] W. H. Heijnis, H. L. Dekker, L. J. de Koning, P. A. Wierenga, A. H. Westphal, C. G. de Koster, H. Gruppen, and W. J. H. van Berkel. Identification of the peroxidase-generated intermolecular dityrosine cross-link in bovine α-lactalbumin. *J. Agric. Food Chem.*, 59(1):444–449, 2010.

[16] S. Improta, H. Molinari, A. Pastore, R. Consonni, and L. Zetta. Probing protein-structure by solvent perturbation of Nmr-spectra - photochemically induced dynamic nuclear-polarization and paramagnetic perturbation techniques applied to the study of the molten globule state of α-lactalbumin. *Eur. J. Biochem.*, 227(1–2):87–96, 1995.

[17] G. Oudgenoeg. *Peroxidase Catalyzed Conjugation of Peptides, Proteins and Polysaccharides Via Endogenous and Exogenous Phenols*. PhD thesis, Wageningen University, Wageningen, The Netherlands, 2004.

[18] L.V. Lopez-Llorca and S.C. Fry. Dityrosine, trityrosine and tetratyrosine, potential cross-links in structural proteins of plant-parasitic nematodes. *Nematologica*, 35(2):165–179, 1989.

[19] D. Stanic, E. Monogioudi, E. Dilek, J. Radosavljevic, M. Atanaskovic-Markovic, O. Vuckovic, L. Raija, M. Mattinen, J. Buchert, and Cirkovic V. T. Digestibility and allergenicity assessment of enzymatically crosslinked β-casein. *Mol. Nutr. Food Res.*, 54(9):1273–1284, 2010.

[20] H. Wu and M. Morbidelli. A model relating structure of colloidal gels to their elastic properties. *Langmuir*, 17(4):1030–1036, 2001.

[21] A. Maltais, G. E. Remondetto, and M. Subirade. Mechanisms involved in the formation and structure of soya protein cold-set gels: A molecular and supramolecular investigation. *Food Hydrocolloid*, 22(4):550–559, 2008.

[22] M. M. Ould Eleya, S. Ko, and S. Gunasekaran. Scaling and fractal analysis of viscoelastic properties of heat-induced protein gels. *Food Hydrocolloid*, 18(2):315–323, 2004.

[23] Y. Saricay. *New insights into enzymatically cross-linked proteins*. PhD thesis, Wageningen University, Wageningen, The Netherlands, 2014.

[24] M. Mellema, J. H. J. van Opheusden, and T. van Vliet. Categorization of rheological scaling models for particle gels applied to casein gels. *J. Rheology (1978-present)*, 46(1):11–29, 2002.

[25] P. Walstra. *Physical Chemistry of Foods*. Marcel Dekker, NY, USA, 2002.

[26] H. Jin, W. Zhou, J. Cao, S. D. Stoyanov, T. B. J. Blijdenstein, P. W. N. de Groot, L. N. Arnaudov, and E. G. Pelan. Super stable foams stabilized by colloidal ethyl cellulose particles. *Soft Matter*, 8(7):2194–2205, 2012.

[27] A. Maestro, E. Rio, W. Drenckhan, D. Langevin, and A. Salonen. Foams stabilised by mixtures of nanoparticles and oppositely charged surfactants: relationship between bubble shrinkage and foam coarsening. *Soft Matter*, 10(36):6975–6983, 2014.

[28] K. D. Martínez, Carrera S. C., J. M. Rodríguez Patino, and A. M. R. Pilosof. Interfacial and foaming properties of soy protein and their hydrolysates. *Food Hydrocolloid*, 23(8):2149–2157, 2009.

[29] I. Nicorescu, A. Riaublanc, C. Loisel, C. Vial, G. Djelveh, G. Cuvelier, and J. Legrand. Impact of protein self-assemblages on foam properties. *Food Res. Int.*, 42(10):1434–1445, 2009.

[30] B. Rullier, M. A. V. Axelos, D. Langevin, and B. Novales. β-Lactoglobulin aggregates in foam films: Effect of the concentration and size of the protein aggregates. *J. Colloid Interface Sci.*, 343(1):330–337, 2010.

[31] A. Stocco, W. Drenckhan, E. Rio, D. Langevin, and B. P. Binks. Particle-stabilised foams: An interfacial study. *Soft Matter*, 5(11):2215–2222, 2009.

[32] P. A. Wierenga, L. van Norel, and E. S. Basheva. Reconsidering the importance of interfacial properties in foam stability. *Colloids Surf., A*, 344(1–3):72–78, 2009.

[33] R.J.B.M. Delahaije, P.A. Wierenga, M.L.F. Giuseppin, and H. Gruppen. Improved emulsion stability by succinylation of patatin is caused by partial unfolding rather than charge effects. *J. Colloid Interface Sci.*, 430(0):69–77, 2014.

[34] I. Nicorescu, C. Loisel, C. Vial, A. Riaublanc, G. Djelveh, G. Cuvelier, and J. Legrand. Combined effect of dynamic heat treatment and ionic strength on the properties of whey protein foams part ii. *Food Res. Int.*, 41(10):980–988, 2008.

[35] B. Rullier, B. Novales, and M. A. V. Axelos. Effect of protein aggregates on foaming properties of β-lactoglobulin. *Colloids Surf., A*, 330(2–3):96–102, 2008.

[36] B. S. Murray and R. Ettelaie. Foam stability: Proteins and nanoparticles. *Curr. Opin. Colloid Interface Sci*, 9(5):314–320, 2004.

[37] D. Saglam, P. Venema, E. van der Linden, and R. de Vries. Design, properties, and applications of protein micro- and nanoparticles. *Curr. Opin. Colloid Interface Sci*, 19(5):428–437, 2014.

[38] I. Blute, R. J. Pugh, J. van de Pas, and I. Callaghan. Industrial manufactured silica nanoparticle sols. 2: Surface tension, particle concentration, foam generation and stability. *Colloids Surf., A*, 337(1–3):127–135, 2009.

[39] S. Damodaran and K. K. Agyare. Effect of microbial transglutaminase treatment on thermal stability and pH-solubility of heat-shocked whey protein isolate. *Food Hydrocolloid*, 30(1):12–18, 2013.

[40] C. V. L. Giosafatto, N. M. Rigby, N. Wellner, M. Ridout, F. Husband, and A. R. Mackie. Microbial transglutaminase-mediated modification of ovalbumin. *Food Hydrocolloid*, 26(1):261–267, 2012.

[41] G. A. H. DE Jong and S. J. Koppelman. Transglutaminase catalyzed reactions: Impact on food applications. *J. Food Sci.*, 67(8):2798–2806, 2002.

[42] P. J. Coussons, N. C. Price, S. M. Kelly, B. Smith, and L. Sawyer. Transglutaminase catalyzes the modification of glutamine side-chains in the C-terminal region of bovine β-lactoglobulin. *Biochemical Journal*, 283:803–806, 1992.

[43] T. Kashiwagi, K. Yokoyama, K. Ishikawa, K. Ono, D. Ejima, H. Matsui, and E. Suzuki. Crystal structure of microbial transglutaminase from Streptoverticillium mobaraense. *J. Biol. Chem.*, 277(46):44252–44260, 2002.

[44] H. L. Monaco, G. Zanotti, P. Spadon, M. Bolognesi, L. Sawyer, and E. E. Eliopoulos. Crystal-structure of the trigonal form of bovine β-lactoglobulin and of its complex with retinol at 2.5 angstrom resolution. *J. Mol. Biol.*, 197(4):695–706, 1987.

[45] E. Y. Lee and J. Park. Pressure inactivation kinetics of microbial transglutaminase from Streptoverticillium mobaraense. *J. Food Sci.*, 67(3):1103–1107, 2002.

[46] H. A. Mckenzie and F. H. White. Lysozyme and α-lactalbumin - structure, function, and interrelationships. *Adv. Protein Chem.*, 41:173–315, 1991.

[47] B. Jacobsen, K. Hoffmann-Sommergruber, T. T. Have, N. Foss, P. Briza, C. Oberhuber, C. Radauer, S. Alessandri, A. C. Knulst, M. Fernandez-Rivas, and V. Barkholt. The panel of egg allergens, Gal d 1-Gal d 5: Their improved purification and characterization. *Mol. Nutr. Food Res.*, 52:S176–S185, 2008.

Summary

Enzymatic cross-linking of food proteins is generally accepted as a method to modify their techno-functional properties, such as gelation, emulsification and foam stabilisation. Some examples of enzymatic cross-linking of globular milk proteins are given in Chapter 1. Literature on enzymatic cross-linking of globular proteins is scant as compared to random coil proteins, such as casein. The aim of this thesis is to understand what kind of protein polymers (nanoparticles) are obtained after cross-linking a globular milk protein and how do they affect functionality. The system chosen for this research is apo α-lactalbumin (α-LA) as a substrate and horseradish peroxidase (HRP) and microbial transglutaminase (mTG) as enzymes for cross-linking α-LA. The characterisation of mesoscale structures that are formed during cross-linking of α-LA with HRP are presented in chapter 2. The formed nanoparticles were separated by asymmetrical flow field flow fractionation (AF4) and characterised inline with multi angle light scattering (MALS). Polymerization of apo α-LA with HRP proceeds in a step growth way i.e. first monomers are reacted to form oligomers and later oligomers are cross-linked to form polymers (nanoparticles). The cross-linked nanoparticles had a size (radius of gyration, R_g) and weight averaged molar mass (M_w), ranging between $2-200$ nm and $0.0142-100$ MDa, respectively. The polymerization of α-lactalbumin could be easily controlled by varying the dosage of co-substrate, hydrogen peroxide (H_2O_2), to produce nanoparticles with controlled size and meso-scale structure. The effects of various process parameters on the sizes of the nanoparticles were investigated. These parameters were protein concentration ($10-30$ g L^{-1}), total dosed concentration of H_2O_2 ($0-10$ mM), the time gap between each dosage of H_2O_2 ($120-600$ s) and ionic strength ($100-200$ mM). The speed of particle formation increased with increasing ionic strength, but their meso-scale structure remained similar. The R_g of these nanoparticles scaled as $M_w^{0.57}$, indicating a fractal structure. The density of the nanoparticles decreased with size. The apparent density (internal protein concentration) of the nanoparticles was between 104 and 10 kg m^{-3} for $R_g \sim 20$ nm and $R_g > 100$ nm, respectively. After knowing the mesoscale structural details, next the molecular scale chemical details of the α-LA/HRP nanoparticles were investigated and are described in chapter 3. Chemical characterisation includes aspects, such as identification of amino acids involved in the cross-links and length of these covalent cross-links. It was believed that HRP-induced cross-linking of α-LA takes place by formation of di-tyrosine. Surprisingly, in this work it was

found that HRP induces not only di-tyrosine, but also oligo-tyrosine cross-links in α-LA particles. So far HRP was thought to do this only for low molar mass tyrosine containing substrates. But, in chapter 3 it is conclusively proved that oligo-tyrosine cross-links can also be formed in proteins. The α-LA nanoparticles made with HRP contained di octa tyrosine cross-links. In the case of α-LA cross-linking, no other cross-links involving different amino acids were found. Two stages of cross-linking of α-LA were identified: 1) $1-2$ cross-links were formed per monomer until the monomers were converted into oligomers and 2) subsequent cross-linking ($3-4$ cross-links per molecule) of oligomers formed in the first stage. Naturally, the next question was, can the average number of cross-links per molecule be increased by using mTG which targets Lys/Gln. Both these residues are abundantly present on the surface of the α-LA. The details of the mTG-induced cross-linking as well as a comparison of the mesoscale structures that are produced with that of HRP-induced cross-linking are presented in chapter 4. The polymerization in the case of mTG is also step growth type. However, the meso-scale structure of the α-LA nanoparticles formed with mTG was denser than that of HRP. For both enzymes, the nanoparticle growth followed a step growth mechanism. Initially, oligomers ($0.0142 < M_w < 1$ MDa) were formed, which were further cross-linked in the later stage to form polymers ($M_w > 1$ MDa). Still significant differences were observed in the mesoscale structure. The density of nanoparticles of $R_g \approx 200$ nm was almost two times higher for α-LA/mTG (20 kg m^{-3}) than the α-LA/HRP. The denser structure was also confirmed by the power law scaling exponent between R_g and M_w, which was 0.38 ± 0.05 and 0.57 ± 0.05 for α-LA/mTG and α-LA/HRP nanoparticles, respectively. The difference in structure was also reflected by a significant difference in thermal stability on extensive heating, water holding capacity as well as by a different swelling behavior of nanoparticles at ionic strengths < 1 mM. Encouraged by these observations, bulk rheological behavior and foaming properties of these two types of nanoparticles were investigated next in chapters 5 and 6, respectively. The differences between the bulk rheological properties of the α-LA nanoparticles made with either HRP or with mTG are shown in chapter 5. This chapter compares their bulk rheological properties, such as storage modulus and shear viscosity, as a function of nanoparticle concentration. Bulk rheological properties of a gel made by concentrating α-LA nanoparticles (2-step gels) were found to be affected by the mesoscale structure of the nanoparticles. Gels made with the compact nanoparticles have around ten times higher storage modulus than that of the open nanoparticles. The aim of this chapter was to investigate 1) the effect of differences in mesoscale structure of protein nanoparticles on bulk rheology of 2-step gels and 2) the differences in rheological properties of 2-step versus 1-step gels (made by continuous cross-linking). For both particles, the jamming concentration was determined by measuring the storage modulus (G'), loss modulus (G'') and shear viscosity (η) as a function of concentration. The jamming concentration for α-LA/mTG nanoparticles ($R_h = 60$ nm) was 55 ± 5 g L^{-1} as compared to 35 ± 5 g L^{-1} for α-LA/HRP ($R_h = 65$ nm). The power law exponent of G' versus concentration curve is much higher ($n = 18.7$) for α-LA/mTG while $n = 5.26$ for α-LA/HRP nanoparticles. There were no major differences between the rheological

properties of α-LA/mTG 1-step and 2-step gels. This implies that gels made by using enzymatically cross-linked protein particles as ingredients can provide rheological properties similar to a gel made by continuous enzymatic cross-linking. Next, it remained to see if the impact of the differences in mesoscale structure are limited only to bulk properties or are they also important for interfacial properties. The interfacial and foaming properties of these two types of α-LA nanoparticles are described in chapter 6. The foam was generated by whipping and sparging method, and nanoparticles of different sizes were foamed at different ionic strengths. Protein particles made by heating are believed to enhance the foam stability through a mechanism analogous to Pickering stabilisation by colloidal particles, such as silica, clay, latex etc. As described in earlier chapters, α-lactalbumin (α-LA) was cross-linked with either microbial transglutaminase (mTG) or horseradish peroxidase (HRP) to produce α-LA nanoparticles (hydrodynamic radius, $R_h = 20 - 100$ nm) with different mesoscale structure. These protein particles were then used for surface and foaming experiments. The adsorption of nanoparticles at the air-water interface as probed by changes in surface pressure (Π) with time was controlled both by diffusion as well as electrostatic barrier to adsorption. The electrostatic barrier was reduced by increasing the ionic strengths ($I = 0 - 125$ mM) resulted in a faster increase of Π with time. The foam-ability of nanoparticles also increased with increasing ionic strengths. At a fixed I, the foam-ability of nanoparticles reduced with increasing size while their foam-stability increased. Foams produced by low-shear whipping were 2 to 6 times more stable for nanoparticles as compared to monomeric protein ($R_h \approx 2$ nm). The higher foam-stability of α-LA nanoparticles as compared to monomeric α-LA was explained based on higher thickness of the interfacial layer and thin films. The enhancement in foam stability is comparable to other heat induced protein aggregates of similar size range reported in literature. But the foam half-life times ($t_{0.5} = 20 - 60$ h) are much less than that of other types of colloidal particles ($t_{0.5} > 30$ days) reported in literature. The Pickering stabilisation with soft nanoparticles is not as strong as in the case of other hard colloidal particles. The $t_{0.5}$ of the foams made with soft α-LA nanoparticles of size around 100 nm is much less than that reported in literature for hard nanoparticles such as silica, i.e. days versus months, respectively. This difference is perhaps due to various relaxation processes associated with soft nanoparticles. Finally, the general outcomes of this thesis are summarised in chapter 7. A set of tool-box has been developed in this thesis for the characterisation of the mesoscale structure of the enzymatically cross-linked protein nanoparticles. Most of the mesoscale structural details can be quantified with the combination of AF4-MALS, DLS and AFM. Still, there are some properties, such as softness of the nanoparticles, that cannot be quantified so easily. Various analytical challenges associated with protein nanoparticles are also discussed in chapter 7. For example, artifacts originating from light scattering during the concentration determination of protein particles in UV cell. This problem can be solved by the use of RI detector in the AF4. Issues with the stability of the nanoparticles during freeze-drying are also discussed. A disaccharide must be used as a cryo-protectant for freeze-drying the soft protein particles. It is suggested that the softness of protein nanoparticles is related to the cross-link density

i.e. number of cross-links per particle. It is seen that in the case of mTG induced cross-linking of apo α-LA, more cross-links are formed per molecule than that of HRP. This results in relatively more dense and rigid α-LA/mTG nanoparticles. An outlook is provided at the end of general discussion. Some examples are given for mTG induced cross-linking of a few other globular proteins. Some issues associated with moving from model α-LA system to mixtures such as WPI are also discussed. In conclusion, enzymatic cross-linking of protein is a nice method to produce protein based particles for food use. With this method, protein particles with controlled size and structure can be produced. The size and structure of the protein particles have a direct effect on their techno-functional properties. Hence, protein particles with different size and structure can be used for imparting a certain functionality when used as ingredients in food applications. Finally, for even higher Pickering effect than that seen in this thesis for foam stabilisation, it is suggested that protein particles with higher cross-link densities are required.

Samenvatting

Enzymatisch crosslinken van voedingseiwitten is een algemeen geaccepteerde methode om de techno-functionele eigenschappen van eiwitten, zoals de vorming en stabilisatie van gelen, emulsies en schuim, te veranderen. Enkele voorbeelden van het enzymatische crosslinken van globulaire eiwitten worden in hoofdstuk 1 gegeven. Er is minder literatuur over het het enzymatisch crosslinken van globulaire eiwitten, dan van random coil eiwitten, zoals casene. Het doel van deze thesis is om te begrijpen welk type eiwitaggregaten (nanodeeltjes) gevormd worden na het crosslinken van een globulair eiwit en hoe dit de functionaliteit benvloedt. Voor dit onderzoek is gekozen voor apo α-lactalbumine (α-LA) als substraat met horseradish peroxidase (HRP) en microbieel transglutaminase (mTG) als enzymen voor het crosslinken van α-LA.

De karakterisatie van mesoscopische structuren welke gevormd worden gedurende het crosslinken van α-LA met HRP zijn weergegeven in hoofdstuk 2. De gevormde nanodeeltjes werden gescheiden met behulp van asymmetric flow field flow fractionatie (AF4) en gekarakteriseerd met statische lichtverstrooiing (MALS). Polymerisatie van apo α-LA met HRP verloopt stapsgewijs d.w.z. eerst reageren de monomeren tot oligomeren en later crosslinken de oligomeren tot polymeren (nanodeeltjes). De gecrosslinkte nanodeeltjes hadden een grootte (gyratieschaal, R_g) en gewichtsgemiddeld molecuulgewicht (M_w) dat respectievelijk tussen $2-200$ nm en $0.0142-100$ MDa varierde. De polymerisatie van α-lactalbumine kon eenvoudig worden gecontroleerd door middel van de dosering van co-substraat, waterstofperoxide (H_2O_2), zodat nanodeeltjes met specifieke grootte en mesocopische structuur kunnen worden gevormd. Het effect van verschillende proces parameters op de grootte van de nanodeeltjes werd onderzocht. Deze parameters waren de eiwitconcentratie, de totale gedoseerde concentratie H_2O_2 $(0-10$ mM), de tijd tussen elke H_2O_2 dosering $(120-600$ s) en de zoutsterkte $(100-200$ mM). De snelheid waarin deeltjes gevormd werden nam toe met toenemende zoutsterkte, maar de mesocopische structuur bleef onveranderd. De Rg van deze nanodeeltjes schaalde met $M_w^{0.57}$, wat duidt op een fractale structuur. De dichtheid van de nanodeeltjes nam af met toenemende grootte. De schijnbare dichtheid (interne eiwitconcentratie) van de nanodeeltjes lag respectievelijk tussen 104 en 10 kg m^{-3} voor deeltjes met een $R_g = 20$ nm en $R_g > 100$ nm. Met kennis van de structurele informatie op mesocopische, de chemische informatie van de α-LA/HRP nanodeeltjes op moleculaire schaal werd onderzocht en beschreven in hoofdstuk 3.

Chemische karakterisatie omvat aspecten zoals identificatie van aminozuren die

betrokken zijn bij het crosslinken en de lengte van deze covalente crosslinks. De aanname was dat het HRP-genduceerd crosslinken van α-LA plaatsvindt door middel van het vormen van di-tyrosine. In dit werk werd verrassenderwijs gevonden dat HRP niet alleen di-tyrosine, maar ook oligo-tyrosine crosslinks vormt in α-LA deeltjes. Tot nu toe werd aangenomen dat HRP deze alleen vormt in het geval van een substraat met een lage moleculaire massa. Maar in hoofdstuk 3 is definitief aangetoond dat oligo-tyrosine crosslinks ook gevormd worden in eiwitten. De α-LA nanodeeltjes gemaakt met HRP bevatte di octa tyrosine crosslinks. Tijdens het crosslinken van α-LA werden geen crosslinks tussen andere aminozuren gevonden. Twee stadia van crosslinken kunnen worden gedentificeerd: 1) 1-2 crosslinks werden gevormd per monomeer voordat de monomeren werden omgezet in oligomeren en 2) daaropvolgend crosslinken van de gevormde oligomeren uit de eerste fase (3-4 crosslinks per molecuul). De volgende vraag was natuurlijk of het gemiddeld aantal crosslinks per molecuul kon worden toegenomen door gebruik te maken van mTG welke doelt op Lys/Gln. Deze beide residueen zijn voornamelijk aanwezig aan het oppervlakte van α-LA. De details omtrent het mTG-genduceerd crosslinken alsmede een vergelijk tussen de mesoscopische structuren die gevormd worden door mTG and HRP staan beschreven in hoofdstuk 4.

De polymerisatie is in het geval van mTG ook een stapsgewijs proces. De mesoscopische structuur van de met mTG gevormde α-LA nanodeeltjes is echter compacter dan die gevormd met HRP. Voor beide enzyme verloopt de groei van de nanodeeltjes via een stapsgewijs mechanisme. Initieel worden oligomeren ($0.0142 < M_w < 1$ MDa) gevormd, welke in een later stadium verder crosslinken tot oligomeren ($M_w > 1$ MDa). Nog steeds werden significante verschillen in de mesoscopische structuur waargenomen. De dichtheid van de nanodeeltjes met een $R_g \approx 200$ nm was bijna twee maal hoger voor α-LA/mTG (20 kg m^{-3}) dan α-LA/HRP. De compactere structuur bleek ook uit de schalings relatie tussen R_g en M_w, voor welke de exponent respectievelijk 0.38 en 0.57 bedroeg voor α-LA/mTG en α-LA/HRP nanodeeltjes. Het verschil in structuur bleek ook uit een significant verschil in thermische stabiliteit tijdens langdurige verhitting, waterhoudend vermogen en een verschil in het zwellen van de nanodeeltjes bij zoutsterktes < 1 mM. Gesterkt door deze observaties worden de bulk reologische en de schuimeigenschappen van deze twee typen nanodeeltjes bestudeerd in respectievelijk hoofdstuk 5 en 6.

Het verschil tussen de bulk reologische eigenschappen van α-LA nanodeeltjes gemaakt met HRP en mTG is weergegeven in hoofdstuk 5. Dit hoofdstuk vergelijkt hun bulk reologische eigenschappen, zoals opslag modulus en afschuif viscositeit, als functie van de nanodeeltjes concentratie. De bulk reologische eigenschappen van een gel gemaakt door middel van het concentreren van α-LA nanodeeltjes (2 staps gelen) bleken beinvloed te worden door de mesocopische structuur van de nanodeeltjes. Gelen gemaakt met de compacte nanodeeltjes hebben een ongeveer tien maal hogere opslag modulus dan de open nanodeeltjes. Het doel van dit hoofdstuk was om uit te zoeken wat 1) het effect van de verschillen in mesocopische structuur van de eiwitnanodeeltjes op de bulk rheologie van de 2 staps gelen is en 2) de verschillen zijn tussen de reologische eigenschappen van 2-staps versus 1-staps gelen (gemaakt door

onafgebroken crosslinken). Voor beide deeltjes werd de overlap concentratie werd bepaald door het meten van de opslag modulus ($G^{'}$), verlies modulus ($G^{''}$) en de afschuif viscositeit (η) als een functie van concentratie. De overlap concentratie was 55–5 g L^{-1} voor α-LA/mTG nanodeeltjes ($R_h = 60$ nm) en 35–5 g L^{-1} voor α-LA/HRP nanodeeltjes ($R_h = 65$ nm). De schalings exponent van $G^{'}$ tegen de concentratie curve is veel hoger ($n = 18.7$) voor α-LA/mTG dan voor α-LA/HRP nanodeeltjes ($n = 5.26$). De reologische eigenschappen van de 1-staps en 2-staps gelen van α-LA/mTG vertoonde geen grote verschillen. Dit impliceert dat gelen die gemaakt zijn met enzymatisch gecrosslinkte eiwitdeeltjes als ingredient dezelfde rheologische eigenschappen kan hebben als een gel gemaakt door middel van onafgebroken enzymatisch crosslinken. Verder moest er nog gekeken worden of de verschillen in mesocopische structuur alleen de bulk eigenschappen beinvloed of dat deze verschillen ook belangrijk zijn voor de oppervlakte eigenschappen.

De oppervlakte- en schuimeigenschappen van deze twee typen α-LA nanodeeltjes staat beschreven in hoofdstuk 6. De schuimen werden gevormd door middel van opkloppen, of door inblazen van lucht waarbij gebruik gemaakt werd van nanodeeltjes van verschillende groottte bij verschillende zoutsterktes. Het wordt aangenomen dat eiwitdeeltjes die gemaakt zijn door verhitting de schuimstabiliteit op een vergelijkbare manier verbeteren als Pickering stabilisatie door colloidale deeltjes zoals silica, klei, latex etc. Zoals beschreven staat in eerdere hoofdstukken wordt α-lactalbumine (α-LA) gecrosslinkt met microbieel transglutaminase (mTG) of horseradish peroxidase (HRP) om α-LA nanodeeltjes (hydrodynamische straal, $R_h = 20 - 100$ nm) met verschillende mesocopische structuur te verkrijgen. Deze eiwitdeeltjes werden daarna gebruikt voor oppervlakte- en schuimexperimenten. De adsorptie van de nanodeeltjes aan het lucht-water grensvlak, bepaald door de verandering in oppervlaktedruk (Π) in de tijd, werd beinvloed door zowel diffusie als een elektrostatische barriere voor adsorptie. Een lagere elektrostatische barriere door toename van de zoutsterkte ($I = 0 - 125$ mM) resulteerde in snellere toename van Π in de tijd. Het schuimvormend vermogen van de nanodeeltjes nam ook toe met toenemende zoutsterkte. Bij een vaste I nam het schuimvormend vermogen van de nanodeeltes af met toenemende grootte terwijl de schuimstabiliteit toenam. Schuimen gemaakt door opkloppen op lage afschuifspanning waren twee tot zes keer stabieler voor de nanodeeltjes in vergelijk met monomeer α-LA ($R_h \approx 2$ nm). Deze verhoogde emulsiestabiliteit van de nanodeeltjes ten opzichte van monomeer α-LA werd verklaard op basis van een dikkere laag aan het oppervlakte en voor de dunne films. De verbeterde emulsiestabiliteit is vergelijkbaar met andere hitte-genduceerde eiwitaggregaten van vergelijkbare grootte die in literatuur beschreven staan. De schuim half-waarde tijden ($t_{0.5} = 20 - 60$ uur) zijn echter veel lager dan die in literatuur beschreven staan voor collodale deeltjes ($t_{0.5} > 30$ dagen). De Pickering stabilisatie door zachte nanodeeltjes is niet zo sterk als door andere harde collodale deeltjes. De $t_{0.5}$ van de schuimen gemaakt met zachte α-LA nanodeeltjes met een grootte van ongeveer 100 nm is veel lager dan de $t_{0.5}$ die in literatuur beschreven staat voor harde nanodeeltjes zoals silica, respectievelijk dagen in plaats van maanden. Dit verschil wordt misschien veroorzaakt door verschillende relaxatie processen die geassocieerd worden met zachte nanodeeltjes.

Ten slotte werden de generieke resultaten van deze thesis samengevat in hoofdstuk 7. In deze thesis is een aantal gereedschappen ontwikkeld voor de karakterisatie van de mesocopische structuur van enzymatisch gecrosslinkte eiwitnanodeeltjes. De meeste mesocopische structurele details kunnen worden gekwantificeerd met een combinatie van AF4-MALS, DLS en AFM. De zachtheid van de nanodeeltjes kan echter niet zo eenvoudig worden gekwantificeerd. Verschillende analytische uitdagingen betreffende eitwitnanodeeltjes worden ook in hoofdstuk 7 bediscussieerd. Bijvoorbeeld, artefacten door lichtverstrooiing tijdens het bepalen van de concentratie van eiwitdeeltjes in een UV cel. Dit probleem kan worden verholpen door gebruik te maken van de RI detector in AF4. Problemen met de stabiliteit van de nanodeeltjes tijdens vriesdrogen worden ook bediscussieerd. Een disaccharide moet dienst doen als cryo-beschermer voor het vriesdrogen van zachte eiwitdeeltjes. Een relatie tussen de zachtheid van eiwitnanodeeltjes en de crosslink dichtheid d.w.z. het aantal crosslinks per deeltje is gesuggereerd. Tijdens het crosslinken van apo α-LA door mTG werden meer crosslinks per molecuul waargenomen dan in het geval van HRP. Dit resulteerde in een relatief compactere en stijvere α-LA/mTG nanodeeltjes. Een vooruitzicht wordt aan het eind van de algemene discussie verschaft. Enkele voorbeelden van andere mTG gecrosslinkte globulaire eiwitten worden beschreven. Enkele problemen gerelateerd aan een verschuiving van een model α-LA systeem naar een mix zoals WPI worden ook bediscussieerd. Concluderend kan gesteld worden dat het enzymatisch crosslinken van eiwit is een goede methode om eiwit-gebaseerde deeltjes te maken voor het gebruik in levensmiddelen. Door middel van deze methode kunnen deeltjes met een specifieke grootte en structuur worden gevormd. De grootte en structuur van de eiwitdeeltjes hebben een direct effect op de techno-functionele eigenschappen. Daarom kan er gebruik worden gemaakt van eiwitdeeltjes met een verschillende grootte en structuur om een bepaalde functionaliteit van een levensmiddel te verkrijgen. Ten laatste, om een nog sterker Pickering effect voor schuimstabilitsatie te krijgen dan is waargenomen in deze thesis werd voorgesteld dat eiwitdeeltjes met een hogere crosslink dichtheid nodig zijn.

List of publications

- **S. K. Dhayal**, R . J. de Vries, H. Gruppen, P. A. Wierenga: *Controlled formation of protein nanoparticles by enzymatic cross-linking of α-lactalbumin with horseradish peroxidase*, Food Hydrocolloids, 2014, 36(0): 53-59.
- **S. K. Dhayal**, R . J. de Vries, H. Gruppen, P. A. Wierenga: *Comparison of mesoscale structures of α-lactalbumin nanoparticles cross-linked with microbial transglutaminase and horseradish peroxidase*, submitted.
- **S. K. Dhayal**, S. Sforza, P. A. Wierenga, H. Gruppen: *Peroxidase induced oligo-tyrosine cross-links during polymerization of α-lactalbumin*, submitted.
- **S. K. Dhayal**, R.J.B.M. Delahaije, R . J. de Vries, H. Gruppen, P. A. Wierenga: *Enzymatic cross-linking of α-lactalbumin to produce nanoparticles with increased foam stability*, submitted.
- **S. K. Dhayal**, Y. Saricay, R . J. de Vries, P. A. Wierenga, H. Gruppen: *Effect of mesoscale structure on rheological properties of enzymatically cross-linked α-lactalbumin nanoparticles*, to be submitted.
- Y. Saricay, **S. K. Dhayal**, P. A. Wierenga, R . J. de Vries: *Protein cluster formation during enzymatic cross-linking of globular proteins*, Faraday Discussions, 2012, 158(1): 51-63.
- Y. Saricay, **S. K. Dhayal**, P. A. Wierenga, R . J. de Vries: *Structure and physical properties of enzymatically cross-linked apo-α-lactalbumin nanoparticles: Laccase versus peroxidase*, Manuscript in preparation.

Acknowledgement

"*Clouds come floating into my life, no longer to carry rain or usher storm, but to add color to my sunset sky.*"
– Rabindranath Tagore

It goes without saying that there are many people who have influenced and made this work possible in various ways. True masters like Tagore could easily describe beauty of human interactions in words, but I am not as capable as him, so would just like to say "**Thank you**". I have a lot of memories and experiences, some to learn and some to cherish. Here, I only mention the names, but there are many things to say, hopefully you know that. I sincerely thank my;

Supervisors: Peter, Renko and Harry

Special supervisor: Stefano

Project partner: Yunus

Students: Zeger, Ning, Yuxi and Giulia

Paranymphs: Alexandra and Roy

Office mates: Annewieke, Edita, Red, Uttara, Wibke, Melliana, Wouter, Alexandra

Protein/Lab mates: Frederik, Emma, Claire, Abhishek, Hans, Anja, Rene, Alexandra, Roy

Lab-trip gals: Milou and Rianne

Colleagues at Food Chemistry: Jolanda, Maxime, Tomas, Marijn, Matthias, Hugo Yannick, Urmila, Lingmin, Aisyah, Carla, Elisabetta, Patricia, Thibaut, Christiane, Anne, Renske, Rudy, Carlos, Ya, Stephanie, Connie, Julia, Lia, Jean-Paul, Mirjam, Henk, Koos, Katharina, Fang-Jie, Martijn, Klaus, Suzanne, Marit, Jesse, Mark, Edwin, Peter G., Margaret, Arjen, Hante, Gerard, Hetty, Marlies, Rinelle, Hilde, Frank, Walter, Geralt, Jorien, Bianca, Rinelle, Annelou, Monique, Wieteke, Kok-Phen, Inma, Mane, Annemieke, Piet, Jesse, Eline and Belen

Colleagues at Fysko: Herman, Remco, Anton, Josie, Mara, Martien, Liyakat, Armando, Dmitri, Evan, Pascal, Sabine, Malgorzata, Kamuran, Gosia, Maria, Jeroen, Joris, Jasper, Marc, Katarzyna, Kathelijne, Lennart, Natalia, Frans, Mieke, Hans, Huanhuan, Thao, Prachi, Jacob, Christian, Hande, Rui, Junyou, Juan, Yuan, Harke and Petya

Other colleagues from FPE, FPH, BIC and VLAG: Ekaraj, Sami, Harry (Baptist), Paul, Elke, Carsten, Kun, Claire, Vaida, Jos, Willem, Vesna and Yvonne

BRM-IPP colleagues: Victor, Rob, Arno, Arjen, Rene

FOM colleagues: Maria (Teuwissen), Victor, Lydia, Pieter, Ria, Renee-Andree, Diana, Ralf, Wessel and Annette.

Unilever Vlaardingen: Theo, Rob and Simeon

Wyatt Dernbach, Germany: Kees, Arthur, Roger and Christian

Other friends: Sidhu, Satesh, Saurabh, Sruti, Umesh, Nagendra, Aparna, Nidhi, Manohar, Madhu, Krithika, Hanneke, Marina, Roelfrike, Marcin, Indira, Ruchika, Sandeep, Alok and Digvijay

Family: Mummy, Papa, Maa, Buba, Naru, Arvi, RukMaa, DewoMaa, Nanuji, Aayush, Shalu, Buaji, Dadoji, Mama(s), Mashi(s) and cousines

Amar Vihaan: Bihu ..
Amar Chirosakhi: Soum

About the author

The author's journey so far has been an outcome of a chance encounter with bubbles and science behind them. Surender Kumar Dhayal was born on 02^{nd} September 1979 in Sikar, Rajasthan, India. During his formative years, he did his schooling in Kendriya Vidyalayas (KV) located in various parts of the country such as Bagdogra-Siliguri, Delhi and Bangalore. After finishing higher secondary education in the faculty of science, he enrolled in a four years course in bachelor of engineering (B.E.) at BMS College of Engineering, Bangalore, studying chemical engineering. During this time he grew deep interest in interfacial phenomena and did a mid-term thesis research with Dr. Samita Maitra on foam, a subject which is still his passion. The B.E. final year thesis research was performed at Indian Institute of Sciences (IISc), Bangalore. After completing his B.E. in the year 2003, he joined Unilever Research India and worked there for five years doing research in various divisions such as chemical engineering and materials science (corporate research) and home and personal care. The research work covered diverse faculties encompassing colloid & interface science and process & materials science. There he also met his wife (Soumi Banerjee) and they both decided to follow their common passion in soft matter science, which led to a move to Wageningen in the year 2009 . He studied masters of science (MSc) in biotechnology, specializing in process technology. To build his skills in working with proteins, he started a MSc thesis with Dr. Renko de Vries and Dr. Peter Wierenga at the Laboratory of Physical Chemistry and Colloid Science, working on enzymatic cross-linking of a milk protein and its impact on foam-stability. This led to start of a PhD research in January 2011 at the Laboratory of Food Chemistry, Wageningen University with Prof. Dr. Harry Gruppen as supervisor and Dr. Wierenga and Dr. de Vries as co-supervisors. He was employed and funded by the Foundation for Fundamental Research on Matter (FOM) during this time on the project titled "Enzymatically Cross-linked Globular Proteins as Hierarchical Biopolymers" supported under the Industrial Partnership Program (IPP) for Bio-Related Materials (BRM) of FOM. This thesis is an outcome of the PhD research performed between January 2011 and December 2014. Currently, he is doing postdoctoral research on self-assembly and colloidal interactions of synthetic protein polymers with Dr. de Vries and Prof. Dr. Martien Cohen Stuart at Physical Chemistry and Soft Matter, Wageningen University.

He can be contacted by email: surender.dhayal@gmail.com

Overview of completed training activities

Discipline specific activity
Food and biorefinery enzymology, Wageningen, 2011†
Rheology and structure of food, Wageningen, 2012†
Zigmondy colloquium, Münster, Germany, 2011‡
From colloids to nano-particles: Historical perspectives on a fascinating world, Utrecht, 2011
ZEFL-soft x-ray, Wageningen, 2012
Food colloids, Copenhagen, Denmark, 2012‡
Soft matter approaches to structured food, Wageningen, 2012
Bio-Related Materials (BRM) conference organized by FOM, Utrecht-2011†, 2012†, 2013‡ and 2014†
Bulk and Surface Rheology, TA instruments, Wageningen, 2013
AF4 training, Wyatt, Germany, 2012

General Courses
PhD Week, VLAG, 2011‡
Philosophy and Ethics of Food Science and Technology, VLAG, 2012
Taking charge of your PhD, FOM, 2011
FOM Young Scientist Day – 2011 and 2012
- The art of presenting science
- Starting a science based company

FOM Young Scientist Day – 2013
- How to get funded
- Academic career development

Art of Scientific writing, FOM, 2013
Career perspectives, WGS, 2013

Other Activities
Protein meetings, FCH, 2011-2014‡
PhD lunch presentations, FCH, 2011-2014‡
Student & other presentations, FCH, PCC, 2011-2014
PhD trip (Singapore and Malaysia)- 2012‡ †
PhD trip (Germany, Denmark, Sweden and Finland)-2014‡ †
Preparing PhD project proposal, FCH, VLAG, 2011

Teaching
Food Processing and Product Properties, Part: Discipline Integrating Product Practical, 2011
Food Related Allergies and Intolerance, 2013
Food Ingredients and Functionality, 2012
Food Ingredients and Functionality, 2013
Supervision of 1 BSc and 3 MSc theses, 2011-2013
*

*‡ Talk, † Poster

This work is part of an Industrial Partnership Programme of the Stichting voor Fundamenteel Onderzoek der Materie (FOM) which is financially supported by the Nederlandse Organisatie voor Wetenschappelijk Onderzoek (NWO). This Industrial Partnership Programme is co-financed by the Top Institute Food & Nutrition and the Dutch Polymer Institute.

Cover design by S. K. Dhayal & S. Banerjee

Printed by Wöhrmann Print Service, Zutphen